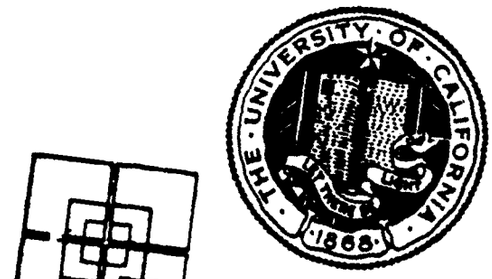

university of california • santa barbara

GENERAL THEORY AND ALGORITHMS FOR THE NON-CAUSAL INVERSION, SLEWING AND CONTROL OF SPACE-BASED ARTICULATED STRUCTURES

Final report to the

Air Force Office of Scientific Research

under

Grant F49620-91-C-0095

by

E. Bayo and B. Paden
Department of Mechanical and Environmental Engineering
University of California
Santa Barbara, CA 93106

October 1993

College of Engineering

REPORT DOCUMENTATION PAGE

Form Approved
OMB No. 0704-0188

1. AGENCY USE ONLY (Leave blank)	2. REPORT DATE	3. REPORT TYPE AND DATES COVERED
	October 31, 1993	Final, Sept. 91 - Aug. 93

4. TITLE AND SUBTITLE
"General Theory and Algorithms for the Non-Causal Inversion, Slewing and Control of Space-Based Articulated Structures"

5. FUNDING NUMBERS
F49620-91-C0095

6. AUTHOR(S)
Bayo, Eduardo
Paden, Bradley

7. PERFORMING ORGANIZATION NAME(S) AND ADDRESS(ES)
Mechanical Engineering Department
University of California
Santa Barbara, CA 93106

8. PERFORMING ORGANIZATION REPORT NUMBER

9. SPONSORING / MONITORING AGENCY NAME(S) AND ADDRESS(ES)
AFOSR
Dr. Spencer Wu, Program Manager
Directorate of Aerospace Sciences
Air Force Office of Scientific Research
Bolling Air Force Base, DC 20332-6448

10. SPONSORING / MONITORING AGENCY REPORT NUMBER

11. SUPPLEMENTARY NOTES

12a. DISTRIBUTION / AVAILABILITY STATEMENT

12b. DISTRIBUTION CODE

13. ABSTRACT (Maximum 200 words)

The following final report describes the accomplishments obtained by the research team at UCSB sponsored by the Directorate of Aerospace Sciences of the AFOSR. The major accomplishments are the following:

- General Procedures for the Non-Causal Inverse Dynamics of Nonlinear Articulated Structures
- Inverse Dynamics of Nonlinear Articulated Structures: Simultaneous Trajectory Tracking and Vibration Reduction
- Buckling Control of a Flexible Beam Using Piezoelectric Actuators
- Nonlinear Inversion-Based Regulation

14. SUBJECT TERMS
Flexible articulated structures, dynamics, control, non-causal inversion, algorithms.

15. NUMBER OF PAGES

16. PRICE CODE

17. SECURITY CLASSIFICATION OF REPORT	18. SECURITY CLASSIFICATION OF THIS PAGE	19. SECURITY CLASSIFICATION OF ABSTRACT	20. LIMITATION OF ABSTRACT
Unclassified	Unclassified	Unclassified	SAR

GENERAL THEORY AND ALGORITHMS FOR THE NON-CAUSAL INVERSION, SLEWING AND CONTROL OF SPACE-BASED ARTICULATED STRUCTURES

Final report to the

Air Force Office of Scientific Research

under

Grant F49620-91-C-0095

by

E. Bayo and **B. Paden**

Department of Mechanical and Environmental Engineering
University of California
Santa Barbara, CA 93106

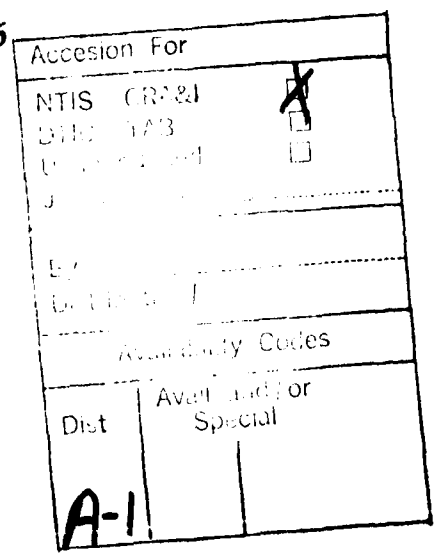

October 1993

Table of Contents

Title Page i

Table of Contents ii

Executive Summary 1

1. General Procedures for the Non-Causal Inverse Dynamics of Nonlinear Articulated Structures 2

2. Inverse Dynamics of Nonlinear Articulated Structures: Simultaneous Trajectory Tracking and Vibration Reduction ... 10

3. Buckling Control of a Flexible Beam Using Piezoelectric Actuators 16

4. Nonlinear Inversion-Based Regulation 21

5. References 29

6. List of Publications under Grant F49620-91-C-0095 32

Appendix: Copies of Publications 33

Executive Summary

The studies reported were carried out during the period September 1991 through August 1993 under the auspices of the Directorate of Aerospace Sciences of the AFOSR. They were concerned with the dynamics and control of spaced based articulated structures, and have led to a better understanding of the theory and procedures for the non-causal inversion, slewing and control of systems characterized by unstable zero-dynamics. In particular the following results can be highlighted:

- general non-recursive procedures to solve the inverse dynamics and kinematics of flexible open-chain and closed-chain nonlinear articulated structures in two and three dimensional settings. These include robust multibody dynamic formulations that are efficient and stable even in singular configurations and in the presence of redundant algebraic constraints.
- a general theory for non-causal inversion of nonlinear non-minimum phase systems which relates invertibility and hyperbolicity of zero dynamics equilibria.
- recursive algorithms in three dimensions for inverse dynamics that include lumped and distributed actuators.
- new methods for the sizing and the placement of distributed actuators on linear and nonlinear configurations.
- a global nonlinear operator framework for controlled dynamical systems which presently handles local dynamics.
- a new approach to nonlinear tracking control which does not require solution of the Byrnes-Isidori PDE. New inverse dynamics based control methods have broad applications (e.g. nonlinear flight control, vibration control of nonlinear structures, trajectory control of towed vehicles, etc.)
- experimental results obtained from a smart articulated structure experiment (see figure 2.1) (funded by Astro-Aerospace Corporation) designed and fabricated at UCSB.

1. General Procedures for the Non-Causal Inverse Dynamics of Nonlinear Articulated Structures.

Summary

This study addresses the problem of end-point trajectory tracking in nonlinear flexible articulated structures through the use of inverse dynamics, and summarizes the work accomplished under the contract and which is described in detail in references 6, 7, and 8. A global Lagrangian approach is employed in formulating the system equations of motion, and an iterative procedure is proposed to achieve end-point trajectory tracking in three-dimensional, flexible multibody systems. Each iteration involves firstly, an inverse kinematics procedure wherein elastic displacements are determined in terms of the rigid body coordinates and Lagrange multipliers, secondly, an explicit computation of the inverse dynamic joint actuation, and thirdly, a forward dynamic analysis wherein generalized coordinates and Lagrange multipliers are determined in terms of the joint actuation and desired end-point coordinates. In contrast with the recursive methods previously proposed, this new method is the most general since it is suitable for both open-chain and closed-chain configurations of three-dimensional multibody systems. The algorithm yields stable, *non-causal* actuating joint torques and associated Lagrange multipliers that account for the constraint forces between flexible multibody components.

Introduction

The problem of end-point trajectory tracking in flexible multibody systems has led to the development of methods for inverse dynamics. Inverse dynamics deals with the problem of determining the joint actuation that will cause a specified control point in the flexible multibody system to follow a desired trajectory. The pioneering work of Reference 1 on the trajectory control of a single flexible link through inverse dynamics showed that the inverse dynamic torque is *non-causal* with respect to the end-point motion, *i.e.*, actuation is required before the end-point has started to move as well as after the end-point has stopped. Moulin and Bayo [2] demonstrated that because of the non-minimum phase character of the inverse dynamics for the trajectory tracking problem, the only bounded solution for the inverse dynamic torque has to be non-causal. Bayo, *et. al.* [3], extended the inverse dynamics to planar, multiple-link systems using an iterative frequency domain approach. The recursive method proposed in that study is suitable for planar open-chain systems, but required an *ad hoc* procedure for planar closed-chain systems. A time domain inverse dynamic technique based on the non-causal impulse response function was presented by Bayo and Moulin [4] for the single link system, with provisions for

extension to multiple link systems. An equivalent time domain approach for a single link arm was proposed by Kwon and Book [5] where the non-causality of the computed torque was captured by dividing the inverse system into causal and anticausal parts.

In this study, a general approach is presented for the solution of the *non-causal* inverse dynamics of three-dimensional, flexible multibody systems, which is suitable for both open-chain and closed-chain configurations. With this work, a methodology is presented that is suitable for all multibody systems, ranging from the single link case to three-dimensional systems with general topologies.

Problem Formulation

Consider an n-body flexible multibody system such as that shown in Fig. 1.1. A typical multibody component, say body i, is shown in Fig. 1.1 along with the floating reference frame associated with that body. The generalized coordinates consist of rigid body coordinates $\mathbf{q}_r^i$ which describe the position and orientation of the floating reference frame associated with each multibody component, and deformation coordinates $\mathbf{q}_f^i$ which describe the deformation of the flexible body with respect to its floating reference frame. The rigid body coordinates $\mathbf{q}_r^i$ consist of the Cartesian coordinates $\mathbf{R}^i$ which describe the position of the origin of the floating reference frame associated with body i, and a set of Euler parameters θ^i which describe the orientation of the floating frame. The deformation from the nominal configuration is assumed to be small, so that the different bending and torsional modes are decoupled.

Considering the reference coordinates $\mathbf{q}^T = \left[\mathbf{R}^T, \theta^T, \mathbf{q}_f^T\right]$ as generalized coordinates for the flexible multibody system, these coordinates are not independent because the motion of specific points in different bodies are related according to the type of mechanical joints that interconnect them. Moreover, in flexible multibody systems, the deformation of a component affects the configuration of adjacent components. As a consequence, the interdependence of the generalized coordinates is expressed by a vector of kinematic constraint equations, such as

$$\Phi(\mathbf{q},t) = 0 \tag{1.1}$$

where $\mathbf{q}$ is the total vector of system generalized coordinates, t is time, and Φ is the vector of linearly independent holonomic constraint equations. These constraint equations can be further classified into:

1. rigid body constraints where only rigid body variables are involved in the constraint equation;

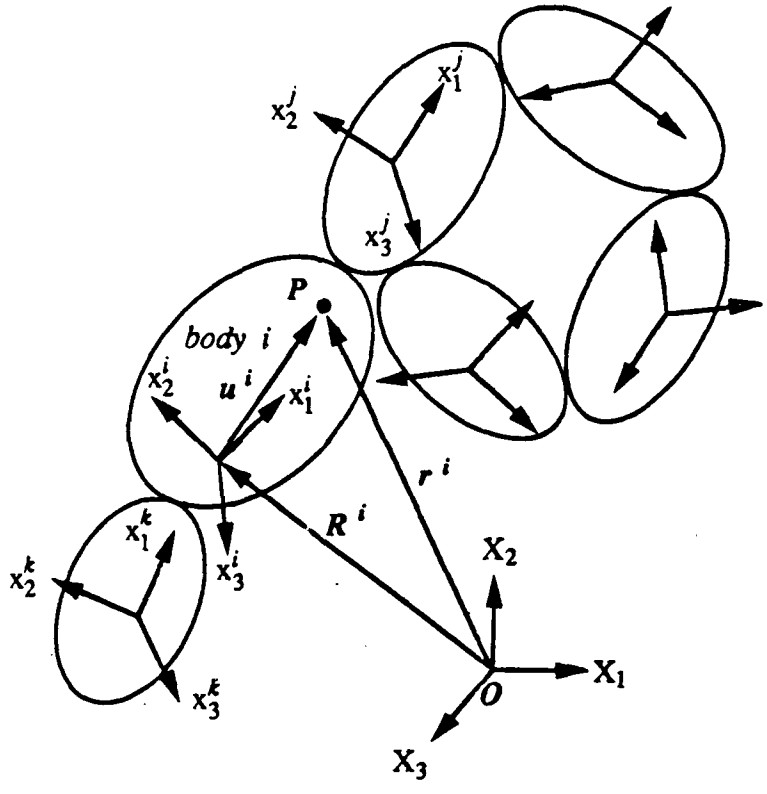

Fig. 1.1. Topological description of a flexible articulated structure.

2. joint constraints where both rigid body and deformation coordinates are included in the constraint equation; and
3. rheonomic constraints wherein the constraint equations can be explicit functions of time as well as generalized coordinates.

The third type of constraint becomes active, for example, in the case of imposing the coordinates of the end-effector to follow a desired trajectory.

Considering the rigid body and deformation coordinates described above as generalized coordinates, and following standard procedures in multibody dynamics, the constrained equations of motion become

$$\mathbf{M}(\mathbf{q})\,\ddot{\mathbf{q}} + \mathbf{C}\,\dot{\mathbf{q}} + \mathbf{K}\,\mathbf{q} + \Phi_{\mathbf{q}}^{\mathbf{T}}\,\lambda = \mathbf{Q}_{\mathbf{e}} + \mathbf{Q}_{\mathbf{v}}(\mathbf{q}, \dot{\mathbf{q}}) \tag{1.2}$$

where $\mathbf{M}$, $\mathbf{C}$, and $\mathbf{K}$ are the system mass, damping and stiffness matrices, respectively, λ is the vector of Lagrange multipliers associated with the constraints, $\Phi_{\mathbf{q}}$ is the constraint Jacobian matrix, $\mathbf{Q}_{\mathbf{e}}$ is the vector of applied external forces, and $\mathbf{Q}_{\mathbf{v}}$ is the quadratic velocity vector. The quadratic velocity vector contains the centrifugal forces and Coriolis forces that result from the differentiation of the kinetic energy expression with respect to the generalized coordinates. Geometric stiffening due to high rotation rates can also be added to the vector $\mathbf{Q}_{\mathbf{v}}$.

In a forward dynamic analysis, *i.e.*, finding the resulting motion given the applied joint forces and external forces, Eqs. (1.1) and (1.2) constitute a mixed system of differential-algebraic equations that have to be integrated simultaneously. The solution to the inverse dynamics problem requires a forward dynamic analysis within an iteration process. We solve the forward dynamics problem by using the augmented Lagrangian penalty formulation [8-9]. Applying the augmented Lagrangian penalty formulation to Eqs. (1.1) and (1.2) results in the following equation:

$$\mathbf{M}(\mathbf{q})\,\ddot{\mathbf{q}} + \mathbf{C}\,\dot{\mathbf{q}} + \mathbf{K}\,\mathbf{q} + \Phi_{\mathbf{q}}^{\mathbf{T}}\,\alpha\left[\ddot{\Phi} + 2\,\mu\,\omega\,\dot{\Phi} + \omega^2\,\Phi\right] = \mathbf{Q}_{\mathbf{e}} + \mathbf{Q}_{\mathbf{v}}(\dot{\mathbf{q}}, \mathbf{q}) - \Phi_{\mathbf{q}}^{\mathbf{T}}\,\lambda^{*} \tag{1.3}$$

where α is a diagonal matrix of penalty factors whose elements are large real numbers that will assure the satisfaction of constraints, ω and μ are diagonal matrices representing the natural frequencies and damping characteristics of the *dynamic penalty system* associated with the constraints. The augmented Lagrangian method requires an iteration for the correct value of the Lagrange multipliers. The iterative equation for the Lagrange multipliers is given by

$$\lambda_{i+1}^{*} = \lambda_{i}^{*} + \alpha\left[\ddot{\Phi} + 2\,\mu\,\omega\,\dot{\Phi} + \omega^2\,\Phi\right]. \tag{1.4}$$

The augmented Lagrangian penalty formulation [8] has several advantages over the standard algorithms used in solving differential-algebraic equations. First, the method obviates the need to solve a mixed set of differential-algebraic equations and does not increase the number of equations to account for the constraints. Second, this method allows the use of standard unconditionally stable algorithms without the need of further stabilization techniques to control the violation of constraints during the integration process. Third, the method can handle redundant constraints and allows the multibody system to undergo singular positions. Fourth, the constraint forces (Lagrange multipliers) can be obtained as a by-product of the integration without having to integrate additional equations for them. Finally, the method assures convergence independent of the penalty values used.

Inverse Kinematics and Inverse Dynamics

The three-dimensional inverse dynamics problem for either open-chain or closed-chain topologies is solved by an iterative Lagrangian procedure. Our overall strategy is to first solve the inverse kinematics problem, *i.e.*, finding the unknown rigid body coordinates $\mathbf{q}_r$ and flexible body displacements $\mathbf{q}_f$, given the desired end-point coordinates as explicit functions of time. Having determined the correct generalized coordinates and their time derivatives, the inverse dynamics joint torques can be obtained explicitly from the equations of motion. Compared to the recursive procedures previously proposed, this new approach is more systematic and becomes the only choice when closed-chain systems are encountered. The elastic links are modeled under pinned-pinned boundary conditions. Furthermore, since torsional deformations cause deviations from the nominal configuration further down the chain, we model the elastic link as fixed with respect to torsion at the distal end of the link.

Our goal then is to formulate an inverse kinematics equation that is linearized about the nominal motion, so that the elastic displacements, which are non-causal with respect to the end-point motion, can be determined through a transformation to the frequency domain. This is possible only if the leading matrix of the linearized equation is time-invariant and if the forcing term is Fourier transformable. This objective has been achieved in the planar case with the use of reference coordinates for the rigid body variables to describe the position and orientation of the floating reference frame [6].

The three-dimensional inverse kinematics problem presents additional difficulties not found in the planar case [7]. First, unlike the planar case, the three-dimensional torque vectors change directions in time, so that the external force vector $\mathbf{Q}_e$ in Eq. (1.3) becomes a nonlinear function of the rigid body orientation coordinates. To overcome this difficulty, a proper

parametrization of the rigid body coordinates and proper bases for the joint torques are necessary to attain the stated objectives in forming the linearized inverse kinematics equations. The desired form of the linearized inverse kinematics equation is possible if Euler parameters are used to describe the rigid body orientation and if the base torque vector of each multibody component is expressed in terms of components along the associated floating reference frame.

For a typical multibody component, say body i, the equations of motion can be written in the following partitioned form [7]:

$$\begin{bmatrix} \mathbf{m}_{RR} & \mathbf{m}_{R\theta} & \mathbf{m}_{Rf} \\ \mathbf{m}_{\theta R} & \mathbf{m}_{\theta\theta} & \mathbf{m}_{\theta f} \\ \mathbf{m}_{fR} & \mathbf{m}_{f\theta} & \mathbf{m}_{ff} \end{bmatrix} \begin{bmatrix} \ddot{\mathbf{R}} \\ \ddot{\theta} \\ \ddot{\mathbf{q}}_f \end{bmatrix} + \begin{bmatrix} 0 & 0 & 0 \\ 0 & 0 & 0 \\ 0 & 0 & \mathbf{c}_{ff} \end{bmatrix} \begin{bmatrix} \dot{\mathbf{R}} \\ \dot{\theta} \\ \dot{\mathbf{q}}_f \end{bmatrix} + \begin{bmatrix} 0 & 0 & 0 \\ 0 & 0 & 0 \\ 0 & 0 & \mathbf{k}_{ff} \end{bmatrix} \begin{bmatrix} \mathbf{R} \\ \theta \\ \mathbf{q}_f \end{bmatrix} + \begin{bmatrix} \Phi_R^T \\ \Phi_q^T \\ \Phi_{q_f}^T \end{bmatrix} = \begin{bmatrix} \mathbf{Q}_{eR} \\ \mathbf{Q}_{e\theta} \\ \mathbf{Q}_{ef} \end{bmatrix} + \begin{bmatrix} \mathbf{Q}_{vR} \\ \mathbf{Q}_{v\theta} \\ \mathbf{Q}_{vf} \end{bmatrix} . \tag{1.5}$$

The elements of the mass matrix and quadratic velocity force vector corresponding to an isoparametric, three-dimensional curved beam finite element are given in Reference 7.

Let τ^i be the torque vector at the base of body i, whose three components τ_r^i, τ_s^i, and τ_t^i are parallel to the associated floating reference axes r^i, s^i, and t^i, respectively. If we use Euler parameters as the rigid body orientation coordinates, the externally applied joint forces $\mathbf{Q}_{e\theta}^i$ associated with the rigid body rotation of body i can be expressed as

$$\mathbf{Q}_{e\theta}^i = \left[\mathbf{G}^i\right]^T \left\{ \tau^i - \left[\mathbf{A}^i\right]^T \mathbf{A}^{i+1} \tau^{i+1} \right\} \tag{1.6}$$

where τ^i is the base torque acting on body i and whose components are parallel to the floating reference axes associated with body i; τ^{i+1} is the vector of joint torques and reaction moments transmitted from body i to body $i + 1$, and whose components are parallel to the floating reference axes associated with body $i + 1$; $\mathbf{A}^i$ and $\mathbf{A}^{i+1}$ are body axes to inertial axes rotation transformation matrices for bodies i and $i + 1$, respectively; and $\mathbf{G}^i$ is a matrix that maps the derivatives of the Euler parameters describing the orientation of the reference frame of body i to the angular velocity of this reference frame, and is given by $\mathbf{G}^i = 2\,\mathbf{E}^i$. Combining Eq. (1.6) with the second set of equations in Eq. (1.5), and after and involved process described in Reference 7, the inverse dynamic equations are obtained as:

$$\tau^i = \left[\mathbf{A}^i\right]^T \mathbf{A}^{i+1}\,\tau^{i+1} + \frac{1}{4}\,\mathbf{G}^i\,\mathbf{m}^i_{\theta R}\,\ddot{\mathbf{R}}^i + \mathbf{J}^i\,\mathbf{G}^i\,\ddot{\theta}^i + \mathbf{J}^i_f\,\ddot{\mathbf{q}}^i_f + \frac{1}{4}\,\mathbf{G}^i\,\Phi^T_{\theta^i}\,\lambda$$

$$+ \frac{1}{2}\,\mathbf{G}^i\left[\dot{\mathbf{G}}^i\right]^T\left\{\mathbf{J}^i\,\mathbf{G}^i\,\dot{\theta}^i + \mathbf{J}^i_f\,\dot{\mathbf{q}}^i_f\right\} \tag{1.7}$$

where $\mathbf{J}^i$ is the 3×3 inertia tensor of body i with respect to the origin of the floating reference frame and measured relative to this frame, and $\mathbf{J}^i_f$ is the inertia matrix coupling the rigid body rotation and the elastic deformation. The key to obtaining a time-invariant leading matrix, that is necessary in transforming the linearized equations of motion into the frequency domain, is the fact that the inertial coupling matrix $\mathbf{J}^i_f$ can be decomposed into the sum of a time-invariant matrix and a time-varying matrix, *i.e.*,

$$\mathbf{J}^i_f = \mathbf{J}^i_{fc} + \mathbf{J}^i_{ft} \tag{1.8}$$

where $\mathbf{J}^i_{fc}$ and $\mathbf{J}^i_{ft}$ are the time-invariant part and time-varying part of $\mathbf{J}^i_f$, respectively. This decomposition is essential to the formulation of the inverse kinematics equations that lead to non-causal solutions of the nonlinear inversion problem and which are given by

$$\tilde{\mathbf{m}}^i_{ff}\,\ddot{\mathbf{q}}^i_f + \mathbf{c}^i_{ff}\,\dot{\mathbf{q}}^i_{ff}\,\mathbf{q}^i_f = \mathbf{F}^i\left(\lambda, \mathbf{q}^i_r, \dot{\mathbf{q}}^i_r, \ddot{\mathbf{q}}^i_r, \mathbf{q}^i_f, \dot{\mathbf{q}}^i_f, \ddot{\mathbf{q}}^i_f\right) \tag{1.9}$$

where

$$\tilde{\mathbf{m}}^i_{ff} = \mathbf{m}^i_{ff} - \mathbf{N}^T_b\,\mathbf{J}^i_{fc} \tag{1.10}$$

and the motion-induced force vector acting on the elastic degrees of freedom is given by

$$\mathbf{F}^i = \mathbf{N}^T_b\left\{\left[\mathbf{A}^i\right]^T \mathbf{A}^{i+1}\,\tau^{i+1} + \mathbf{T}^i_b\right\} - \mathbf{N}^T_t\left[\mathbf{A}^i\right]^T \mathbf{A}^{i+1}\,\tau^{i+1}$$

$$+ \mathbf{Q}^i_{vf} - \Phi^T_{q^i_f}\,\lambda - \mathbf{m}^i_{fR}\,\ddot{\mathbf{R}}^i - \mathbf{m}^i_{f\theta}\,\ddot{\theta}^i\,. \tag{1.11}$$

The modified mass matrix $\tilde{\mathbf{m}}^i_{ff}$ is non symmetric and it is precisely this non symmetry that produces elastic displacements which are non-causal with respect to the end-point motion when non-causal techniques are employed to obtain the proper inversion of the nonlinear, non-minimum phase systems.

The non-causal inversion can now be carried out efficiently in the frequency domain since the leading matrices have been constructed such that they remain constant throughout the motion. Equation (1.9) can be written as a set of complex equations for a particular frequency ω

$$\left[\bar{\mathbf{m}}^i_{ff} + \frac{1}{i\omega}\mathbf{c}^i_{ff} - \frac{1}{\omega^2}\mathbf{k}^i_{ff}\right] \hat{\ddot{\mathbf{q}}}^i_f(\omega) = \hat{\mathbf{F}}^i(\omega) \tag{1.12}$$

where $\hat{\ddot{\mathbf{q}}}^i_f(\omega)$ is the Fourier transform of $\ddot{\mathbf{q}}^i_f(t)$ and $\hat{\mathbf{F}}^i(\omega)$ is the Fourier transform of $\mathbf{F}^i(t)$.

Alternatively, the computation of the elastic displacements and their derivatives in each iteration can also be carried out in the time domain through the use of the non-causal impulse response function and the bilateral Laplace transform, *e.g.*,

$$\ddot{\mathbf{q}}_f(t) = \int_{-\infty}^{\infty} \sum_{j=1}^{j=n} \mathbf{h}_j(t-\tau) f_j(\tau)\, d\tau \tag{1.13}$$

where $\mathbf{h}_j(t)$ is the non-causal acceleration response vector to an impulse applied to the j^{th} degree of freedom and $\mathbf{f}_j(t)$ is the jth component of the forcing term on the right hand side of Eq. (1.9). We note that the integration from $-\infty$ to ∞ is necessary to capture the non-causal effects.

Once the non-causal elastic displacements and their derivatives are known, Eq. (1.7) can be used to explicitly compute the non-causal inverse dynamics joint efforts that will move the end effector according to a desired trajectory. We note, however, that the joint torques and elastic displacements given by Eqs. (1.7) and (1.9), respectively, depend on the Lagrange multipliers and rigid body coordinates, which in turn depend on the elastic displacements and the applied torque. Moreover, the rigid body coordinates and Lagrange multipliers are different from their nominal values when the components of the multibody system are flexible. Therefore, a forward dynamic analysis is required to obtain an improved estimate of the generalized coordinates and Lagrange multipliers.

Results

Figure 1.2 shows a closed-chain, three-dimensional flexible articulated structure, where the selected control torques are shown in the figure. Joints 1-4 are revolute joints while joint 5 is a spherical joint. The desired end-point (joint 5) trajectory is a motion in the $x_2 - x_3$ plane with the x_2 coordinate and x_3 coordinate of the end-point following the trajectories shown in Fig. 1.3. The four links share the following geometric and material properties:

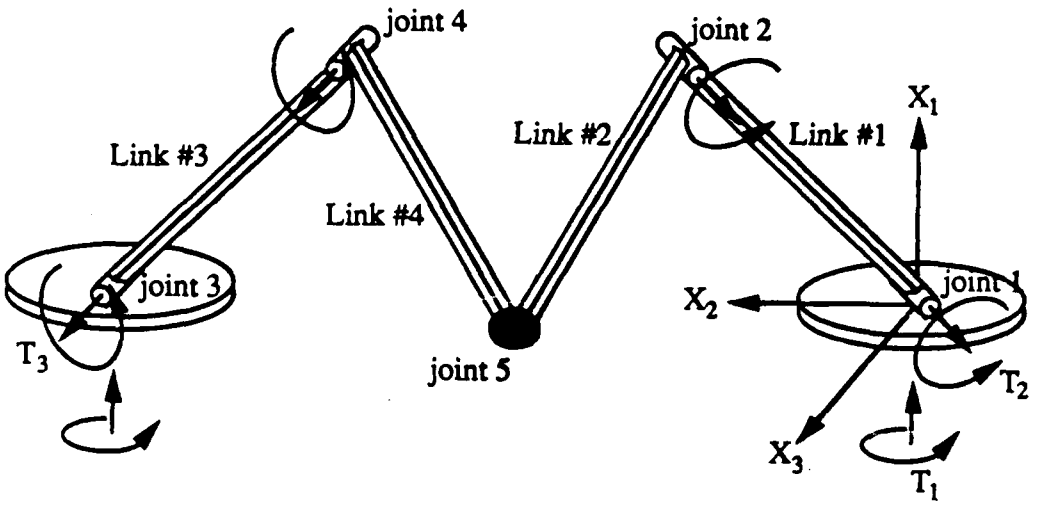

Fig. 1.2. Close-chain 3-D Flexible articulated structure.

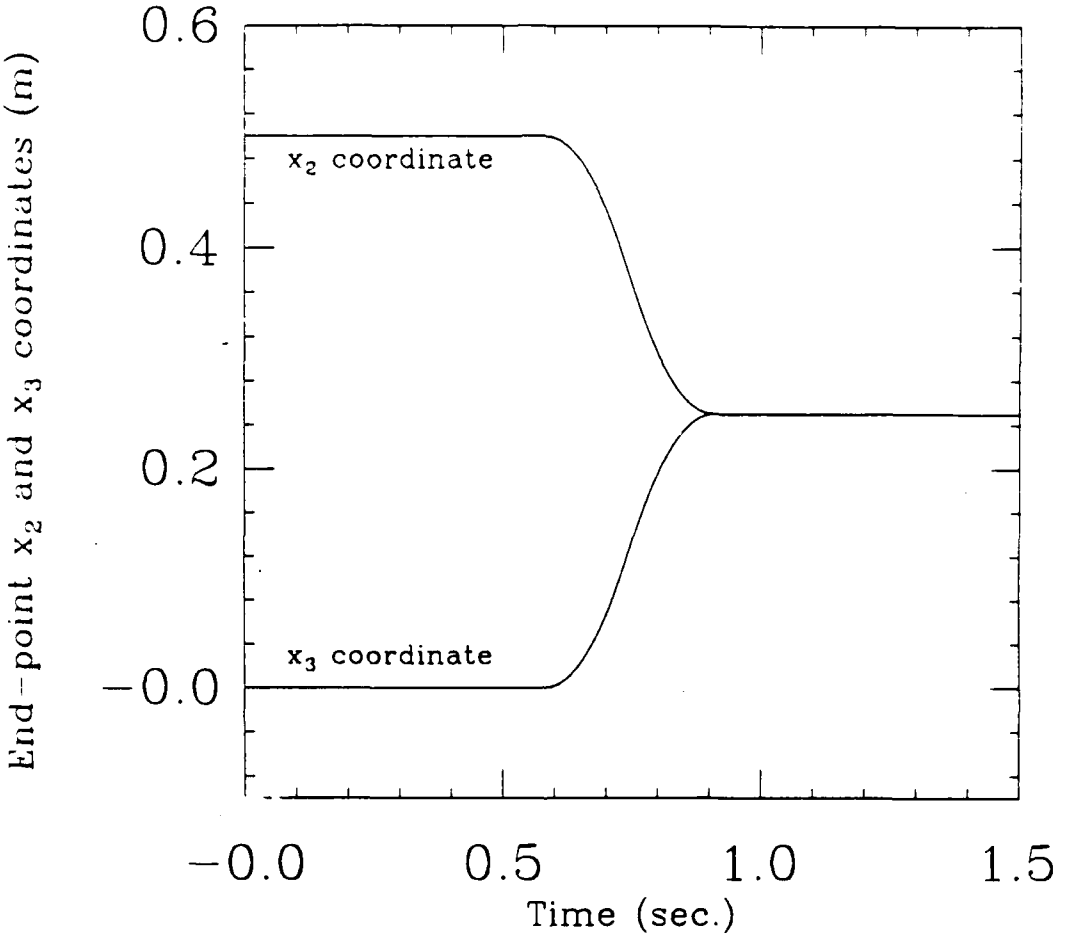

Fig. 1.3. Required end-point trajectory.

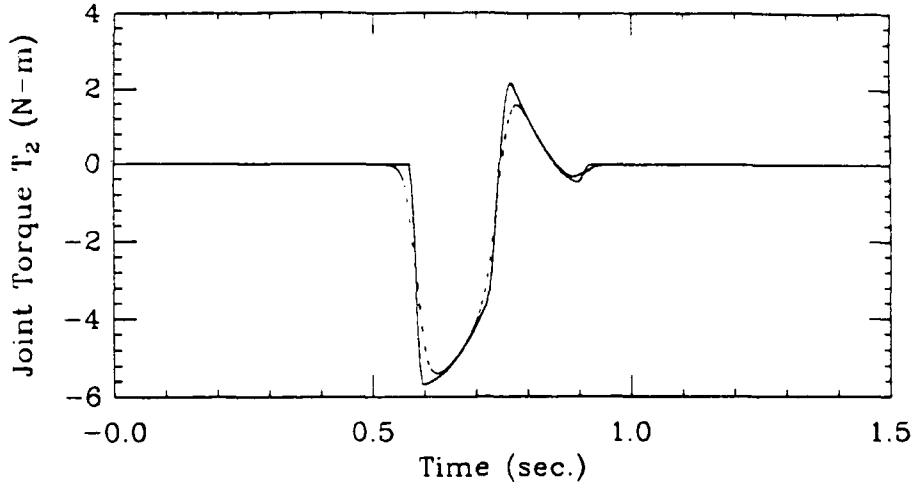

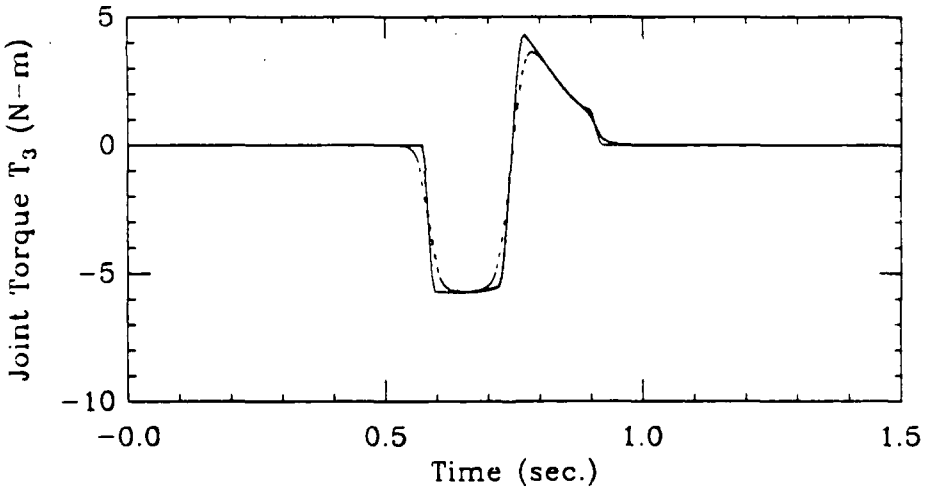

Fig. 1.4. Inverse dynamics torques.

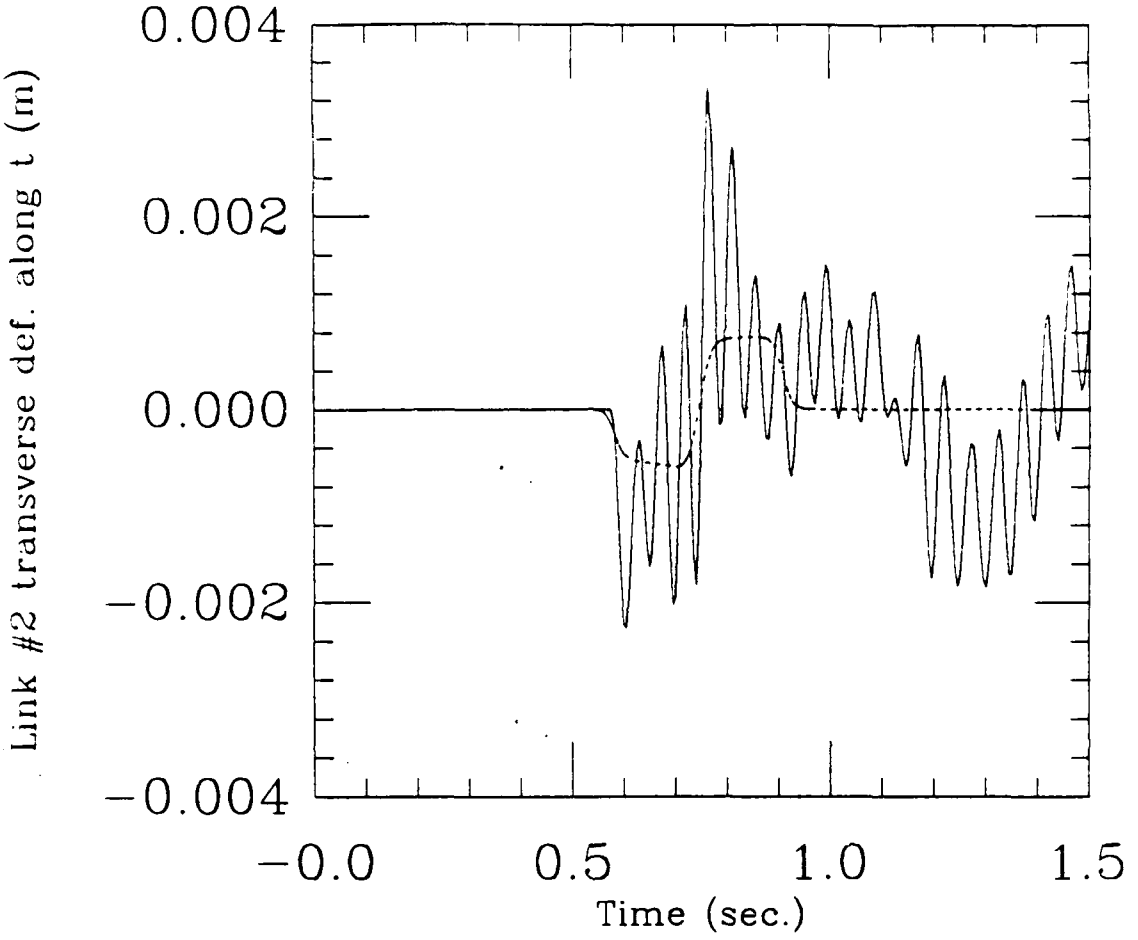

Fig. 15. Elastic deflection in an internal point.

Length: 1.0m; Cross section dimensions: 1.0 cm x 1.0 cm; Young's modulus: 40 GPa; Shear modulus: 15 GPa; Mass density: 2715 kg/m3; Tip mass: 0.1 kg.

The procedure is applied to the closed-chain system by introducing a cut at the end-point (joint 5), thus creating two open-chain systems. The internal constraint forces exposed by the cut are automatically taken into account by the Lagrange multipliers in the equations of motion. Figures 1.4a and 1.4b show joint torques T_2 and T_3, respectively, that are needed to achieve the desired end-point trajectory. In these figures, the dashed curves refer to the inverse dynamic torques obtained by the present procedure while the solid curves refer to the corresponding rigid body torques. Observe the pre and post activation required by the inverse dynamics situation. Figure 1.5 shows the transverse deflections at a third point in link #2, obtained from a feed-forward of the inverse dynamic torques (dashed curve) and the corresponding deflection obtained from a feed-forward of the rigid body torque (solid curve). It may be observed that the inverse dynamic torques minimize the residual structural vibrations that are otherwise present when rigid body torques are used to actuate the system.

Conclusion

A new and general procedure for determining the inverse dynamics and kinematics of 2-D and 3-D flexible articulated structures and multibody systems has been developed. An iterative procedure is necessary because of the interdependence between the elastic coordinates, the rigid body coordinates and the associated Lagrange multipliers in the system equations of motion. The procedure is general since it is valid for both open-chain and closed-chain configurations, and differs from the previously proposed recursive methods in the sense that the rigid body coordinates are not assumed to follow the nominal motion. The conditions for trajectory tracking are now met in a more general way through the satisfaction of rheonomic constraint conditions. For closed-chain systems, the new method is the only valid procedure for determining the inverse dynamic torques since in this case, the number of control torques is smaller than the number of joints and therefore, the recursive methods can not be applied.

2. Inverse Dynamics of Nonlinear Articulated Structures: Simultaneous Trajectory Tracking and Vibration Reduction.

Summary

The problem of inverse dynamics for flexible multibodies, which arises, in trajectory tracking control of flexible multibodies such as space manipulators and articulated flexible structures is studied. Previous research has resolved this trajectory tracking problem by computing the system inputs for feed-forward control of actuators at the joints. Recently, the use of distributed actuators like electro-strictive actuators in flexible structures has introduced a new dimension to this trajectory tracking problem. In this paper we optimally utilize such actuators to aid joint actuators for tracking control, and introduce a new inverse dynamics scheme for simultaneously (1) tracking a prescribed trajectory and (2) minimizing ensuing elastic deflections. We apply this scheme for trajectory tracking of a two-link two-joint planar manipulator with joint motors and distributed electro-strictive actuators. Experimental results are presented to contrast our new scheme with other existing methods. The study summarizes the work done under the contract and described in references 14 and 15.

Introduction

Inverse dynamics provides an excellent means for trajectory tracking of flexible multibodies. Methods to pre compute the actuator inputs required to exactly track a given output trajectory of a control point on open-chain flexible multibodies have been developed [1-5] where the inverse dynamics and kinematics produce bounded feed-forward inputs for actuators, like motors at articulations and joint angles, to track a reference point on the structure. The closed-chain cases have been recently presented by Ledesma and Bayo [6-7]. If the sensors and actuators are non-collocated then the flexible structure has nonminimum phase dynamics and the only stable inverse dynamics solution to the tracking problem is non-causal [2]. Once a trajectory is specified, the feed-forward control input obtained by inverse dynamics for exact trajectory tracking, has a unique bounded solution. Therefore, the subsequent elastic structural vibrations induced on the structure (except at the control point where these vibrations are zero) during the trajectory tracking motion are also defined uniquely. These vibrations could be detrimental to the performance of sensitive on-board systems and hence it is desirable to minimize them. For some time, distributed actuators have been successfully used to control structural vibrations [10-11]. Recent success in their experimental use [12] motivates the use of such actuators to aid joint actuators, like motors, for trajectory tracking.

The trajectory tracking objective can be accomplished by the point actuators alone [13] and in this sense the distributed actuators are redundant. In this study (which summarizes the contribution of references) the concept of using the extra actuation available through the distributed actuators in the structure is introduced to not only satisfy the trajectory tracking constraint, but also minimize the accompanying elastic displacements during the motion. A new inverse dynamics method is presented to compute the feed-forward inputs which includes the cases of redundantly actuated structures. This use of distributed actuators for end effector trajectory control is contrasted with the use of only the joint actuators in feed-forward. The method proposed is shown to substantially reduce the induced vibrations in the structure. The results are experimentally verified using a flexible two link articulated truss structure with distributed electro-strictive actuators and joint motors.

Formulation

The inverse dynamics of a flexible multibody is a nonlinear problem. We solve this non-linear problem recursively, one element of the multibody at a time. This algorithm proposed by Bayo et al in [3], for general multibody inverse dynamics involves, 1) studying an individual component (link) in the chain; 2) coupling the equations of the individual links; and 3) recursively converging to the desired actuator inputs and corresponding displacements. Following this general procedure, a new scheme is proposed which incorporates distributed actuators in the solution of the inverse dynamics problem [14-15]. This approach leads to the following inverse dynamics equations in terms of joint torque and piezoelectric voltages:

$$\mathbf{M}\ddot{\mathbf{z}} + \left[\mathbf{C} + \mathbf{C}_c(\omega_h)\right]\dot{\mathbf{z}} + \left[\mathbf{K} + \mathbf{K}_c(\alpha_h, \omega_h)\right]\mathbf{z} = \mathbf{B}_T\mathbf{T} + \mathbf{B}_p\mathbf{V}_p + \mathbf{F} \qquad (2.1)$$

where $\mathbf{z}$ is an $\mathbf{R}^n$ vector of the finite element degree of freedom. $\mathbf{M}$ and $\mathbf{K}$ belong to $\mathbf{R}^{n\times n}$ and are the conventional finite element mass and stiffness matrices respectively; $\mathbf{C}_c$ and $\mathbf{K}_c \in \mathbf{R}^{n\times n}$ and are the time varying Coriolis and centrifugal stiffness matrices, respectively. The $\mathbf{R}^{n\times n}$ matrix $\mathbf{C}$ represents the internal viscous damping of the material. $\mathbf{T}$ is the unknown joint actuation $\mathbf{F} \in \mathbf{R}^n$ contains the reactions at the end of the link, and the known forces produced by the rotating frame effect. The distributed actuator inputs $\mathbf{V}_p \in \mathbf{R}^{np}$ are the equivalent nodal forces at the FEM degrees of freedom, where np is the number of distributed actuator inputs. $\mathbf{B}_T$ and $\mathbf{B}_p$ are constant matrices inputs influence matrices of dimensions $\mathbf{R}^n$ and $\mathbf{R}^{n\times np}$, respectively.

The requirement is to accurately track the end effector of the link along the given nominal trajectory without overshoot and residual vibrations. If the distributed actuators were not

available then the exact tip trajectory tracking requirement defines the joint input torque **T**. The objective is to use the additional actuation available through the distributed actuators to reduce the ensuing structural vibrations at locations away from the control point during this motion by minimizing $\mathbf{J}(\mathbf{T}, \mathbf{V}_p)$, a measure of elastic deflections in the structure defined as follows:

$$\mathbf{J}(\mathbf{T}, \mathbf{V}_p) \underline{\Delta} \int_{-\infty}^{\infty} \mathbf{z}(t)^T \mathbf{z}(t) dt \tag{2.2}$$

Mathematically the objective can be stated as

$$\min_{(\mathbf{T},\mathbf{V}_p)\in\overline{\mathbf{T}}} \mathbf{J}(\mathbf{T},\mathbf{V}_p) \tag{2.3}$$

Where $\overline{\mathbf{T}}$ is the set of all pairs of stable actuator inputs that when used to actuate the system defined by Eq. (2.1) yields $\mathbf{z}_t(t) = 0$ for all t.

The solution process starts by rewriting Eq. (2.2) as

$$\mathbf{M}\ddot{\mathbf{z}} + \mathbf{C}\dot{\mathbf{z}} + \mathbf{K}\mathbf{z} = \mathbf{B}_T\mathbf{T} + \mathbf{B}_p\mathbf{V}_p + \mathbf{F} - \mathbf{C}_c(\omega_h)\,\dot{\mathbf{z}} - \mathbf{K}_c(\alpha_h,\omega_h)\,\mathbf{z} \tag{2.4}$$

where the time dependent Coriolis and centrifugal terms are kept on the RHS of the equation. The iteration procedure starts with the absence of the last two terms involving $\mathbf{C}_c$ and $\mathbf{K}_c$ in the right hand side. Then, the system of equations can be transformed into independent sets of simultaneous complex equations by means of the Fourier transform. For each of the evaluation frequency ω, Eq. (2.5) becomes

$$\left[\mathbf{M} + \frac{1}{i\omega}\mathbf{C} - \frac{1}{\omega^2}\mathbf{K}\right]\begin{bmatrix}\hat{\ddot{\mathbf{z}}}_h\\ \hat{\ddot{\mathbf{z}}}_i\\ \hat{\ddot{\mathbf{z}}}_t\end{bmatrix} = \begin{bmatrix}\hat{\mathbf{T}}\\ 0\\ 0\end{bmatrix} + \begin{bmatrix}\hat{\mathbf{F}}_h\\ \hat{\mathbf{F}}_i\\ \hat{\mathbf{F}}_t\end{bmatrix} + \begin{bmatrix}\mathbf{B}_{ph}\\ \mathbf{B}_{pi}\\ \mathbf{B}_{pt}\end{bmatrix}\hat{\mathbf{V}}_p \tag{2.5}$$

where the symbol $\wedge$ stands for Fourier transform, and $\hat{\mathbf{F}}$ represents the known forcing terms. After the first iteration it will also include the updated contributions from the Coriolis and centrifugal terms appearing in the RHS of Eq. (2.4). For any $\omega \neq 0$, the matrix

$$\mathbf{H} \triangleq \left[\mathbf{M} + \frac{1}{i\omega}\mathbf{C} - \frac{1}{\omega^2}\mathbf{K}\right] \tag{2.6}$$

is a complex, symmetric and invertible matrix. For $\omega = 0$ the system undergoes a rigid body motion and $\mathbf{H} \triangleq \mathbf{M}$, the positive definite invertible mass matrix. Let $\mathbf{G} \triangleq \mathbf{H}^{-1}$. Then a relationship between the joint actuation and the distributed actuator inputs and is obtained [14-15] as:

$$\hat{\mathbf{T}} = -\mathbf{G}_{th}^{-1}[\mathbf{G}_{th}\mathbf{G}_{ti}\mathbf{G}_{tt}]\,(\hat{\mathbf{F}} + \mathbf{B}_p\hat{\mathbf{V}}_p) \tag{2.7}$$

Substituting this expression for the input hub torque in Eq. (2.3) and using the property that $\ddot{\hat{\mathbf{z}}} = -\omega^2\hat{\mathbf{z}}$ yields

$$\hat{\mathbf{z}} = -\frac{1}{\omega^2}(\mathbf{A}\hat{\mathbf{V}}_p + \mathbf{B}) \tag{2.8}$$

where

$$\mathbf{A} \triangleq \left[= \mathbf{G}_{th}^{-1}\mathbf{G}\mathbf{B}_T(\mathbf{G}_{th}\mathbf{G}_{ti}\mathbf{G}_{tt}) + \mathbf{G}\right]\mathbf{B}_p \tag{2.9}$$

and

$$\mathbf{B} \triangleq \left[= \mathbf{G}_{th}^{-1}\mathbf{G}\mathbf{B}_T(\mathbf{G}_{th}\mathbf{G}_{ti}\mathbf{G}_{tt}) + \mathbf{G}\right]\hat{\mathbf{F}} \tag{2.10}$$

Next using Parseval's theorem the piezo-electric voltages are obtained as [14-15]:

$$\hat{\mathbf{V}}_p = -(\mathbf{A}^*\mathbf{A})^{-1}\mathbf{A}^*\mathbf{B} \tag{2.11}$$

where the symbol * denotes conjugate transpose. A sufficient and necessary condition for **A** to have rank np is given in references [14-15].

The distribution of actuation effort depends on the mode-shapes of the structure and the actuator placement, and can be modeled easily using FEM [16]. In the problem at hand, the best placement for a given trajectory depends not only on the structure but also the component frequencies of the desired motion. Thus the optimal placement of the actuator would in general be trajectory dependent. In most structures, such a freedom of changing the actuator placement with the prescribed trajectory is not available. The design of such structures with fixed actuator placements, is based on minimizing the induced structural vibrations over sets of disturbances with a specified energy [16]. In systems where the required motions are largely repetitive, the actuator placement can be optimized over a specified set of trajectories; this warrants a separate treatment to be considered in a future work.

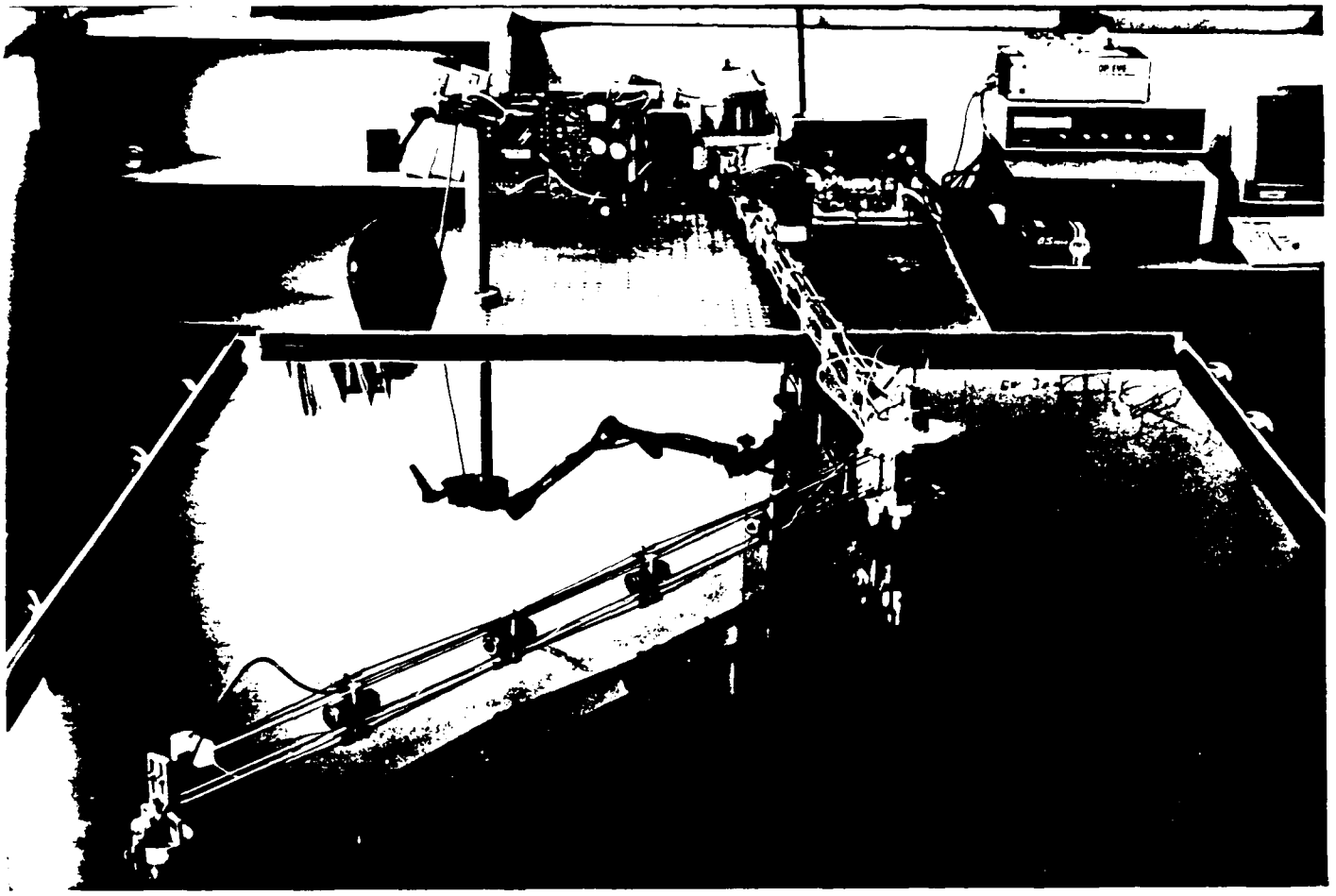

Fig. 2.1. Experimental set up.

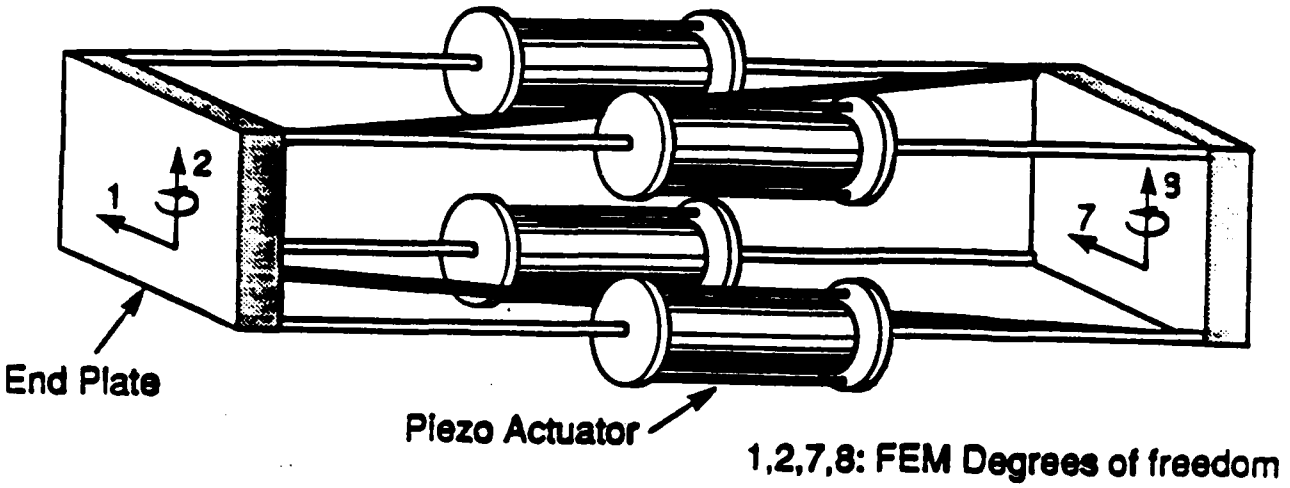

Fig. 2.2. Detail of active bay.

Experimental Verification

An experimental truss structure developed at UCSB is shown in Figure 2.1. The structure has 16 spans and two articulations forming a planar manipulator. The trusses are made of aluminum and have lumped masses (net 2 Kgs for each link) distributed along their lengths in order to lower the links modal frequencies and hence the control sample rate. In addition, the first (base) and the second links have tip loads of 3.5 and 1 Kgs respectively. These loads further increase the flexibility of the structure and the natural frequencies of the first and second links with clamped free boundary conditions are 0.6 Hz and 1.2 Hz respectively. Actuation consists of low-inertia dc-motors at the two joints and an active bay (Figure 2.2) with four electro-strictive actuators. Sensing consists of resolvers at the joints and collocated strain sensors on the four electro-strictive actuators. In addition, an optical sensor measures the position of an infra-red LED mounted about the midpoint of the first link, thus providing information of the induced structural vibrations during the tracking operation. The entire structure is supported on air bearings and controlled with an Intel 386-based PC, servo amplifiers for the motors and 150V servo amplifiers for the electro-strictive actuators.

To evaluate the proposed use of distributed actuators, we apply it to track the end-effector of the two link flexible articulated structure. The desired trajectory of the end-effector is a series of rest to rest motions, while the first link is stationary. The nominal motion of the second link is shown in Figure 2.3. The objective is to track the desired trajectory and minimize the vibrations in the first link which is equipped with electro-strictive actuators. To evaluate the vibration reduction achieved, the following tracking experiments are conducted: (1) feed-forward of torques computed without inverse dynamics, i.e. assuming the links to be rigid; (2) using the torques computed by inverse dynamics for only the joint actuators; and (3) incorporating the distributed electro-strictive actuators on the first truss along with joint actuators in the inverse dynamics computation and using these as feed-forward. In each case a joint based PD controller was used for controlling errors due to unmodeled dynamics, friction and other modeling errors.

Plots of the inputs to he electro-strictor and joint motors are presented in Figures 2.4 and 2.5. Note that the actuations start before the tip trajectory begins. This non-causality due to the propagation delays is reduced when additional actuation is available through the piezos as seen in Figure 2.5. To illustrate the viability of the proposed method we plot the transverse structural deflections at the midpoint of the first link (Figure 2.6) during the motion obtained by an infra-red led mounted on the structure and an over-head optical sensor. These elastic deflections in the structure are considerably reduced when electro-strictive actuators are also used in addition to the joint motors. On the contrary if inverse dynamics is not used and the rigid body torques are used then the resulting motion has much larger vibrations.

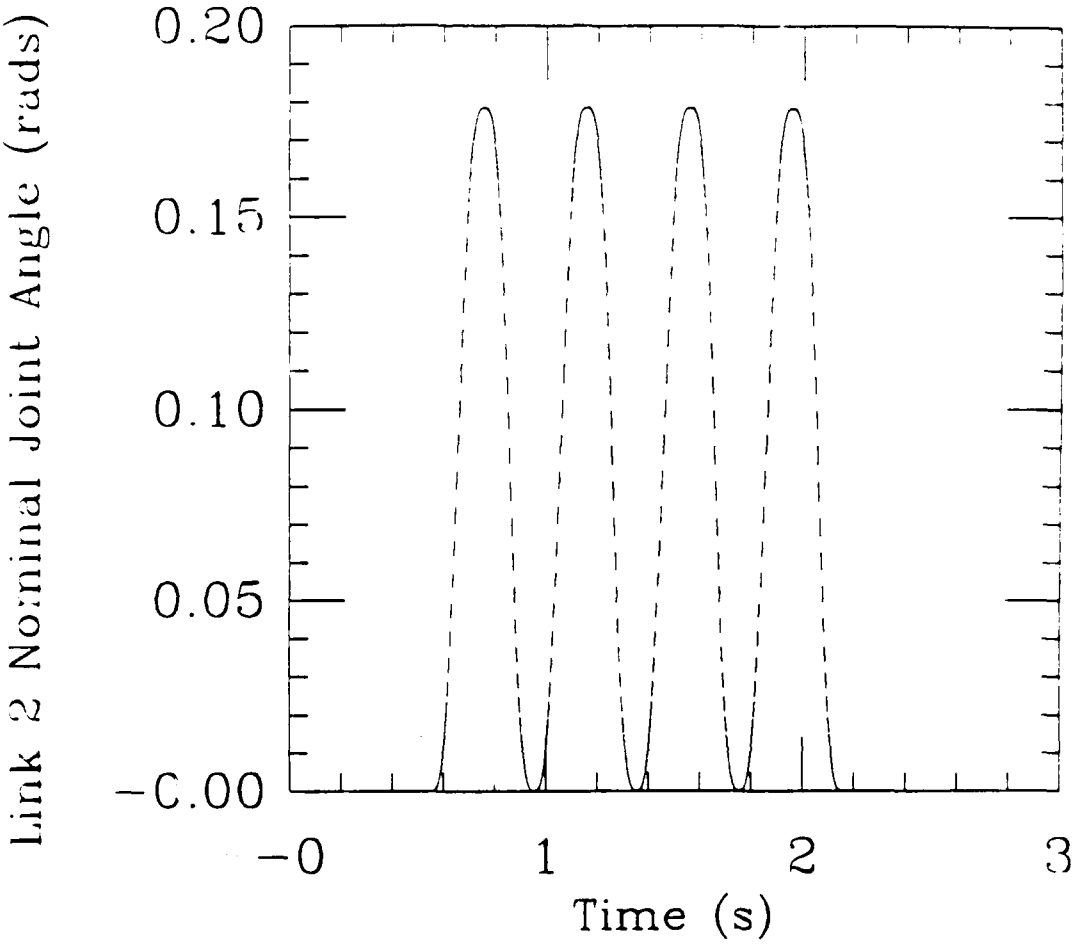

Fig. 2.3. Desired nominal rotations of second link.

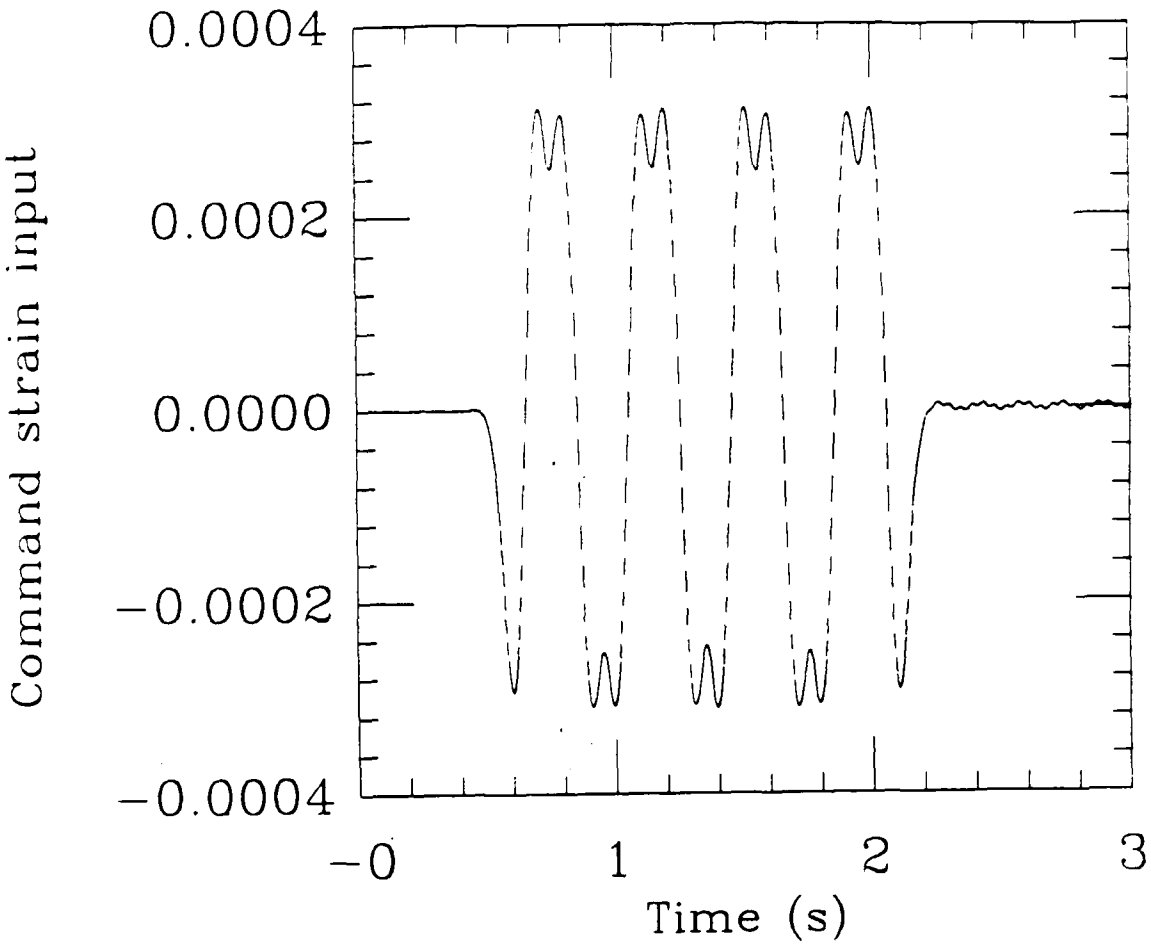

Fig. 2.4. Command strain input to the electro-strictor.

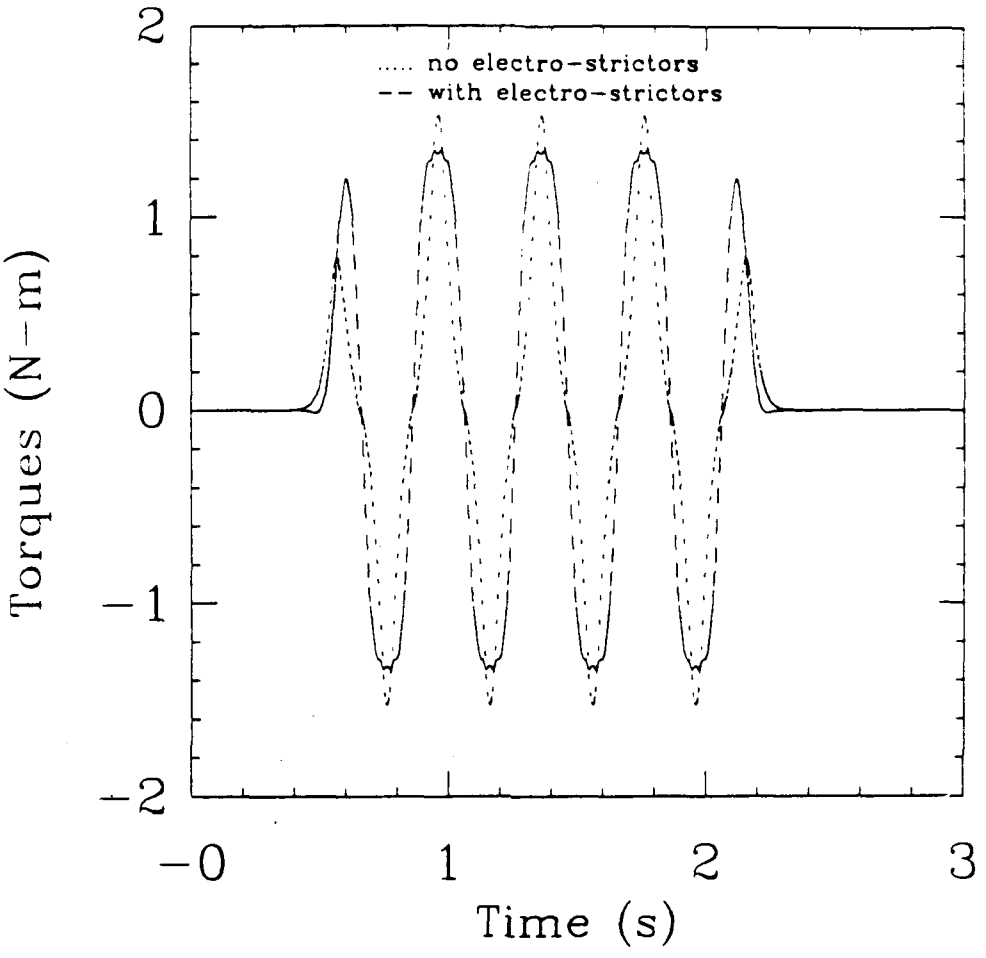

Fig. 2.5. Applied joint torques.

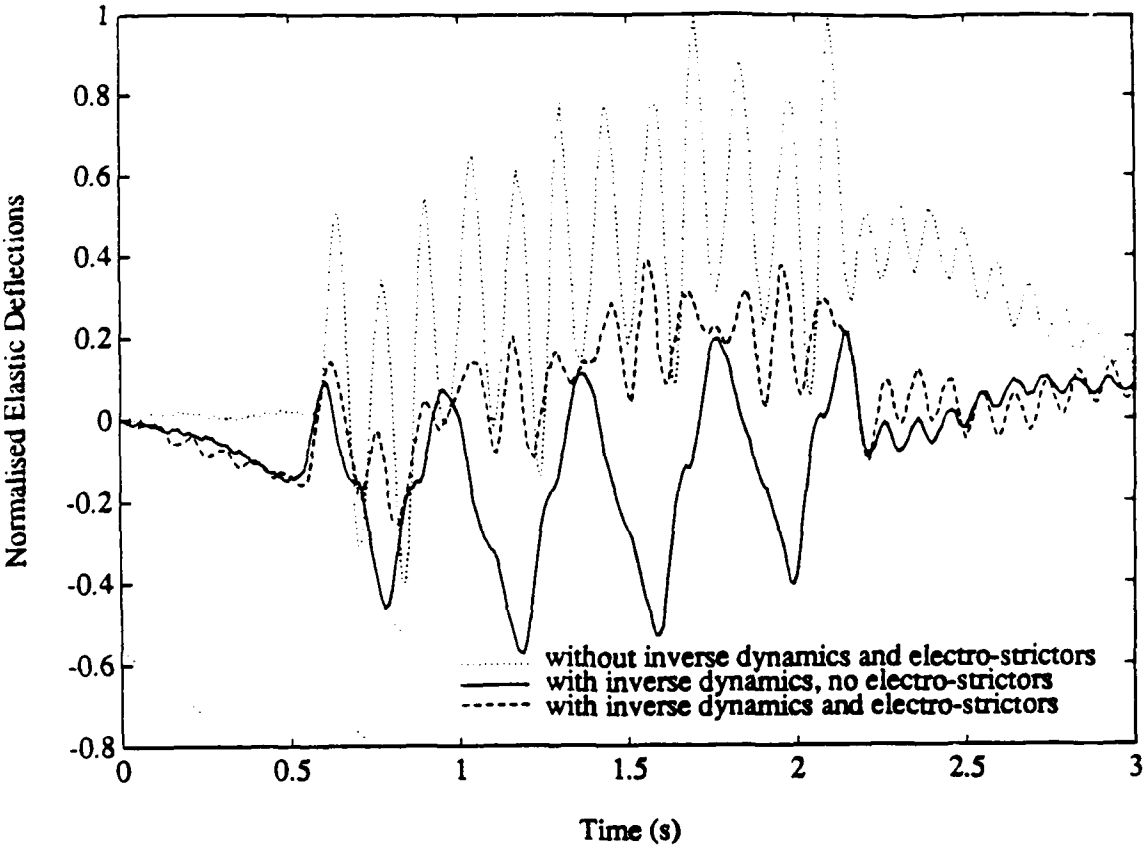

Fig. 2.6. Measurcd vibrations.

Thus the incorporation of electro-strictive actuators results in a significant reduction in the structural vibrations and demonstrates the viability of the proposed method. The consequent reduction (50%) in the induced vibrations of the structure allows the use of lighter elements and therefore smaller joint actuators, especially in space structures where the loads are mainly inertial.

Conclusion

Typically distributed actuators like the electro-strictive ones cannot garner enough actuation to cause large motions in the multibody system. However they could be very effective in reducing structural deformation. To reduce such vibrations by the use of distributed actuators in feedforward aiding joint actuators for trajectory tracking is a novel idea developed in this study. The method proposed is extremely efficient as it optimally reduces structural vibrations and the theory developed was verified by experiments. The use of the redundant distributed actuators seems promising in the slewing control of flexible manipulators and other space structures, and motivates further work on distributed actuators for the control of flexible multibodies.

3. Buckling Control of a Flexible Beam Using Piezoelectric Actuators

Summary

A new application of piezoelectric actuation is described for enhancing the load capacity of a beam under compression. By feedback control, the first buckling mode is stabilized and the buckling load is dramatically increased to the critical load of the second buckling mode of the beam. The approach uses a truncated modal model of the beam, distributed piezo actuators, and strain gauges for feedback.

Introduction

Active damping and control of flexible structures has been an area of research focus for some time. However, the recent application of distributed piezoelectric actuators to structure control by Crawley and De Luis [17], Bailey and Hubbard [18], and Fisher [20] has posed new and challenging problems. Following the initial experiments of these researchers, where a single vibrational mode is controlled, Fisher addressed the actuator placement problem to control several modes.

We address the new problem of buckling control using smart materials. In contrast to the dynamic stability issues of vibration control, buckling is a static instability of axially loaded members of a structure. It is well known that as the axial compressive load P in an initially straight beam increases, the beam remains straight and undeformed until the load reaches a certain critical value $P_{cr,1}$, where the stable equilibrium of the first bending mode bifurcates into one unstable and two stable equilibria (pitchford bifurcation). The two stable equilibria correspond to buckled configurations.

Here we use piezoelectric actuators and strain gauge sensors to show that buckling of a simply supported beam can be postponed beyond the first critical load. The load deflection characteristic for large deflections of a beam in a buckled configuration is highly nonlinear and involves numerical solution of elliptic integrals. Figure 3.1a shows a typical load deflection curve where $P_{cr,n}$ is the buckling load of the nth mode. If $P < P_{cr,1}$, the undeflected beam is stable. For $P_{cr,n} < P < P_{cr,n+1}$ all modes are stable except for the first n bending modes. The idea reflected in our work is the use of feedback control in conjunction with piezoactuators to stabilize the first bending mode beyond $P_{cr,1}$ and achieve a bifurcation diagram of the form shown in Fig. 3.1b, where the buckling force $P_{cr,1}$ is greater than that for the uncontrolled beam.

We use the linearized equations of motion and the associated modal equations of a simply supported flexible beam with piezoelectric actuators subjected to slowly varying

axial load. A finite-dimensional state-space model is then derived for a reduced order system and a controller is designed to increase the stiffness of the first bending mode to exceed that of the second bending mode.

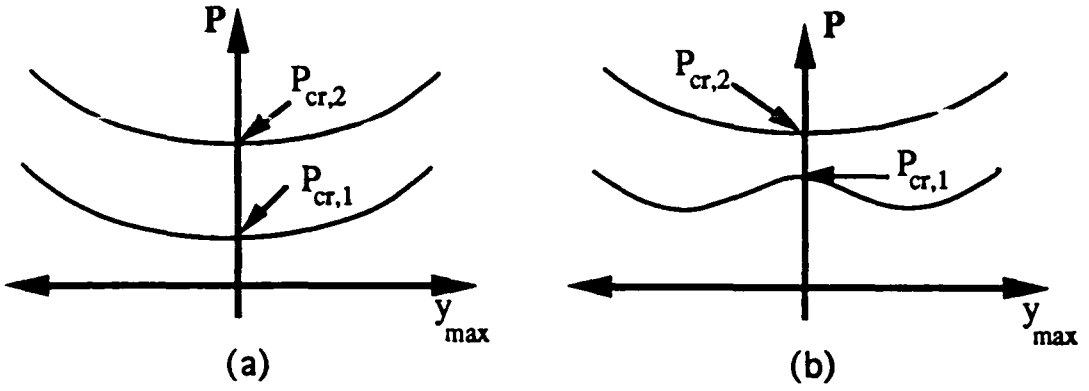

Fig. 3.1. Load deflection curve of a) uncontrolled beam and b) controlled beam.

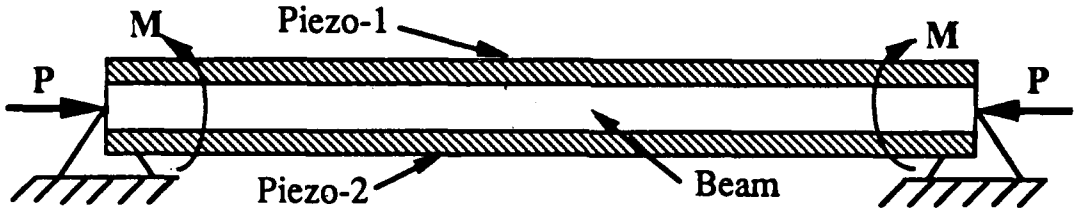

Fig. 3.2. Simply supported column with piezoelectric actuators.

Problem Formulation

We use a truncated modal expanstion of the deflection of a beam to derive a linear finite-dimensional model. We emphasize that the beam is assumed to be uniform with no manufacturing imperfections. Since the aim is to stabilize the beam in its straight configuration, it is natural to assume small deflections and linearize the equations of motion about this configuration. Note that the strain induced by ppezoelectric actuators is usually small and, therefore, the small deflection assumption is consistent with the capacity of the actuators.

Figure 3 2 shows a simply supported uniform beam with piezoelectric actuators of equal thickness bonded to both sides by a suitable adhesive. The beam of width b and thickness t_b is subjected to an axial compressive load, and control moments are applied by

the piezoactuators. The actuator being modeled is a piezoelectric polymer, poly vinylidene fluoride. For an axially polarized piezo, a voltage applied across its thickness results in strain along its length. For simplicity the width of each piezolayer is assumed to be the same as that of the beam.

The strain Λ_i developed in an unconstrained piezo is given by $\Lambda_i = v_i(t)d_{31}/t_p$ where $v_i(t)$; i = 1, 2 is the voltage applied to the ith piezostrip, d_{31} the piezoelectric strain constant, and t_p the thickness of the piezolayer. If v_1 and v_2 are the voltages applied on the top and bottom piezolayers, respectively, and E_p is the Young's modulus of the piezo, the resulting moment on the piezobeam segment is given by

$$M = bE_p t_p(\Lambda_2 - \Lambda_1)\left(\frac{t_b}{2} + t_a + \frac{t_p}{2}\right)$$

$$= bE_p d_{31}\left(\frac{t_b}{2} + t_a + \frac{t_p}{2}\right)(v_2 - v_1) \triangleq \underline{k}^*(v_2 - v_1) \tag{3.1}$$

The equation of motion of the beam can be derived using Hamilton's variational principle. Under small deflection assumption Hamilton's principle yields

$$\rho A\ddot{y} + (EIy'') + (Py')' = M\left[\delta'(x - x_2) - \delta'(x - x_1)\right] \tag{3.2}$$

where ρ is the density of the beam; y is the transverse deflection; $\dot{y}$ and y' are the time and spatial derivatives of y, respectively; EI is the stiffness of the beam; A is the cross-sectional area of the beam; δ' is the spatial derivative of the delta function; and x_1 and x_2 are the locations of the two ends of the piezolayer.

Modal states are estimated from strain gauge measurements at discrete locations. It is easy to see that observability of the modes of the system depends on the location of the sensors; a mode with its node at the location of a strain gauge is unobservable with that sensor. To reduce the number of sensors, modal control of flexible structures is usually based on the first few modes of vibration. This is justified by the fact that higher vibrational modes are in general difficult to excite and have higher structural damping. However, the unmodeled dynamics can cause instability through what are known as control and observation spillover. It has been shown that both control and observation spillover of unmodeled modes are necessary to cause instability in a closed-loop system.

The sensors are placed so that the second and third modes and their multiples are unobservable. Thus the first and fifth modes are the first two modes in a minimal

realization of the system. We ignore higher order modes and discuss the associated spillover problems in [20]. If a small amount of structural damping is present, all of the unobservable modes remain stable even in the presence of spillover. Similarly the dynamics of the even modes are not affected by the control, and hence they remain stable.

We model the sensors as follows. The bending moment at the location of a strain gauge, a distance x from the lift end of the beam, is given by

$$M_b = -E_b I_{eq} y''(x,t) = \sqrt{\frac{2}{L}}\, E_b I_{eq} \frac{\pi^2}{L^2} \sum_{n=1}^{n=\infty} n^2 \eta_n \sin\left(\frac{n\pi x}{L}\right) \qquad (3.9)$$

where E_b is the Young's modulus of the beam material and I_{eq} is the equivalent moment of inertia of the composite piezo-beam segment based on beam material. The resulting strain in a strain gauge attached to one side of the beam is

$$\varepsilon = \pm \frac{M_b \left[(t_b/2) + t_a + t_p\right]}{E_b I_{eq}} - \frac{P}{A_{eq} E_b} \qquad (3.10)$$

where A_{eq} is the equivalent area based on beam material. The sign of the first term in Eq. (3.10) depends on which side of the beam the strain gauge is bonded to. Therefore, the output of a *differential* strain gauge is *independent of the load P* and is given by

$$v_s = 2\,\varepsilon\, k_g = 2\sqrt{\frac{2}{L}}\, k_g \frac{\left[(t_b/2) + t_a + t_p\right]\pi^2}{L^2} \sum_{n=1}^{n=\infty}$$

$$\times\, n^2 \eta_n \sin\left(\frac{n\pi x}{L}\right) \triangleq k_s \sum_{n=1}^{n=\infty} n^2 \eta_n \sin\left(\frac{n\pi x}{L}\right) \qquad (3.11)$$

where k_g is the strain gauge constant. If differential strain gauges are placed as $x = L/3$ and $x = 2L/3$, and the sum of their measurements is taken as the system output, we have

$$v_o \triangleq v_s\left(x = \frac{L}{3}\right) + v_s\left(x = \frac{2L}{3}\right)$$

$$= k_s \sum_{n=1}^{n=\infty} n^2 \eta_n \left(\sin\frac{n\pi}{3} + \sin\frac{2n\pi}{3}\right) \qquad (3.12)$$

Results

The modal model developed above was truncated to form the actuated beam model and sensor model. A standard linear quadratic regulator was then designed. We showed that the buckling of a flexible beam can be postponed beyond the first critical load by means of feedback using piezoelectric actuators and strain gauge sensors [20]. It is observed that a controller design based on a fixed axial load P_{max} stabilizes the modeled modes for any $P \leq P_{max}$ and, therefore, is robust to slow load variations. Hence buckling in the first mode is inhibited, and the beam can support a load up to the second critical load. Actuator and sensor placement is discussed with regard to problems of spillover. Finally, spillover has not posed serious problems as we are able to design the controller, in the case of a beam, using a low-order model and verify stability for a high-order model.

4. Nonlinear Inversion-Based Regulation

Summary

In this study a new inverse is introduced for nonlinear systems. This inverse agrees with that of Hirschorn for minimum phase nonlinear systems, but is noncausal (rather than unstable) in the nonminimum phase case. Further, a geometric connection is made between the unstable manifold of the system zero dynamics and the noncausality in the inverse. With the inverse used for generating feedforward, exact regulation along a desired trajectory is easily accomplished with the addition of stabilizing feedback; this is demonstrated with a numerical example and compared to the Byrnes-Isidori regulator. Rather than solving a PDE to construct a regulator, the inverse is easily constructed using a Picard-like iteration. Moreover, when preactuation is not possible, noncausal inverse trajectories can be truncated. The result is the introduction of transients common in other regulators.

Introduction

Tracking control and regulation are common problems in applications and have thus attracted considerable attention from control researchers. Asymptotic tracking has been solved for arbitrary reference trajectories in the context of linear-quadratic optimal control [21]. Also for linear systems, the asymptotic regulation and tracking of signals generated by finite dimensional linear systems has been studied in a general framework by Francis and Wonham [22]. These authors show that the tracking problem is solvable if and only if a set of linear matrix equations is solvable. In the nonlinear case, the Francis-Wonham equations have been generalized to a first-order partial differential algebraic equation (PDE) by Byrnes and Isidori [23]. This fundamental work has been augmented with tests for approximate solvability of the Byrnes-Isidori PDE [24] and methods for optimal regulator design [25]. In addition, extensions to the Byrnes-Isidori regulator have been described in [26], and [27]. In this paper we introduce a new inversion-based approach to exact nonlinear output tracking control. The basic idea presented is to use feedforward of a nominal input which forces a given system along a desired trajectory, and then to stabilize the trajectory using feedback. We use preactuation to establish initial conditions in the nonminimum phase case, in contrast to setting initial conditions as is done in [28]. Our approach eliminates the requirement for solving the partial differential algebraic equation (of potentially high dimension) encountered in the Byrnes-Isidori regulator by tracking a

specific trajectory rather than any one of a family. Moreover, no exosystem is required, and the specification of trajectories is simplified. We do, however, introduce boundedness and integrability requirements on the trajectory. The key to our approach is finding a bounded inverse, even for nonminimum phase nonlinear systems, for use in generating feedforward inputs. In contrast to the inversion approach of Hirschorn [29] where unstable zero dynamics lead to unbounded responses of the inverse system, we introduce a nonlinear operator which is noncausal in the nonminimum phase case. Noncausal feedforward can be used in the case where trajectory preview is possible, or truncated to a causal signal at the cost of introducing transient tracking errors. Such noncausal character is seen in the linear quadratic setting, but the use of exact inverses in both linear and nonlinear tracking control is new. The noncausal inverses used here are motivated by the work of Bayo [30] in flexible multibodies and have been applied to the control of flexible-link robots in [31].

Problem Formulation

Consider the nonlinear system

$$\dot{x} = f(x) + g(x)u \tag{4.1}$$

$$y = h(x), \tag{4.2}$$

defined on a neighborhood X of the origin of $\Re^n$, with input $u \in \Re^p$ and output $y \in \Re^q$. The functions f(x), $g_i(x)$ (the ith column of g(x)) i - 1, 2, . . ., p are smooth vector fields and $h_i(x)$ for i = 1, 2, . . ., q are smooth functions on X, with f(0) = 0 and h(0) = 0.

In the context of the above system pose the following

Stable Inversion Problem: Given a smooth reference output trajectory $y_d(t) \in L_1 \cap L_\infty$, (bounded, integrable signals) find a control input $u_d(t)$ and a state trajectory $x_d(t)$ such that

1) u_d and x_d satisfy the differential equation

$$\dot{x}_d(t) = f\big(x_d(t)\big) + g\big(x_d(t)\big)\, u_d(t), \tag{4.3}$$

2) exact output tracking is achieved:

$$h\big(x_d(t)\big) = y_d(t), \tag{4.4}$$

3) u_d and x_d are bounded, and

$$u_d(t) \to 0,\ x_d(t) \to 0 \text{ as } t \to \pm\infty. \tag{4.5}$$

We call x_d the desired state trajectory and u_d the nominal control input. These can be incorporated into a regulator by using the nominal control input as a feed-forward signal and $x - x_d$ as an error signal for feedback.

Results

In solving for the nominal trajectories x_d and u_d the concepts of stable and unstable manifolds of an equilibrium point arise naturally [32]. For the sake of completeness we review the definitions here. Let $z = 0$ be an equilibrium point of an autonomous system defined in a open neighborhood U of the origin of $\Re^n$:

$$\dot{z} = f(z), \tag{4.6}$$

and $\phi_t(z)$ be the flow passing through z at $t = 0$. We define the (local) stable and unstable manifolds W^s, W^u as follows:

$$W^s = \left\{z \in U | \phi_t(z) \in U \forall t \geq 0, \phi_t(z) \to 0 \text{ as } t \to \infty\right\} \tag{4.7}$$

$$W^u = \left\{z \in U \mid \phi_t(z) \in U \forall t \geq 0, \phi_t(z) \to 0 \text{ as } t \to -\infty\right\} \tag{4.8}$$

The equilibrium point $z = 0$ is said to be hyperbolic if the Jacobian matrix Df of f at $z = 0$ has no eigenvalues on the $j\omega$ axis. Let n^s denote the number of eigenvalues of Df in the open left half complex plane, and n^u the number in the open right half plane. Stable and unstable manifolds W^s and W^u exist locally in the neighborhood of hyperbolic fixed point and have dimensions n^s and n^u respectively.

For convenience, we will use the following notation. Let $\underline{N} \underline{\Delta} \{0, 1, 2, \ldots\}$, $r = (r_1, r_2, \ldots, r_q)^t \in \underline{N}^m$ and $y = \left[y_1(t), y_2(t), \ldots, y_q(t)\right]^t; t \in \Re$. Then we define $|r| \underline{\Delta} r_1 + r_2 + \ldots + r_q$ and write

$$y^{(r)} \triangleq \begin{bmatrix} \frac{d^{r_1} y_1}{dt^{r_1}} \\ \frac{d^{r_2} y_2}{dt^{r_2}} \\ \frac{d^{r_q} y_q}{dt^{r_q}} \end{bmatrix} \tag{4.9a}$$

We will use the bold number **1** to denote the vector $(1, 1, \ldots, 1)^t$ so that

$$y^{(1)} = y = \left(\frac{dy_1}{dt}, \frac{dy_2}{dt}, \ldots, \frac{dy_q}{dt} \right)^t . \tag{4.9b}$$

If $y: \Re^n \rightarrow \Re^q$ and $f: \Re^n \rightarrow \Re^n$, we define

$$L_f^r y \triangleq \begin{bmatrix} L_f^{r_1} y_1 \\ L_f^{r_2} y_2 \\ \cdots \\ L_f^{r_q} y_q \end{bmatrix} . \tag{4.10}$$

Partial linearization and inversion

The system dynamics (4.1, 4.2) is written in the following form, where the number of inputs (p) is assumed to be the same as the number of outputs,

$$\dot{x} = f(x) + \sum_{i=1}^{p} g_i(x)\, u_i \tag{4.11a}$$

$$\begin{aligned} y_1 &= h_1(x) \\ &\cdots \\ y_m &= h_p(x) . \end{aligned} \tag{4.11b}$$

We assume that the system has well-defined relative degree $r = (r_1, r_2, \ldots, r_p)$ at the equilibrium point 0, that is,

(i) for all $1 \le j \le p$, for all $1 \le i \le p$, for all $k < r_i - 1$, and for all x in a neighborhood of the origin,

$$L_{g_j} L_f^k h_i(x) = 0 , \tag{4.12}$$

(ii) the $p \times p$ matrix

$$\beta(x) = \begin{bmatrix} L_{g_1} L_f^{r_1-1} h_1(x) & \cdots & L_{g_p} L_f^{r_1-1} h_1(x) \\ L_{g_1} L_f^{r_2-1} h_2(x) & \cdots & L_{g_p} L_f^{r_2-1} h_2(x) \\ \cdots & \cdots & \cdots \\ L_{g_1} L_f^{r_p-1} h_p(x) & \cdots & L_{g_p} L_f^{r_p-1} h_p(x) \end{bmatrix} \tag{4.13}$$

is nonsingular in a neighborhood of the origin.

Under this assumption, the system can be partially linearized. To do this, we differentiate y_i until at least one u_j appears explicitly. This will happen at exactly the r_ith derivative of y_i due to (4.12). Define $\xi_k^i = y_i^{(k-1)}$ for $i = 1, \ldots p$ and $k = 1, \ldots, r_i$, and denote

$$\begin{aligned} \xi &= \left(\xi_1^1, \xi_2^1, \cdots, \xi_{r_1}^1, \xi_1^2, \cdots, \xi_{r_2}^2, \cdots, \xi_{r_p}^p \right)^t \\ &= \left(y_1, \dot{y}_1, \cdots, y_1^{(r_1-1)}, y_2, \cdots, y_2^{(r_2-1)}, \cdots, y_p^{(r_p-1)} \right)^t . \end{aligned} \tag{4.14}$$

Choose η, an $n - |r|$ dimensional function on $\Re^n$ such that $\left(\xi^t, \eta^t\right)^t = \psi(x)$ forms a change of coordinates with $\psi(0) = 0$ [32]. In this new coordinate system, the system dynamics of equation (4.1) becomes

$$\begin{cases} \xi_1^i = \xi_2^i \\ \cdots \\ \xi_{r_i-1}^i = \xi_{r_i}^i \\ \xi_{r_i}^i = \alpha_i(\xi, \eta) + \beta_i(\xi, \eta)u \end{cases} \quad \text{for } i = 1, \cdots, p \tag{4.15a}$$

$$\dot{\eta} = q_1(\xi, \eta) + q_2(\xi, \eta)\, u, \tag{4.15b}$$

which, in a more compact form, is equivalent to

$$y^{(r)} = a(\xi, \eta) + \beta(\xi, \eta)u\,, \tag{4.16}$$

$$\dot{\eta} = s_1(\xi, \eta) + s_2(\xi, \eta)\, u\,, \tag{4.17}$$

where

$$y = \left(y_1, y_2, \cdots, y_p\right)^t,$$

$$u = \left(u_1, u_2, \cdots, u_p\right)^t,$$

$$\alpha(\xi, \eta) = L_f^r\, h\left(\psi^{-1}(\xi, \eta)\right), \tag{4.18}$$

$$\beta(\xi, \eta) = L_g^1\, L_f^{r-1}\, h\left(\psi^{-1}(\xi, \eta)\right). \tag{4.19}$$

Here β is actually the same $\beta(x)$ matrix defined in the equation (4.13), $\alpha(0, 0) = 0$ since $f(0) = 0$, and

$$h(x) = \left[h_1(x), h_2(x), \cdots, h_p(x)\right]^t,$$

$$g(x) = \left[g_1(x), g_2(x), \cdots, g_p(x)\right].$$

Since by the relative degree assumption, $\beta(\xi, \eta)$ is nonsingular, the following feedback control law

$$u \triangleq [\beta(\xi, \eta)]^{-1} [v - \alpha(\xi, \eta)] \tag{4.20}$$

is well defined and partially linearizes the system such that the input-output relationship is given by a chain of integrators:

$$y^{(r)} = v \tag{4.21}$$

where $v \in \Re^p$ is the new control input. Assume both y and y_d start from rest and choose

$$v = y_d^{(r)}. \tag{4.22}$$

Then immediately we have

$$\xi = \xi_d \triangleq \left(y_{d1}, \dot{y}_{d1}, \cdots, y_{d1}^{(r_1-1)}, y_{d2}, \cdots, y_{d2}^{(r_2-1)}, \cdots, y_{dp}^{(r_p-1)} \right)^t \tag{4.23}$$

and equation (16) becomes, which we call the *reference dynamics*, or the zero dynamics driven by the reference output trajectory,

$$\dot{\eta} = s\left(y_d, \dot{\xi}_d, \eta\right) \tag{4.24}$$

where

$$s\left(y_d, \dot{\xi}_d, \eta\right) \triangleq s_1(\xi_d, \eta) + s_2(\xi_d, \eta) [\beta(\xi_d, \eta)]^{-1} \left[y_d^{(r)} - \alpha(\xi_d, \eta) \right]. \tag{4.25}$$

under certain technical conditions on s (see [33]) there exists a solution $\eta_d(\cdot) \in L_1 \cap L_\infty \cap C^0$, to (51). Once the solution to the zero dynamics is found, an integration of the reference dynamics gives rise to a trajectory of the original state through the inverse coordinate transformation $x_d = \psi^{-1} \begin{pmatrix} \xi_d \\ \eta_d \end{pmatrix}$ and an input trajectory, u_d, by equation (4.20).

If $\left(\dot{\zeta}_d, y_d\right)$ has a compact support, $[t_0, t_1]$, then it is possible to give a geometric interpretation of the evolution of $x_d(t)$ [34]. The noncausal part of the nominal control drives the internal states of the system along the unstable manifold of the zero dynamics manifold to a particular initial condition $x_d(t_0)$ while maintaining zero system output. This initial condition guarantees two things: 1) the desired reference output trajectory is easily reproduced with bounded input and states; 2) the internal states land on the stable manifold of the zero dynamics manifold at the end of output tracking. With this nice final condition, the internal states will converge to zero along the stable manifold without affecting the output.

Conclusions

We have introduced a new nonlinear operator whose application in nonlinear inversion yields a clear connection between unstable zero dynamics and noncausal inversion. When noncausal inversion is incorporated into tracking regulators, we can see that it is a powerful tool for control -- particularly when computation is considered. An important fact is that a given system model defines different input-output operators depending on how boundary conditions are applied. For the study of feedforward control, boundary conditions at infinity give a useful perspective on a system. We have considered only the case of hyperbolic zero dynamics. Cases where zero dynamics have a center manifold or a hyperbolic orbit should prove interesting as well.

5. References

1. Bayo, E., "A Finite Element Approach to Control the End-Point Motion of a Single Link Flexible Robot," *Journal of Robotic Systems*, Vol. 4, No. 1, pp. 63-75. 1987.
2. Moulin, H. and Bayo, E., "On the End-Point Trajectory Tracking for Flexible Manipulators through Non-Causal Inverse Dynamics," *Journal of Dynamic Systems, Measurement and Control*. Vol. 113, No. 2, pp. 320-324. 1991.
3. Bayo, E., Serna, M. A., Papadopoulos, P. and Stubbe, J.R., "Inverse Dynamics and Kinematics of Multi-Link Elastic Robots: An Iterative Frequency Domain Approach," The *International Journal of Robotics Research*. Vol 8, No 6, pp. 49-62. 1989.
4. Bayo, E. and Moulin, H., "An Efficient Computation of the Inverse Dynamics of Flexible Manipulators in the Time Domain," Proceedings of the 1989 IEEE Conference on Robotics and Automation. Vol 2 pp. 710-715. Scottsdale, Arizona, May 1989.
5. Kwon, D. S. and Book, W. J., "An inverse dynamic method yielding flexible manipulators state trajectories". Proc. ACC, Vol. 1, pp. 186-193, San Diego, CA, 1990.
6. Ledesma, R. and Bayo, E., "A non recursive Lagrangian solution to the non-causal inverse dynamics of flexible multibody systems: The planar case". *Int. J. Numerical Methods in Engineering*. Vol. 36, pp. 2725-2741. 1993.
7. Ledesma, R. and Bayo, E., "A Lagrangian approach to the non-causal inverse dynamics of flexible multibody systems: the three dimensional case". Submitted to the *Int. J. Numerical Methods in Engineering*.
8. Bayo, E. and Avello, A., "Singularity Free Augmented Lagrangian Algorithms for Constraint Multibody Dynamics". To appear in the *Journal of Nonlinear Dynamics*, Vol. 5, No. 1. 1994.
9. Bayo, E., Garcia de Jalon, J. and Serna, M. A., "A Modified Lagrangian Formulation for the Dynamic Analysis of Constrained Mechanical Systems," *Computer Methods in Applied Mechanics and Engineering*, Vol. 71, pp. 183-195. 1988.
10. Mierovitch, L., and Baruh, H., "Control of self-adjoint distributed-parameter systems," *AIAA Journal*, Vol. 5, pp. 60-66, 1980.
11. Balas, M. J., "Active control of flexible systems," *Journal of Optimization Theory and Applications*, Vol. 25, pp. 415-436, 1987.
12. Fanson, J. L. and Garba, J. A., "Experimental studies of active members in control of large space structures," *Proceedings of the 29th AIAA SDM Conference*, Williamsburg, VA, pp. 9-17, 1988.
13. Paden, B., Chen, D., Ledesma, R. and Bayo, E. "Exponentially Stable Tracking Control for Multi-Joint Flexible-Link Manipulators," *Journal of Dynamic Systems, Measurement and Control*, Vol. 115, pp. 53-59. 1993.
14. Devasia, S. and Bayo, E., "Inverse dynamics of articulated flexible structures: simultaneous trajectory tracking and vibration reduction". Accepted for publication to the *Journal of Dynamics and Control*.
15. Devasia, S. and Bayo, E. "Redundant actuators to achieve minimal vibration trajectory tracking of flexible multibodies: theory and application". Accepted for publication to the *Journal of Nonlinear Dynamics*.
16. Devasia, S., Meressi, T., Paden, B. and Bayo, E. "Piezo-electric actuators design for vibration suppression: placement and sizing". *AIAA J. Guidance, Control and Dynamics*. Vol. 16, pp. 859-864, Sept-Oct. 1993.

17. Crawley, E. F., and De Luis, J., "Use of Piezoelectric Actuators as Elements of Intelligent Structures," *AIAA Journal*, Vol. 25, No. 10, pp. 1373-1385, 1987.

18. Bailey, T., and Hubbard, J. E., "Distributed Piezoelectric-Polymer Active Vibration Control of a Cantilever Beam," *Journal of Guidance, Control, and Dynamics*, Vol. 8, No. 5, pp. 605-611, 1985.

19. Fisher, S., "Application of Actuators to Control Beam Flexure in a Large Space Structure," Journal of Guidance, Control, and Dynamics, Vol. 12, No. 6, pp. 874-879, 1989.

20. Meressi, T. and Paden, B., "Buckling control of a flexible beam using piezoelectric actuators," AIAA *Journal of Guidance, Control and Dynamics.*, Vol. 16, No. 5, pg. 977-980, 1993.

21. Anderson, B. D. O. and Moore, J., Optimal Control-Linear Quadratic Methods, Prentice-Hall, Englewood Cliffs, New Jersey, 1990.

22. Francis, B. A. and Wonham, W. M., "The internal model principle of control theory," Automatica, vol. 12, pp. 457-465, 1976.

23. Isidori, A. and Byrnes, C. I., "Output regulation of nonlinear systems," IEEE Transactions on Automatic Control, vol. 35, No. 2, pp. 131-140, 1990.

24. Huang, J. and Rugh, W. J., "On a Nonlinear Multivariable Servomechanism Problem," Automatica, vol. 26, No. 6, pp. 963-972, 1990.

25. Krener, A. J., "Optimal Model Matching Controllers for linear and Nonlinear Systems," Proc. of NOLCOS, Bordeaux, France, 1992.

26. Gopalswamy, S. and Hedrick, J. K., "Tracking nonlinear non-minimum phase systems using sliding control," International Journal of Control, vol. 57, No. 5, pp. 1141-1158, 1993.

27. Castillo, B., "Output regulation of nonlinear systems with more inputs than outputs," International Journal of Control, vol. 57, No. 6, pp. 1343-1356, 1993.

28. Di Benedetto, M. D. and Lucibello, P., "Inversion of Nonlinear Time-Varying Systems," IEEE Transactions on Automatic Control, vol. 38, No. 8, pp. 1259-1264, August, 1993.

29. Hirschorn, R. M., "Invertibility of nonlinear control systems," SIAM J. of Control and Optimization, vol. 17, No. 2, pp. 289-297, 1979.

30. Bayo, E., "A finite-element approach to control the end-point motion of single-link flexible robot," J. of Robotic Systems, vol. 4, No. 1, pp. 63-75, 1987.

31. B. Paden, D. Chen, R. Ledesma and E. Bayo "Exponentially Stable Tracking Control for Multi-Joint Flexible-Link Manipulators", ASME Journal of Dynamic Systems, Measurement and Control, Vol. 115, pp. 53-59, March 1993.

32. Isidori, A., Nonlinear Control Systems: An introduction, Springer-Verlag, 1989.

33. "Nonlinear Inversion-Based Regulation," submitted to IEEE Transaction on Automatic Control.

34. Paden, B. and Chen. D., "A state-Space Condition for the Invertibility of Nonlinear Nonminimum-Phase Systems," ASME Winter Annual Meeting, 1992.

6. List of Publications under Grant F49620-91-C-0095

1. Bayo, E. and Avello, A., "Singularity Free Augmented Lagrangian Algorithms for Constraint Multibody Dynamics". To appear in the *Journal of Nonlinear Dynamics*. Vol. 5, No. 1. 1994.
2. Devasia, S. and Bayo, E., "Inverse dynamics of articulated flexible structures: simultaneous trajectory tracking and vibration reduction". Accepted for publication to the *Journal of Dynamics and Control.*
3. Devasia, S., Meressi, T., Paden, B. and Bayo, E. "Piezo-electric actuators design for vibration suppression: placement and sizing". *AIAA J. Guidance, Control and Dynamics*. Vol. 16, pp. 859-864, Sept-Oct. 1993.
4. Devasia, S., Paden, B. and Bayo, E. "Actuator placement for articulated flexible manipulators and space structures". Submitted to the *AIAA Journal.*
5. Devasia, S. and Bayo, E. "Redundant actuators to achieve minimal vibration trajectory tracking of flexible multibodies: theory and application". Accepted for publication to the *Journal of Nonlinear Dynamics.*
6. Devasia, S., Paden, B., and Bayo, E. "Vibration control of an experimental two-link manipulator," American Control Conference, pp. 2093-2098, San Francisco, 1993
7. Ledesma, R. and Bayo, E., "A non recursive Lagrangian solution to the non-causal inverse dynamics of flexible multibody systems: The planar case". *Int. J. Numerical Methods in Engineering*. Vol. 36, pp. 2725-2741. 1993.
8. Ledesma, R. and Bayo, E., "A Lagrangian approach to the non-causal inverse dynamics of flexible multibody systems: the three dimensional case". Submitted to the *Int. J. Numerical Methods in Engineering.*
9. Ledesma, R., Devasia, S. and Bayo, E., "Inverse dynamics of spatial open-chain flexible manipulators with lumped and distributed actuators. Accepted for publication to the *J. of Robotic Systems.*
10. Meressi, T. and Paden, B., "Buckling control of a flexible beam using piezoelectric actuators," AIAA *Journal of Guidance, Control and Dynamics.*, Vol. 16, No. 5, pg. 977-980, 1993.
11. B. Paden and D. Chen, "Zero dynamics and inversion of nonlinear systems" US-Japan Conference on Flexible Automation, San Francisco, 1992. Also submitted to *Systems and Control Letters.*
12. Paden, B. and Chen, D. "A state-space condition for the invertibility of nonlinear non-minimum phase systems," DSC-Vol. 43, pp. 37-41. Anaheim CA, November 1992.

Appendix: Copies of Publications

Nonlinear Dynamics 5: 1–22, 1994.

Singularity-Free Augmented Lagrangian Algorithms for Constrained Multibody Dynamics

E. BAYO
Department of Mechanical Engineering, University of California, Santa Barbara, California 93106, U. S. A.

and

A. AVELLO
Dept. of Applied Mechanics, University of Navarra and CEIT, Manuel de Lardizábal 15, 20009 San Sebastián, Spain

(Received: 13 March 1992; accepted: 4 August 1992)

Abstract. After a general review of the methods currently available for the dynamics of constrained multibody systems in the context of numerical efficiency and ability to solve the differential equations of motion in singular positions, we examine the acceleration based augmented Lagrangian formulations, and propose a new one for holonomic and non-holonomic systems that is based on the canonical equations of Hamilton. This new one proves to be more stable and accurate that the acceleration based counterpart under repetitive singular positions. The proposed algorithms are numerically efficient, can use standard conditionally stable numerical integrators and do not fail in singular positions, as the classical formulations do. The reason for the numerical efficiency and better behavior under singularities relies on the fact that the leading matrix of the resultant system of ODEs is sparse, symmetric, positive definite, and its rank is independent of that of the Jacobian of the constraint equations. The latter fact makes the proposed method particularly suitable for singular configurations.

Key words: *Constrained multibody systems, penalty and augmented Lagrangian method, holonomic and non-holonomic constraints, canonical equations of Hamilton.*

1. Review of Current Approaches for Multibody Dynamics

Computer systems, while increasing tremendously in power in recent years, are so affordable nowadays, that their use have become widely spread in many different fields and for a number of applications. The computer kinematic and dynamic analysis of multibody systems is increasingly being used in fields such as the automobile industry, aerospace, robotics, machinery, biomechanics, etc., and it has been receiving considerable attention recently, as seen by the amount of literature on multibody simulation and computer aided analysis programs being sold in the market of engineering software. Nevertheless, there is an increasing demand for faster and more reliable simulations that must be based on more efficient and robust algorithms for multibody dynamics.

The dynamic analysis of multibody systems is a process which is most appropriately performed using interactive (rather than batch) type of analysis. The analyst is interested in visualizing a whole set of successive responses of the multibody, a simulation of its behavior and operation over all the mechanism workspace and over a certain period of time. In certain cases it may be even necessary to introduce the engineer as an additional element in the simulation, called "man-in-the-loop", who may act by introducing external forces or control over specific degrees of freedom. In any case, each response over a time step needs to be calculated and displayed at the highest speed possible in order to give a picture that will possibly resemble the actual motion of the system in both time and space: *the real time behavior.*

While it is important for multibody dynamic simulations to have fast and accurate inter-

J.R.: PIPS Nr.: 19345
nody9212.tex - Date: October 28, 1993 Time: 11:33

active graphical interfaces, it is essential that the computer software relies on good numerical algorithms that will permit a fast and reliable solution of the resulting algebraically constrained differential equations of motion. Consequently, it becomes very important that numerical efficiency and stability be combined with robustness so that the simulation does not reach dead-lock situations due to singularity positions in the multibody motion.

In recent years, some important advances have been made in the development of new formulations for multibody dynamics. Some formulations, stemming mainly from the robotics field, have been especially conceived for real-time simulation and are based on the recursive computation of some or all of the terms in the equations of motion [1-4]. Some of these algorithms are $O(N)$ meaning that the number of floating point arithmetic operations grows linearly with the number of degrees of freedom. Others require the solution of a system of N linear equations and, therefore, are of order $O(N^3)$ (if Gaussian elimination is used). Although it has been demonstrated by Featherstone [3] that the best $O(N^3)$ algorithms are faster than the best $O(N)$ algorithms for $N < 10$, the elegance and attractiveness of the $O(N)$ Featherstone's formulation has exerted a strong influence on later developments that have generalized these ideas for non-serial (tree-configuration) and closed-loop systems [6-7]. A limitation arises when closed-chain multibodies are analyzed, since for these cases special provisions must be made to account for the reaction forces between the different loops [6].

The second group of methods encompasses those that reduce the equations of motion in dependent coordinates to a minimum set of independent ones via a transformation matrix obtained from the nullspace of the Jacobian of the constraint equations. Different methods of choosing the independent set of coordinates and generating the transformation matrix have been proposed [8-14]. The concept of *velocity transformations*, initially introduced by Jerkovsky [15], has been subsequently extended into efficient algorithms [16-19] that avoid the Jacobian factorization, and allow for an efficient and simple way of generating the equations of motion in independent coordinates in a way that can be fully parallelized [19].

The classical way to generate the equations of motion is to use dependent (or absolute) coordinates to generate and solve the equations of motion [14]. These algorithms are based on the classical Lagrange's formulation which leads to a set of differential and algebraic equations (DAE) of motion with the coordinates and multipliers as unknowns. The solution of these equations require special techniques [20] whose merit has not been thoroughly calibrated yet for the integration of multibody systems. A way to avoid the DAE is by differentiating the constraints. The resulting constraint violations are commonly stabilized using the method proposed by Baumgarte [21]. An extension for violation stabilization of holonomic systems based on the use of the canonical momenta has been proposed in [22].

Although the methods described above are well established (some of them very efficient numerically), they can not directly handle redundant constraints. In fact these have to be eliminated prior to the dynamic analysis. In addition they all fail to give successful solutions when the multibody undergoes a singular position. A partial solution to the problem of singular positions was provided in [23] where a method is developed that detects the ill-conditioning of the Jacobian matrix so that the integrator can step over it. In [24-25] *a regularization method* is proposed to cope with singularities. The main idea consists in adding to the vanishing and the linearly dependent constraints their third derivatives, and this turns the Jacobian non-singular. A staggered stabilization approach was presented by Park and Chiou [26] which was later refined by means of an explicit-implicit integration procedure [27]. This method integrates two different sets of equations one for the coordinates and another for the Lagrange multipliers, and avoids the singular position problem of the equations of motion. A small

limitation, however, is that it requires the inversion of the mass matrix, which is in general semi-positive definite and may not have an inverse in certain instances (in particular when redundant dependent coordinates are used).

Bayo, Garcia de Jalon and Serna proposed a penalty method [28] by which the acceleration, velocity and position constraint conditions are added to the equations of motion as a "dynamical penalty system" to obtain a simple and efficient formulation for the dynamic equations. The appeal of this formulation lies in two main points. Firstly, it leads to a reduced set of equations in the form $\dot{\mathbf{y}} = \mathbf{g}(\mathbf{y}, t)$ that can be integrated by standard conditionally stable numerical algorithms, without the need of further stabilization techniques to control the violation of the constraints during the integration process. Secondly, unlike the classical methods which rely on the Jacobian, this penalty formulation leads to matrices that can be inverted even in singular positions, and in the presence of redundant (linearly dependent) constraints and coordinates. Important theoretical studies of its convergence and stability have been carried out in [29] and [30]. The penalty method of [28] has also been successfully extended to real time dynamics within the context of fully Cartesian coordinates in [31]. There, it has been shown that the penalty method requires the factorization of a symmetric matrix that is dominated by the terms in the main diagonal (no pivoting is required), and is strongly banded, feature that makes it an order n method, where n is the number of coordinates. In addition, the different steps of the algorithm can be parallelized, making this method suitable for very large systems.

It was also proposed in [28] a more complete and accurate *augmented Lagrangian* method (combination of the penalty formulation and Lagrange's multipliers), which allows for convergence independently of the penalty values and which yields the constraint forces (Lagrange multipliers) as a by-product without having to integrate additional equations. In this paper we examine this augmented Lagrangian formulation within the context of singular positions and, in addition, propose a new one based on the use of the canonical equations of Hamilton that is even more stable and numerically efficient than the previous one.

2. Preliminaries on the Classical Formulations

2.1. Acceleration Based Lagrange's Multiplier Formulation

Let us consider a multibody system whose configuration is characterized by n generalized coordinates $\mathbf{q}$ that are interrelated through the m holonomic kinematic constraint conditions

$$\Phi(\mathbf{q}, t) = \mathbf{0} \tag{1}$$

Let L be the system Lagrangian, defined by $L = T - V$, where T and V are the kinetic and potential energy, respectively; and let $\mathbf{Q}$ be the vector of external and non-conservative forces. The Lagrange equations of such a system can be written as [32]

$$\frac{\mathrm{d}}{\mathrm{dt}}\left(\frac{\partial L}{\partial \dot{\mathbf{q}}}\right) - \frac{\partial L}{\partial \mathbf{q}} + \Phi_{\mathbf{q}}^{T}\lambda = \mathbf{Q}, \tag{2}$$

which for a general multibody system leads to:

$$\mathbf{M}\ddot{\mathbf{q}} + \Phi_{\mathbf{q}}^{T}\lambda = \mathbf{Q} + L_{\mathbf{q}} - \dot{\mathbf{M}}\dot{\mathbf{q}}, \tag{3}$$

where $\mathbf{M}$ is the mass matrix, $L_{\mathbf{q}}$ is the partial derivative of the Lagrangian with respect to the coordinates, $\Phi_{\mathbf{q}}$ is the Jacobian of the constraint equations, $\mathbf{Q}$ is the vector of external and non-conservative forces, and λ is the vector that contains the Lagrange's multipliers.

Equations (1) and (3) constitute a set of $n + m$ mixed differential algebraic equations (DAE) of index three [20], with $\mathbf{q}$ and λ as unknowns. In order to avoid the direct integration of DAEs, a double differentiation of the constraints equations may be carried out, which along with the Baumgarte's stabilization [21] yields:

$$\begin{bmatrix} \mathbf{M} & \boldsymbol{\Phi}_{\mathbf{q}}^T \\ \boldsymbol{\Phi}_{\mathbf{q}} & \mathbf{0} \end{bmatrix} \begin{Bmatrix} \ddot{\mathbf{q}} \\ \lambda \end{Bmatrix} = \begin{Bmatrix} \mathbf{Q} + L_{\mathbf{q}} - \dot{\mathbf{M}}\dot{\mathbf{q}} \\ -\dot{\boldsymbol{\Phi}}_{\mathbf{q}}\dot{\mathbf{q}} - \dot{\Phi}_t - a\dot{\Phi} - b\Phi \end{Bmatrix}, \tag{4}$$

where a and b are the stabilization constants. These equations can now be integrated using standard numerical integrators [33] with each function evaluation performed using equation (4).

2.2. Lagrange's Multiplier Formulation in Canonical Form

The definition of the *conjugate or canonical momenta* can be taken from classical mechanics [32]

$$\mathbf{p} = \frac{\partial L}{\partial \dot{\mathbf{q}}} \tag{5}$$

along with the *Hamiltonian*

$$H = \mathbf{p}^T\dot{\mathbf{q}} - L. \tag{6}$$

The *canonical equations of Hamilton* for a constrained system are formulated as

$$\dot{\mathbf{q}} = \frac{\partial H}{\partial \mathbf{p}} \tag{7a}$$

$$-\dot{\mathbf{p}} = \frac{\partial H}{\partial \mathbf{q}} - \mathbf{Q} + \boldsymbol{\Phi}_{\mathbf{q}}^T\lambda. \tag{7b}$$

In the case of multibody systems the Lagrangian L is defined in terms of $\mathbf{q}$, $\dot{\mathbf{q}}$ and t, and rather than following a lengthy process to form the Hamiltonian as an explicit function of $\mathbf{q}$, $\mathbf{p}$ and t, and then differentiate as in (7a), the canonical equations can be directly obtained from (5) and (7b). Since the system kinetic energy is a quadratic function of the generalized velocities, (5) and (7b) directly lead to the following set of equations in matrix form

$$\mathbf{p} = \mathbf{M}\dot{\mathbf{q}} \tag{8a}$$

$$\dot{\mathbf{p}} = L_{\mathbf{q}} + \mathbf{Q} - \boldsymbol{\Phi}_{\mathbf{q}}^T\lambda. \tag{8b}$$

The combination of (8a-b) and (1) constitutes a system of $2n + m$ differential and algebraic equations (DAE), of index two. Note, that although equations (8a-b) have n more equations than (3), $\dot{\mathbf{p}}$ can be obtained explicitly from (8b). In addition, index two DAEs are better behaved than index three DAEs [20], and therefore the consideration of equations (8a-b) may be numerically more advantageous than (3), when using algorithms for the solution of the mixed differential algebraic equations.

In order to avoid the mixed differential and algebraic equations, the system Lagrangian is modified in [22] and [34] to include the kinematic velocity constraints as

$$L^* = L + \dot{\boldsymbol{\Phi}}^T\sigma, \tag{9}$$

where σ are the new Lagrange multipliers. The new Hamiltonian is $H = \mathbf{p}^T\dot{\mathbf{q}} - L^*$ and the application of (3) and (5b) leads to

$$\mathbf{p}_{new} = \mathbf{M}\,\dot{\mathbf{q}} + \boldsymbol{\Phi}_{\mathbf{q}}^T\sigma \tag{10a}$$

$$\dot{\mathbf{p}}_{new} = L_{\mathbf{q}} + \mathbf{Q} + \dot{\boldsymbol{\Phi}}_{\mathbf{q}}^T\sigma \tag{10b}$$

that along with

$$\dot{\boldsymbol{\Phi}} + \gamma\boldsymbol{\Phi} = \boldsymbol{\Phi}_{\mathbf{q}}\dot{\mathbf{q}} + \boldsymbol{\Phi}_t + \gamma\boldsymbol{\Phi} = \mathbf{0} \tag{11}$$

constitutes a set of $2n+m$ ordinary differential equations (ODE), with p, q and σ as unknowns. The real constant γ provides asymptotic stability of the stabilization scheme. It can be very easily verified by differentiation of (10a) and substitution in (10b) that $\dot{\sigma} = \lambda$.

It is worth mentioning that only the following $n+m$ equations need be solved at each time step in the numerical implementation of the algorithm:

$$\begin{bmatrix} \mathbf{M} & \boldsymbol{\Phi}_{\mathbf{q}}^{\mathbf{T}} \\ \boldsymbol{\Phi}_{\mathbf{q}} & 0 \end{bmatrix} \begin{Bmatrix} \dot{\mathbf{q}} \\ \sigma \end{Bmatrix} = \begin{Bmatrix} \mathbf{p}_{new} \\ -\boldsymbol{\Phi}_t - \gamma\boldsymbol{\Phi} \end{Bmatrix}. \tag{12}$$

The numerical simulations of [34] show that since only the first time derivative of the constraints is used, the integration of this equations is more efficient and more stable, than the acceleration based counterparts.

2.3. Reduction to an Independent Set of Coordinates

The other widely accepted group of methods for multibody dynamics is based on the use of a transformation matrix $\mathbf{R}$ that will reduce the equations of motion to a minimum set of coordinates. The matrix $\mathbf{R}$ is obtained from the concept of the *nullspace* of the Jacobian, and allows one to express equation (3) in terms of an independent set of coordinates. The procedure starts by differentiating the constraint equations $\boldsymbol{\Phi}(\mathbf{q}) = \mathbf{0}$, that for simplification purposes we assume are sclerenomous, to obtain

$$\boldsymbol{\Phi}_{\mathbf{q}}\dot{\mathbf{q}} = \mathbf{0}. \tag{13}$$

It may be seen from equation (13) that $\dot{\mathbf{q}}$ belongs to the nullspace of the Jacobian $\boldsymbol{\Phi}_{\mathbf{q}}$. The dimension of the nullspace is equal to f, where f is the number of degrees of freedom of the multibody system. We can always express $\dot{\mathbf{q}}$ as a linear combination of the vectors of a nullspace's basis, in the form

$$\dot{\mathbf{q}} = \mathbf{R}\dot{\mathbf{z}}, \tag{14}$$

where $\mathbf{R}$ is an $n \times f$ matrix whose columns constitute a basis of the nullspace, and $\dot{\mathbf{z}}$ are the f independent velocities. Since $\mathbf{R}$ constitutes a basis of the nullspace of the Jacobian, it satisfies the relationship $\boldsymbol{\Phi}_{\mathbf{q}}\mathbf{R} = \mathbf{0}$. The matrix $\mathbf{R}$ may be obtained from the Jacobian by projection methods using Gauss factorization [8], the singular value decomposition [9] or the QR method [10]. It can also be obtained more efficiently by velocity transformations [15-19]. The substitution of (14) into (3) and premultiplication by $\mathbf{R}^T$ yields:

$$\mathbf{R}^T\mathbf{M}\,\mathbf{R}\,\ddot{\mathbf{z}} = \mathbf{R}^T(\mathbf{Q} + L_{\mathbf{q}} - \dot{\mathbf{M}}\dot{\mathbf{q}}) - \mathbf{R}^T\mathbf{M}\,\dot{\mathbf{R}}\,\dot{\mathbf{z}} \tag{15}$$

from which $\ddot{\mathbf{z}}$ can be calculated. An extension of this method within the setting of canonical equations has been proposed in [35], where the same leading matrix is obtained.

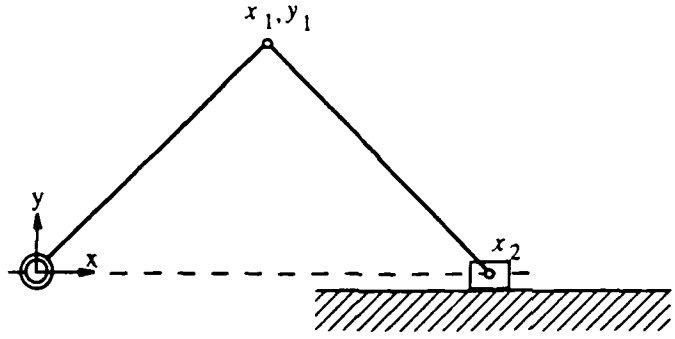

Fig. 1. Slider-crank mechanism.

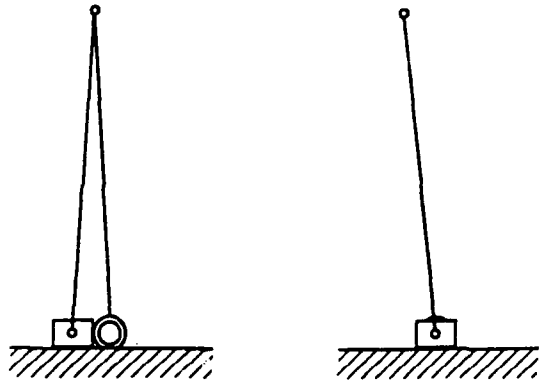

Fig. 2. a. Slider-crank mechanism motion. b. Rotating bar motion.

2.4. Why the Classical Formulations Fail in Singular Positions

As mentioned before, a singular position is encountered when the multibody reaches a configuration in which there is a sudden change in the number of degrees of freedom. For instance, a slider-crank mechanism as the one shown in Figure 1, reaches a singular position when the two links are in vertical position. In that configuration, both links are coincident and the mechanism has not one but two degrees of freedom. These two degrees of freedom correspond to the two possible motions (bifurcations) that the mechanism can undergo, and which are illustrated in Figure 2. Figure 2a shows the first possible motion that corresponds to a slider-crank mechanism, Figure 2b, shows the second motion corresponding to a rotating bar (in fact two coincident rotating bars). As may be seen, a singular position implies a bifurcation point, in which the mechanism can, at least theoretically, undergo different paths.

The existence of a singular position with both, the classical Lagrange's multipliers approach and the reduction to a set of independent coordinates, is invariably detected when the Jacobian matrix of the constraints becomes rank deficient. These formulations are based on the decomposition of the Jacobian and since its rank suddenly falls at a singular position, the decomposition fails and therefore no solution can be found. The simulation then crashes not because of the physics of the problem, but because of the inability of the dynamic formulation to overcome the sudden change in the rank of the Jacobian.

Equations (4) and (12) are the key equations for the solution of the dynamics using the Lagrange's multipliers method. Assuming that all the constraints are independent, that is if

$m = n - f$, the rank of the leading matrices in those equations is $n + m$. Since the Jacobian becomes rank deficient in singular positions, this matrix becomes singular. This means that the accelerations (or velocities) may not be computed unless special care is taken to eliminate (or regularize), at that particular position of the multibody system, all the vanishing constraints. Otherwise, the dynamic simulation crashes at this point. Equation (15) is the alternate key equation for the independent coordinate method. Again, when a singular position is reached special provisions have to be made for the computation of the matrix R.

If a singular position is not exactly reached, the leading matrix of both classical methods will not be strictly singular, but near singular, with a very high condition number. If this situation is not correctly tracked, the integration and round-off errors will be amplified and the resulting solutions may be totally erroneous.

It is important at this stage to emphasize the difference between a singular Jacobian and a singular position. While a singular position always implies a singular Jacobian, the converse is not always true. A Jacobian can become singular when redundant constraints are present, a dead-lock position is reached, or, when the coordinate partitioning between dependent and independent coordinates is not made properly or has not been updated for a while. Contrary to the case of a singular position, these singularities can be easily avoided and the simulation may proceed smoothly. The difference between singular Jacobian and singular positions can be better understood by partitioning the columns of the Jacobian $\Phi_{\mathbf{q}}$ into two submatrices $\Phi_{\mathbf{q}}{}^{d}$ and $\Phi_{\mathbf{q}}{}^{i}$, corresponding to the dependent and independent coordinates, respectively. This partition is made so that $\Phi_{\mathbf{q}}{}^{d}$ has full row rank. When $\Phi_{\mathbf{q}}{}^{d}$ is rank-deficient but $\Phi_{\mathbf{q}}$ has full row rank the singularity is easily avoidable since the full rank of $\Phi_{\mathbf{q}}{}^{d}$ can be recovered by a new suitable choice of independent coordinates. However, at a singular position $\Phi_{\mathbf{q}}$ looses rank all of a sudden, and the singularity may only be avoided by eliminating the non-active constraints. As pointed out in [25] if these non-active constraints are eliminated in the neighborhood of the singular configurations the corresponding constraint forces become zero and this may result in a fast deviation of the simulation from the constrained behavior.

3. Acceleration Based Augmented Lagrangian Formulation

3.1. Description of the Method

For the sake of completeness and in order to facilitate the understanding of the methods proposed in sections 4 and 6, we present in this section the augmented Lagrangian method introduced in [28]. Later we will address its behavior in singular positions. Given a multibody system with holonomic constraint equations of the form given in (1), which represent a set of nonlinear algebraic equations in the coordinates and the time variable. The penalty-augmented Lagrangian formulation proposed in [28] is derived by adding to the Lagrangian two terms: a fictitious potential

$$V^{*} = \sum_{k} \frac{1}{2} \alpha_k \, \omega_k^2 \equiv \frac{1}{2} \Phi^T \alpha \, \Omega^2 \Phi \tag{15}$$

and a fictitious kinematic energy term

$$T^{*} = \sum_{k} \frac{1}{2} \alpha_k \left(\frac{d\Phi_k}{dt} \right)^2 \equiv \frac{1}{2} \dot{\Phi}^T \alpha \, \dot{\Phi}. \tag{17}$$

A set of Rayleigh's dissipative forces is also added to the system

$$G_k = -2\alpha_k \omega_k \mu_k \frac{d\phi_k}{dt} \equiv -2\alpha \Omega \mu \dot{\Phi}, \tag{18}$$

where α_k are large positive real values (penalty numbers), and ω_k and μ_k represent the natural frequency and the damping ratio of the dynamic penalty system (mass, dashpot and spring) corresponding to the constraint $\Phi_k = 0$. Matrices α, Ω and μ are $m \times m$ diagonal matrices that contain the values of the penalty numbers, the natural frequencies and the damping ratios of the penalty systems assigned to each constraint condition. If the same values are used for each constraint these matrices become identity matrices multiplied by the respective penalty numbers. Note that in equations (16) through (18) we have used both index as well as matrix notation, hoping that this will lead to a better understanding of the physical significance of the different terms. In the following discussion we will only use the matrix form in order to be consistent with the notation used so far in the paper.

The differentiation of the new Lagrangian leads to

$$\frac{\partial L^*}{\partial \mathbf{q}} = L_{\mathbf{q}} + \dot{\Phi}_{\mathbf{q}}^T \alpha \dot{\Phi} - \Phi_{\mathbf{q}}^T \alpha \Omega^2 \Phi \tag{19}$$

$$\frac{\partial L^*}{\partial \dot{\mathbf{q}}} = \mathbf{M}\dot{\mathbf{q}} + \dot{\Phi}_{\mathbf{q}}^T \alpha \dot{\Phi} \tag{20}$$

$$\frac{\mathrm{d}}{\mathrm{d}t}\left(\frac{\partial L^*}{\partial \dot{\mathbf{q}}}\right) = \mathbf{M}\ddot{\mathbf{q}} + \dot{\mathbf{M}}\dot{\mathbf{q}} + \dot{\Phi}_{\mathbf{q}}^T \alpha \dot{\Phi} + \Phi_{\mathbf{q}}^T \alpha \ddot{\Phi}, \tag{21}$$

where the relation $\ddot{\Phi}_{\mathbf{q}}^T = \dot{\Phi}_{\mathbf{q}}^T$, which can be easily verified, has been used. L is the Lagrangian corresponding to the system without constraints.

The work done by the fictitious Rayleigh forces is

$$\delta W_R = -2(\delta\Phi)^T \alpha \Omega \mu \dot{\Phi} = -2\delta \mathbf{q}^T \Phi_{\mathbf{q}}^T \alpha \Omega \mu \dot{\Phi}. \tag{22}$$

Therefore the final expression obtained by the application of the Lagrange's equations (3) is

$$\mathbf{M}\ddot{\mathbf{q}} + \Phi_{\mathbf{q}}^{\mathbf{T}} \alpha \left(\ddot{\Phi} + 2\Omega\mu\dot{\Phi} + \Omega^2\Phi\right) + \Phi_{\mathbf{q}}^{\mathbf{T}} \lambda^* = \mathbf{Q} + L_{\mathbf{q}} - \dot{\mathbf{M}}\dot{\mathbf{q}}, \tag{23}$$

where λ^* are the new Lagrange multipliers of the modified system. Note that the second term in the LHS of equation (23) represents the projection in the direction of the coordinates $\mathbf{q}$ of all the internal forces that are generated by the penalty system when the constraints Φ, $\dot{\Phi}$ and $\ddot{\Phi}$ are violated. Introducing $\ddot{\Phi} = \Phi_{\mathbf{q}}\ddot{\mathbf{q}} + \dot{\Phi}_{\mathbf{q}}\dot{\mathbf{q}} + \dot{\Phi}_t$ the final result is obtained

$$\begin{aligned}&\left(\mathbf{M} + \Phi_{\mathbf{q}}^{\mathbf{T}} \alpha \Phi_{\mathbf{q}}\right)\ddot{\mathbf{q}} + \Phi_{\mathbf{q}}^{\mathbf{T}} \lambda^* \\ &\quad = \mathbf{Q} + L_{\mathbf{q}} - \dot{\mathbf{M}}\dot{\mathbf{q}} - \Phi_{\mathbf{q}}^{\mathbf{T}} \alpha \left(\dot{\Phi}_{\mathbf{q}}\dot{\mathbf{q}} + \dot{\Phi}_t + 2\Phi\mu\dot{\Phi} + \Omega^2\Phi\right).\end{aligned} \tag{24}$$

This equation may be viewed as the "generic penalty method" [28] to which the Lagrange's multipliers are added. As clearly shown in [28] this augmented Lagrangian formulation allows the analyst to choose from a wide range of penalty values that assure convergence and avoid numerical ill-conditioning. As we will see later, the solution provided by this method is not sensitive to the value taken by the penalty factor, and therefore, equation (24) represents and

elegant and attractive way of avoiding the problems customarily attributed to the penalty formulations.

It is important to note that there is a very important difference between equation (24) and the classical dynamic algorithms represented by (4) and (15). As we indicated before, the leading matrices of the latter equations become singular in singular positions. However, although the mass matrix M is in general positive semi-definite, it is always strictly positive definite in the nullspace of the Jacobian matrix. Therefore, a look at equation (24) reveals that its leading matrix $(\mathbf{M} + \Phi_{\mathbf{q}}{}^{T}\alpha\Phi_{\mathbf{q}})$ is always positive definite, which means that it can always be factorized, even in singular positions and/or with linearly dependent constraints. In practice, the augmented Lagrangian formulation is superior to the generic penalty method since the former allows for smaller values of the penalty parameter, hence, for a better conditioning of the leading matrix.

In equation (24) the Lagrange's multipliers λ^* play the role of correcting terms. In the limit the constraint conditions are satisfied, thus $\lambda = \lambda^*$ and equations (4) and (24) become equivalent except for round off errors induced by the penalty parameter and finite machine precision. By comparing those two equations one can infer that

$$\lambda \cong \lambda^* + \alpha\left(\ddot{\Phi} + 2\Omega\mu\dot{\Phi} + \Omega^2\Phi\right). \tag{25}$$

We are seeking the solution of (24) without having to use the algebraic constraint equations (1). This requires that the correct values of λ^* be known so that they can be inserted in (24). Since those values are not known in advance we need to set up an iterative process that calculates the unknown multipliers λ^*. The iteration is easily established by taking advantage of equation (25)

$$\lambda^*_{i+1} = \lambda^*_i + \alpha\left(\ddot{\Phi} + 2\Omega\mu\dot{\Phi} + \Omega^2\Phi\right)_{i+1}, \qquad i = 0, 1, 2, \ldots \tag{26}$$

with $\lambda^*_0 = 0$ for the first iteration. Equation (26) physically represents the introduction at iteration $i+1$ of forces that tend to compensate the fact that the addition of all the constraint terms are not exactly zero. It turns out that with the augmented Lagrangian formulation, the penalty numbers do not need to be very large (thus leading to a better numerical conditioning) since the resulting error in the constraint equations will be eliminated by the Lagrange's terms during the iteration procedure. Also note that the "generic penalty" [28] method corresponds to the augmented Lagrangian formulation in which the iteration process is only carried out once.

The matrix formulation of (24), including the iterative process defined in (26), is given by the following expression:

$$\left(\mathbf{M} + \Phi_{\mathbf{q}}^{\mathbf{T}}\alpha\Phi_{\mathbf{q}}\right)\ \ddot{\mathbf{q}}_{i+1} = \mathbf{M}\ddot{\mathbf{q}}_i - \Phi_{\mathbf{q}}^{\mathbf{T}}\alpha\left(\dot{\Phi}_{\mathbf{q}}\dot{\mathbf{q}} + \dot{\Phi}_t + 2\Omega\mu\dot{\Phi} + \Omega^2\Phi\right)$$
$$i = 0, 1, 2, \ldots \tag{27}$$

where the subscript i represents the iteration number, and $\mathbf{M}\,\ddot{\mathbf{q}}_{\mathbf{o}} = \mathbf{Q} + L_{\mathbf{q}} - \dot{\mathbf{M}}\dot{\mathbf{q}}$ for the initial iteration. Equation (27) may be used to iterate until $\|\ddot{\mathbf{q}}^{(i+1)} - \ddot{\mathbf{q}}^{(i)}\| < \varepsilon$, where ε is a user-specified tolerance.

The main advantage of using equation (27) is that the penalty terms are in fact used as an intermediate tool in order to compute the Lagrange's multipliers for which no new equations are integrated: only n equations are solved in the integration process. Therefore, the value of the penalty factor α does not affect the solution, but only the convergence rate. Experience

shows that when the constraints are scaled to unity, penalty factors ranging from 10^5 to 10^7 give a good convergence rate, and only 2 to 4 iterations are required to converge to the machine precision, in double precision arithmetic.

Note that the added cost of using equation (27) to refine the solution and obtain the Lagrange multipliers is fairly small, since its leading matrix remains constant during the iteration process needed for a function evaluation. Therefore, at each iteration step only the computation of the independent term and a forward and a backward substitutions are required. The numerical implementation of the algorithm using standard integrators [33], available in commercial mathematical libraries, is rather simple and may be described as follows

ALGORITHM ALF1

Given $\mathbf{q}$ and $\dot{\mathbf{q}}$ at time step l.

1. Use (27) iteratively to solve for $\ddot{\mathbf{q}}$, with $\mathbf{M}\,\ddot{\mathbf{q}}_0 = \mathbf{Q} + L_{\mathbf{q}} - \dot{\mathbf{M}}\dot{\mathbf{q}}$ for the initial iteration. At the end of each iteration use (26) to calculate the Lagrange multipliers λ^*, if desired
2. Call the numerical integration subroutine (n.i.s) to compute $\mathbf{q}$ and $\dot{\mathbf{q}}$ at time step $l + 1$.
3. Upon convergence of the n.i.s update the time variable and go to step 1.

We have used this algorithm very successfully in multibody dynamics simulation and has turned out to be very efficient and accurate. However, we have noticed that under repetitive singular conditions this algorithm may lead to unstable behavior (see examples below) due to the accumulation of small violations of the constraints during the integration process. This lead us to propose a more robust augmented Lagrangian method based on the canonical equations of Hamilton that is presented in the next section.

4. Augmented Lagrangian Formulation in Canonical Form

4.1. Basic Augmented Lagrangian Formulation in Canonical Form

Let us consider equation (9) as the starting point to build a modified Lagrangian that will not only contain the Lagrange multipliers σ but also the penalty terms of the previous section. Accordingly:

$$L^* = L + \frac{1}{2}\dot{\Phi}^T\alpha\dot{\Phi} - \frac{1}{2}\Phi^T\Omega^2\alpha\Phi + \dot{\Phi}^T\sigma^*. \tag{28}$$

In the limit when the constraint conditions are satisfied, the penalty terms vanish and $\sigma = \sigma^*$. Similar to the Lagrange's formulation $\dot{\sigma}^* = \lambda^*$ and after the augmented Lagrangian iteration when the constraints are satisfied to machine precision $\dot{\sigma} = \lambda$. The differentiation of L^* with respect to $\dot{\mathbf{q}}$ leads to the following new canonical momenta in matrix form

$$\mathbf{p} = \frac{\partial L^*}{\partial \dot{\mathbf{q}}} = \mathbf{M}\dot{\mathbf{q}} + \mathbf{\Phi}_\mathbf{q}^\mathbf{T}\alpha\dot{\mathbf{\Phi}} + \mathbf{\Phi}_\mathbf{q}^\mathbf{T}\sigma^*, \tag{29}$$

where we have eliminated the subindex 'new' of (10a) for practical convenience. The modified *Hamiltonian* can be written as $H^* = \mathbf{p}^T\dot{\mathbf{q}} - L^*$ and the use of (7), including the Rayleigh forces of (18), leads to

$$\left[\mathbf{M} + \mathbf{\Phi}_\mathbf{q}^\mathbf{T}\alpha\mathbf{\Phi}_\mathbf{q}\right]\dot{\mathbf{q}} = \mathbf{p} - \mathbf{\Phi}_\mathbf{q}^\mathbf{T}\alpha\mathbf{\Phi}_\mathbf{t} + \mathbf{\Phi}_\mathbf{q}^\mathbf{T}\sigma^* \tag{30a}$$

$$\dot{\mathbf{p}} = \mathbf{Q} + L_{\mathbf{q}} + \dot{\mathbf{\Phi}}_{\mathbf{q}}^{\mathbf{T}} \alpha \dot{\mathbf{\Phi}} - \mathbf{\Phi}_{\mathbf{q}}^{\mathbf{T}} \alpha \left(\mathbf{\Omega}^2 \mathbf{\Phi} + 2\mathbf{\Omega} \mu \dot{\mathbf{\Phi}} \right) + \dot{\mathbf{\Phi}}_{\mathbf{q}}^{\mathbf{T}} \sigma^*. \tag{30b}$$

Equations (30a–b) constitute a set of $2n$ first order ordinary differential equations. However, $\dot{\mathbf{p}}$ is given in explicit form, and therefore only n algebraic equations need be solved at each function evaluation for the numerical implementation of the algorithm.

Our numerical simulations have shown that equations (30) tend to be numerically stiff due to all the penalty terms concentrated in the RHS of (30b). This numerical stiffness limits the possible choices of numerical integrators. Standard ODE integrators [33] that are based on conditionally stable predictor-corrector multi-step formulae, lead to an increased number of function evaluations. We propose in the next section a modification of (30) that circumvents this problem.

4.2. Modified Augmented Lagrangian Formulation in Canonical Form

The canonical equation (30a) may be also written as

$$\mathbf{p} = \mathbf{M}\dot{\mathbf{q}} + \mathbf{\Phi}_{\mathbf{q}}^{\mathbf{T}} \alpha \dot{\mathbf{\Phi}} + \mathbf{\Phi}_{\mathbf{q}}^{\mathbf{T}} \sigma^*, \tag{31}$$

which indicates that the canonical momenta is stabilized through the addition of penalty terms that are proportional to the violation of the velocity constraint equations. It is important to realize that if equation (31) is differentiated and substituted into the acceleration based augmented Lagrangian equation (24) the result is precisely the additional canonical equation (30b), which lead us to see that *the canonical equations originate from the acceleration based equations by the mere canonical transformation* indicated in (31).

However, we can achieve a better stabilization of the canonical momenta if we add to the RHS of (31) two additional penalty terms: one term proportional to the constraint violation and the other to its integral. Accordingly we define a new momenta p as

$$\mathbf{p} = \mathbf{M}\dot{\mathbf{q}} + \mathbf{\Phi}_{\mathbf{q}}^{\mathbf{T}} \alpha \left(\dot{\mathbf{\Phi}} + 2\mu\mathbf{\Omega}\mathbf{\Phi} + \mathbf{\Omega}^2 \int_{t_o}^{t} \mathbf{\Phi} dt \right) - \mathbf{\Phi}_{\mathbf{q}}^{\mathbf{T}} \sigma^*. \tag{32}$$

By expanding the term $\dot{\mathbf{\Phi}}$ equation (32) becomes:

$$\left(\mathbf{M} + \mathbf{\Phi}_{\mathbf{q}}^{\mathbf{T}} \alpha \mathbf{\Phi}_{\mathbf{q}} \right) \dot{\mathbf{q}} = \mathbf{p} - \mathbf{\Phi}_{\mathbf{q}}^{\mathbf{T}} \alpha \left(\mathbf{\Phi}_t + 2\mu\mathbf{\Omega}\mathbf{\Phi} + \mathbf{\Omega}^2 \int_{t_o}^{t} \mathbf{\Phi} dt \right) - \mathbf{\Phi}_{\mathbf{q}}^{\mathbf{T}} \sigma^*. \tag{33a}$$

The differentiation of (33a) and substitution into (24) leads to the second set of modified canonical equations

$$\dot{\mathbf{p}} = \mathbf{Q} + L_q + \dot{\mathbf{\Phi}}_{\mathbf{q}}^{\mathbf{T}} \alpha \left(\dot{\mathbf{\Phi}} 2\mathbf{\Omega}\mu\mathbf{\Phi} + \mathbf{\Omega}^2 \int_{t_o}^{t} \mathbf{\Phi} dt \right) + \dot{\mathbf{\Phi}}_{\mathbf{q}}^{\mathbf{T}} \sigma^*, \tag{33b}$$

which along with (33a) constitute a set of $2n$ first order ordinary differential equations in the unknowns p, q and σ^*. Again only n algebraic equations need be solved at each function evaluation for the numerical implementation of the algorithm. A very important point is that, contrary to equations (30a-b), equations (33a-b) do not become stiff, and all our numerical experiments show that they even provide more numerical accuracy and better constraint stabilization than the acceleration based formulation of equation (24).

In fact we can compare this set of equations with the n second order ordinary differential equations resulting from the acceleration based formulation of (24). While both formulations

require the triangularization of the same leading matrix for each function evaluation, there is a serious advantages in the use of (33a-b) as compared to (24): the kinematic constraint conditions are differentiated only once with the canonical procedure (twice in the acceleration based formulation) and this will lead to lesser violations of the constraints. We will see in the numerical simulations of Section 6, how this factor becomes detrimental for the acceleration based formulation under repetitive singular positions, whereas the canonical approach leads to a much better performance.

Note again, that the multipliers σ^* do not need to be solved for explicitly. Following the same procedure as that used with the acceleration based augmented Lagrangian formulation, the σ^* may be obtained in an iterative manner as:

$$\sigma^*_{i+1} = \sigma^*_i + \left(\dot{\Phi} + 2\mu\Omega\Phi + \Omega^2 \int_{t_o}^{t} \Phi d\tau\right)_{i+1}, \qquad i = 0, 1, 2, \ldots \tag{34}$$

with $\sigma^*_0 = 0$ for the first iteration. Equation (33a) including the iterative process of (34) becomes

$$\left(\mathbf{M} + \Phi_{\mathbf{q}}^{\mathbf{T}} \alpha \Phi_{\mathbf{q}}\right) \dot{\mathbf{q}}_{i+1} = \mathbf{M}\dot{\mathbf{q}}_i - \Phi_{\mathbf{q}}^{\mathbf{T}} \alpha \left(\Phi_t + 2\mu\Omega\Phi + \Omega^2 \int_{t_o}^{t} \Phi d\tau\right), \quad i = 0, 1, 2, \ldots \tag{35}$$

with $\mathbf{M}\,\dot{\mathbf{q}}_{\mathbf{o}} = \mathbf{p}$ for the first iteration. Equation (35) shows that the velocity calculation at each function evaluation is refined so that the weighted summation of the constraint equations (34) are satisfied to machine precision. After the velocity calculation equation (33b) may be used to evaluate the derivative of the canonical momenta.

The algorithm may be presented as

ALGORITHM ALF2

Given p and q at time step l.

1. Use (35) iterativeiy to solve for $\dot{\mathbf{q}}$, with $\mathbf{M}\,\dot{\mathbf{q}}_{\mathbf{o}} = \mathbf{p}$ for the first iteration. At the end of each iteration use (34) to calculate the Lagrange multipliers σ^*
2. Use (33b) to compute $\dot{\mathbf{p}}$ explicitly (no solution of equations involved).
3. Call the numerical integration subroutine to compute p and q at time step $l + 1$.
4. Upon convergence of the n.i.s.
   - If desired, use a differentiation scheme to obtain $\lambda = \dot{\sigma}$
   - Update the time variable and go to step 1.

This algorithm is as efficient numerically as ALF1 but much more stable under repetitive singular positions.

5. Canonical Augmented Lagrangian Formulation for Non-Holonomic Systems

The modified augmented Lagrangian formulation described above may also be extended to non-holonomic systems with constraints of the form

$$\Phi\ (\dot{\mathbf{q}}, \mathbf{q}, t) = \mathbf{0}. \tag{36}$$

The acceleration based augmented Lagrangian formulation for this type of constraints is:

$$\mathbf{M}\ddot{\mathbf{q}} = \mathbf{Q} + L_{\mathbf{q}} - \dot{\mathbf{M}}\dot{\mathbf{q}} - \Phi_{\mathbf{q}}^{\mathbf{T}} \alpha \left(\dot{\Phi} + \beta\Phi\right) - \Phi_{\mathbf{q}}^{\mathbf{T}} \lambda^*. \tag{37}$$

In order to obtain the canonical counterparts we follow a procedure similar to that used for the holonomic case, and establish the following canonical transformation:

$$\mathbf{p} = \mathbf{M}\dot{\mathbf{q}} + \mathbf{\Phi}_{\mathbf{q}}^{\mathbf{T}}\alpha\left(\mathbf{\Phi} + \beta\int_{t_o}^{t}\mathbf{\Phi}d\tau\right) + \mathbf{\Phi}_{\mathbf{q}}^{\mathbf{T}}\sigma^{*}, \tag{38a}$$

which indicates that a better stabilization of the canonical momenta may be achieved by considering one penalty term proportional to the constraint violation and other to its integral. The differentiation of (38a) and posterior substitution into (37) leads to the second set of canonical equations

$$\dot{\mathbf{p}} = \mathbf{Q} + L_{\mathbf{q}} + \dot{\mathbf{\Phi}}_{\mathbf{q}}^{\mathbf{T}}\alpha\left(\mathbf{\Phi} + \beta\int_{t_o}^{t}\mathbf{\Phi}d\tau\right) + \dot{\mathbf{\Phi}}_{\mathbf{q}}^{\mathbf{T}}\sigma^{*}, \tag{38b}$$

which along with (38a) constitute a set of $2n$ first order ordinary differential equations in the unknowns p, q and σ^{*}. Again only n equations need be solved at each function evaluation.

Typically, non-holonomic constraint conditions for multibody systems take the following form

$$\mathbf{\Phi} = \mathbf{A}(\mathbf{q}, t)\,\dot{\mathbf{q}} + \mathbf{B}(\mathbf{q}, t) \tag{39}$$

and consequently the application of (38a–b) leads to

$$\left(\mathbf{M} + \mathbf{A}^{\mathbf{T}}\alpha\mathbf{A}\right)\,\dot{\mathbf{q}} = \mathbf{p} - \mathbf{A}^{\mathbf{T}}\alpha\left(\mathbf{B} + \beta\int_{t_o}^{t}\mathbf{\Phi}d\tau\right) - \mathbf{A}^{\mathbf{T}}\sigma^{*} \tag{40a}$$

$$\dot{\mathbf{p}} = \mathbf{Q} + L_{\mathbf{q}} + \dot{\mathbf{A}}^{\mathbf{T}}\alpha\left(+\beta\int_{t_o}^{t}\mathbf{d}\tau\right) + \dot{\mathbf{A}}^{\mathbf{T}}\sigma^{*} \tag{40b}$$

and

$$\sigma_{i+1}^{*} = \sigma_{i}^{*} + \left(\mathbf{\Phi} + \beta\int_{t_o}^{t}\mathbf{\Phi}d\tau\right)_{i+1}, \quad i = 0, 1, 2, \ldots \tag{41}$$

with $\sigma_0^{*} = 0$ for the first iteration.

6. Numerical Examples

6.1. A Simple Example

To better understand the application of the augmented Lagrangian formulation in singular and non-singular positions, let us consider the slider-crank mechanism shown in Figure 1. Both links are of length $l = 1$m, with a uniformly distributed mass of $m = 1$ Kg. We take as position coordinates q, the x and y coordinates of the crank end, and the x coordinate of the slider, thus $\mathbf{q}^{\mathbf{T}} = \{x_1,\ y_1,\ x_2\}$. We consider the gravity force, with a value $g = 9.81$ m/s^2 acting in the negative Y axis direction.

The 3×3 mass matrix corresponding to these variables is

$$\mathbf{M} = \frac{1}{6}\begin{bmatrix} 4 & 0 & 1 \\ 0 & 4 & 0 \\ 1 & 0 & 2 \end{bmatrix}$$

Table 1. Convergence rate with $\alpha = 10^4$

Iteration #	Error
1	$6.5792\ 10^{-4}$
2	$4.3705\ 10^{-8}$
3	$2.9206\ 1\text{-}^{-12}$
4	$1.6107\ 10^{-14}$

This mechanism has one degree of freedom only, and therefore there are two geometrical constraints that correspond to the constant distance conditions

$$\Phi = \begin{Bmatrix} \frac{1}{2}(x_1^2 + y_1^2 - 1) \\ \frac{1}{2}\left[(x_2 - x_1)^2 + y_1^2 - 1\right] \end{Bmatrix}$$

When the crank forms an angle of $\pi/2$ radians with the horizontal, the coupler is coincident with the crank and the crank axis is also coincident with the slider. In this position the mechanism has two instantaneous degrees of freedom, since it can undergo either the motion of a slider-crank or the motion of two superimposed rotating bars. Let us now apply the algorithm ALF1 for the instantaneous solution of the accelerations, for both a nonsingular position and a singular position.

Nonsingular Position. Consider the mechanism in an initial position in which the crank forms an angle of $\pi/4$ with the horizontal and in which the slider has a velocity $\dot{x}_2 = -2$ m/s. The exact acceleration has been computed first with the classical Lagrange's multiplier method of equation (4). Then, the accelerations have been calculated with the algorithm ALF1, using equation (27) iteratively, with a value $\alpha = 10^4$. Table I shows the norm of the difference between the exact acceleration and the one obtained with ALF1.

Table I also shows that the convergence rate of the iterative algorithm is considerably fast. This rate agrees with that predicted analytically in [36]. A higher penalty value gives a faster convergence rate but a lower precision. For instance, a value of $\alpha = 10^7$ yields an error of the order of 10–12 in one iteration, however, further iterations are unable to improve the solution, since some precision is lost in floating point arithmetic operations between numbers with exponents of significantly different values.

Singular Position. Now, consider the crank in a vertical position, forming and angle of $\pi/2$ radians with the horizontal. As we did in the nonsingular case, we take again a slider velocity value $\dot{x}_2 = -2$ m/s. Since the mechanism is in a singular position with 2 instantaneous degrees of freedom, we also have to specify the horizontal velocity of the crank end. It can be easily shown that, theoretically, the crank end can have any velocity value $\dot{x}_1 = v$. However, the slider-crank motion must satisfy the condition $x_1 = x_2/2$ over all its motion, and therefore the velocity $\dot{x}_1 = -1$ seems the obvious choice. Note that in this example the choice for the crank-end velocity is being made explicitly, but during a dynamic simulation the numerical integrator will provide the value of the crank-end velocity. Since the integrator assumes a continuous variation of the variables, this condition will be automatically guaranteed.

In this case, the exact acceleration value cannot be computed with equation (4) because the leading matrix is singular. However, the application of equation (27) with a value of $\alpha = 10^4$ leads to

$$\begin{bmatrix} \frac{2}{3} & 0 & \frac{1}{6} \\ 0 & 2\left(10^4 + \frac{1}{3}\right) & 0 \\ \frac{1}{6} & 0 & \frac{1}{3} \end{bmatrix} \begin{Bmatrix} \ddot{x}_1 \\ \ddot{y}_1 \\ \ddot{x}_2 \end{Bmatrix} = \begin{Bmatrix} 0 \\ -(2(10)^4 + 9.81) \\ 0 \end{Bmatrix}$$

which can be inverted and leads to the solution $(0, -1.0004738254362427 29, 0)$. After 3 iterations, the result is $(0, -1, 0)$, accurate to 14 digits.

This simple example clearly and simply illustrates that the penalty-augmented Lagrangian formulation works in singular positions, when the classical formulations, such as the Lagrange's multipliers method or the reduction to independent coordinates, fail. Also note that the condition number of the leading matrix increases at the same rate as the penalty parameter.

6.2. Dynamic Smulation of the Slider-Crank Mechanism

Let us consider again the same slider-crank mechanism of Section 6.1, in an initial position such that the crank forms an angle of $\pi/4$ radians with the X axis and that the slider's velocity is $\dot{x}_2 = -4$ m/s.

We perform a dynamic simulation by integrating the equations of motion for a total of 10 seconds, using a conditionally stable variable step and order integrator based on predictor-corrector multistep formulae [33]. We set the error tolerance to 10^{-5} and choose as penalty parameters $\alpha = 10^7$, $\Omega = 10$ and $\mu = 1$. During the simulation, the mechanism goes through the singular position 11 times, following a periodical response.

First, the simulation was carried out with the acceleration based algorithm ALF1. Figure 3 shows the X acceleration of the crank-end over the time period of 10 seconds. Figure 4 shows the value of the Lagrange multiplier λ_1, corresponding to the constant distance constraint condition between the crank axis and the crank end. Finally, Figure 5 shows the time history of the total energy, which should be kept constant, since the system is conservative. A very interesting point can be noted in Figures 3, 4 and 5. The value of the acceleration of the crank-end and λ_1 present spikes around $t = 9.25$ s and, at the same time, the energy presents a sudden discontinuity. The cause of this phenomenon is a small violation of the constraints around the singular position, due to the combination of the errors produced by the numerical integration routine and by the round-off errors produced by augmented Lagrangian procedure. These errors are more critical in the acceleration based algorithm ALF1 because the constraint equations are differentiated twice.

The simulation was repeated, this time using the algorithm ALF2, with the same error tolerance and values for the penalty parameters. This time, the values of λ_1 and the crank-end acceleration, illustrated in Figures 6 and 7, no longer show the spikes resulting from ALF1. In addition, the total energy, shown in Figure 8, does not show the sudden discontinuity that results in Figure 5.

The accumulation of integration errors that lead to small constraint violations in the neighborhood of the singular position is the cause for the sudden peaks and jumps in the constraint forces and accelerations produced by ALF1. These can be removed by tighter error tolerances in the integrator. The better results obtained under the same conditions with ALF2 are due to its better constraint stabilization properties.

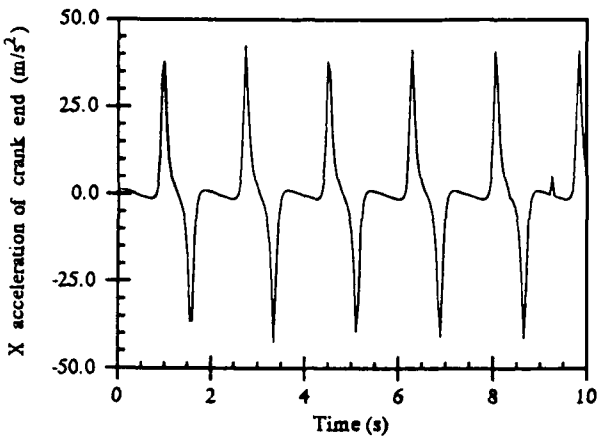

Fig. 3. Acceleration of the crank end with ALF1.

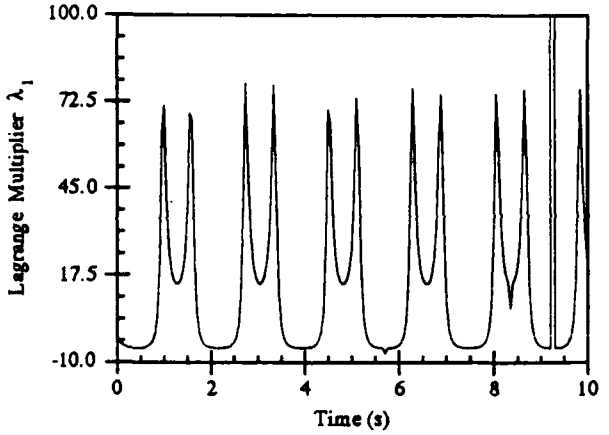

Fig. 4. Lagrange's multiplier with ALF1.

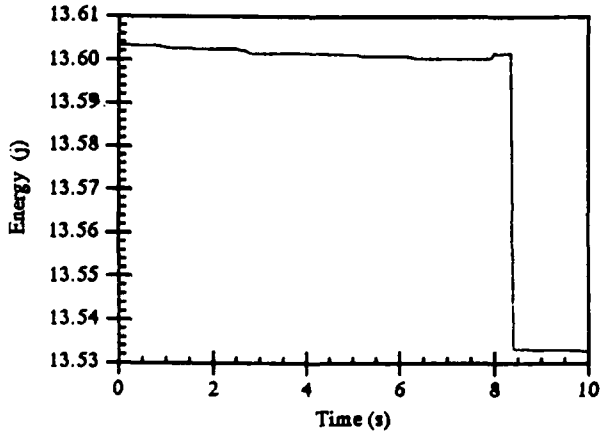

Fig. 5. Total energy with ALF1.

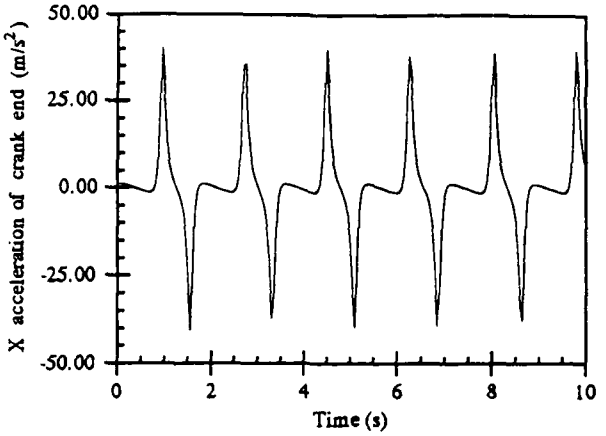

Fig. 6. Acceleration of the crank end with ALF2.

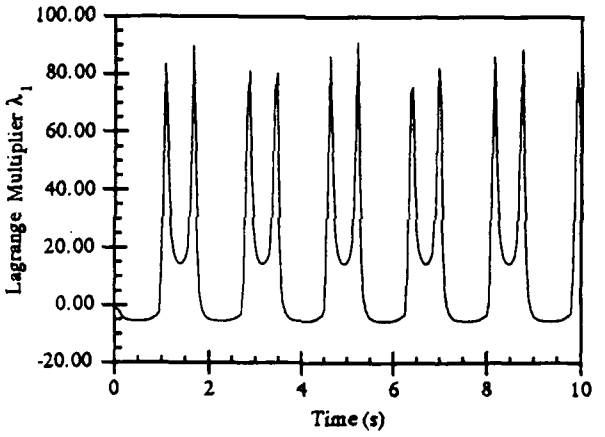

Fig. 7. Lagrange's multiplier with ALF2.

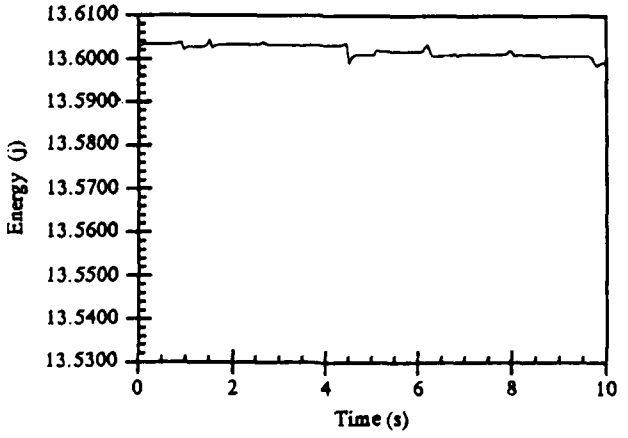

Fig. 8. Total energy with ALF2.

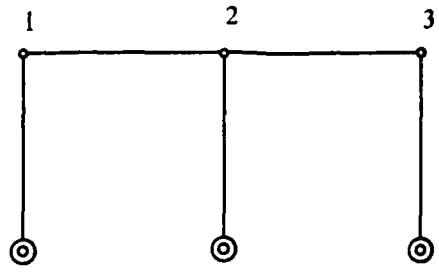

Fig. 9. Assembly of two four-bar linkages.

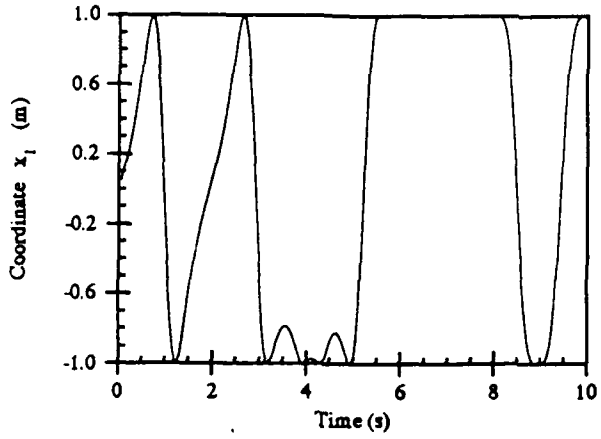

Fig. 10. Time history of x_1 with *ALF1*.

6.3. AN ASSEMBLY OF TWO FOUR-BAR LINKAGES

Figure 9 shows the initial position of a one degree-of-freedom assembly of two four-bar linkages. This mechanism constitutes a particularly critical example, because when it reaches the horizontal position the number of degrees of freedom increases instantaneously from 1 to 3. To define the position of the system, we use the 6 position variables $(x_1, y_1, x_2, y_2, x_3, y_3)$. All the links are of length $l = 1$ m and have a uniformly distributed mass $m = 1$ Kg. The gravity force acts in the negative Y direction, with a value $g = 9.81$ m/s^2. At $t = 0$ the initial velocity is $\dot{x}_1 = 1$. We integrate the motion for 10 seconds, using the same integrator and tolerance as before, and the values $\alpha = 10^7$, $\Omega = 10$ and $\mu = 1$ for the penalty parameters.

The analysis was carried out twice, first with the algorithm ALF1 and then with the algorithm ALF2. The results obtained with ALF1 are displayed in Figures 10 and 11, which show the time variation of the coordinate x_1 and the Lagrange multiplier λ_1, corresponding to a constant distance constraint between point 1 and the fixed end of the leftmost link. Figures 12 and 13 show the variation of the same variables, obtained this time with the algorithm ALF2. As may be seen, the solution with ALF1 becomes unstable after 3.3 seconds, while ALF2 gives congruent results.

The reason for the failure of ALF1 and the success of ALF2 are found again in the better stability properties of ALF2 with respect to constraint violations (it even yields a successfull integration when just the generic penalty formulation is used with no augmented lagrangian iteration). The way ALF1 may be improved, if it is to be used in repetitive singular positions, is by setting tighter error tolerances and rising the value of the parameter Ω. However, this will

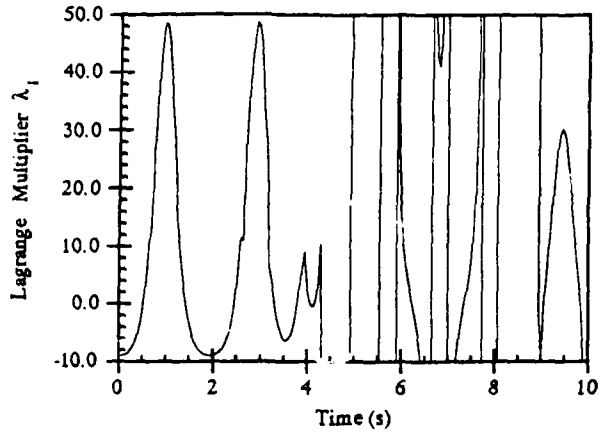

Fig. 11. Lagrange's multiplier with ALF1.

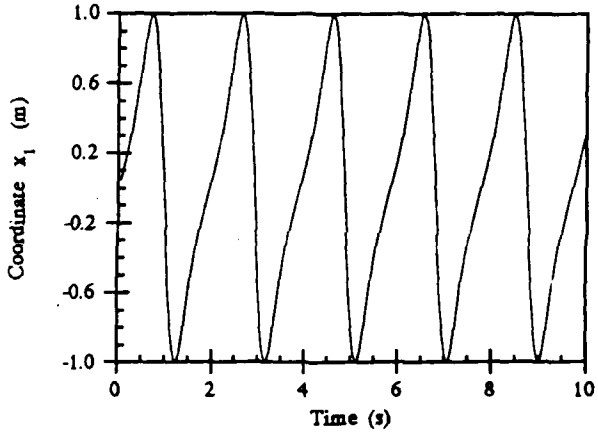

Fig. 12. Time history of x_1 with ALF2.

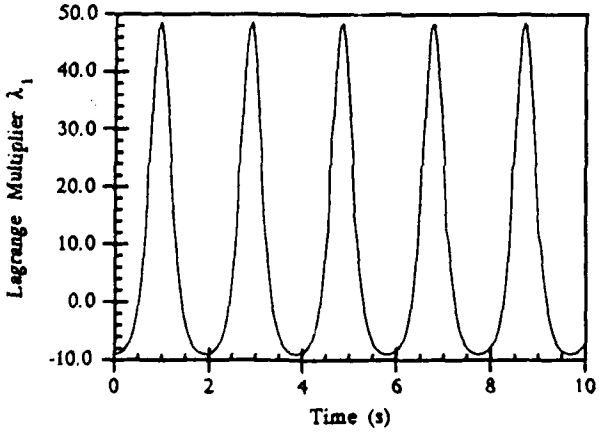

Fig. 13. Lagrange's multiplier with ALF2.

introduce numerical stiffness in the problem and therefore will increase the computational effort. In this example, the value of $\omega = 20$ solves the problem satisfactorily at the cost of a lengthier integration.

7. Conclusions

In this paper we have concisely reviewed the state of the art in multibody dynamic simulation. We have also revisited the acceleration based augmented Lagrangian formulation in the context of singular positions (ALF1) and proposed a new one based on the canonical equations of Hamilton (ALF2) for both holonomic and non-holonomic systems. Both formulations, ALF1 and ALF2, successfully solve the simulation problem in singular positions, however the canonical formulation ALF2 proves to be more accurate and robust than ALF1 under repetitive singular configurations.

The advantages of the proposed method can be summarized as follows:

- The method is very simple to implement and can use standard off the shelf conditionally stable numerical integrators such as those available in commercial mathematical libraries.
- The fact that the leading matrix of the equations of motion is always positive definite, symmetric and sparse, allows for a very efficient solution of the equations without the use of pivoting. This applies even in the presence of redundant (linearly dependent) constraints and coordinates, and most importantly in singular positions.
- Both the generic penalty and augmented Lagrangian methods do not require special provisions such as, detection, elimination of constraints or regularization, near the singular position. The integration goes through the singularity in a procession manner with no need for additional changes.
- The Lagrange multipliers (reaction forces at the constraints) are obtained without having to integrate additional equations.
- The leading matrix is strongly banded, feature that in principle makes it an order n method, where n is the number of dependent coordinates. Therefore it may become a very efficient formulation for those systems with a large number of multibodies, although this assertion needs to be corroborated by further research.
- The acceleration based formulation ALF1 shows numerical inestabilities under repetitive singular positions that are due to the accumulation of round-off and constraint errors. These can be circumvented with tighter tolerances and increased values in the frequency of the dynamical penalty system at the expense of additional computational cost.
- The canonically based method ALF2 is more robust and has not shown pathological behavior in any of our simulations (even when we used it in the generic penalty way). These authors do not know of any other algorithm that can simulate the motion of a multibody undergoing repetitive singular positions as ALF2 does.

As a final remark, one must keep in mind that the actual behavior of multibody systems around singular positions is physically uncertain, due to the uncertainty in the manufacturing tolerances. It is, therefore, unlikely that the behavior of the systems simulated with the algorithms presented in this paper may be experimentally reproduced. However, the usefulness of the algorithms and numerical results presented herein is twofold. Firstly, they provide an efficient and reliable tool for multibody dynamics, which avoids the program crashing that

occurs with the classical formulations. Secondly, these algorithms become useful for the study of the different alternative motions that a multibody system may undergo in the neighborhood of a singular position, when one or several geometrical parameters are slightly varied to simulate manufacturing errors.

Acknowledgments

The partial support of this work by the Air Force Office of Scientific Research under contract #F49620-91-C-0095, and the NATO travel grant 0877-87 that has allowed team cooperation between the University of Navarra and the University of California are greatly acknowledged. The authors wish to thank Dr. Chang and Dr. Wu of the AFOSR for their interest in our work, and Prof. Andrew Kurdila for his helpful comments.

References

1. rmstrong, W. W., 'Recursive solution to the equations of motion of an N-link manipulator', *Proceedings 5th World Congress on Theory of Machines and Mechanisms* **2**, 1979, 1343–1346, Montreal, Canada.
2. eatherstone, R., 'The calculation of robot dynamics using articulated body inertias', *The International Journal of Robotic Research* **2**, 1983, 13–30.
3. eatherstone, R., *Robot Dynamics Algorithms*, Kluwer Academic Publishers, Boston, MA, 1987.
4. alker, M. W. and Orin, D. E., 'Efficient dynamic computer simulation of robotic mechanisms', *Journal of Dynamic Systems, Measurements and Control, ASME* **104**, 1982, 205–211.
5. ae, D. S. and Haug, E. J., 'A recursive formulation for constrained mechanical system dynamics. Part I: Open loop systems', *Mechanics of Structures and Machines* **15**, 1987, 359–382.
6. ae, D. S. and Haug, E. J., 'A recursive formulation for constrained mechanical system dynamics. Part II: Closed loop systems', *Mechanics of Structures and Machines* **15**, 1987–88, 481–506.
7. odriguez, G., Jain A., and Kreutz K., 'A spatial operator algebra for manipulator modelling and control', *International Journal of Robotics Research* **10**, 1991, 371–381.
8. arcía de Jalón, J., Unda, J., Avello, A., and Jiménez, J. M., 'Dynamic analysis of three-dimensional mechanisms in natural coordinates', *Computer Methods in Applied Mechanics and Engineering* **56**, 1986, 309–327.
9. ani, N. K., Haug, E. J., and Atkinson, K. E., 'Application of singular value decomposition for analysis of mechanical system dynamics', *Journal of Mechanisms, Transmissions and Automation in Design* **107**, 1985, 82–87.
10. im, S. S. and Vanderploeg, M. J., 'QR decomposition for state space representation of constrained mechanical dynamic systems', *Journal of Mechanisms, Transmissions and Automation in Design* **108**, 1986, 183–188.
11. iang, C. G. and Lance, G. M., 'A differentiable null space method for constrained dynamic analysis', *Journal of Mechanisms Transmissions and Automation in Design* **109**, 1987, 405–411.
12. ehage, R. A. and Haug, E. J., 'Generalized coordinate partitioning for dimension reduction in analysis of constrained dynamic systems', *Journal of Mechanical Design* **104**, 1982, 247–255.
13. der, S. K. and Amirouche, F. M. L., 'Coordinate reduction in constrained spatial dynamic systems – a new approach', *Journal of Applied Mechanics* **55**, 1988, 899–905.
14. uhrer, C. and Schwertassek, R., 'Generation and solution of multibody systems equations', *International Journal Non-Linear Mechanics* **25**, 1990, 127–141.
15. erkovsky, W., 'The structure of multibody dynamic equations', *Journal of Guidance and Control* **1**, 1978, 173–182.
16. im, S. S. and Vanderploeg, M. J., 'A general and efficient method for dynamic analysis of mechanical systems using velocity transformations', *Journal of Mechanisms, Transmissions and Automation in Design* **108**, 1986, 176–182.
17. ikravesh, P. E. and Gim, G.,'Systematic construction of the equations of motion for multibody systems containing closed kinematic loops', *Advances in Design Automation* **3**, 1989, 27–33.
18. ane, T. R. and Levinson, D. A., *Dynamics: Theory and Applications*, McGraw-Hill, New York, NY, 1985.
19. arcía de Jalón, J., Jiménez, J. M., Martín, F., and Cuadrado. J., 'Real-time simulation of complex 3-D multibody systems with realistic graphics', *Real Time Integration Methods for Mechanical System Simulation*. Edited by E. Haug and R. Deyo. NATO ASI Series **69**, 1990, 261–293.
20. renan, K. E, Campbell, S. L., and Petzold, L. R., *The Numerical Solution of Initial Value Problems in Differential-Algebraic Equations*, Elsevier, New York, NY, 1989.

21. aumgarte, J., 'Stabilization of constraints and integrals of motion in dynamical systems', *Computer Methods in Applied Mechanics and Engineering* **1**, 1972, 1–16.
22. aumgarte, J., 'A new method of stabilization for holonomic constraints', *Journal of Applied Mechanics* **50**, 1983, 869–870.
23. ark, T. and Haug, E. J., 'Ill-conditioned equations in kinematics and dynamics of machines', *International Journal of Numerical Methods in Engineering* **26**, 1988, 217–230.
24. der, S. K. and Amirouche, F. M. '..., 'Numerical stability of the constraints near singular positions in the dynamics of multibody systems, *C mputers & Structures* **33**, 1989, 129–137.
25. mirouche, F. M. L. and Chin-Wei, T., 'Regularization and stability of the constraints in the dynamics of multibody systems', *Nonlinear Dynamics* **1**, 1990, 459–475.
26. ark K. C. and Chiou J. C., 'Stabilization of computational procedures for constrained dynamical systems', *Journal of Guidance, Control and Dynamics* **11**, 1988, 365–370.
27. ark K. C., Chiou J. C., and Downer, J. D., 'Explicit-implicit staggered procedure for multibody dynamic analysis', *Journal of Guidance, Control and Dynamics* **13**, 1990, 562–570.
28. ayo, E., García de Jalón, J., and Serna, M. A., 'A modified Lagrangian formulation for the dynamic analysis of constrained mechanical systems', *Computer Methods in Applied Mechanics and Engineering* **71**, 1988, 183–195.
29. urdila, A. J., Junkins, J. L., and Hsu, S., 'Lyapunov stable penalty methods for imposing nonholonomic constraints in multibody system dynamics', *Nonlinear Dynamics*, to appear.
30. urdila, A. J. and Narcowich, F. J.,'Sufficient conditions for penalty formulation methods in analytical dynamics', *Computational Mechanics*, to appear.
31. ayo, E., García de Jalón, J., Avello, A., and Cuadrado, J., 'An efficient computational method for real time multibody dynamic simulation in fully Cartesian coordinates', *Computer Methods in Applied Mechanics and Engineering* **92**, 1991, 377–395.
32. oldstein H., *Classical Mechanics*, Second Edition, Addison-Wesley, London, 1980.
33. hampine, L. F. and Gordon, M. K., *Computer Solution of Ordinary Differential Equations: the Initial Value Problem*, W. J. Freeman, San Francisco, CA, 1975.
34. ankarani, H. M and Nikravesh, P. E., 'Application of the canonical equations of motion in problems of constrained multibody systems with intermittent motion', *Advances in Design Automation* **1**, 1988, 417–423.
35. ae, D.-S. and Won, Y. S., 'A Hamiltonian equation of motion for real time vehicle simulation', *Advances in Design Automation* **2**, 1990, 151–157.
36. lowinski, R. and LeTallec, P., *Augmented Lagrangian and Operator-Splitting Methods in Nonlinear Mechanics*, SIAM, Philadelphia, PA, 1989.

To appear in the Journal of Dynamics and Control

Inverse Dynamics of Articulated Flexible Structures: Simultaneous Trajectory Tracking and Vibration Reduction

Santosh Devasia

Eduardo Bayo

Dept. of Mechanical & Environmental Engineering

University of California, Santa Barbara, CA 93106

ABSTRACT

This paper addresses the problem of inverse dynamics for articulated flexible structures with both lumped and distributed actuators. This problem arises, for example, in the combined vibration minimization and trajectory control of space robots and structures. For such flexible structures, closed loop passive joint based controllers have been shown to be effective in trajectory control by Paden et al. Crucial to the development of such closed loop controllers, which are robust to external perturbations, is the problem of dynamic inversion which yields the nominal state trajectories and the feedforward inputs. In this paper we propose a new inverse dynamics scheme for computing the nominal lumped and distributed feedforward inputs for tracking a prescribed trajectory.

1. Introduction

Inverse dynamics is an important problem in the control of articulated flexible structures such as space stations and manipulators. A solution for the nonredundant lumped actuator case has been provided by Bayo et. al., [1] and Book, [2]. This method produces bounded inputs which move a reference point on the structure along a desired trajectory. The inputs are necessarily non-causal when the structure dynamics are nonminimum phase. Elastic deformation which may cause vibration of the structure is also determined by the trajectory; our goal is to minimize such vibrations. The viability of distributed actuators for the control of structural vibrations, [3] , [4] and [5] , has motivated their use here for trajectory tracking.

Trajectory tracking of the structure can be accomplished by the use of the joint actuators alone [6] and in this sense the distributed actuators are redundant. However, if only the joint actuators are used, once the trajectory to be tracked is prescribed, the feedforward inputs and consequently the induced structural vibrations during motion are determined uniquely. Note that there are many state trajectories that could yield the same output response, but we can only access a particular one, with a given set of nonredundant number of actuators. On the contrary if additional actuation is available, we have the freedom of choosing a more favorable state dynamics. In this paper, we develop the concept of using the extra actuation available through the distributed actuators in the structure to not only satisfy the trajectory tracking constraint but also minimize the accompanying elastic displacements during the motion. To obtain these new feedforward inputs, the inverse dynamics method suggested in [1] is extended to cover cases of redundantly-actuated structures. To verify the efficay of the proposed method, an example of a flexible two link truss structure with distributed piezo-electric actuators was studied to contrast the use of distributed actuators along with the joint actuators for end effector trajectory control with the use of only the joint actuators. The inverse dynamics problem studied in this paper, yields the nominal desired state trajectories and the feed-

forward input which can be used to develop closed loop controllers to achieve robust trajectory tracking[6].

The remainder of the paper is organized in the following format. The modeling of flexible structures with joint and distributed actuators, the formulation of the problem and its solution are presented in Section 2. Section 3 deals with an application of the proposed method to the example of a two link flexible truss. The discussions and conclusions are presented in section 4.

2. Formulation

The solution to the general multi-link inverse dynamics problem involves studying an individual link in the chain, coupling the equations of the individual links, and then recursively converging to the desired actuator inputs and corresponding displacements. This approach is presented below, beginning with a single link.

2.1 Equation of motion of a single link

To simplify the equations, we present the equations for a link with a revolute joint. The flexible link depicted in figure 1 forms part of a multi-link system. The link is shown with a revolute joint, however the formulation remains identical for a link with translational joint. The elastic deflections in the structure are defined with respect to a nominal position characterized by a moving frame whose origin coincides with the location of the hub of the link. The nominal motion of this frame is prespecified by its angular velocity ω_h, angular acceleration α_h and the translational motion of its origin. The above definition of the elastic displacements with respect to this nominal frame permits the linearization of the problem from the outset. Incorporating the kinematic model followed by Naganathan and Soni [7] in a finite element model (FEM), the equations of motion for a single link at any time t can be written as [1]

$$M\ddot{z} + \left[C + C_c(\omega_h)\right]\dot{z} + \left[K + K_c(\alpha_h, \omega_h)\right] z = B_T T + B_p V_p + F. \qquad (2.1)$$

Where z is an R^n vector of the finite element degrees of freedom. M and K belong to $R^{n\times n}$ and are the conventional finite element mass and stiffness matrices respectively; C_c and $K_c \in R^{n\times n}$ and are the time varying Coriolis and centrifugal stiffness matrices, respectively. The $R^{n\times n}$ matrix C represents the internal viscous damping of the material. T is the unknown joint actuation. $F \in R^n$ contains the reactions at the end of the link, and the known forces produced by the rotating frame effect. The distributed actuator input, $V_p(t) \in R^{np}$, is the equivalent nodal forces at the FEM degrees of freedom, where np is the number of distributed actuator inputs. B_T and B_p are constant matrices of dimensions R^n and $R^{n\times np}$, respectively. The set of finite element equations (2.1) may be partitioned as follows

$$M\begin{bmatrix}\ddot{\theta}_h\\ \ddot{z}_i\\ \ddot{z}_t\end{bmatrix} + \left[C + C_c(\omega_h)\right]\begin{bmatrix}\dot{\theta}_h\\ \dot{z}_i\\ \dot{z}_t\end{bmatrix} + \left[K + K_c(\alpha_h,\omega_h)\right]\begin{bmatrix}\theta_h\\ z_i\\ z_t\end{bmatrix} = \begin{bmatrix}1\\ 0\\ 0\end{bmatrix} T + \begin{bmatrix}B_{p_h}\\ B_{p_i}\\ B_{p_t}\end{bmatrix} V_p + \begin{bmatrix}F_h\\ F_i\\ F_t\end{bmatrix} \tag{2.2}$$

where θ_h is the elastic rotation of the hub, z_t is the elastic deflection at the tip in the y direction, and the other $n-2$ finite element degrees of freedom are included in the vector z_i. The force vector, F, and the B_p and B_T matrices are also partitioned similarly.

2.2 Minimization Objective

The requirement is to accurately track the end effector of the link along the given nominal trajectory without overshoot and residual vibrations. Additionally we also seek to minimize the ensuing structural vibrations during this motion by minimizing $J(T,V_p)$, a measure of elastic deflections in the structure defined as follows

$$J(T,V_p) \triangleq \int_{-\infty}^{\infty} z(t)^T z(t)\,dt. \tag{2.3}$$

Mathematically the objective can be stated as

$$\min_{(T,V_p)\in \hat{T}} J(T,V_p). \tag{2.4}$$

Where $\hat{T}$ is the set of all pairs of stable joint torque and distributed actuator inputs that when used to actuate the system defined by equation (2.2) yields $z_t(t) = 0$ for all t.

2.3 Solution Methodology

An iterative scheme is described below for each link. Equation (2.2) can be rewritten as

$$M\ddot{z} + C\dot{z} + Kz = B_T T + B_p V_p + F - C_c(\omega_h)\,\dot{z} - K_c(\alpha_h,\omega_h)\,z \tag{2.5}$$

where the time dependent Coriolis and centrifugal terms are kept on the RHS of the equation. The iteration procedure starts with the absence of the last two terms involving C_c and K_c in the right hand side. Then, the system of equations can be transformed into independent sets of simultaneous complex equations by means of the Fourier transform. For each of the evaluation frequency $\bar{\omega}$, equation (2.5) becomes

$$\left[M - \frac{1}{i\omega}C - \frac{1}{\omega^2}K\right]\begin{bmatrix}\bar{z}_h\\ \bar{z}_i\\ \bar{z}_t\end{bmatrix} = \begin{bmatrix}\bar{T}\\ 0\\ 0\end{bmatrix} + \begin{bmatrix}\bar{F}_h\\ \bar{F}_i\\ \bar{F}_t\end{bmatrix} + \begin{bmatrix}B_{p_h}\\ B_{p_i}\\ B_{p_t}\end{bmatrix}\bar{V_p} \tag{2.6}$$

where the bar stands for the Fourier transform, and F represents the known forcing terms. After the first iteration it will also include the updated contributions from the Coriolis and centrifugal terms appearing in the RHS of equation (2.5). For any $\bar{\omega} \neq 0$, the matrix

$$H \triangleq \left[M - \frac{1}{i\omega}C - \frac{1}{\omega^2}K\right] \tag{2.7}$$

is a complex, symmetric and invertible matrix. For $\bar{\omega} = 0$ the system undergoes a rigid body motion and $H \triangleq M$ which is the positive definite invertible mass matrix. Let $G \triangleq H^{-1}$. Then the above equation can be re-written as

$$\begin{bmatrix}\bar{z}_h\\ \bar{z}_i\\ \bar{z}_t\end{bmatrix} = \begin{bmatrix}G_{hh} & G_{hi} & G_{ht}\\ G_{ih} & G_{ii} & G_{it}\\ G_{th} & G_{ti} & G_{tt}\end{bmatrix}\left\{\begin{bmatrix}\bar{T}(\bar{\omega})\\ 0\\ 0\end{bmatrix} + \begin{bmatrix}\bar{F}_h\\ \bar{F}_i\\ \bar{F}_t\end{bmatrix} + \begin{bmatrix}B_{p_h}\\ B_{p_i}\\ B_{p_t}\end{bmatrix}\bar{V_p}\right\}. \tag{2.8}$$

The condition that the tip should follow the nominal motion is equivalent to $\overline{z_t} = 0$ for all $\bar{\omega}$. This induces a relationship between the joint actuation and the distributed actuator inputs and is obtained from the last row of the previous equation.

$$\bar{T} = -G_{th}^{-1}\left[G_{th}\ G_{ti}\ G_{tt}\right]\ (\bar{F} + B_p \overline{V_p}) \tag{2.9}$$

Substituting this expression for the input hub torque in equation (2.8) and using the property that $\overline{\frac{d^2 z}{dt^2}} = -\bar{\omega}^2 \bar{z}$ yields

$$\bar{z} = -\frac{1}{\omega^2}(A\overline{V_p} + B)\,. \tag{2.10}$$

Where

$$A \triangleq [-G_{th}^{-1} G B_T (G_{th}\ G_{ti}\ G_{tt}) + G]\, B_p \tag{2.11}$$

and

$$B \triangleq [-G_{th}^{-1} G B_T (G_{th}\ G_{ti}\ G_{tt}) + G]\, \bar{F}\,. \tag{2.12}$$

Next we determine $\overline{V_p}$. Using Parseval's theorem, minimizing $J(T, V_p)$ in equation (2.4) is equivalent to minimizing $\|\bar{z}\|_2^2$ at each $\bar{\omega}$. This is a standard least squares approximation problem [8] and results in the following solution for the distributed actuator inputs,

$$\overline{V_p} = -U\begin{bmatrix}\Sigma^{-1} & 0\\ 0 & 0\end{bmatrix} V^* B \tag{2.13}$$

where Σ, U and V define the standard singular value decomposition of A as follows

$$V^* A U = \begin{bmatrix}\Sigma & 0\\ 0 & 0\end{bmatrix}. \tag{2.14}$$

Where the conjugate transpose matrix operator is denoted by *. In addition if A has rank np, which is the number of distributed actuator inputs, then the least squares approximation yields

$$\overline{V_p} = -(A^* A)^{-1} A^* B\,. \tag{2.15}$$

A sufficient and necessary condition for A to have rank np is given next.

Lemma

$$\text{rank } [A] = np \quad \text{iff} \quad \text{rank } [B_T \mid B_p] = np+1 \tag{2.16}$$

Proof

$$\text{Rank } [B_T] = 1 \implies \text{rank } [GB_T(G_{th}\ G_{ii}\ G_{tt})] = 1$$

$$\implies \text{rank} \left[\hat{A} \triangleq [-G_{th}^{-1}\, GB_T(G_{th}\ G_{ti}\ G_{tt}) + G] \right] \geq n-1.$$

Since $B_T = [1\ 0\ 0]^*$, it is easy to see that the null space of $\hat{A}$ is the span of $[1\ 0\ 0]^*$. Hence rank $\hat{A}$ is $n-1$. Noting that $A = \hat{A}\, B_p$, the lemma follows easily. □

The above lemma requires that all the columns of the input matrices B_T and B_p be independent. This is computationally more efficient than checking the rank of A for each $\bar{\omega}$. Next, the corresponding joint torque component, $\bar{T}$ is then evaluated from equation (2.9). The inverse Fourier transforms for the feedforward inputs completes the first iteration and results in torques, T^1 and distributed inputs V_p^1. Then the forward dynamic analysis is carried out to compute K_c and C_c. F in the RHS of equation (2.5) is updated and the process is repeated to find the new input torques and voltages. The process is stopped at the n^{th} iteration if $\| T^n - T^{n-1} \|_2 + \| V_p{}^n - V_p{}^{n-1} \|_2 < \varepsilon$, where ε is some small positive constant. It may be noted that for slow motions the terms involving K_c and C_c are small relative to the other terms in equation (2.1) and the iterations converge in a few steps [1].

2.4 The Algorithms for the Multi-Link Cases

In the previous sub-section the procedure to evaluate the joint actuations of a single link was presented. This can be recursively extended for multi-link flexible manipulators. Algorithms are presented below for both open and closed chain multi-link mechanisms.

Multi-Link Open Chain Case

1. Define the nominal motion (Inverse Kinematics of rigid manipulator).

2. For each link j, starting from the last one in the chain:

   a) Compute torque (or force) T^j and distributed actuator inputs P^j

imposing $z_i^j = 0$ (Section 2)

b) Compute the link reaction forces R^j from equilibrium.

3. Use equation (2.1) to compute the elastic displacement and joint angles.

4. Compute the inputs for the next link, $j-1$.

Multi-Link Closed Chain Case

1. Define the nominal motion (Inverse Kinematics of rigid robot).

2. Define an independent set of joint forces and reactions equal in number to the degrees of freedom of the robot.

3. For each link j, starting from the last one in the chain:

a) Compute torque (or force) T^j and distributed actuator

inputs P_i^j imposing $z_i^j = 0$ (Section 2)

b) Compute the link reaction forces R^j from equilibrium.

4. Use equation (2.1) to compute the elastic displacements and joint angles

5. Use elastic deflections to correct the nominal motion of each link.

6. Repeat steps 3 to 5 until convergence in the forces/torques is obtained

This concludes the methodology. In the next section we present an application to a two-link flexible manipulator.

3. Example

A twolink truss experiment under development at UCSB is shown in figure 2. The trusses are made of lexan and have lumped masses (net 2 Kg for each link) distributed along their lengths. The first and the second links are tip loaded with 3.5 and 1 Kg respectively. Equivalent beam properties of the trusses used in the FEM model for simulations are Youngs modulus = 7 e^9 GPa, Link length = 1.2 m, density = 1500 Kg/m^3, cross sectional area = 4.378 e^{-5} m^2 and cross sectional area moment of inertia = 4.7244 e^{-9} m^4. Of the 10 spans in each link, two are piezo-electrically actuated. They are

located at the second and ninth spans as shown in the figure 2. The piezo-electric stack actuators in those spans have the following properties. Cross sectional area, $A_{cs} = 7.3\ e^{-6}\ m^2$, piezo strain to voltage constant, $d_{sv} = .731\ e^{-6}\ V^{-1}$, Youngs modulus, $E_p = 73\ e^9\ Gpa$ and distance of the actuator from the neutral axis of the truss, $d_t = 1.27\ e^{-2}\ m$. Following the standard Bernoulli-Euler modeling for an applied voltage V_{input}, the piezo-electric actuation can be considered as two concentrated moments M acting at the two ends of the actuator [9] and [10]. Where M is given by

$$M = (d_{sv}\ N_p\ E_p\ A_{cs}\ d_t)V_{input} \tag{3.1}$$

and $N_p = 4$ is the number of piezos in each span. For the truss considered above $M = = 0.0198V_{input}$. The desired trajectory is a rest to rest motion of the structure with initial conditions given by $\theta_1 = \theta_2 = 0$ and final conditions $\theta_1 = 11.25^o$ and $\theta_2 = -22.5^o$. Where $\theta's$ are the absolute angles of the links with respect to a frame fixed on the ground and are shown in figure 2. The nominal motion of the tip for each link are the trajectories followed by the tips of the links if the structure were rigid and followed the nominal angular motions shown in figure 3. Using the procedure in section 2.4 for open-chain mechanisms, open loop simulations were performed (1) using only the joint actuation for feedforward and (2) using the distributed piezo-electric actuators along with joint actuators in feedforward and the results are presented below.

Plots of the input piezo voltages and joint torques are presented in figures 4 and 5 respectively. To illustrate the viability of the proposed method figures 6 and 7 show the transverse structural midpoint deflections of the two links during the motion with and without the distributed actuators. Similar plots for the elastic hub rotations are shown in figures 8 and 9.

Thus the piezo-electric actuators show a significant reduction in the structural vibrations and demonstrates the viability of the proposed method. The consequent reduction in the induced strains in the structure allows the use of lighter elements and smaller actuators, especially in space structures where the loads are mainly inertial.

4. Conclusion

Typically distributed actuators like the piezo-electric ones cannot garner enough actuation to cause large motions in the structure. However they could be very effective in controlling the small structural deformations in the structure. Their use in the feedforward to aid the joint actuators for trajectory tracking is a novel idea developed in this paper. The method proposed was shown to be extremely efficient in removing structural vibrations from structures as seen in the example. Thus these feedforward actuations, obtained through the proposed inverse dynamics, augmented with joint angle feedback based closed loop controllers seem promising in the slewing control of flexible manipulators. This encouraging result motivates further work on distributed actuators in the control of flexible structures.

ACKNOWLEDGEMENT

Support from Air Force Office of Scientific Research through grant F49620-91-C-0095, the Astro Aerospace Corporation and TRW are gratefully acknowledged.

References

1. E. Bayo., M.A. Serna , P. Papadopoulos, and J. Stubbe , "Inverse Dynamics and Kinematics of Multi-Link Elastic Robots. An Iterative Frequency Domain Approach," *The International J. of Robotics Research*, vol. 8, No 6, Dec 1989.
2. D. Kwon. and W.J. Book, "An inverse dynamic method yielding flexible manipulator state trajectories," *Proc. of ACC*, pp. 186-193, 1990.
3. Fanson, J. L. and Garba, J. A., "Experimental Studies of Active members in Control of Large Space Structures," *Proc. AIAA 29th SDM Conf.*, pp. 9-17, 1988.
4. L. Meirovitch and H. Baruh, "Control of Self-Adjoint Distributed-Parameter Systems," *AIAA*, vol. 5, No 1, pp. 60-66, 1980.
5. M. J. Balas, "Active Control of Flexible Systems," *Journal of Optimization Theory and Applications*, vol. 25, No 3, pp. 415-436, 1978.
6. B. Paden, D. Chen, R. Ledesma, and E. Bayo, "Exponentially Stable Tracking Control for Multi-Joint Flexible-Link Manipulators," *ASME J. of Dynamic Systems, Measurement and Control*, vol. 115, pp. 53-59, 1993.
7. G. Naganathan and A.H. Soni, "Coupling Effects of Kinematics and Flexibility in Manipulators," *International Journal of Robotics Research*, vol. 6, No 1, pp. 75-85, 1987.
8. G.W. Stewart, *Introduction to Matrix Computations*, pp. 319-325, Academic Press, Inc., 1973.
9. E.F. Crawley and E.H. Anderson, "Detailed Models of Piezoceramic Actuation of Beams," *J. of Intelligent Material Systems and Structures*, vol. 1, pp. 4-24, 1990.
10. S. Devasia, "Modeling of Piezo Electric Actuators," *M.S. Thesis*, UCSB, 1990.

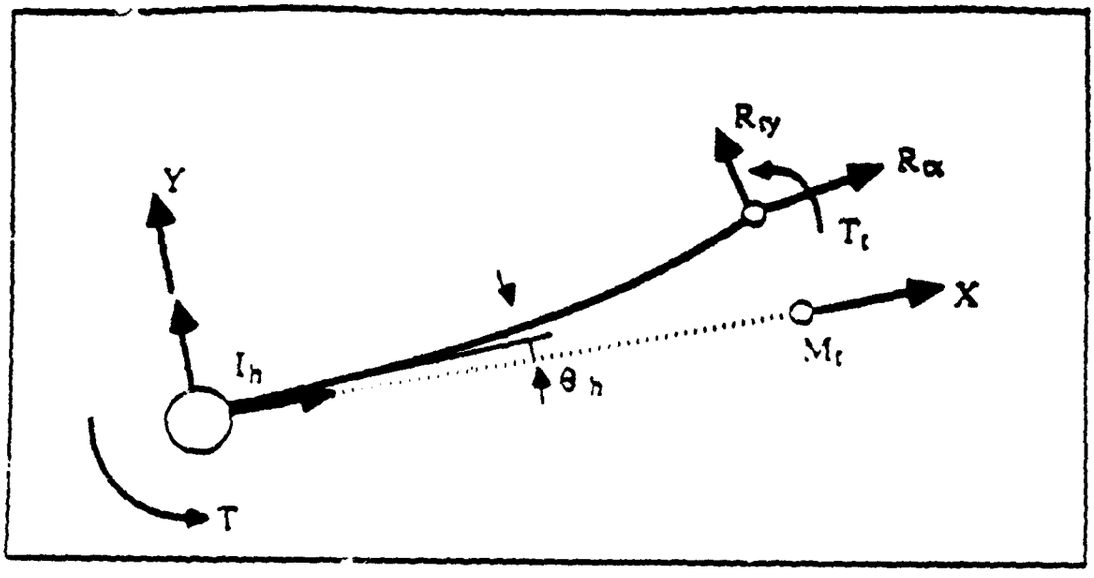

Figure 1. A Single Flexible Link

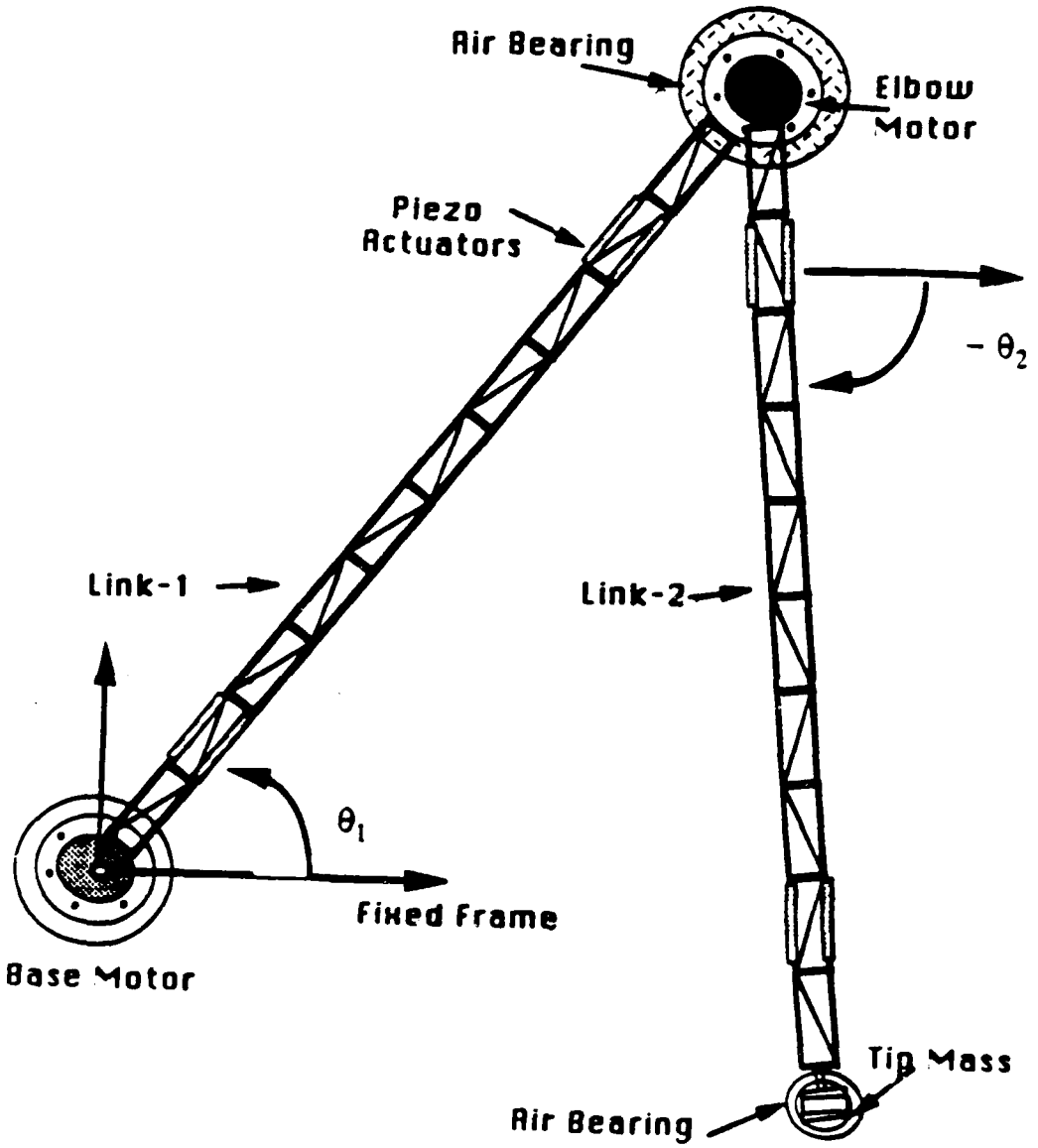

Figure 2. The Two Link Truss Structure

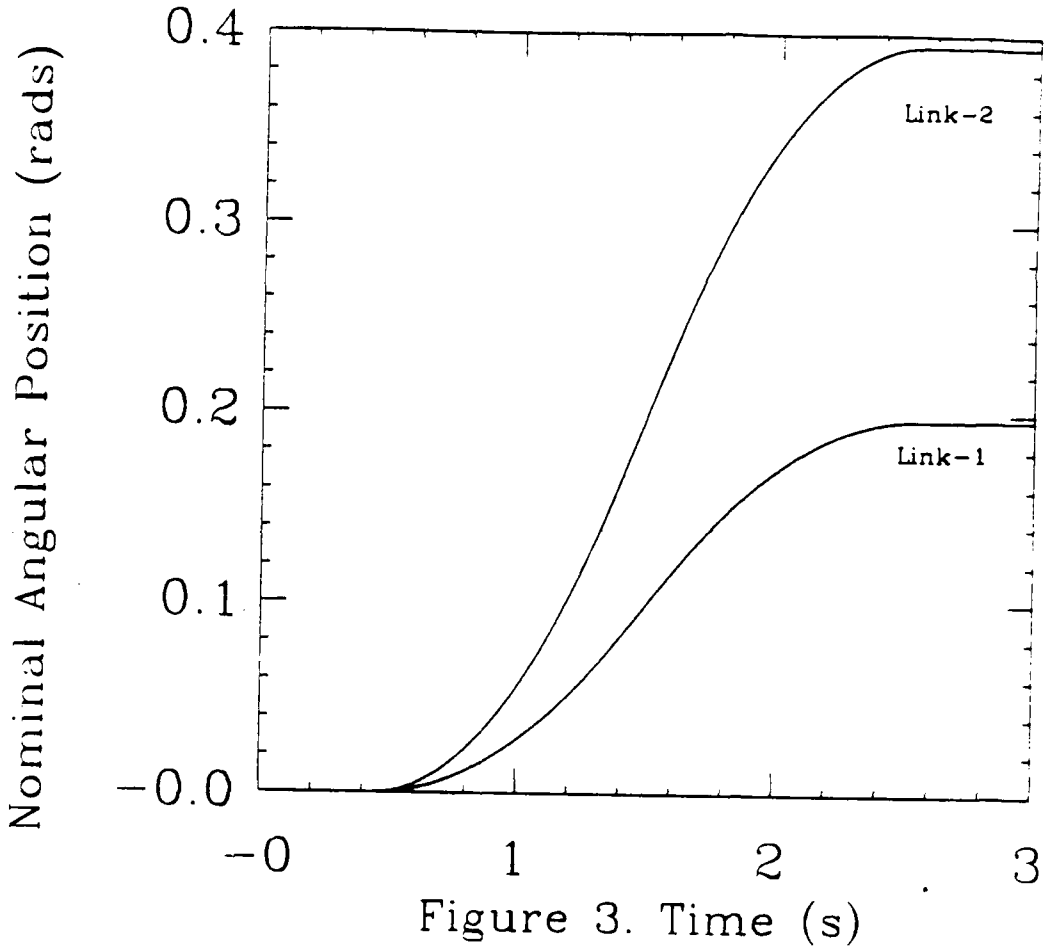
0.4
0.3
0.2
0.1
-0.0
-0
1
2
3
Link-2
Link-1
Nominal Angular Position (rads)
Time (s)

Figure 3.

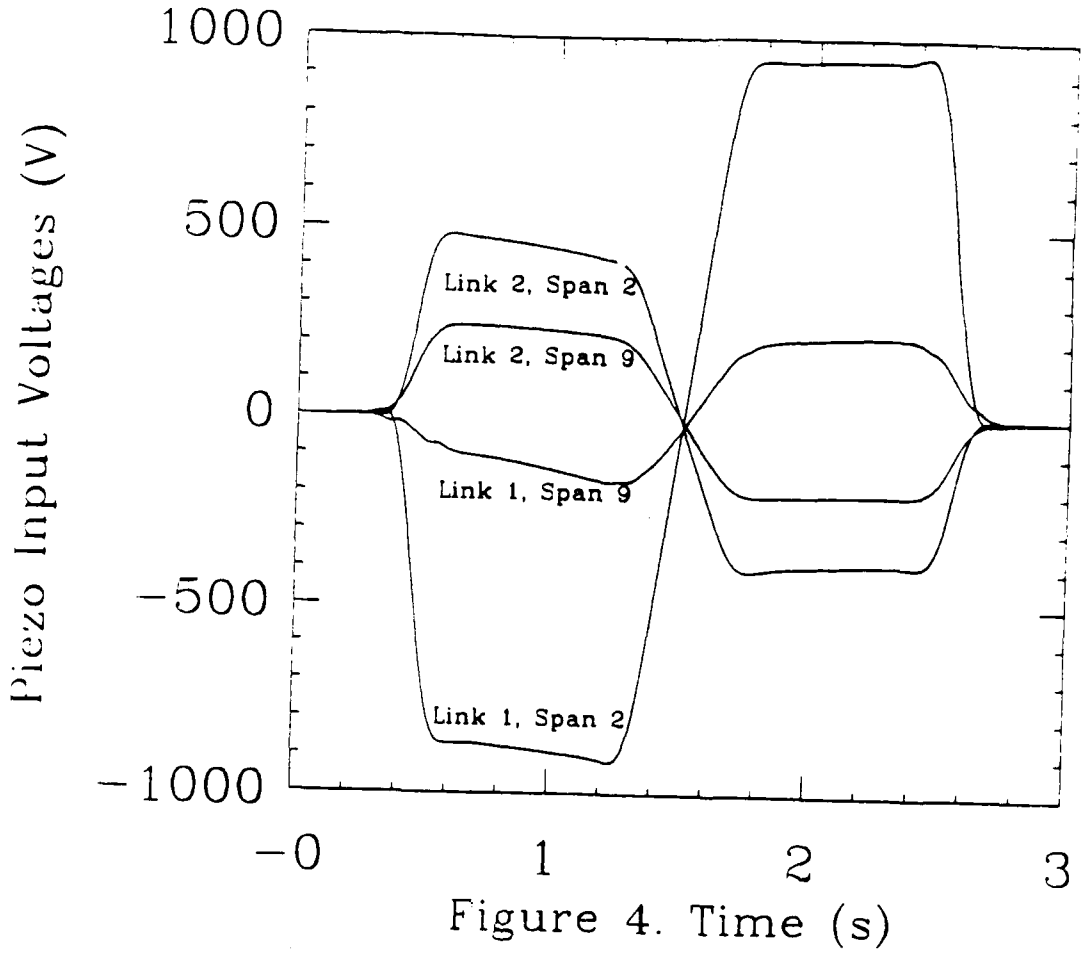
1000
500
0
−500
−1000
−0
1
2
3
Piezo Input Voltages (V)
Time (s)
Link 2, Span 2
Link 2, Span 9
Link 1, Span 9
Link 1, Span 2

Figure 4.

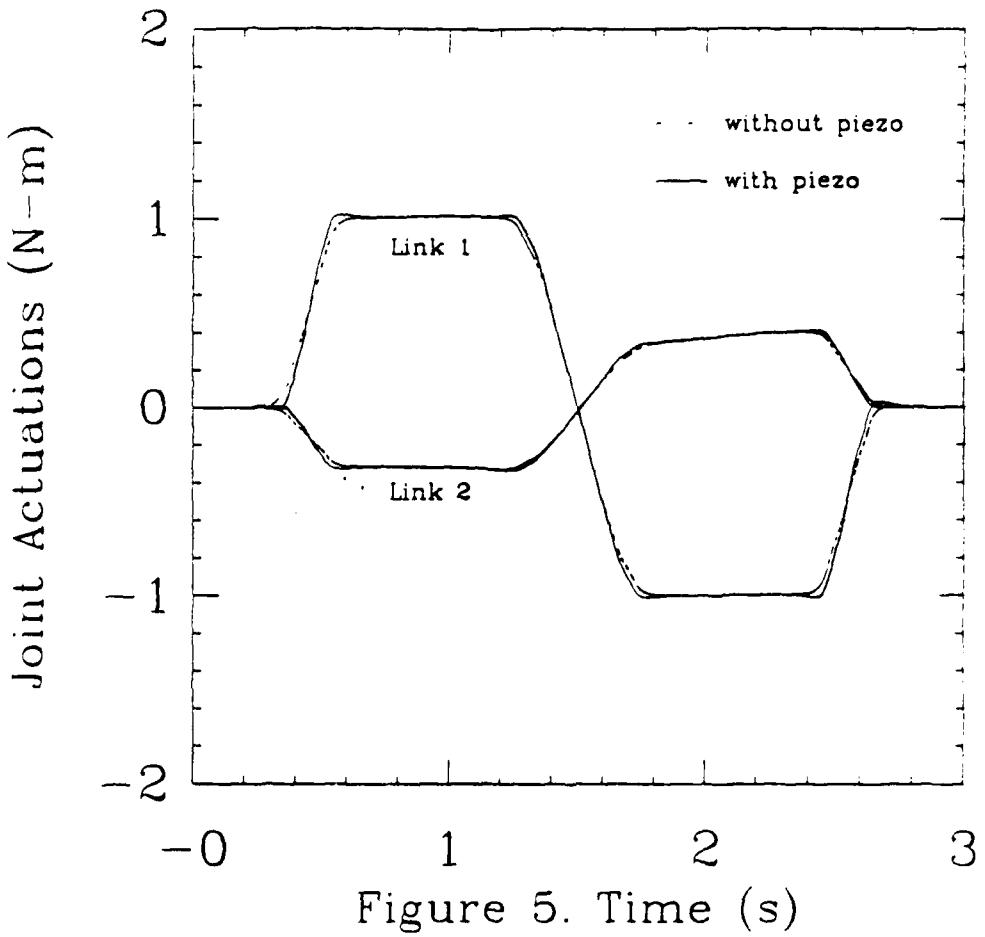
2
1
0
−1
−2
−0
1
2
3
Joint Actuations (N−m)
without piezo
with piezo
Link 1
Link 2
Time (s)

Figure 5.

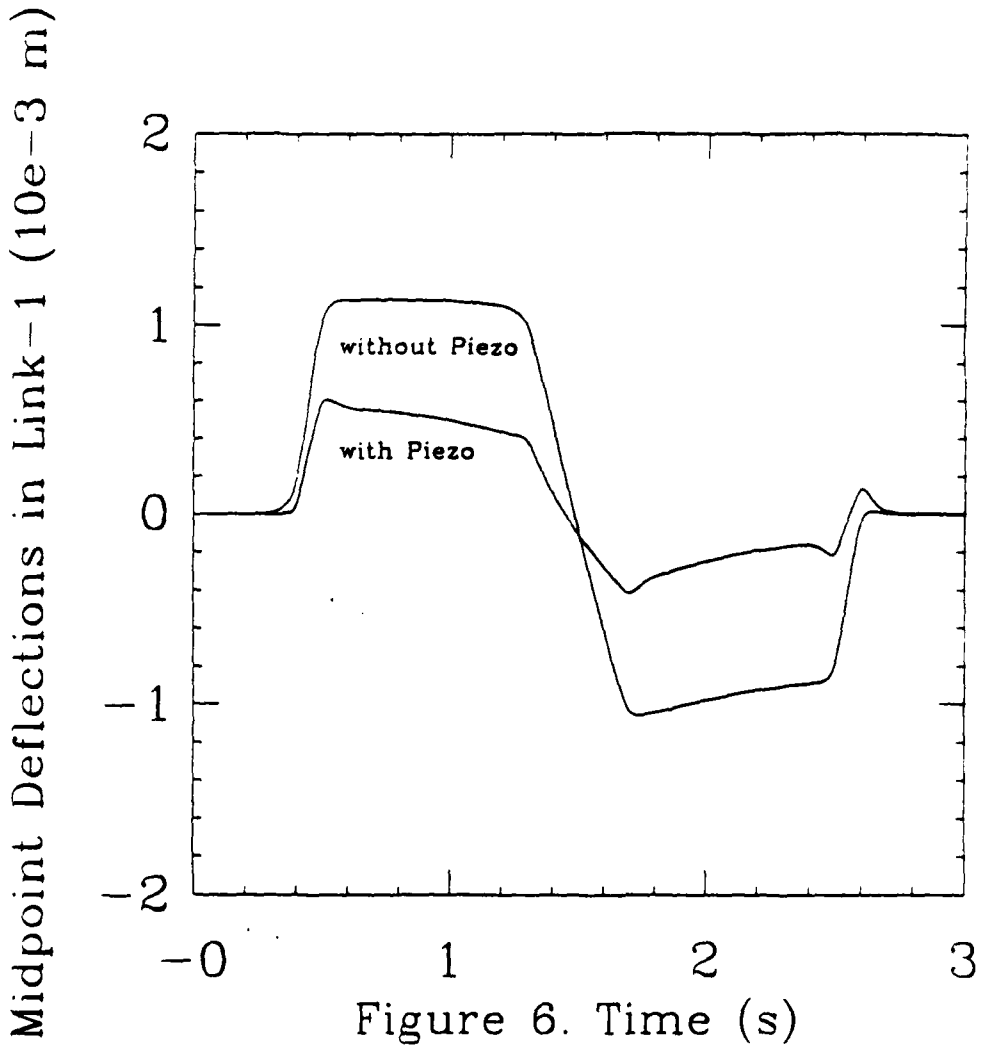
Midpoint Deflections in Link-1 (10e-3 m)
2
1
0
-1
-2
-0
1
2
3
without Piezo
with Piezo
Time (s)

Figure 6.

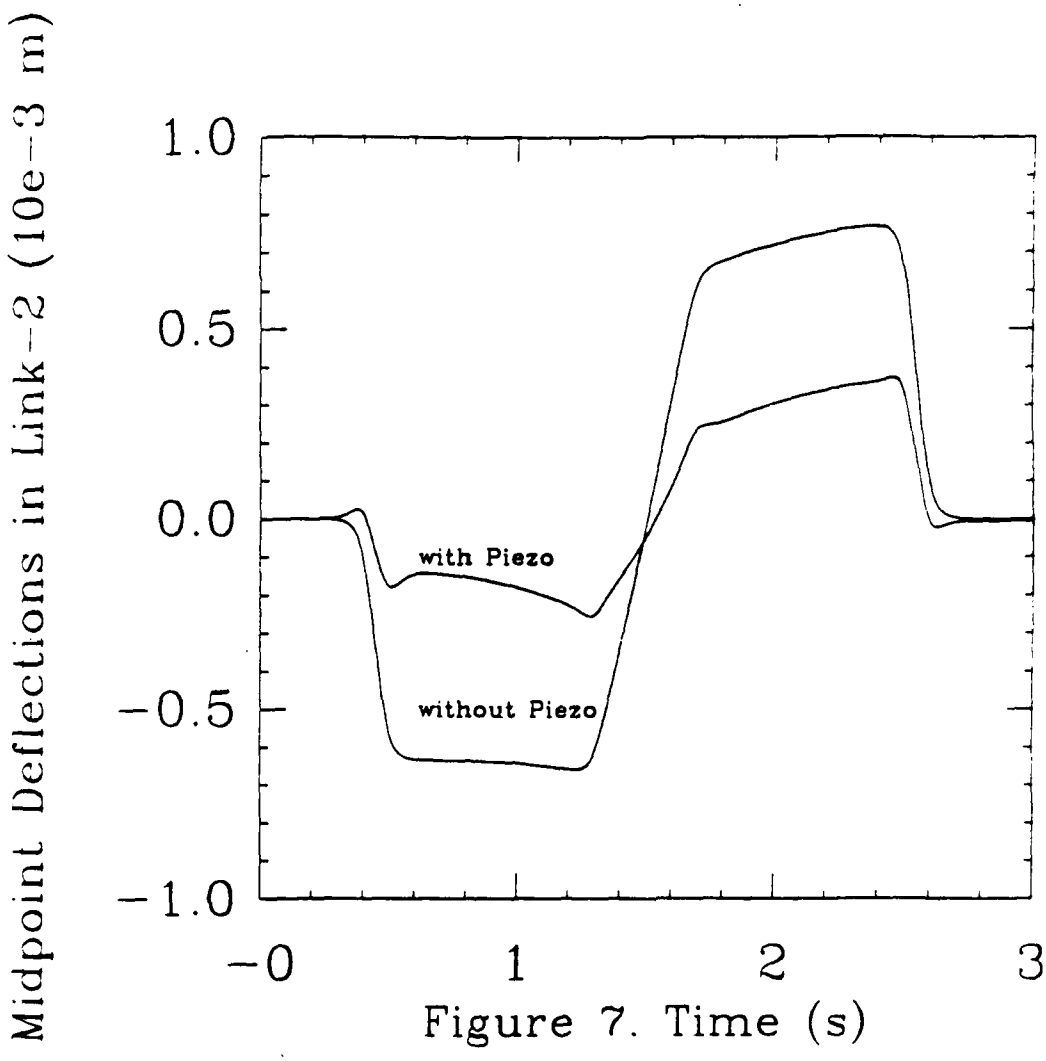
Midpoint Deflections in Link-2 (10e-3 m)
1.0
0.5
0.0
-0.5
-1.0
-0
1
2
3
with Piezo
without Piezo
Time (s)

Figure 7.

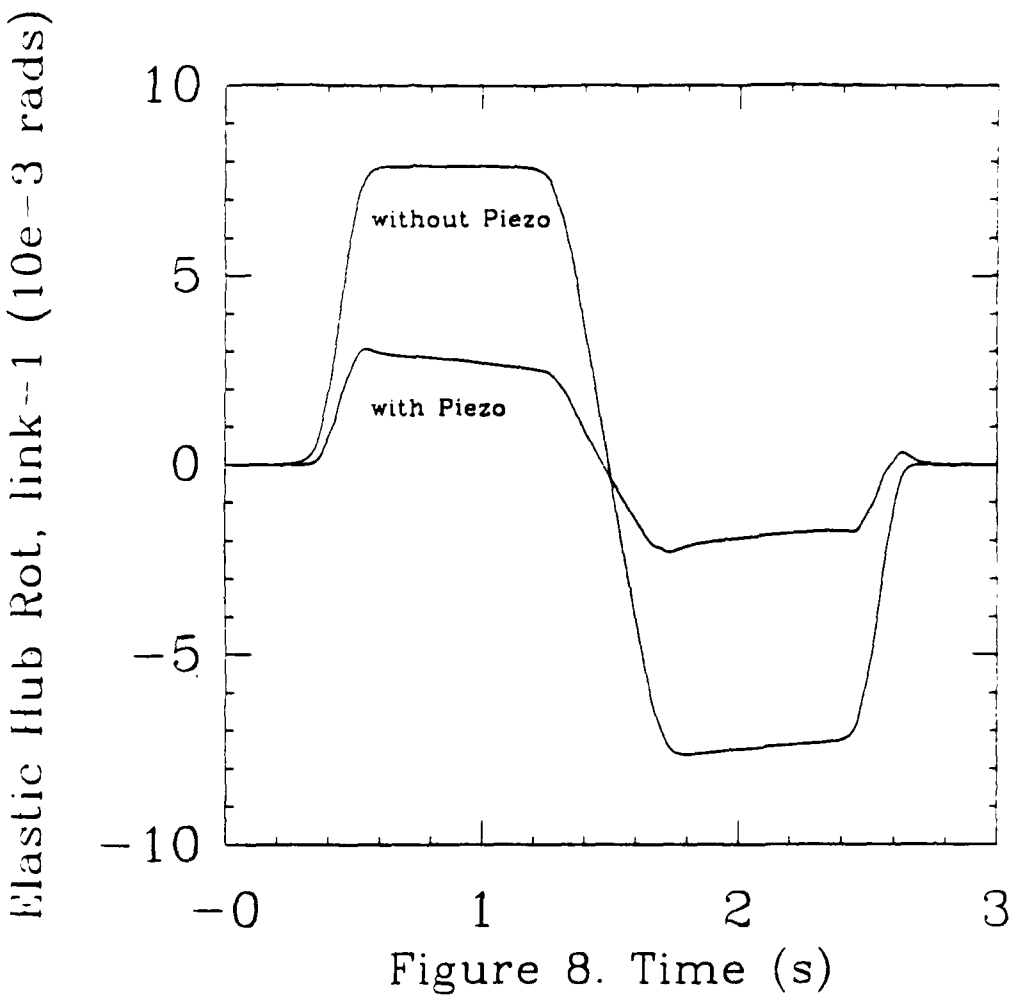

Figure 8. Time (s)

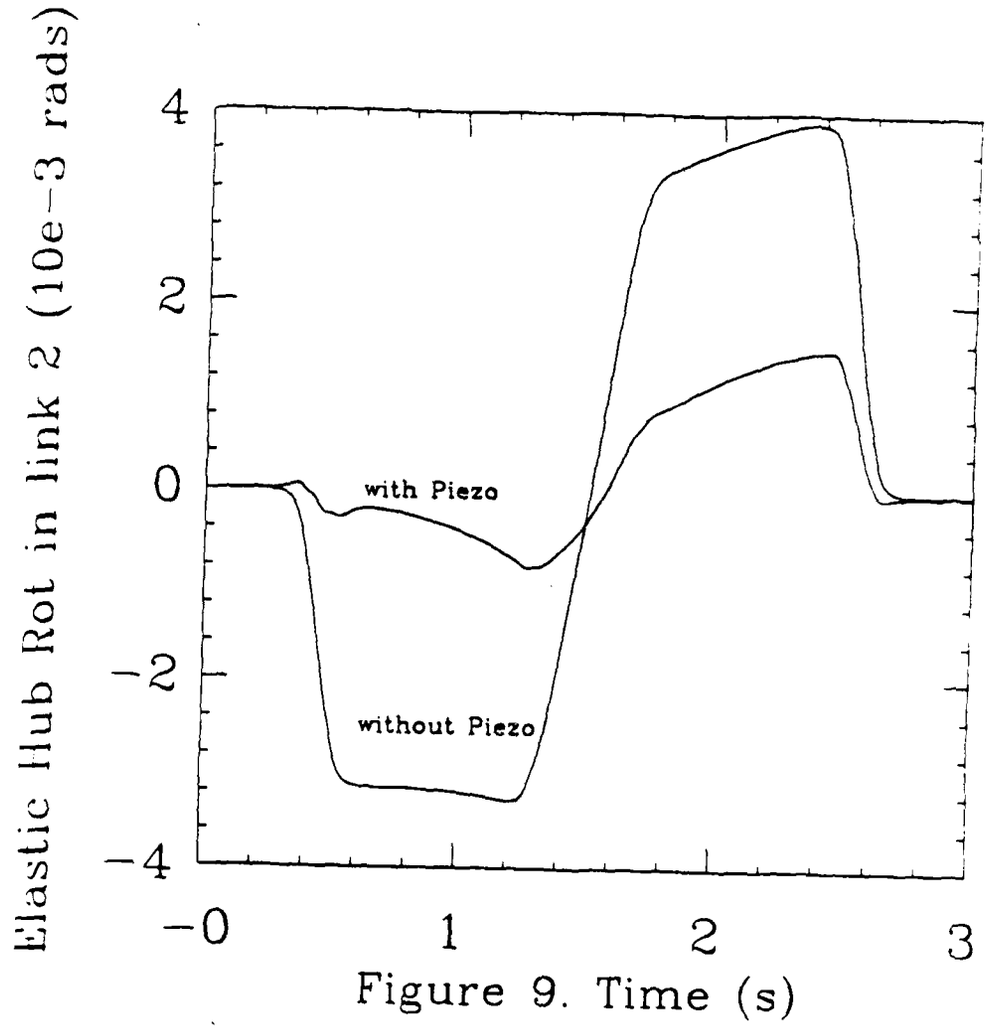
Elastic Hub Rot in link 2 (10e−3 rads)
4
2
0
−2
−4
−0
1
2
3
with Piezo
without Piezo
Time (s)

Figure 9.

JOURNAL OF GUIDANCE, CONTROL, AND DYNAMICS
Vol. 16, No. 5, September–October 1993

Piezoelectric Actuator Design for Vibration Suppression: Placement and Sizing

Santosh Devasia,* Tesfay Meressi,* Brad Paden,† and Eduardo Bayo†
University of California, Santa Barbara, Santa Barbara, California 93106

In this paper we consider the problem of simultaneous placement and sizing of distributed piezoelectric actuators to achieve the control objective of damping vibrations in a uniform beam. For several closed-loop performance measures we obtain optimal placement and sizing of the actuators using a simple numerical search algorithm. These measures are applied to the specific example of a simply-supported beam with piezoelectric actuators, and their relative effectiveness is discussed. We demonstrate that the controllability grammian is not suitable to determine actuator placement for vibration suppression problems.

Nomenclature

A_b = cross-sectional area of the beam
b = cross-sectional width
C_p = capacitance of the piezoelectric actuator
d_{31} = piezoelectric constant
E_a = Young's modulus of the adhesive layer
E_b = Young's modulus of the beam column
E_p = Young's modulus of the piezoactuator
g_{31} = strain to voltage constant
I_b = area moment of inertia of the beam
I_{EQ} = equivalent area moment of inertia
t_a = thickness of the adhesive layer
t_b = thickness of the beam column
t_p = thickness of the piezoactuator
v_1 = voltage applied to the top piezo
v_2 = voltage applied to the bottom piezo
$y(x)$ = vertical displacement of the neutral axis
δ' = derivative of the delta function
ρ_b = density of the beam

I. Introduction

THE control of large flexible structures has been considered for some time.[1,2] However, the recent application of piezoelectric materials by Crawley[3] and Bailey and Hubbard[4] for actuation of flexible structures has added new dimensions to the control problem. This comes from the fact that these actuators can be distributed along structural members for vibration and shape control. In this paper we consider the problem of simultaneous *placement* and *sizing* of distributed piezoelectric actuators to achieve the control objective of damping vibrations in a uniform beam.

Figure 1 shows a specific example of a simply-supported beam with piezoelectric actuator strips attached to both sides. Our goal is to find the position and length of piezoelectric actuators to maximize modal damping when feedback control is applied. In contrast to previous approaches, we simultaneously optimize the position and length of the actuator strips. For several *closed-loop* performance measures we obtain optimal placement and sizing of the actuators using a simple numerical search algorithm.

In Crawley's early work the actuator was simply placed with one bending mode in mind at the location of maximum strain for that mode.[3] However the placement problem for the case with two or more controlled modes was not addressed. Kondoh et al.[5] used the linear quadratic-optimal control framework to perform sensor and actuator placement, but formulated the problem such that the solution is initial condition dependent—this dependence is removed here. Controllability was used as a performance measure for placement of a point actuator in Refs. 6 and 7. These methods are shown to yield less effective results for vibration damping in beams than those based on closed-loop performance measures. Previous works on actuator placement have not dealt with the sizing problem. We incorporate this as an additional optimization parameter and show that increasing the size of the actuator is not necessarily better.

Questions of robustness to spillover and actuator dynamics have been raised and addressed in Refs. 1, 2, and 8, but are not addressed here. Another important issue is the problems involved in the implementation of controllers for the distributed piezoactuators. These include depoling, nonlinearity, hysteresis, and creep effects in the actuator.[9] Depoling may be avoided by maintaining the applied field below the coercive field. Within the depoling limits, the nonlinearity between the applied electric field and the resulting actuation strain may require the use of more complex models.[10] An alternative is the linearization of this relationship about the operating point.[11] Creep and strain rate dependence of the actuator become important at large strains and low frequencies. Hysteresis also plays an important role at low frequencies. Significant performance improvement over such behavior is possible by commanding the induced charge rather than the voltage applied to the actuator.[12] Other related issues due to actuator dynamics are considered in Refs. 13 and 14, but not addressed in this paper. We note, however, that piezoactuators have fast dynamics relative to electromagnetic actuators and are attractive in this regard.

The remainder of the paper is organized in the following format. In Sec. II a state-space model of a piezoelectric actuated beam of finite length is derived. Section III formulates the placement problem with respect to three performance cri-

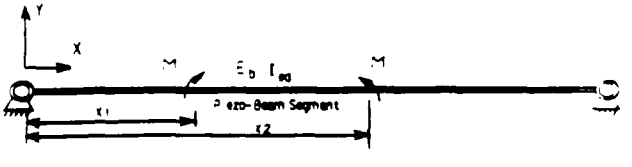

Fig. 1 Simply-supported beam.

Received April 13, 1992; revision received Nov. 6, 1992; accepted for publication Nov. 14, 1992.

*Research Assistant, Department of Mechanical and Environmental Engineering.
†Associate Professor, Department of Mechanical and Environmental Engineering.

teria. These are applied to the simply-supported beam in Sec. IV and compared. Our conclusions are made in Sec. V. The Appendix contains detailed calculations of the mechanics of a piezoactuated beam.

II. State-Space Model of Actuated Beam

In this section we develop a state-space model for the transverse vibrations of the finite beam. The boundary conditions are any combination of pinned, clamped, or free. A pair of piezos attached to the top side and bottom side of the beam is used to actuate the beam as shown in Fig. 2. A second pair is used as sensors. Collocation is achieved since the two pairs are located side by side. The input to the system is the voltage v applied to the actuator pair and the output is the strain-induced voltage generated by the sensors. We show in the Appendix that the net forcing of the beam is equivalent to two equal and opposite moments, M and $-M$ (Fig. 3), applied to the beam at the piezo endpoints x_1 and x_2. Moreover, the moment M is proportional to the input voltage

$$M = Kv \tag{1}$$

The partial differential equation describing the distributed parameter system is therefore

$$E_b I_b y'''' + \rho_b A_b \ddot{y} = M\left[\delta'(x-x_2) - \delta'(x-x_1)\right] \tag{2}$$

We assume that the effects of the actuator on the mode shapes are negligible, which is valid if the dimensions of the piezo are small compared with those of the beam. This formulation is simple and is sufficient for the work presented in this paper. More detailed models are available in Ref. 9. Our assumption of a finite beam with pinned, clamped, or free boundary conditions guarantees a modal decomposition of the form

$$y(x,t) = \sum_{i=1}^{\infty} \Phi_i(x)\eta_i(t) \tag{3}$$

where the $\Phi_i(x)$ are the normalized orthogonal mode shapes and the $\eta_i(t)$ are the modal amplitudes. Substituting Eqs. (1) and (3) into (2) and projecting onto the ith mode yields decoupled modal equations

$$\rho_b A_b \ddot{\eta}_i(t) + E_b I_b \psi_i \eta_i(t) = \left[\Phi_i'(x_2) - \Phi_i'(x_1)\right] Kv(t) \tag{4}$$

where ψ_i determines the modal stiffness and is given by

$$\psi_i \triangleq \int_0^{L_b} \Phi_i \cdot \Phi_i'''' \, dx \tag{5}$$

Define

$$\omega_i^2 \triangleq \frac{E_b I_b \psi_i}{\rho_b A_b} \quad \text{and} \quad B_i \triangleq \frac{1}{\rho_b A_b}\left[\Phi_i'(x_2) - \Phi_i'(x_1)\right] K \tag{6}$$

Then equation (4) can be written as

$$\ddot{\eta}_i(t) + \omega_i^2 \eta_i(t) = B_i v(t) \tag{7}$$

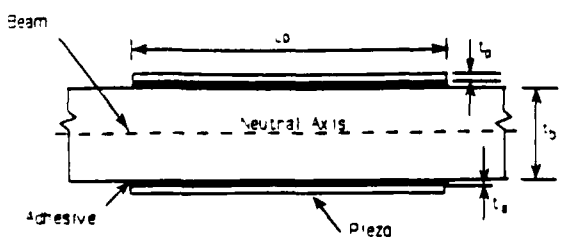

Fig. 2 Beam segment with actuator.

It is clear from Eq. (7) that the ith mode is controllable if and only if B_i is nonzero. In this paper we are trying to control multiple modes with a single piezo and so there must be a compromise placement and sizing such that B_i for each controlled mode is nonzero.

With the sensor placed as shown in Fig. 2, the output of the sensor piezos is a linear combination of the modal amplitudes. Substituting Eq. (3) into Eq. (A9) of the Appendix yields

$$V_s(t) = K_s \sum_{i=1}^{\infty} \eta_i(t)\left[\Phi_i'(x_2) - \Phi_i'(x_1)\right] \tag{8}$$

Define C_i by

$$C_i \triangleq K_s\left[\Phi_i'(x_2) - \Phi_i'(x_1)\right] \tag{9}$$

then

$$\hat{y}(t) = \sum_{i=1}^{\infty} C_i \eta_i(t) \tag{10}$$

If C_i is nonzero then the ith mode is observable. In our case of collocated sensors and actuators (Fig. 2), the ith mode is observable if and only if it is controllable.

If we truncate our representation to n modes, the dynamics can be written as

$$\dot{z}(t) = \bar{A}z(t) + \bar{B}v(t)$$
$$V_s(t) = \bar{C}z(t) \tag{11}$$

where

$$z \triangleq \left[\eta_1 \quad \eta_2 \quad \cdots \quad \eta_n \quad \dot{\eta}_1 \quad \dot{\eta}_2 \quad \cdots \quad \dot{\eta}_n\right]^T \tag{12}$$

$$\bar{A} \triangleq \begin{bmatrix} O_n & I_n \\ -\Omega^2 & 0_n \end{bmatrix}$$

$$\bar{B} \triangleq \begin{bmatrix} O_{n\times 1} \\ \hat{B} \end{bmatrix} = \begin{bmatrix} O_{n\times 1} \\ B_1 \\ \vdots \\ B_n \end{bmatrix}$$

$$\bar{C} \triangleq \left[\hat{C} \quad O_{1\times n}\right] = \left[C_1 \, C_2 \cdots C_n \quad O_{1\times n}\right] \tag{13}$$

and $\Omega \triangleq \operatorname{diag}(\omega_1, \ldots, \omega_n)$.

We emphasize the fact that $\bar{B}$ and $\bar{C}$ depend on the piezo position and length through x_1 and x_2.

III. Optimal Placement and Sizing of Piezoactuators

In this section we formulate three optimization problems for determining a good placement and length of the piezoactuator. In words they are the following: 1) subject to the constraint that collocated damping control is used, find the placement and length that maximizes damping uniformly in the modes;

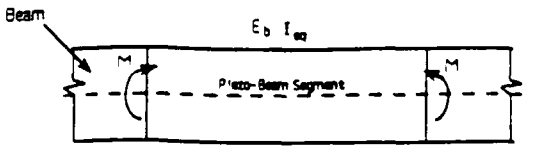

Fig. 3 Equivalent beam segment.

2) assuming the system is detectable and stabilizable, find the placement and length that minimizes a standard linear quadratic cost functional uniformly in initial conditions; and 3) find the placement and length that maximizes the minimum eigenvalue of the controllability grammian (as is done only for the actuator placement problem by Arbel[6]).

Passive Damping Case

For the first optimization problem, we assume a pure collocated damping control given by

$$v(t) = k_d \hat{C} \dot{\eta} \tag{14}$$

where $\eta = [\eta_1\ \eta_2\ \cdots\ \eta_n]$ and k_d is the controller gain. With this control, Eq. (11) can be written in vector form as

$$\ddot{\eta} + \Omega^2 \eta = k_d \hat{B} \hat{C} \dot{\eta} \tag{15}$$

and the state-space description becomes

$$\dot{z}(t) = Az(t) \tag{16}$$

where

$$A \triangleq \begin{bmatrix} O_n & I_n \\ -\Omega^2 & -k_d \hat{B} \hat{C} \end{bmatrix} \tag{17}$$

The advantage of such a collocated passive control is that controllers designed for a finite-dimensional model retain the stability of the infinite dimensional plant provided that actuator dynamics can be neglected.[15] Since the bandwidth of a piezo is only limited by its capacitance, actuator dynamics can be justifiably ignored for large space structures. The implementation issues of such controllers have been addressed in Refs. 9 and 14.

We measure the system performance for a particular choice of controller, placement, and piezo length by the rate of decay of system states and therefore seek to place the poles of the system far into the left half of the complex plane. More formally, we perform the following optimization

$$\min_{\substack{L_p \in [0, L_b] \\ X_p \in [L_p/2,\ L_b - L_p/2]}} \max_i Re\lambda_i(A) \tag{18}$$

where $\lambda_i(A)$ is the ith eigenvalue of A. We vary the length of the piezo L_p from zero to the length of the beam L_b. The piezo must not overlap the ends of the beam hence the center position X_p of the piezo is varied from $L_p/2$ to $L_b - L_p/2$.

Linear Quadratic Regulator Case

The linear quadratic regulator (LQR) is attractive because the controller stabilizes the closed-loop system and also allows for user defined weights on the inputs and states. LQR optimization has been used to reduce the structural vibrations in the control of large flexible structures in Refs. 4 and 7 for a fixed-size actuator. Here we include placement and sizing in the optimization. For the system described by Eq. (11), consider the infinite-horizon time-optimal control problem of minimizing a quadratic cost functional given by

$$J_v \triangleq \int_0^\infty \left[Rv(t)^2 + z^T(t) Q z(t) \right] dt \tag{19}$$

where R is a positive scalar and Q is a positive semidefinite matrix such that the pair $(\bar{A}, Q^{1/2})$ is observable. Provided system (11) satisfies the standard conditions of stabilizability and detectability, the minimum cost $\min J_v$ is given by $z^T(t_0) P z(t_0)$, where P is the unique nonnegative-definite solution to the algebraic Riccati equation[16]

$$P\bar{A} + \bar{A}^T P - P\bar{B} R^{-1} \bar{B}^T P + Q = 0 \tag{20}$$

The corresponding control is

$$v(t) = -R^{-1} \bar{B}^T P z(t) \tag{21}$$

We propose minimizing J_v for the worst case initial condition and therefore pose the following optimization for computing X_p and L_p.

$$\min_{\substack{L_p \in [0, L_b] \\ X_p \in [L_p/2,\ L_b - L_p/2]}} \max_{z_0 = 1} z_0^T P z_0 \qquad z_0 = z(t_0) \tag{22}$$

This method optimizes performance uniformly in initial conditions in contrast to the approach by Kondoh et al.[5] where a solution sensitive to initial conditions is proposed.

Controllability Grammian Method

Finally, we describe a placement procedure based on the controllability grammian proposed by Ref. 6. This method is useful, but has certain disadvantages discussed in the Conclusion. With the inclusion of structural damping the matrix $\bar{A}$ in the state-space description Eq. (11) becomes

$$A_s \triangleq \begin{bmatrix} O_n & I_n \\ -\Omega^2 & -2\zeta\Omega \end{bmatrix} \tag{23}$$

where ζ is the structural damping coefficient. Since A_s is stable, as the final time T tends to infinity, it can be shown that the finite time controllability grammian $W(0,T)$ approaches W, which is the solution of the Lyapunov equation

$$WA_s^T + A_s W + \bar{B}\bar{B}^T = 0 \tag{24}$$

Based on Arbel's method we perform the optimization

$$\max_{\substack{L_p \in [0, L_b] \\ X_p \in [L_p/2,\ L_b - L_p/2]}} \min_i \lambda_i(W) \tag{25}$$

to maximize the controllability of all the modes. The three approaches discussed here are compared via an example in the next section.

IV. Example: Simply-Supported Beam

Consider the simply-supported actuated beam (Fig. 1) having the following properties.

Beam properties

$\zeta = 0.01$ $\quad E_b = 70$ GPa $\quad L_b = 0.5$ m

$t_b = 0.01$ m $\quad b = 0.05$ m $\quad \rho_b = 2500$ Kg/m^3

Piezoactuator-sensor properties

$E_p = 63$ GPa $\quad L_p \in [0, L_b]$ $\quad t_p = 2 \times 10^{-4}$ m

$d_{31} = 120 \times 10^{-12}$ m/V $\quad g_{31} = 10.6 \times 10^{-3}$ Vm/N

$C_p = 35$ pC

Adhesive properties

$E_a = 2.4$ GPa $\quad L_a = L_p$ $\quad t_a = 2 \times 10^{-5}$ m

Using the geometric boundary conditions

$$y(0,t) = y(L,t) = y''(0,t) = y''(L,t) = 0 \tag{26}$$

together with Eqs. (2) and (3), we obtain the equation for the ith mode shape normalized so that

$$\int_0^{L_b} \Phi_i^2\, dx = 1$$

$$\Phi_i(x) = \sqrt{2/L_b}\, \sin(i\pi x / L_b) \tag{27}$$

Substituting this into Eqs. (5) and (6), we have

$$\omega_i = \frac{i^2\pi^2}{L_b^2}\sqrt{\frac{E_b I_b}{\rho_b A_b}} \tag{28}$$

The ith component of the input vector $\hat{B}$ is obtained from Eqs. (6) and (27) and is given by

$$B_i = \frac{ibt_b^3 K^* \pi}{12\rho_b A_b I_{Eq} L_b}\sqrt{\frac{2}{L_b}}\left[\cos\left(\frac{i\pi x_2}{L_b}\right) - \cos\left(\frac{i\pi x_1}{L_b}\right)\right] \tag{29}$$

where K^* and I_{Eq} are as defined in the Appendix by equations (A3) and (A4), respectively. The ith component C_i of the output vector $\hat{C}$ is obtained from Eqs. (9) and (27):

$$C_i = \frac{bt_b g_{31}\pi i}{2C_p L_b}\sqrt{\frac{2}{L_b}}\left[\cos\left(\frac{i\pi x_2}{L_b}\right) - \cos\left(\frac{i\pi x_1}{L_b}\right)\right] \tag{30}$$

Note that a necessary condition for observability and controllability of the ith mode is for the term in parentheses in Eq. (30) to be nonzero. From Eq. (29) we see that B_i is large if x_1 and x_2 are chosen to lie near two different nodes of the ith mode separated by an odd number of half cycles of the mode shape (hence a bigger actuator is not necessarily better!). Also the ith ($i > 1$) mode becomes uncontrollable if the center of the piezo coincides with one of its nodes or the piezo length is an integral multiple of $2L_b/i$. For example, if the piezo length L_p is the same as the beam length L_b, then all of the even modes are uncontrollable.

Simulations were performed for each of the optimization schemes discussed in Sec. III applied to the earlier truncated beam model (with the first two modes). A uniform structural damping coefficient of 0.01 is considered for both of the modes. This implies that the system is stable and hence both detectable and stabilizable. For the passive damping case a controller gain $k_d = 1e-6$ was used. In the LQR based design the placement depends on Q, especially if some states are not penalized. However, to uniformly penalize all modes, Q was taken as $I_{4\times4}$. It was observed in the simulations that the optimum placement and sizing did not vary with R. The results presented are for the $R = 1$ case. The variations of the objective function for the passive damping case with 1) the position of the center of the piezo X_p (optimal over all possible actuator lengths) and 2) the length of the piezo L_p (optimal over possible piezo placements) are shown in Fig. 4. Similar simulation results for the LQR and the controllability grammian methods are shown in Figs. 5 and 6, respectively. Note that as the piezo length L_p approaches the beam length L_b, its midpoint is pushed toward $L_p/2$, making the second mode less controllable. Hence the cost increases as L_p tends to L_b and leads to an optimal actuator length less than L_b. The optimal lengths and positions for the three methods are given in Table 1.

To make a comparison between our LQR method and the initial condition dependent methods described in Refs. 3 and 5 we consider the following two different initial conditions $z_1^T = [1\ 0\ 0\ 0]$ and $z_2^T = [0\ 1\ 0\ 0]$, which correspond to unit displacements in the first and the second modes, respectively. The variation of the cost of control over different actuator

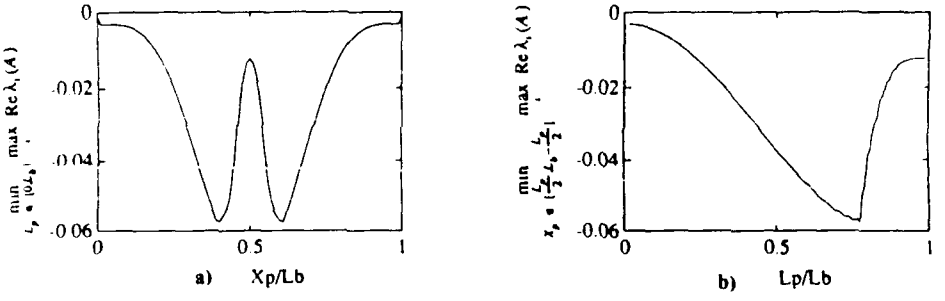

Fig. 4 Passive damping based optimization.

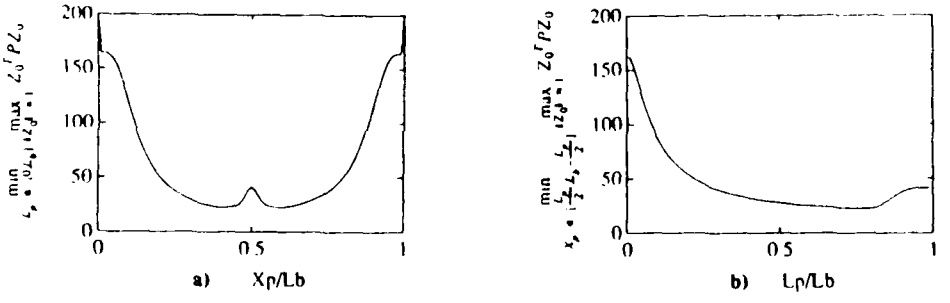

Fig. 5 Linear quadratic regulator based optimization.

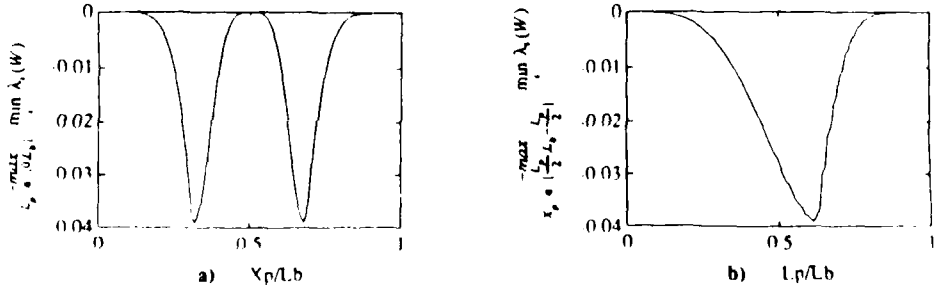

Fig. 6 Controllabilty grammian based optimization.

locations for each of the earlier initial conditions is shown in Fig. 7. The optimization based on these initial conditions results in two different optimum piezo positions at $L_b/2$ and $L_b/4$ suggesting piezo placement at locations where the strain is maximum for the corresponding initial condition. The optimal piezo positions for various initial conditions that are linear combinations of the two modes will vary widely. This problem is easily resolved by the LQR methodology proposed in this paper as it optimizes over all initial conditions.

Next we discuss the controllability grammian method applied by Arbel.[6] The optimized minimum energy control cost for given initial condition $z(t_0)$ and final condition $z(T)$ is equivalent to

$$J \triangleq \left[z(T) - e^{A_s(T-t_0)}z(t_0)\right]' W^{-1}(0,T)\left[z(T) - e^{A_s(T-t_0)}z(t_0)\right] \tag{31}$$

where $e^{A_s(T-t_0)}$ is the state transition matrix.[16] J is the energy required to deviate from the natural motion of the system, which would have reached the state $e^{A_s(T-t_0)}z(t_0)$ at time T without the application of any control. Arbel's method is based on optimizing J (over all possible initial and final conditions) and results in minimizing the maximum eigenvalue of the inverse of the controllability grammian, $W^{-1}(0,T)$, over different actuator positions. However, the control cost J for the finite time regulator problem $[z(T)=0]$ is given by

$$J_r \triangleq \left[e^{A_s(T-t_0)}z(t_0)\right]' W^{-1}(0,T)\left[e^{A_s(T-t_0)}z(t_0)\right] \tag{32}$$

and is not suitably evaluated by Arbel's controllability grammian approach because it fails to consider the effect of $e^{A_s(T-t_0)}$ on J_r in Eq. (32). Next we show that the maximum eigenvalue of $W^{-1}(0,T)$ increases as the system poles move far into the left half of the complex plane. Let γ_i be an eigenvalue of W and let V_i be the corresponding eigenvector such that $\|V_i\|_2 = 1$. Pre- and post-multiplying the Lyapunov Eq. (24) by V_i^T and V_i, respectively, we obtain

$$V_i^T W A_s^T V_i + V_i^T A_s W V_i + V_i^T B B^T V_i = 0 \tag{33}$$

Then

$$\gamma_i = -\frac{V_i^T B B^T V_i}{2 V_i^T A_s V_i} \leq \frac{|\max_i \lambda_i(BB^T)|}{\min_i |\lambda_i(A_s)|} \tag{34}$$

This result implies that for a given B the eigenvalues of W^{-1} increase if the eigenvalues of A_s move far into the left half plane. Hence Arbel's approach deems the system as less controllable and therefore not desirable even though the shifting of the poles is advantageous for vibration reduction.

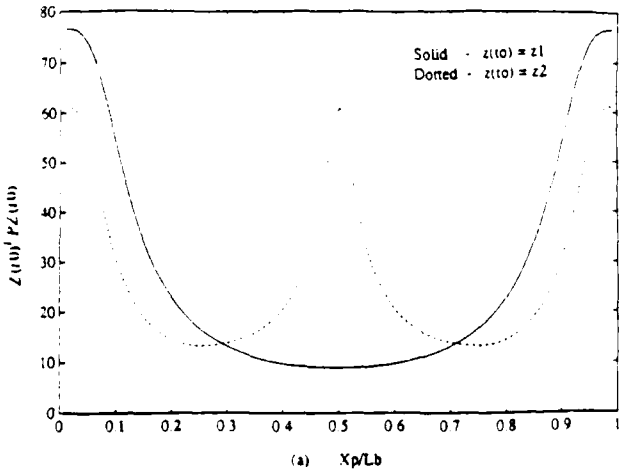

Fig. 7 Initial conditions based optimization.

Table 1 Results

Controller	Optimal $\frac{L_p}{L_b}$	Optimal $\frac{X_p}{L_b}$
Passive	0.7723	0.3961
LQR	0.7921	0.4060
Contr. Gramm.	0.6139	0.3267

This decrease in controllability can be easily illustrated through a scalar example described by

$$\dot{x}(t) = -ax(t) + bu(t) \tag{35}$$

Using Arbel's method, for a large final time T, the eigenvalue of $W(0,T)$ tends to $b^2/2a$, which decreases as a increases, and subsequently the controllability measure deems the system as less controllable even though from a vibration reduction perspective it is more desirable. A similar effect due to the high decay rate in the second mode is seen in the example of the simply-supported beam. The two modes have the same damping coefficient, and so the second mode has a faster decay rate. Arbel's placement method therefore assigns the second mode as less controllable relative to the first mode and hence pushes the placement toward $L_b/4$ where the second mode has maximum strain. Because of a lower decay rate, control of the first mode (which is more controllable when the placement is at the center of the beam) is more critical from a vibration suppression perspective. However, the placement obtained by Arbel's method is further away from the center of the beam and hence results in slower vibration decays in the system as compared to the results obtained through LQR or passive damping methods (Table 1). Thus for vibration reduction, passive damping or LQR based objective functions are more suitable to design the placement of actuators.

V. Conclusion

In this paper we formulated actuator placement and sizing methodologies for vibration suppression in uniform beams. Several closed-loop performance criteria were considered to derive objective functions for optimum placement and sizing of piezoelectric actuators in uniform beams. The paper illustrated through an example that passive damping or linear quadratic regulator based measures are more suitable than the controllability measure for the placement and sizing of actuators to obtain vibration reduction. The procedures developed led to solutions that are independent of initial conditions. The design is also formulated as an eigenvalue problem thereby reducing the required computation considerably.

We also note that the measures proposed in this paper can be applied to any general linear time invariant system and hence the actuator design for vibration suppression can be based on these measures. The question of the existence of optimal designs over different controllers (e.g., all passive controllers) for general linear time invariant systems is the subject of further research.

Appendix: Mechanics of Piezo Actuated Beam

Consider a segment of the piezo beam as shown in Fig. 2. It is assumed for simplicity that the width of the piezo is equal to that of the beam. Using the standard Bernoulli-Euler beam approach, the moment generated by voltage applied to the piezos is given by Ref. 9

$$M^* = b t_p E_p \left[(\Lambda_1 - \Lambda_2)(t_b/2 + t_a + t_p/2)\right] \tag{A1}$$

where

$$\Lambda_i = \frac{d_{31} v_i}{t_p} \qquad i = 1,2 \tag{A2}$$

Thus

$$M^* = bE_p d_{31}(t_b/2 + t_a + t_p/2)(v_1 - v_2) \triangleq K^*(v_1 - v_2)/2 \quad \text{(A3)}$$

M^* is the effective bending moment acting on a beam of equivalent area moment of inertia given by

$$I_{Eq} = \frac{bt_b^3}{12} + 2\frac{b_a t_a^3}{12} + 2b_a t_a\left(\frac{t_b}{2} + \frac{t_a}{2}\right)^2 + 2\frac{b_p t_p^3}{12} + 2b_p t_p\left(\frac{t_b}{2} + t_a + \frac{t_p}{2}\right)^2 \quad \text{(A4)}$$

where $b_a = b(E_a/E_b)$ and $b_p = b(E_p/E_b)$ are the equivalent adhesive and piezo widths, respectively. Then the resultant strain of the actuator is

$$\epsilon(x,h) = \frac{M^*(x)h}{E_b I_{Eq}} \quad \text{(A5)}$$

where x is measured along the length of the piezo and h is the distance from the neutral axis. The previous expression is based on the Bernoulli-Euler model described in Ref. 9 and a detailed explanation of the results based on this model can be found in Ref. 17. If the voltages applied at the top and bottom layers of the piezoactuators are equal in magnitude and opposite in sign ($v_1 = -v_2 \triangleq v$), then equation (A3) becomes $M^* = K^* v$. Without loss of generality one can write the effect of the piezo on the beam as two equal and opposite concentrated moments whose magnitudes are given by $M = Kv$ as shown in Fig. 3, where

$$K \triangleq K^* \frac{bt_b^3}{12I_{Eq}} \quad \text{(A6)}$$

The sensor output is obtained as follows. The incremental charge dQ generated on an infinitesimal area $b\ dx$ is given by

$$dQ = g_{31}\frac{t_b}{2}\frac{d^2y(x)}{dx^2}\,b\,dx \quad \text{(A7)}$$

This may be integrated over the sensor covered length of the beam to yield the sensor output voltage

$$V_s(t) = \frac{bt_b g_{31}}{2C_p}\left[y'(x_2,t) - y'(x_1,t)\right] \quad \text{(A8)}$$

$$\triangleq K_s\left[y'(x_2,t) - y'(x_1,t)\right] \quad \text{(A9)}$$

where g_{31} is the strain to voltage constant, C_p is the capacitance and x_1 and x_2 are the locations of the piezo ends.

Acknowledgments

Support from the Air Force Office of Scientific Research through Grant F9620-91-C-0095 and the Astro Aerospace Corporation is gratefully acknowledged.

References

[1]Balas, M. J., "Active Control of Flexible Systems," *Journal of Optimization Theory and Applications*, Vol. 25, No. 3, 1978, pp. 415–436.

[2]Meirovitch, L., and Baruh, H., "Control of Self-Adjoint Distributed-Parameter Systems," *AIAA Journal*, Vol. 5, No. 1, 1980, pp. 60–66.

[3]Crawley, E. F., and De Luis, J., "Use of Piezoelectric Actuators as Elements of Intelligent Structures," *AIAA Journal*, Vol. 25, No. 10, 1985, pp. 1373–1385.

[4]Bailey, T., and Hubbard, J. E., Jr., "Distributed Piezoelectric-Polymer Active Vibration Control of a Cantilever Beam," *Journal of Guidance, Control, and Dynamics*, Vol. 8, No. 5, 1985, pp. 605–611.

[5]Kondoh, S., Yatomi, C., and Koichi, I., "The Positioning of Sensors and Actuators in the Vibration Control of Flexible Systems," *JSME International Journal*, Vol. 33, No. 2, 1990, pp. 145–152.

[6]Arbel, A., "Controllability Measures and Actuator Placement in Oscillatory Systems," *International Journal of Control*, Vol. 33, No. 3, 1981, pp. 565–574.

[7]Fisher, S., "Application of Actuators to Control Beam Flexure in a Large Space Structure," *Journal of Guidance, Control, and Dynamics*, Vol. 12, No. 6, 1989, pp. 874–879.

[8]Goh, C. J., and Caughey, T. K., "On the Stability Problem Caused by Finite Actuator Dynamics in the Collocated Control of Large Space Structures," *International Journal of Control*, Vol. 41, No. 3, 1985, pp. 787–802.

[9]Crawley, E. F., and Anderson, E. H., "Detailed Models of Piezoceramic Actuation of Beams," *Journal of Intelligent Material Systems and Structures*, Vol. 1, No. 1, 1990, pp. 4–25.

[10]Crawley, E. F., and Lazarus, K. B., "Induced Strain Actuation of Isotropic and Anisotropic Plates," AIAA 30th Structural, Structural Dynamics, and Materials Conference, AIAA Paper 89-1326, 1989.

[11]De Luis, J., "Design and Implementation of Optimal Controllers for Intelligent Structures Using Infinite Order Structural Models," Ph.D. Thesis, Massachusetts Inst. of Technology, Cambridge, MA, 1989.

[12]Comstock, R. H., "Charge Control of Piezoelectric Actuators as Elements of Intelligent Structures," U.S. Patent 4,263,527, Draper Laboratories, Cambridge, MA, 1981.

[13]Fanson, J. L., and Garba, J. A., "Experimental Studies of Active Members in Control of Large Space Structures," *Proceedings of the AIAA 29th Structures, Structural Dynamics, and Materials Conference*, AIAA, Washington, DC, 1988, pp. 9–17.

[14]Fanson, J. L., and Caughey, T. K., "Positive Position Feedback Control for Large Space Structures," *AIAA Journal*, Vol. 28, No. 4, 1990, pp. 717–724.

[15]Bhaya, A., and Desoer, C. A., "On the Design of Large Flexible Space Structures (LFSS)," *IEEE Transactions on Automatic Control*, Vol. AC-30, No. 11, 1985, pp. 1118–1120.

[16]Kwakernaak, H., and Sivan, R., *Linear Optimal Control Systems*, Wiley-Interscience, New York, 1972.

[17]Devasia, S., "Modeling of Piezo Electric Actuators," M.S. Thesis, Univ. of California, Santa Barbara, Santa Barbara, CA, 1990.

ACTUATOR PLACEMENT FOR ARTICULATED FLEXIBLE MANIPULATORS AND SPACE STRUCTURES

Santosh Devasia * Brad Paden ** Eduardo Bayo **

University of California, Santa Barbara, CA 93106

ABSTRACT

In this paper we consider the problem of placing piezoelectric vibration dampers in an experimental articulated flexible structure (AFS). The placement problem for these jointed structures is complicated by their nonlinear dynamics. Even with small linear vibrations about a given rigid body configuration, a good placement for one configuration should not necessarily work well after the structure's joints are rotated. With a finite-element model, we have indeed observed a large variation in modal frequencies (for the linearized dynamics) as the joint angles are varied. However, we have observed that for our structure the mode *shapes* are relatively invariant to joint configuration and hence uniformly good placements are possible. We also show, using a singular perturbation argument, that such uniformly good placements can be expected in a class of AFS with joint dominated inertias. Two methods of placement are explored. The first is based on a simple damping controller where placements are chosen to maximize the decay rate of vibrations. The second method optimizes placement based on closed-loop performance of Linear-Quadratic Regulator. The two methods are contrasted using a finite-element model of our structure.

* Research Assistant, Department of Mechanical & Environmental Engineering
** Associate Professor, Department of Mechanical & Environmental Engineering

1. Introduction

Control of Articulated Flexible Structures (AFS) is important in many space and aerospace applications. The control objectives are application dependent, for example in articulated flexible manipulators the objective may be to track a given end-effector trajectory or to reduce the elastic vibrations in the structure. The problem of using point actuators has been addressed in [1] and [2] where the inverse dynamics problem has been solved to obtain the control inputs. Closed loop controllers which achieve exponentially stable trajectory tracking have been proposed by Paden *et al* [3]. However, errors in the modeling of the structure, approximations in the implementation of the controllers and disturbances from external sources introduce vibrations in the structure. This vibration problem is compounded by backlash and friction in the motor drives which make small amplitude vibrations difficult to control. These vibrations adversely affect the system performance and are to be minimized. This problem can be mitigated by using piezoelectric or electrostrictive actuators. Substantial success in vibration reduction has been reported [4] by incorporating such distributed actuators in the flexible structures. To optimize the vibration reduction with distributed actuators, synergistic structure-controller designs are necessary, [5] and [6]. A key issue in any such design is actuator placement.

In this paper the placement problem for distributed actuators in articulated flexible structures is addressed. In contrast to this nonlinear problem the placement issue for linear systems is well studied in literature. In Crawley's early work on systems with linear dynamics, the distributed actuator was simply placed with one bending mode in mind at the location of maximum strain for that mode [7]. However the placement problem for the case with two or more controlled modes was not addressed. This was done using a controllability based performance measure by Arbel [8]. The effectiveness of measures based on closed loop controllers ([9] and[10]) over those based on the controllability grammian for vibration damping in linear flexible structures was demonstrated by Devasia *et al* [11]. However, the computations of such measures are not tractable for general trajectories in systems like AFS which have nonlinear dynamics.

We introduce two measures in this paper which are useful to determine the placement of

actuators to achieve structural vibration reduction in AFS. The goal of vibration damping based actuator placements is to improve the convergence rate for a set of equilibrium points. For our case these equilibria are rigid body configurations with zero elastic deflections. Our approach can be summarized as 1) linearizing about equilibrium points, 2) evaluation of a local cost functional at the different equilibrium points and 3) selection of placement based on a suitably constructed global measure (pertaining to the entire set of equilibrium points). The measures are then applied to an example two-link flexible manipulator to solve the placement problem for a piezoelectric actuator.

The remainder of the paper is organized in the following format. Our approach is described in section 2. In section 3 we illustrate the methodology with an example of actuator placement in a two-link flexible truss structure (figure 1). For this articulated structure, modal frequencies of linearizations change considerably with configuration and one may expect that a uniformly good placement is impossible. The saving fact is that, although the frequencies change, the mode shapes are relatively invariant. This results in placements that are uniformly "good" over all configurations. Section 4 studies a class of systems (with joint dominated inertias) where such uniformly good placements can be expected due to mode shape invariance. Our conclusions are in section 5.

2. Performance Measures for Actuator Placement

In this section we formulate the problem for the placement of distributed actuators in a general articulated flexible structure (AFS). The set of equilibria in AFS consists of rigid body configurations with zero elastic deformations. Our objective is to damp elastic vibrations about these rigid body equilibrium configurations. In the following section solution methodologies based on two different measures are described in detail. We start with a description of the general actuator placement problem.

General Placement Problem

The general equation of motion for an articulated flexible structure can be described by a nonlinear differential equation as,

$$\dot{x}(t) = f_p(x, u(t))$$
$$y = h_p(x), \tag{2.1}$$

where x is a vector of the system states and p belongs to the set of possible actuator placements X_p. A formal design procedure for actuator placement involves the following: Given a set X_d of desired state trajectories, a set U of possible inputs and a set X_p of possible placements, evaluate the formal expression

$$\min_{p \in X_p} \max_{x_u \in X} \min_{u \in U} J_u(u, (x_u - x_d)),$$

where x_u is the actual trajectory followed by the system when actuated by input u and $J_u(u, (x_u - x_d))$ is a functional that defines the design objectives. The issue is to choose an appropriate functional J_u which penalizes undesirable behavior and is also computationally viable -- an example is a cost functional which is quadratic in control input u and the state trajectory error $(x_u - x_d)$. However, in the general nonlinear setting (2.1) the minimax problem is intractable.

Here we address the simpler issue of actuator placement to suppress elastic deflections about given rigid body configurations. Therefore, our control objective is to obtain uniformly good regulation of elastic deformations at any equilibrium state (rigid body configuration) of the articulated structure. This implies that the set of desired trajectories X_d, are constant trajectories. Our approach is based on linearization of the system equations at each equilibrium point in the set X_o followed by a local cost measure evaluation at these equilibrium points. In the following sub-section we describe this procedure.

Linearized State Space Model and Local Measures

Low amplitude elastic deformations, about a given rigid body equilibrium configuration x_o and for a given placement p, of an articulated flexible structure can be approximated by a finite

number of equations using the Finite Element Method (FEM) or assumed modes method as given below [12]

$$\dot{z}(t) = A_{p,x_o} z(t) + B_{p,x_o} u(t) \tag{2.2a}$$

$$y(t) = C_{p,x_o} z(t)\,, \tag{2.2b}$$

where $z \in R^m$ represents deformations and deformation rates, $u \in R^l$ is a vector of the l inputs, and $y(t) \in R^q$ is the output vector.

Using the model (2.2), we introduce two measures to determine local costs for different actuator placement. In words they are the following. (1) Subject to the constraint that a given "passive" control is used, find the placement that maximizes damping uniformly in the elastic modes. (2) Assuming all states of equation (2.2) are stabilizable and detectable, find the placement that minimizes a standard Linear Quadratic Regulator (LQR) cost functional uniformly in initial conditions and rigid body configurations.

Passive Control Case

We use the term "passive" to mean input-output passivity as defined by [13]. A dynamical system is passive if, whenever its initial states $x_0 = \underline{0}$ at time t_0, its input $u(\tau) \in R^k$ and output $y(\tau) \in R^k$ satisfy $\int_{t_0}^{t} u^T(\tau)\, y(\tau)\, d\tau \geq 0$ for all time $t > t_0$. Local collocated controllers like the rate-based damping controllers for flexible structures fall under this category. In addition to the simplicity of these passive controllers, they exhibit robustness to spill-over problems due to unmodeled dynamics [14]. For this optimization problem, let the feedback control input be specified by

$$u(t) = -K_d C_{p,x_o} z\,. \tag{2.3}$$

With this control, equation (2.2a) can be written in vector form as

$$\dot{z}(t) = \bar{A}_{p,x_o} z(t) \tag{2.4}$$

where

$$\bar{A}_{x_o,p} = A_{p,x_o} - B_{p,x_o} K_d C_{p,x_o} . \tag{2.5}$$

We measure the system performance for a particular choice of controller and placement by the decay rate of the linearized system states and therefore seek to place the poles of the system (2.4) far into the left half of the complex plane. More formally, we generate the following local cost measure at a configuration x_o and placement p.

$$c(p, x_o) \triangleq \max_i \operatorname{Re} \lambda_i(\bar{A}_{p,x_o}) \tag{2.6}$$

where $\lambda_i(\bar{A}_{p,x_o})$ is the i^{th} eigenvalue of $\bar{A}_{p,x_o}$.

Linear Quadratic Regulator Case

The Linear Quadratic Regulator (LQR) is attractive because the controller stabilizes the closed loop system and also allows for user defined weights on the inputs and states. LQR optimization has been used to reduce the structural vibrations in the control of large flexible structures in [9] , [10] and [15]. For the system described by equation (2.2), consider the infinite-horizon time-optimal control problem of minimizing a quadratic cost functional given by

$$J_u \triangleq \int_0^\infty [\, Ru(t)^2 + z^T(t) Q z(t) \,] dt \tag{2.7}$$

where R is a positive scalar. Q is a positive semi-definite matrix such that the pair $(A_{p,x_o}, Q^{1/2})$ is observable. Provided system (2.2) satisfies the standard conditions of stabilizability and detectability, the minimum cost, $\min_u J_u$, is given by $z^T(t_0) P z(t_0)$ where P is the unique positive definite solution to the algebraic Ricatti equation [16]

$$P A_{p,x_o} + A_{p,x_o}^T P - P B_{p,x_o} R^{-1} B_{p,x_o}^T P + Q = 0. \tag{2.8}$$

The corresponding control is

$$u(t) = -R^{-1} B_{p,x_o}^T P z(t). \tag{2.9}$$

We propose minimizing J_u for the worst case initial condition and therefore evaluate the local cost function as

$$c(p, x_o) \triangleq \max_{\|z_0\|=1} z_0^T P z_0 = \bar{\sigma}(P), \quad z_0 = z(t_0), \tag{2.10}$$

where $\bar{\sigma}(P)$ is the maximum eigenvalue of P implicitly dependent on the placement p. This method optimizes the local performance uniformly in initial conditions in contrast to the approach by Kondoh *et al* [9] where a solution sensitive to initial conditions is proposed.

We state the placement problem in the next sub-section.

Problem Statement

Based on the local cost measures defined in the previous section we can state the placement problem as

$$\min_{p \in X_p} C(p) \tag{2.11}$$

where the functional $C(p)$ assigns a global cost for each placement by evaluating a suitable norm on the function $c(p, .) : X_o \rightarrow R^1$. If for example, the set of equilibrium points, X_o, is contained in R^n, then two possible choices of the the function $C(p)$ are the average and worst case:

$$\frac{\int_{X_o} c(x_o, p)\, dx}{\int_{X_o} dx} \tag{2.12}$$

and

$$\max_{x_o \in X_o} c(p, x_o). \tag{2.13}$$

The measures described in the above section are used to numerically solve the problem of placing distributed piezoelectric actuators in a two-link flexible manipulator-strictive in the next section.

3. Example

The effectiveness of distributed actuators has been demonstrated for vibration reduction ([17] and [18]) and tracking control of flexible manipulators [19]. Such structures exhibit residual vibrations due to imperfections in the controller and disturbances like impacts, thermal heating and micro-gravity. For example, in space station mobile transporter units, power and weight restrictions require that only small actuators be used at the joints. Consequently the large numbe

of gear trains, required to amplify the torques provided by these small actuators, exhibit substantial friction, stiction and backlash. Therefore the joint actuators are ineffective in controlling low amplitude structural vibrations. The placement of distributed actuators plays a critical role in their ability to control these vibrations.

Experimental Set-up

The example considered is an experimental two-link truss structure (figure 1) built at UCSB. The structure has 16 spans and two articulations forming a planar manipulator. The trusses are made of aluminum and have lumped masses (net 2 kg for each link) distributed along their lengths in order to lower the modal frequencies and hence the control sample rate. In addition, the first and the second links have tip loads of 3.5 and 1 kg respectively, and their lengths are 1.8 and 1.1 m respectively. Actuation consists of low-inertia dc-motors at the two joints and an active bay with four piezoelectric actuators. Sensing consists of resolvers at the joints and collocated strain sensors on the four piezoelectric actuators. The bays structural properties are only minimaly affected by the addition of piezoelectric actuators as the the Youngs modulus of the piezoelectric actuator (83 Gpa) is similar to that of the aluminum (77Gpa) used for the truss, and the added mass is negligible compared to the lumped masses and end plates (see figure 2) at each end of the bay. However these effects will be included in the model considered for consistency. The entire structure is supported on air bearings and controlled with an Intel 386-based PC, servo amplifiers for the motors and 150V servo amplifiers for the piezoelectric actuators.

Modeling Issues

Our interest is to study piezoelectric actuator placement for optimally controlling structural vibrations. A related issue is the implementation of controllers for the distributed actuators. The problems of implementation include depoling, nonlinearity, hysteresis, and creep effects in the actuator [20]. Depoling may be avoided by maintaining the applied field below the coercive field. Within the depoling limits, the nonlinearity between applied electric field and the resulting

actuation strain may require the use of more complex models [21]. An alternative is the linearization of this relationship about the operating point [22]. Creep and strain rate dependence of the actuator become important at large strains and low frequencies. Hysteresis also plays an important role at low frequencies. Significant performance improvement over such behavior is possible by commanding the induced charge rather than the voltage applied to the actuator [23]. Other related issues due to actuator dynamics are considered in [4] and [24], but not addressed in this paper. We note, however, that piezoelectric actuators have fast dynamics relative to electromagnetic actuators and are attractive in this regard.

In this section we study the placement problem to optimally control structural vibrations when the joint motors are locked because of friction. In the flexible manipulator this corresponds to clamped boundary conditions at the joints. Our objective is to find the best placement of the active bay in the truss structure which minimizes the given cost functional. We study the actuator placement at a single shoulder joint configuration because the system dynamics are independent of the shoulder joint angle. Also, the elbow joint θ is constrained to $|\theta| \leq 90^o$ in the experiment. Then by symmetry it is sufficient to study the problem for elbow joint angles between 0^o and 90^o. Hence the set of equilibrium states X_o, containing rigid body configurations with zero elastic deflections, is parametrized by the elbow joint angle θ and is independent of the placement p.

For a given θ and $p \in X_p$, the linearized system equations for the two-link flexible manipulator generated via Finite Element Method (FEM) [1] can be written as

$$M_{p,\theta}\ddot{x} + D_{p,\theta}\dot{x} + K_{p,\theta}x = \bar{B}_{p,\theta}u_p \tag{3.1a}$$

$$y = \bar{C}_{p,\theta}x \,, \tag{3.1b}$$

where $x \in R^n$ denotes the flexible degrees of freedom. $M_{p,\theta}$, and $K_{p,\theta}$, are the mass and stiffness matrices respectively. $D_{p,\theta}$ includes a uniform structural damping coefficient (0.001) in the elastic modes. Hence the system is stable and thus trivially stabilizable and detectable. $u_p \in R^1$ is the input voltage to the actuator. The effect of the piezoelectric actuators is modeled as two point moments M (figure 3) acting at the ends of the actuator ([20] and[25]) and is included in the $\bar{B}_{p,\theta}$ matrix. The output $y \in R^1$ is obtained from a strain gauge collocated with

the actuator and is linear in the state [11]. From equation (3.1) it is seen that at each p, the system can be considered as a family of linear systems parametrized by θ. Noting that at each equilibrium point is defined by $x = \dot{x} = 0_{n\times 1}$, the state equation (3.1) can be rewritten in the form (2.2) as

$$\dot{z}(t) = A_{p,\theta} z(t) + B_{p,\theta} u(t) \tag{3.2a}$$

$$y(t) = C_{p,\theta} z(t) . \tag{3.2b}$$

where

$$z = \left[x^T \;\; \dot{x}^T \right]^T \in R^{2n} , \tag{3.2c}$$

$$A_{p,\theta} = \begin{bmatrix} O_{n\times n} & I_{n\times n} \\ -M_{p,\theta}^{-1} K_{p,\theta} & -M_{p,\theta}^{-1} D_{p,\theta} \end{bmatrix} \in R^{2n\times 2n} , \tag{3.2d}$$

$$B_{p,\theta} = \begin{bmatrix} O_{n\times 1} \\ M_{p,\theta}^{-1} \bar{B}_{p,\theta} \end{bmatrix} \in R^{2n\times 1} , \tag{3.2e}$$

and

$$C_{p,\theta} = \left[\bar{C}_{p,\theta} \;\; O_{1\times n} \right] \in R^{1\times 2n} . \tag{3.2f}$$

Controller Choice

The two measures defined in section 2 are used to generate solutions to the placement problem of the piezoelectric actuators. The passive collocated damping controller considered can be parametrized by a scalar feedback gain K_d and the feedback law can be written as [11]

$$u = -K_d \left[O_{1\times n} \;\; \bar{C}_{p,\theta} \right] z . \tag{3.3}$$

While computing the cost, an optimization is also performed over the scalar controller gain K_d. This implies that the local measure $c(p, x_o)$, with the passive damping controller is given by

$$c(p, x_o) \;\; \triangleq \min_{K_d \in R^1} \max_{i} \; \mathrm{Re}\,\lambda_i(\bar{A}_{p,x_o}) . \tag{3.4}$$

For the LQR controller based measure, weighting matrix Q is chosen to be uniform in the elastic

displacements as

$$Q = \begin{bmatrix} I_{n\times n} & 0_{n\times n} \\ O_{n\times n} & O_{n\times n} \end{bmatrix} . \tag{3.5}$$

The choice of the weight R on the control input depends on the depoling limit of the actuator and the initial conditions. For a given R, and optimal placement p_{op}, the maximum input voltage $u_{\max}(R)$ over all the configurations is found. This variation of $u_{\max}(R)$ as a function of R and α the bound on the initial conditions i.e. $\| x_o \| \leq \alpha$ is shown in figure 4. Based on depoling limits for the actuator, the maximum applied voltage is limited to $300V$ which corresponds to an applied field of $2\ MV/m$. For $\alpha = 1e-3$ which corresponds to a maximum transverse elastic deflections of approximately $3cm$, $R = 1e-6$ falls in the suitable region, with maximum input voltages below the actuator depoling limit.

Simulation Results

For a given elbow joint configuration the variation of the passive damping and LQR based costs with placement are shown in figures 8 and 9 respectively. The optimal placement at each configuration is marked by an asterik. Figure 8 shows that for all joint configurations the passive damping based cost is minimal when the placement is at the root of the first link. For the averaging global measure defined by equation (2.12), the LQR based measure resulted in a placement at the root of the second link. To illustrate the improvements achieved by the proper placement of the piezoelectric actuators, simulations of the equations of motions for the passive damping controller case are carried out. Note that there are an uncountably infinite set of possible initial conditions, and hence as many possible system responses. A major advantage of our formulation is that the design is optimized over an entire set of initial perturbations with the same energy. The *worst case* vibration response, for the passive damping case, over all configurations and all perturbations of a fixed energy is shown in figure 10, which shows the decay of the systems energy (kinetic energy + potential energy) for different placements. The rate of vibrational energy decay is maximum when the actuators are placed at the first bay. In theory, this decay rate can be arbi-

trarily chosen by appropriate feedback, but at the cost of larger inputs to the piezoelectric actuators. To avoid the saturation of these actuators, the input is penalized in the LQR controller based design measure. The average variation of these costs over the different placements is shown in figure 11 and the resultant placement of the actuator with the LQR controller is at the the root of the second link.

Discussion of Results

As the joint angle θ varies from 0 to 90^o, there is a substantial variation in the system modal frequencies. This is represented in figure 5, where the variation of the lowest modal frequency with elbow joint angle is shown. These significant (40% increase) changes in the modal frequencies might deem uniformly good placements impossible. The uniformity of placement location is a desirable result because it implies that a a single placement is effective in reducing vibrations at the different configurations. The placement based on passive damping controller is seen to be invariant with joint configuration. when the LQR based measure is used, the resultant global optimal placement (at the root of the second link) is not the best for certain configurations. For example, when the structure is fully extended, i.e. the elbow joint angle is zero, the optimal placement of the active bay (for this particular configuration) with an LQR controller is at the root of the first link. However the increase in cost due to placing the actuator at the root of the second link is negligible (1%, figure 9). Hence the placement is not very sensitive to gross changes of system configuration. This near optimality over all configurations is attributed to the relative invariance of the rotational components of the mode shapes, and is discussed next.

The placement invariance is due to the fact that in our example the *eigenvectors* are relatively invariant with the joint configuration. This is illustrated in figure 6, where the projection of the eigenvectors, associated with the least two eigenvalues, onto the rotary elastic displacements at the FEM nodes of the manipulator model is shown. These correspond to the spatial derivative of the projection of the eigenvectors onto the transverse elastic displacements of the manipulator. Note that the rotary mode shapes shown in figure 6, vary little with joint angle. As the placement

varies over the length of the manipulator, the relative control over each mode and its variation are determined by these mode shapes [24]. Consequently, the invariance of these mode shapes with the joint angle implies the relative invariance of the distribution of effective control over different modes. It is this control distribution of the different modes that determines the cost for the possible placement and therefore its invariance results in a uniformly good placement.

The performance measure based on passive damping is determined by the distance of system eigenvalues from the imaginary axis. This distance is an estimate of the slowest decay rate of elastic perturbations in the structure. In our example, the decay rate tends to increase with the elbow joint-angle as shown in figure 7. This is mainly due to the increase in the system natural frequencies, but with constant structural damping. For such a system, the elastic vibration modes associated with higher modal frequencies tend to have higher decay rates. Thus in the case of the passive controller based performance measure, it is the variation of the eigenvalue associated with the lowest frequency that determines the cost and therefore the placement. To control a single eigenvector, the optimal placement is at the location of maximum strain [26] where the effective control over that mode is maximized. Hence the passive damping based measure yields the placement at the first span of the structure. As discussed above, this placement is uniformly good for all joint configurations because the *rotary* mode shapes are relatively invariant.

The LQR based performance measure resulted in a placement where the control objective to minimize the quadratic cost functional given by equation (2.7) is achieved. The optimization of this quadratic cost functional results in a compromise placement between high decay rates of perturbations and small control effort. Note that the placement obtained on using this performance measure is relatively good over all configurations. Thus the invariance of the mode shapes resulted in placements which were near-optimal for each of the possible configurations. In the next section we study a class of AFS where such uniformly good actuator placements can be expected.

4. Mode Shape Invariance in Structures with Joint Dominated Inertias

In this section we show that "high frequency" mode shapes are configuration invariant in AFS with joint dominated inertias. We also show that this invariance results in actuator placements which are uniformly good over different configurations. We begin with the following lemma dealing with the eigenvalues and eigenvectors of a singularly perturbed eigenvalue problem arising in our analysis.

Lemma

Consider the problem of finding the eigen pair (λ, v), $v \triangleq [v_1\ v_2]^T$, which satisfies

$$\begin{bmatrix} \lambda A_{11}+B_{11} & \lambda A_{12}+B_{12} \\ \lambda A_{21}+B_{21} & \lambda A_{22}/\varepsilon+\lambda\delta_{22}+B_{22} \end{bmatrix} \begin{bmatrix} v_1 \\ v_2 \end{bmatrix} = \underline{0}, \tag{5.1}$$

where $A_{11} \in R^{n\times n}$, $A_{22} \in R^{m\times m}$, the other submatrices A_{21}, A_{12}, etc. have compatible dimensions, and $\det(A_{22}) \neq 0$.

Then

(1) The eigenvalues of the singularly perturbed system are close to the roots of $\det(lambdaA_{11}+B_{11})=0$, or are close to zero. More precisely, given $r>0$, there exists $\varepsilon_0(r)>0$ such that $0<\varepsilon\leq\varepsilon_0(r)$ implies

$$|\lambda_i(\varepsilon)-\beta_i| < r, \qquad i=1,\ldots,n, \text{ and} \tag{5.2}$$

$$|\lambda_i(\varepsilon)| < r, \qquad i=n+1,\ldots,n+m, \tag{5.3}$$

where $\{\beta_1,\ldots,\beta_n\}$ are the roots of $\det[\beta A_{11}+B_{11}]=0$, and $(\lambda_i(\varepsilon), v_i(\varepsilon))$ are solutions to (5.1) (renumbered if necessary), with the dependence on ε explicitly stated.

(2) If λ_i is an eigenvalue satisfying (5.2) is not too small (i.e. $\beta_i \neq 0$), then the norm of $v_{i,2}$ is small relative to $v_{i,1}$. That is, for all $\beta_i \neq 0$, given $r>0$, there exists $\varepsilon_1(r)>0$ such that $0<\varepsilon\leq\varepsilon_1(r)$ implies

$$\| v_{i,2}(\varepsilon) \|_2 < r \| v_{i,1}(\varepsilon) \|_2, \qquad i = 1,\ldots,n \tag{5.4}$$

where (λ_i, v_i) is the solution to (5.1) such that $\| v_i \|_2 = 1$.

Proof

(1) This follows from standard arguments in singular perturbations theory,

for example, see [27].

(2) if $\beta_i \neq 0$, from equation (5.1),

$$\left\{ \lambda A_{22}/\varepsilon + \lambda \delta_{22} + B_{22} \right\} v_{i,2} = -\left[\lambda A_{21} + B_{21} \right] v_{i,1}. \tag{5.5}$$

By continuity of matrix inversion in a neighborhood of A_{22}, given $\delta_1 > 0$ there exists $\varepsilon_{i,2}(\delta_1) > 0$ such that, whenever $0 < \varepsilon \leq \varepsilon_{i,2}(\delta_1)$,

$$\| \left[\beta_i A_{22} + \varepsilon \beta_i \delta_{22} + \varepsilon B_{22} \right]^{-1} \|_2 < \varepsilon \frac{\| A_{22}^{-1} \|_2}{|\beta_i|} (1 + \delta_1). \tag{5.6}$$

Choose $\varepsilon_{i,0}$ (from first part of the theorem) such that $0 < \varepsilon \leq \varepsilon_{i,0}$ implies that $|\lambda_i - \beta_i| < \frac{|\beta_i|}{2}$. Let $\varepsilon_{i,3} \triangleq \min(\varepsilon_{i,0}, \varepsilon_{i,2}(1))$.

Then

$$\| v_{i,2} \|_2 < \frac{4 \varepsilon K}{|\beta_i|} \| A_{22}^{-1} \|_2 \| v_{i,1} \|_2 \tag{5.7}$$

whenever $0 < \varepsilon \leq \varepsilon_{i,3}$, where

$$K \triangleq \max \left\{ \| \left[\beta_i A_{21} + B_{21} + |\beta_1| \frac{A_{21}}{2} \right] \|_2, \| \left[\beta_i A_{21} + B_{21} - |\beta_1| \frac{A_{21}}{2} \right] \|_2 \right\} \tag{5.8}$$

If $K = 0$ then choose $\varepsilon_1 = \varepsilon_3$, else choose $\varepsilon_1 = \min_{i=1,\ldots,n} \left[\varepsilon_{i,3}, \frac{r |\beta_i|}{4 K \| A_{22}^{-1} \|_2} \right]$.

Then for all ε such that $0 < \varepsilon \leq \varepsilon_1$,

$$\| v_{i,2} \|_2 < r \| v_{i,1} \|_2 \tag{5.9}$$

and this completes the proof. □

Next we use the lemma to show that for planar AFS (figure 12) 1) consisting of interconnected beams and 2) having joint dominated inertias, the modal frequencies can be partitioned into two groups. One "low frequency" set corresponds to eigenvalues that tend to zero as the joint inertias become large. The other group of relatively "higher frequency" modes corresponds to the eigenvalues of the AFS, simply supported at the joints. We show that these high frequency mode shapes are joint configuration invariant. Due to bandwidth restrictions, joint actuators on the AFS are ineffective in controlling these high-frequency vibrations, but the distributed actuators are highly effective in controlling them. Due to the invariance of these mode shapes in AFS with joint dominated inertias, we can expect to find distributed actuator placements that are uniformly good over all joint configurations.

To show the mode shape invariance we generate a dynamic model for the beams Using the Finite Element Method (FEM), with degrees of freedom (dof) as shown in figure 13, each of the individual beam's mass and stiffness matrices can be assembled to obtain the total mass and stiffness matrices, M_t and K_t, of the structure. The system equations can be written as

$$M_t \ddot{X} + K_t X = B F, \tag{5.10}$$

where F is the external force. X can be partitioned into X_1 and X_2, where the later consists of the translational dof at the joints. Moreover, the matrices M_t and K_t can be partitioned such that the dynamic equations become

$$\begin{bmatrix} M_{11} & M_{21} \\ M_{12} & M_{22} \end{bmatrix} \begin{bmatrix} \ddot{X}_1 \\ X_2 \end{bmatrix} + \begin{bmatrix} K_{11} & K_{21} \\ K_{12} & K_{22} \end{bmatrix} \begin{bmatrix} X_1 \\ X_2 \end{bmatrix} = B F \,, \tag{5.11}$$

where

$$X_2 = \begin{bmatrix} X_{j(1)} \\ Y_{j(1)} \\ X_{j(2)} \\ Y_{j(2)} \\ \cdots \\ \cdots \\ X_{j(n)} \\ Y_{j(n)} \end{bmatrix} \tag{5.12}$$

represents the translational degrees of freedom at the joints. Since all degrees of freedom, except those of the joints, are defined in local beam co-ordinates, only the joint related inertias (M_{12}, M_{21}, M_{22}) and stiffnesses (K_{12}, K_{21}, K_{22}) are dependent on the joint angles, θ_k. However, $M_{11} \in R^{n \times n}$ and $K_{11} \in R^{n \times n}$, which also include terms corresponding to the rotary degrees of freedom, are *independent* of θ_k. The submatrix $M_{22} \in R^{m \times m}$ consists of two components-- the contribution from the joint masses M_{joints}, and the contribution from the link inertias, δ_{22}. Since M_{joints} is large by assumption, we express it as $\frac{M^*}{\varepsilon}$, where ε is small. Therefore M_{22} can be written as

$$M_{22} = \frac{M^*}{\varepsilon} + \delta_{22} \tag{5.13}$$

Note that δ_{22} depends on θ_k, and M^* does not. For the system described by 5.11, its eigenvalues λ_i and the corresponding eigenvectors, v_i, satisfy

$$\begin{bmatrix} \lambda_i M_{11} - K_{11} & \lambda_i M_{12} - K_{12} \\ \lambda_i M_{21} - K_{21} & \lambda_i M^*/\varepsilon + \lambda_i \delta_{22} - K_{22} \end{bmatrix} \begin{bmatrix} v_{i,1} \\ v_{i,2} \end{bmatrix} = \underline{0}. \tag{5.14}$$

From the lemma proved earlier, in the limit as $\varepsilon \to 0$ (large joint inertias), the system eigenvalues can be partitioned into the "high frequency" group $\left\{ \bar{\alpha}_i \right\}_{i=1}^{i=m}$ and the "low frequency" $\left\{ \underline{\alpha}_j \right\}_{j=1}^{j=n}$, such that

$$\lim_{\varepsilon \to 0} | \bar{\alpha}_i - \beta_i | = 0 \tag{5.15}$$

$$\lim_{\varepsilon \to 0} | \underline{\alpha}_i | = 0 \tag{5.16}$$

where β_i satisfies $\det \left[\beta_i M_{11} - K_{11} \right] = 0$. Moreover, in the limit as $\varepsilon \to 0$, the eigenvectors $\bar{v}_i$, corresponding to $\bar{\alpha}_i$, are those of the structure, simply supported at the joints. Hence

$$\bar{v}_{i,2} = \underline{0}, \tag{5.17}$$

$$\bar{\alpha}_i M_{11} \bar{v}_{i,1} = K_{11} \bar{v}_{i,1}. \tag{5.18}$$

Since M_{11} and K_{11} are independent of joint configurations, equation 5.18, and consequently the eigenpairs $(\bar{\alpha}_i, \bar{\nu}_i)$ are also configuration invariant in AFS with joint dominated inertias. Hence the associated "high frequency" mode shapes and in particular their rotary components do not change much with joint configuration if ϵ is small. This leads to placements that are good over large variations in joint configurations as discussed in section 3. The above arguments can also be extended for spatial AFS with complex structural connections between joints. Thus we can expect to find uniformly good distributed actuator placements in AFS with joint dominated inertias.

5. Conclusion

In this paper we formulated the actuator placement for Articulated Flexible Structures. Two closed loop performance criteria were considered to derive objective functions for optimum placement of actuators in such systems. The procedures, developed independent of initial conditions and formulated as eigen-value problems, are easy to compute. In the example two-link manipulator, these measures are computationally tractable and effective to solve the distributed actuator placement problem for optimal structural vibration reduction. An important observation is that the mode shapes associated with nodal rotations for the example two-link flexible manipulator are relatively invariant with joint configuration. This invariance resulted in a placement which is effective in reducing vibrations over all the different configurations. We further investigate the invariance of the mode shapes and identify a class of articulated structures, with joint dominated mass distributions, where we can expect such uniformly good placements.

The measures suggested in this paper can also be used for actuator placement in set point controllers of nonlinear systems. In this sense the approach is a modest attempt at the larger problem of nonlinear actuator placement. The existence and computability of optimal designs for general trajectory tracking in nonlinear systems is the subject of further work.

Acknowledgment

Support from the Air Force Office of Scientific Research through grant F9620-91-C-0095 and the Astro Aerospace Corporation is gratefully acknowledged.

References

1. E. Bayo, M.A. Serna, P. Papadopoulos, and J. Stubbe, "Inverse Dynamics and Kinematics of Multi-Link Elastic Robots. An Iterative Frequency Domain Approach," *The International J. of Robotics Research*, vol. 8, No 6, Dec 1989.

2. D. Kwon and W.J. Book, "An inverse dynamic method yielding flexible manipulator state trajectories," *Proc. of ACC*, pp. 186-193, 1990.

3. B. Paden, D. Chen, R. Ledesma, and E. Bayo, "Exponentially Stable Tracking Control for Multi-joint Flexible_Link Manipulators," *ASME Journal of Dynamic Systems, Measurement and Control*, vol. To Appear.

4. J.L. Fanson and J.A. Garba, "Experimental Studies of Active members in Control of Large Space Structures," *Proc. AIAA 29th SDM Conf.*, pp. 9-17, 1988.

5. A. Messac and K. Malek, "Control-Structure Integrated Design," *AIAA Journal*, vol. 30. No 8, pp. 2124-2131, Aug 1992.

6. I. M. Jin and L. A. Schmit, "Control Design Variable Linking for Optimization of Structural/Control Systems," *AIAA Journal*, vol. 30 No. 7, pp. 1892-1900, July 1992.

7. E. F. Crawley and J. De Luis, "Use of Piezoelectric Actuators as Elements of Intelligent Structures," *AIAA Journal*, vol. 25, No 10, pp. 1373-1385, 1985.

8. A. Arbel, "Controllability Measures and Actuator Placement in Oscillatory Systems," *Int. J. Control*, vol. 33, No.3; pp. 565-574, 1981.

9. S. Kondoh, C. Yatomi, and Koichi Inoue, "The Positioning of Sensors and Actuators in the Vibration Control of Flexible Systems," *JSME International Journal*, vol. 33, No.2, pp. 145-152, 1990.

10. S. Fisher, "Application of Actuators to Control Beam Flexure in a Large Space Structure," *J. Guidance*, vol. 12, No.6, pp. 874-879, Dec 1989.

11. S. Devasia, T. Meressi, B. Paden, and E. Bayo, "Piezo-Electric Actuator Design for Vibration Suppression: Placement and Sizing," *Proc. of CDC*, Dec,1992.

12. R. R. Craig, *Structural Dynamics, An introduction to Computer Methods*, John Wiley & Sons, inc . 1981.

13. P. J. Moylan, "Implications of Passivity in a Class of Nonlinear Systems," *IEEE Transactions on Automatic Control*, vol. AC-19, No. 4, pp. 373-381, 1974.

14. A. Bhaya and C. A. Desoer, "On the Design of Large Flexible Space Structures(LFSS)," *IEEE trans. on Automatic Control*, vol. AC-30, No.11, pp. 1118-1120, Nov,1985.

15. G. P. Gibbs and C. R. Fuller, "Experiments on Active Control of Vibrational Power Flow Using Piezoceramic Actuators/Sensors," *AIAA Journal*, vol. 30 No. 2, pp. 457-463, Feb 1992.

16. H. Kwakernaak and R. Sivan, *Linear Optimal Control Systems*, Wiley-Interscience, 1972.

17. M. J. Balas, "Active Control of Flexible Systems," *Journal of Optimization Theory and Applications*, vol. 25, No 3, pp. 415-436, 1978.

18. L. Meirovitch and H. Baruh, "Control of Self-Adjoint Distributed-Parameter Systems," *AIAA*, vol. 5, No 1, pp. 60-66, 1980.

19. S. Devasia and E. Bayo, "Inverse Dynamics: Simultaneous Trajectory Tracking and Vibration Reduction with Distributed Actuators," *Journal of Dynamics and Control* , Accepted for Publication, 1993.

20. E. F. Crawley and E. H. Anderson, "Detailed Models of Piezoceramic Actuation of Beams," *J. of Intell. Mater. Syst. and Struct.*, vol. 1, pp. 4-25, Jan, 1990.

21. Crawley E. F. and Lazarus K.B., "Induced Strain Actuation of Isotropic and Anisotropic Plates," *AIAA Paper 89-1326, 30th AIAA Structural, Structural Dynamics and Materials Conference*, 1989.

22. J. De Luis, "Design and Implementation of Optimal Controllers for Intelligent Structures Using Infinite Order Structural Models," *PhD Thesis*, MIT, Cambridge, MA, 1989.

23. R.H. Comstock, "Charge Control of Piezoelectric Actuators as Elements of Intelligent Structures," *AIAA Journal*, vol. 25, No 10, pp. AIAA paper 86-0878, Oct 1987.

24. J.L. Fanson and T.K. Caughey, "Positive Position Feedback Control for Large Space Structures," *AIAA Journal*, vol. 28, No.4, pp. 717-724, April 1990.

25. C. J. Goh and T. K. Caughey, "On the Stability Problem Caused by Finite Actuator Dynamics in the Collocated Control of Large Space structures," *Int. J. Control*, vol. 41, No. 3, pp. 787-802, 1985.

26. E. F. Crawley and J. De Luis, "Use of Piezo-ceramics as distributed actuators in large space structures," *AIAA Journal*, pp. 126-133, 1985.

27. Vidyasagar, M., *Nonlinear System Analysis*, pp. 126-128, Prentice-Hall, 1978.

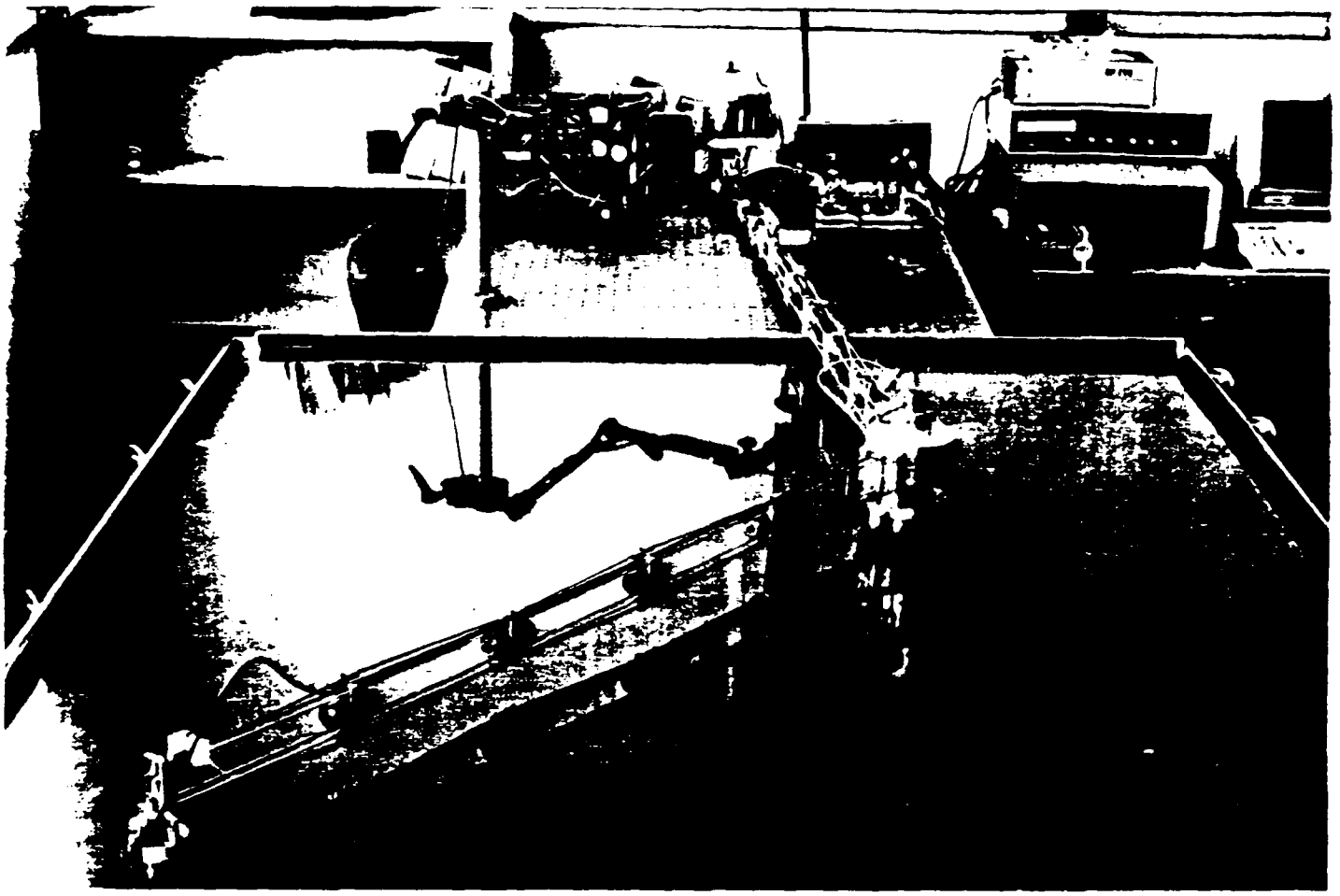

Figure 1. Experimental Smart Flexible Structure

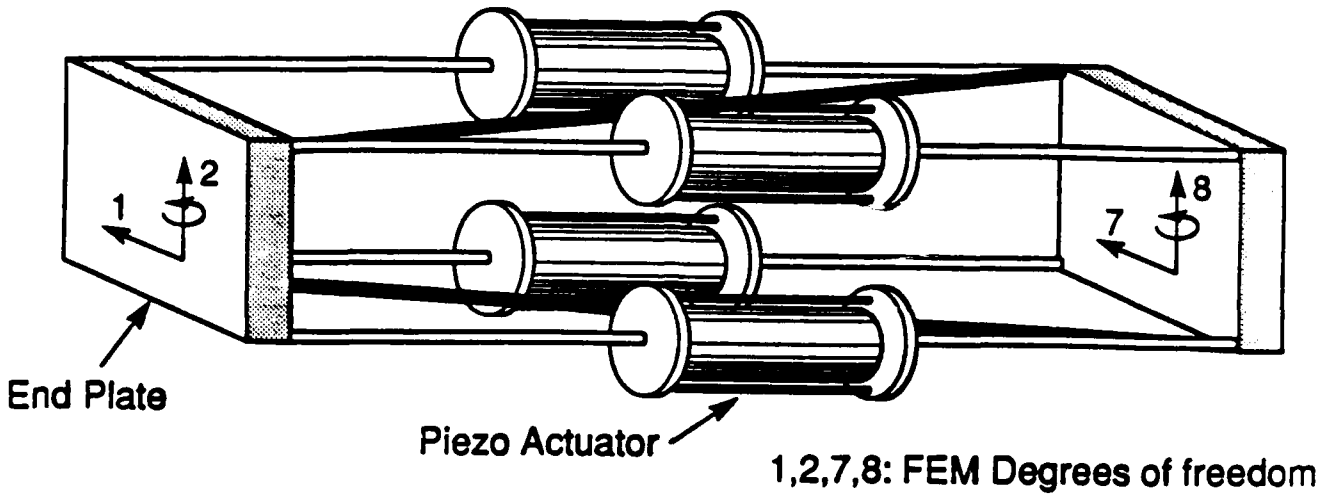

Figure 2. The Active Bay

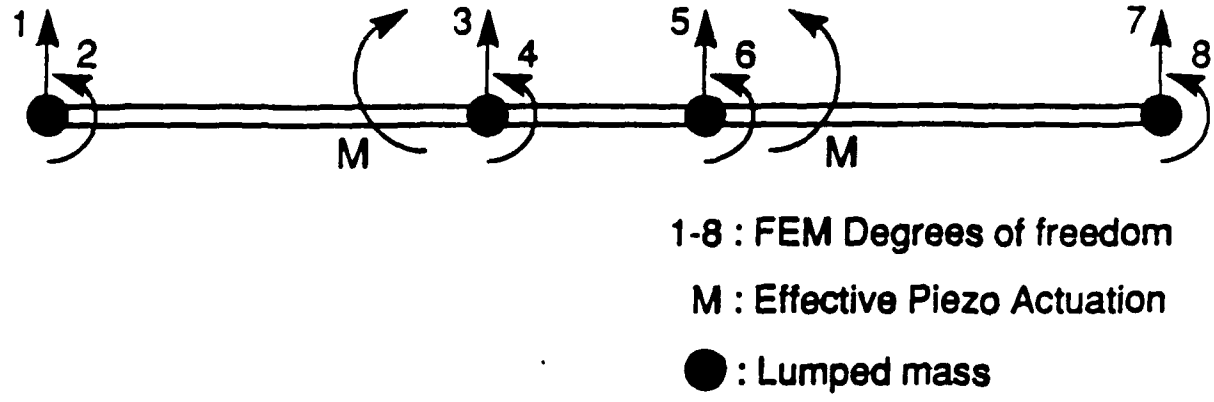

Figure 3. Equivalent FEM representation

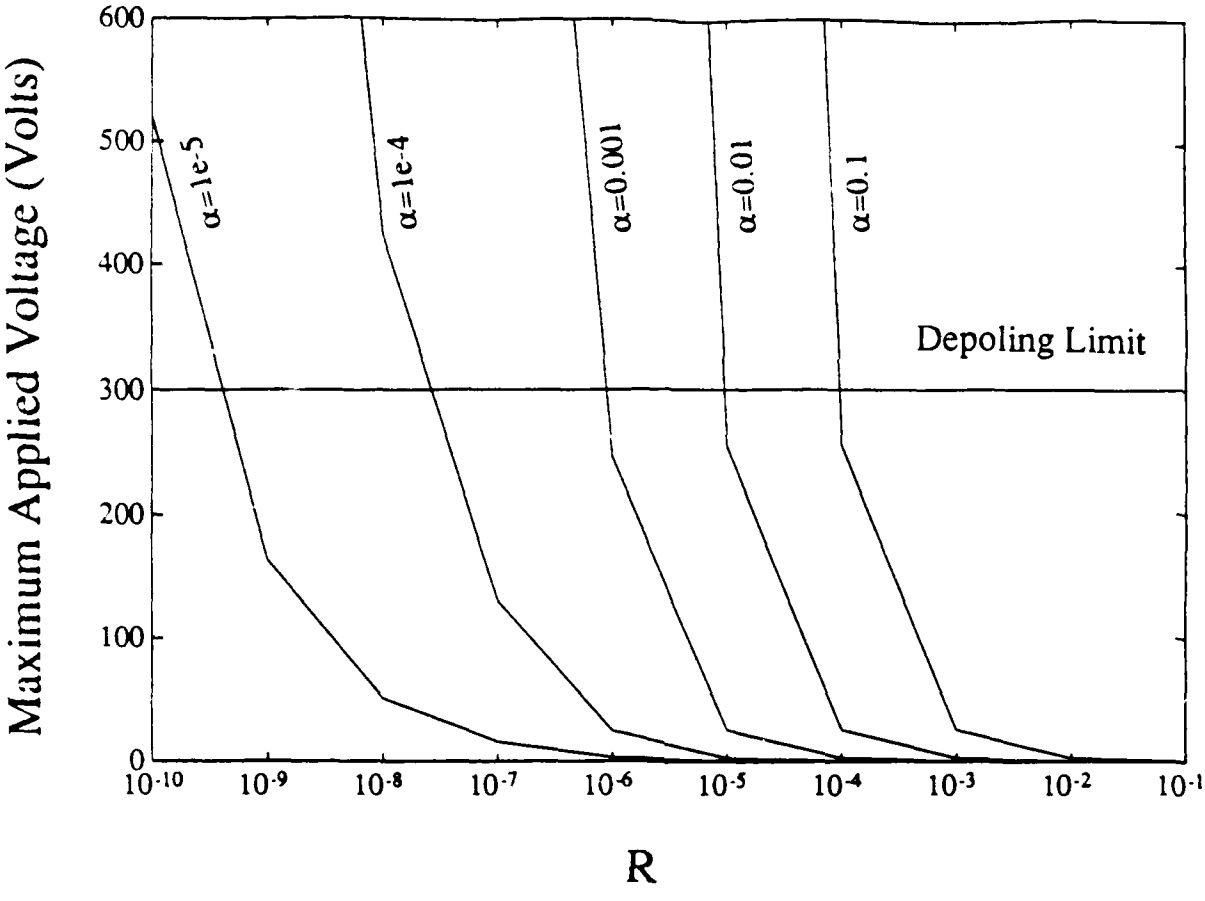

Figure 4. Variation of Maximum Applied Voltage with R

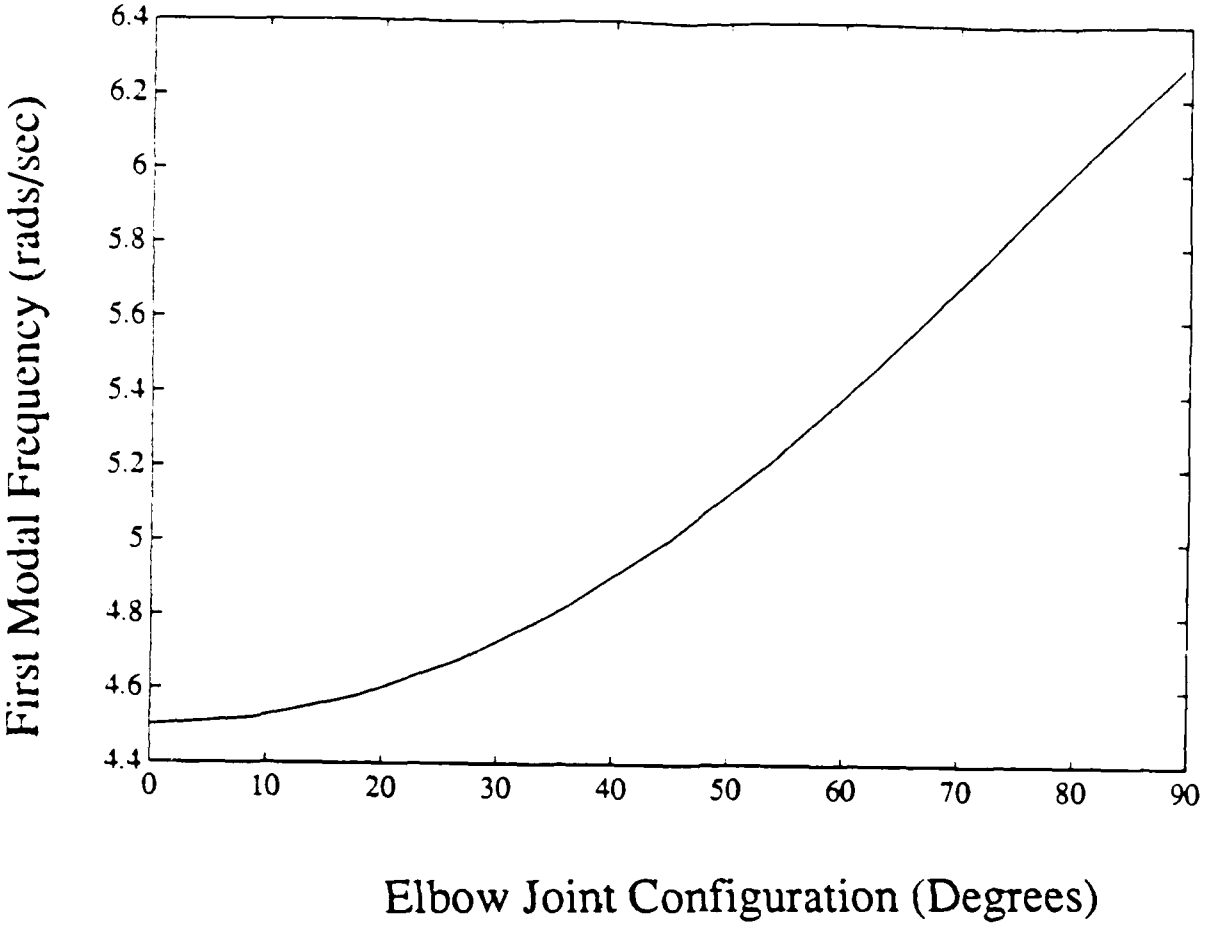

Figure 5. Variation of First Modal Frequency of the Structure

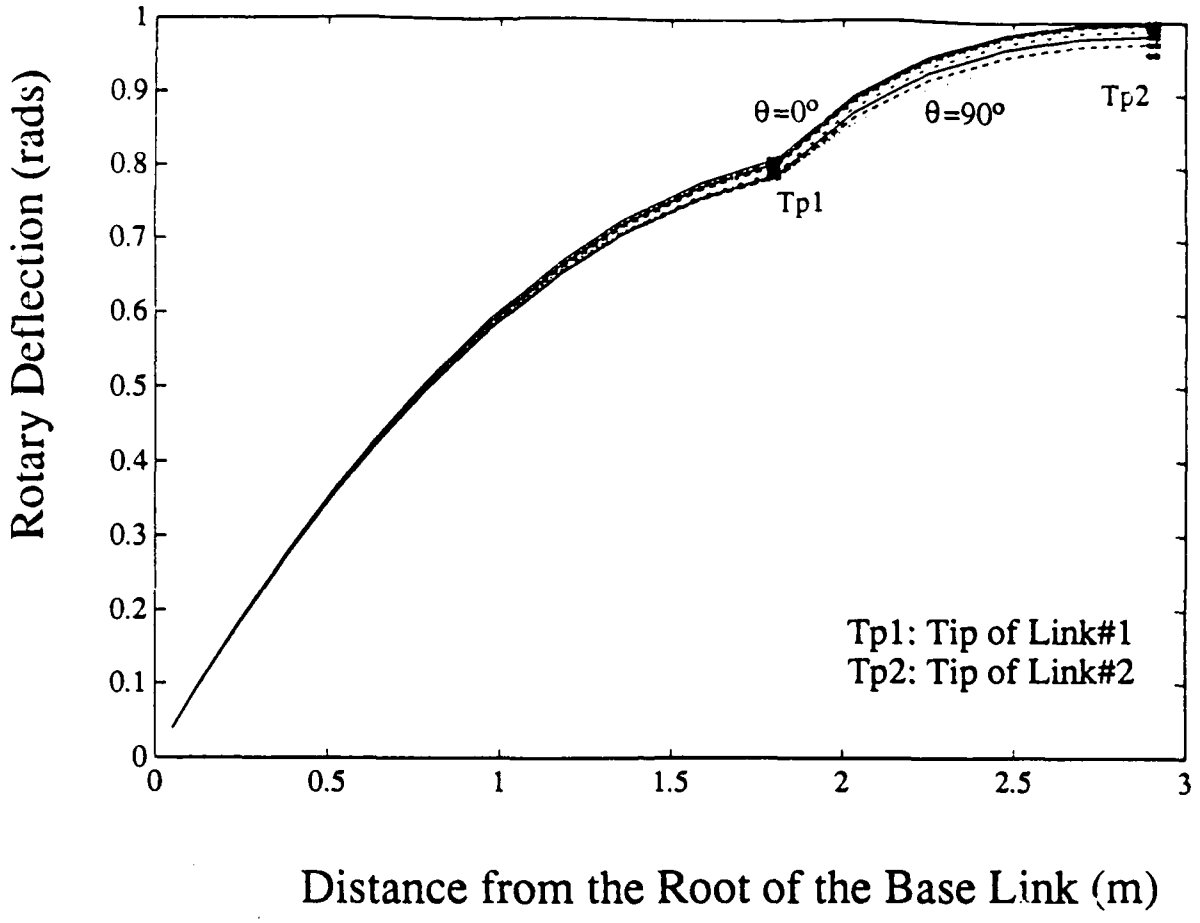

Figure 6a. Variation of Rotary Components of the 1st Eigenvector with Joint Configuration

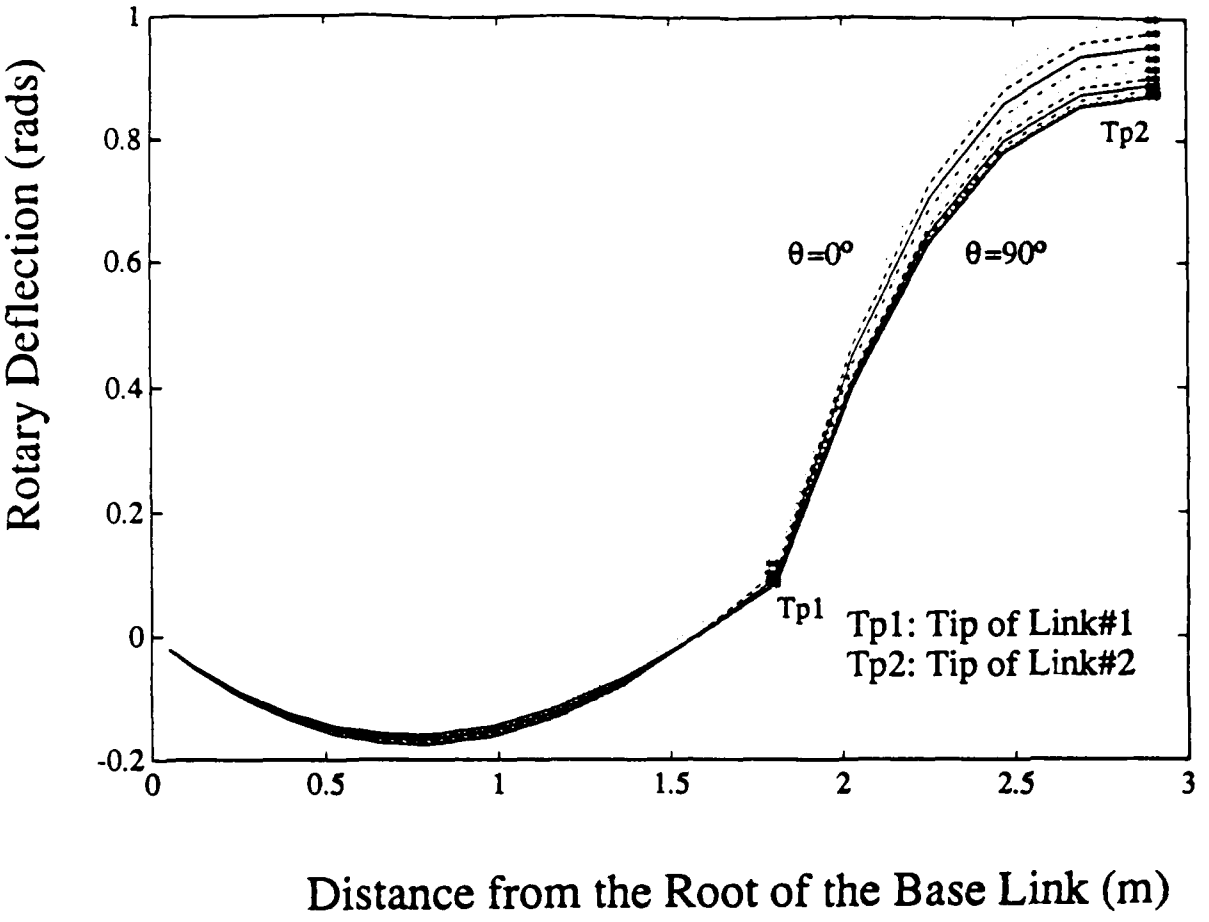

Figure 6b. Variation of Rotary Components of the 2nd Eigenvector with Joint Configuration

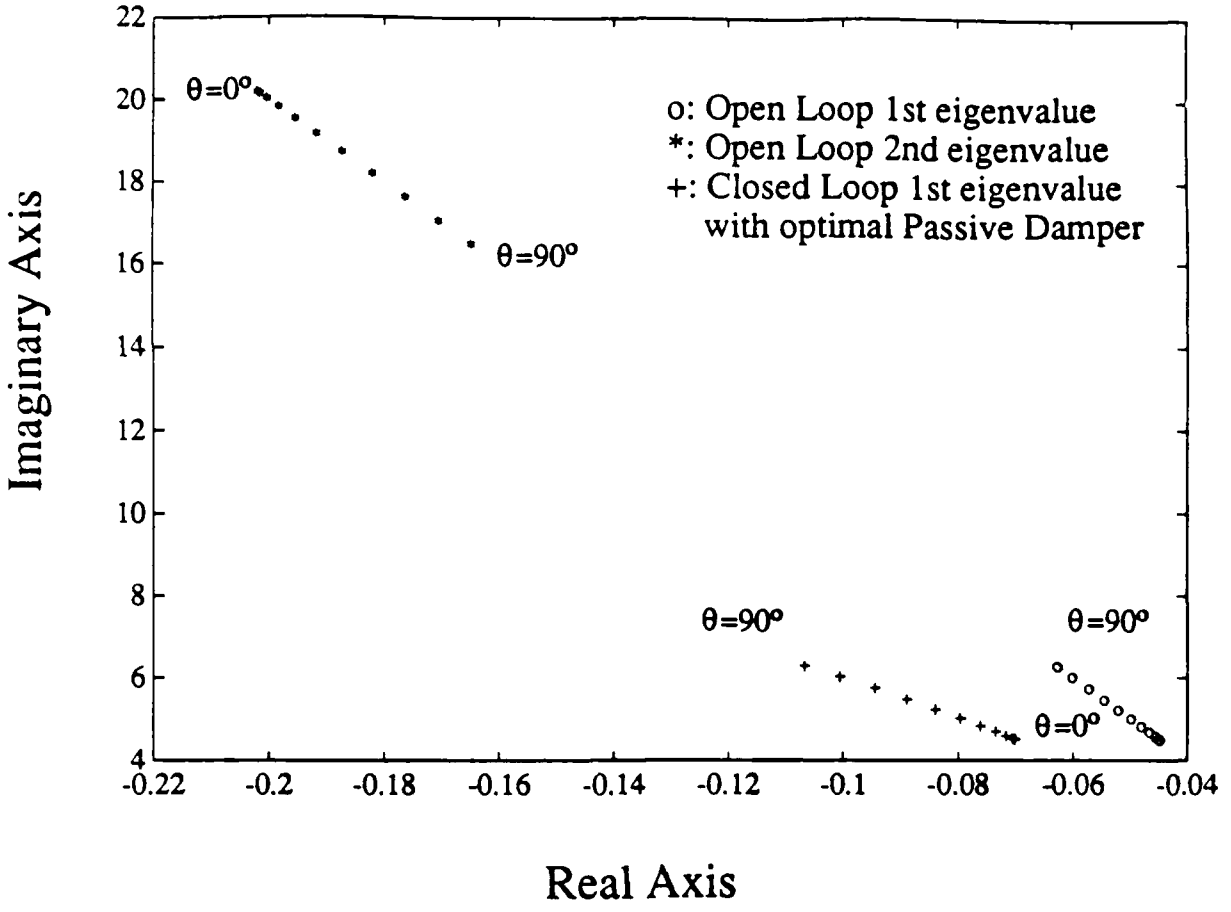

Figure 7. Variation of Eigenvalues with Joint Configuration

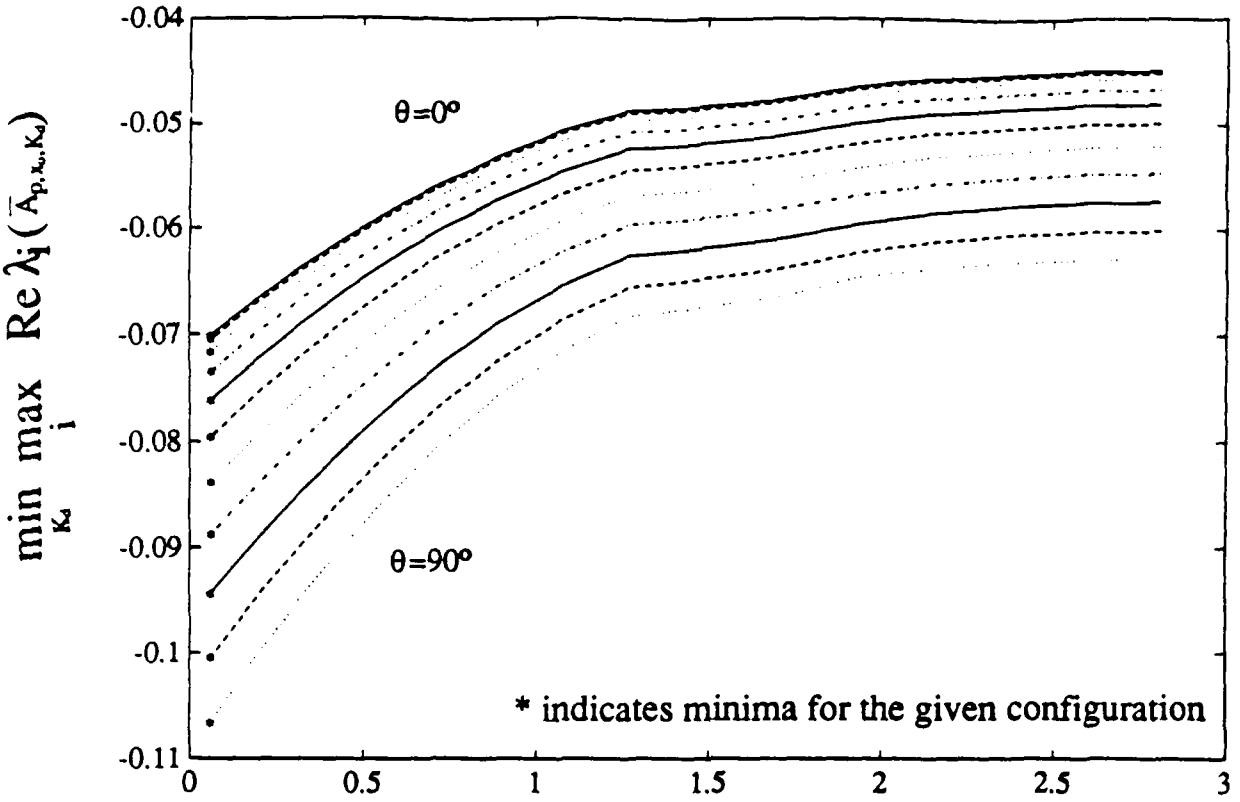

Figure 8. Variation of Passive Damping Based Cost over Joint Configurations

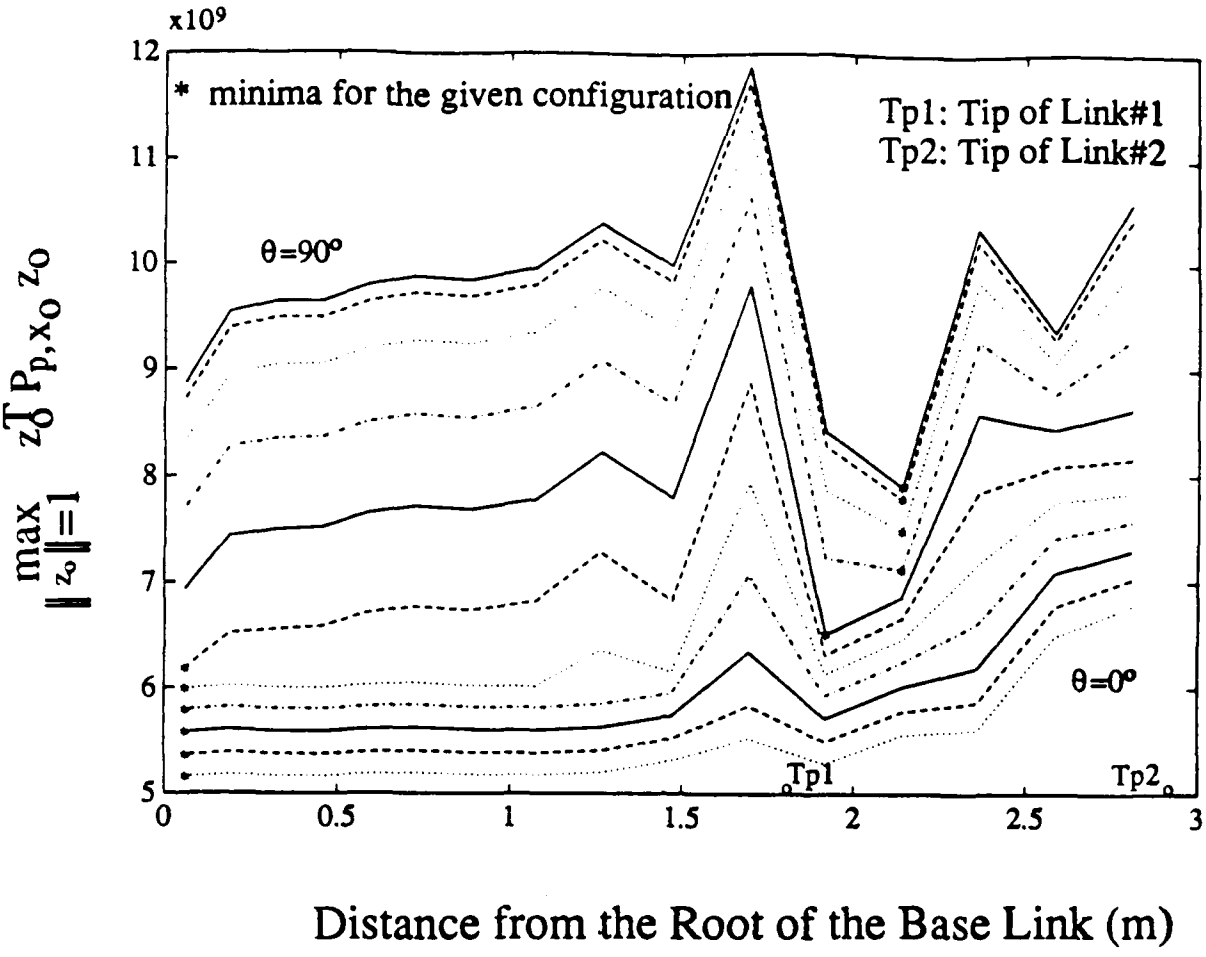

Figure 9. Variation of LQR Based Cost Measure over Joint Configurations

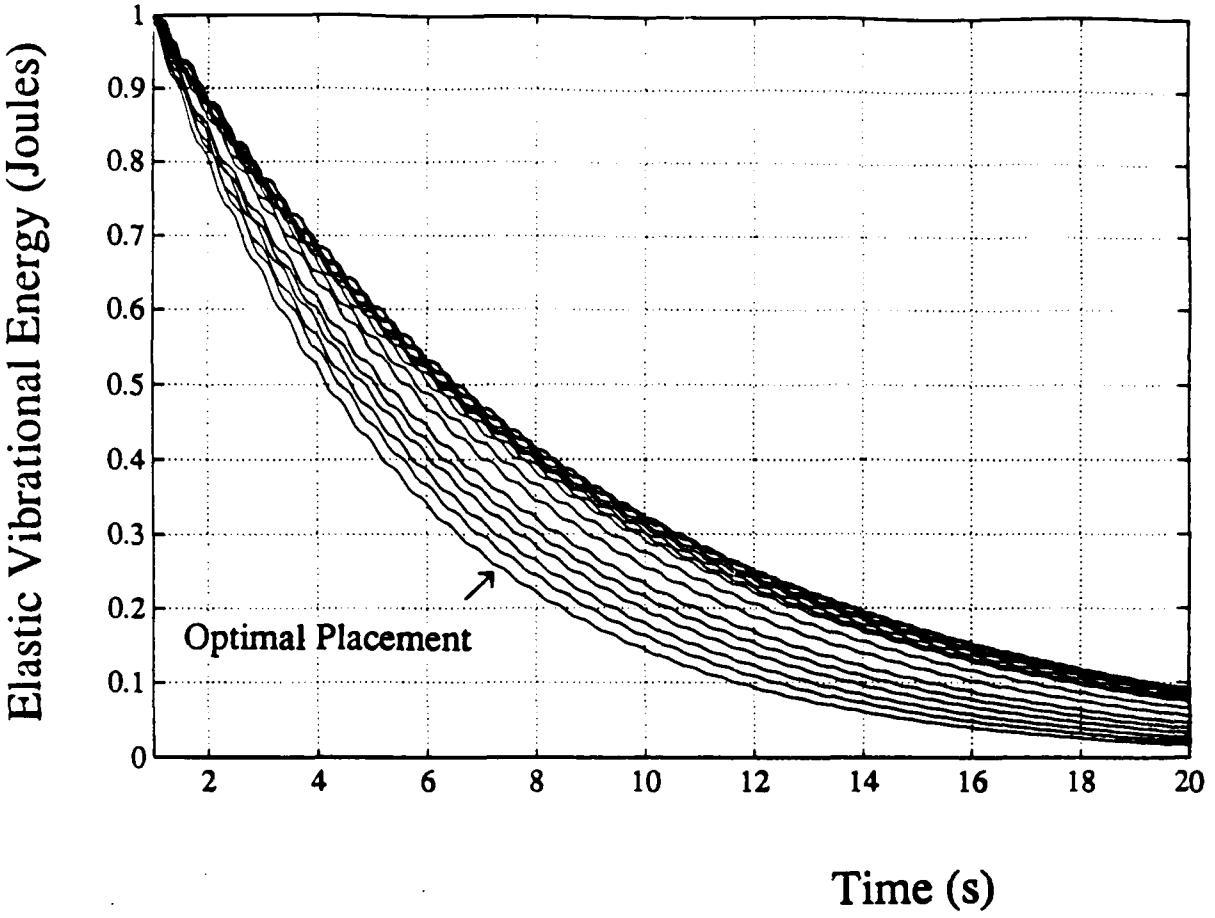

Figure 10. Worst Case Vibration Response for Different Placements

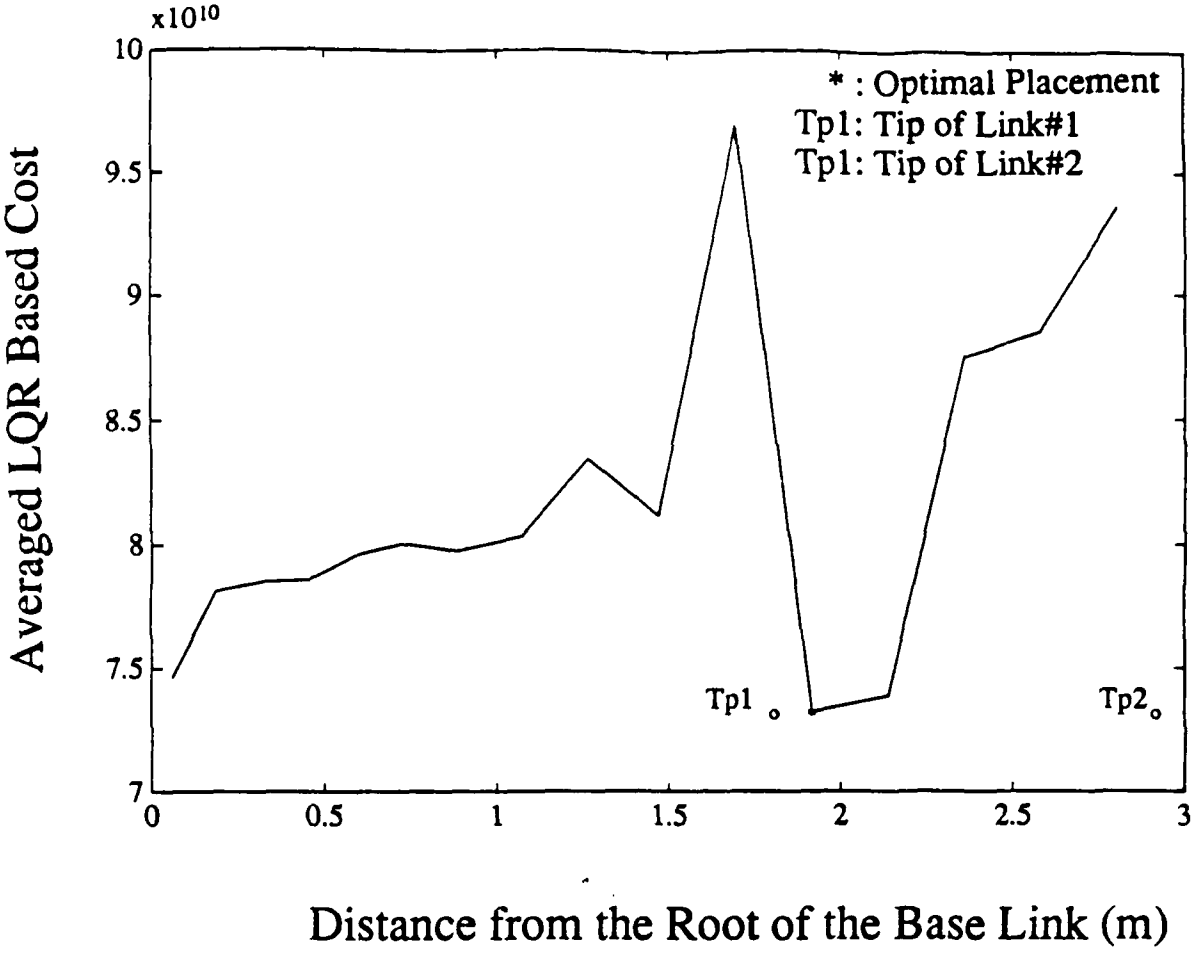

Figure 11. The Average Global LQR Based Cost for Different Placements

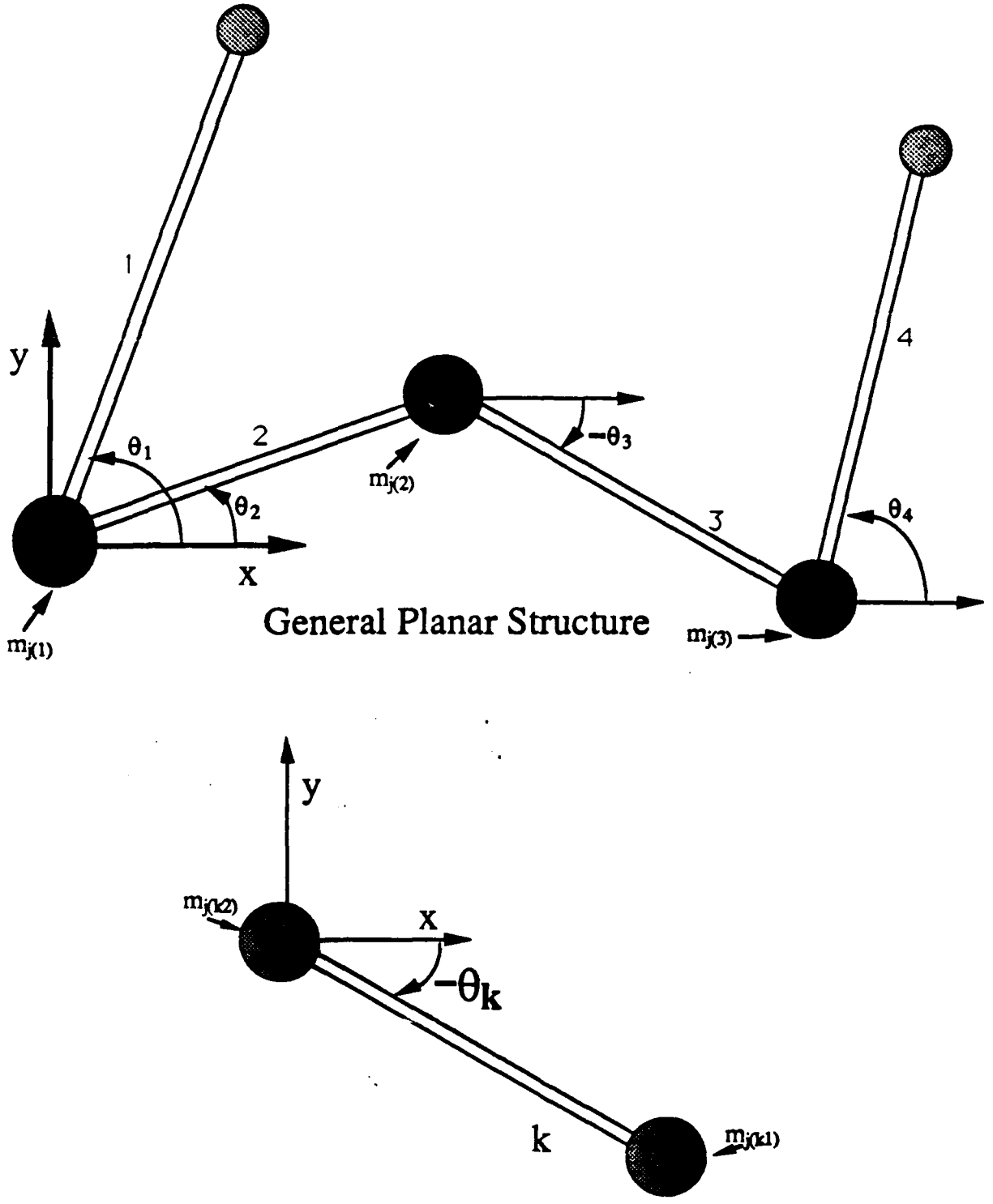

Figure 12. The k^{th} Beam Segment of a General Planar Structure

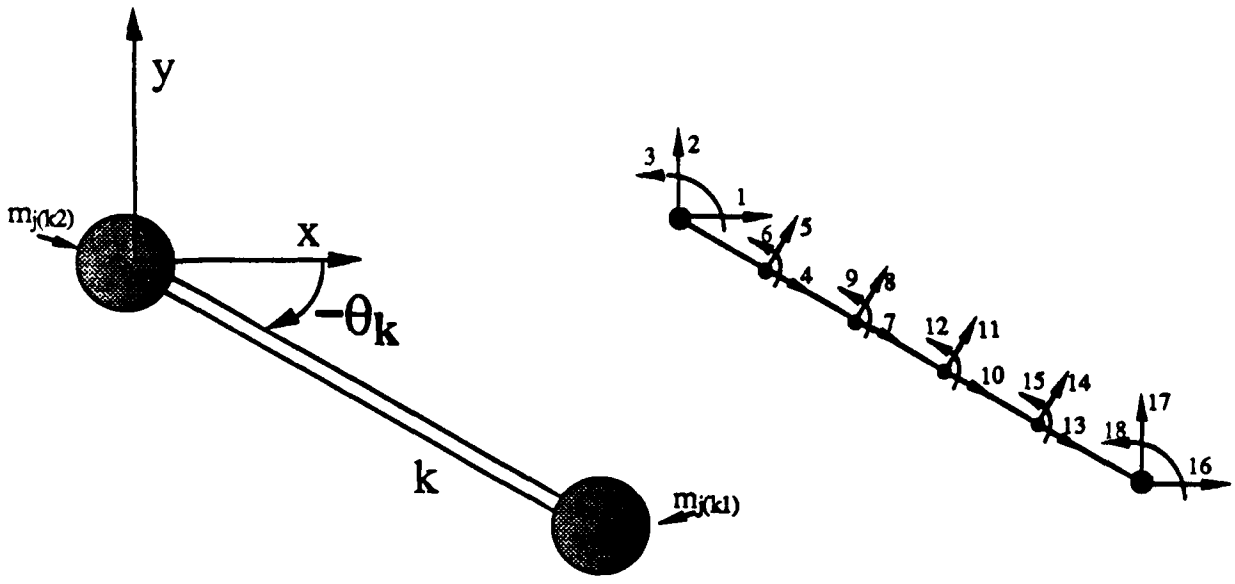

Figure 13. Global FEM Degrees of Freedom of Beam Element

Redundant Actuators to Achieve Minimal Vibration Trajectory Tracking of Flexible Multibodies: Theory and Application

SANTOSH DEVASIA and EDUARDO BAYO
Mechanical & Environmental Engineering Department, University of California, Santa Barbara, CA 93106

Abstract. We address the problem of inverse dynamics for flexible multibodies, which arises, in trajectory tracking control of flexible multibodies such as space manipulators and articulated flexible structures. Previous research has resolved this trajectory tracking problem by computing the system inputs for feedforward control of actuators at the joints. Recently, the use of distributed actuators like electro-strictive actuators in flexible structures has introduced a new dimension to this trajectory tracking problem. In this paper we optimaly utilize such actuators to aid joint actuators for tracking control, and introduce a new inverse dynamics scheme for simultaneously (1) tracking a prescribed trajectory and (2) minimizing ensuing elastic deflections. We apply this scheme for trajectory tracking of a two-link two-joint planar manipulator with joint motors and distributed electro-strictive actuators. Experimental results are presented to contrast our new scheme with other existing methods.

Key words: Flexible articulated structures, multibody dynamics, actuator redundancy, trajectory tracking, inverse dynamics.

1. Introduction

Inverse dynamics provides an excellent means for trajectory tracking of flexible multibodies. Methods to precompute the actuator inputs required to exactly track a given output trajectory of a control point on a single link flexible arm were provided by Bayo [1] and by Kwon and Book, [2]. The solution for multi-link open-chain applications has been proposed by Bayo et al. [3] where the inverse dynamics and kinematics produce bounded feedforward inputs for actuators, like motors at articulations and joint angles, to track a reference point on the structure. The closed-chain planar case has been recently presented by Ledesma and Bayo [4]. If the sensors and actuators are non-collocated then the flexible structure has *nonminimum* phase dynamics and the only stable inverse dynamics solution to the tracking problem is *non-causal* [5]. Once a trajectory is specified, the feedforward control input obtained by inverse dynamics for exact trajectory tracking, has a unique bounded solution. Therefore, the subsequent elastic structural vibrations induced on the structure (except at the control point where these vibrations are zero) during the trajectory tracking motion are also defined uniquely. These vibrations could be detrimental to the performance of sensitive on-board systems and hence it is desirable to minimize

them. For some time, distributed actuators have been strongly considered successfully used to to control structural vibrations ([6] and [7]). Recent success in their experimental use [8] motivates the use of such actuators to aid joint actuators, like motors, for trajectory tracking.

The trajectory tracking objective can be accomplished by the point actuators alone [9] and in this sense the distributed actuators are redundant. In this paper we introduce the concept of using the extra actuation available through the distributed actuators in the structure to not only satisfy the trajectory tracking constraint, but also minimize the accompanying elastic displacements during the motion. A new inverse dynamics method is presented to compute the feedforward inputs which includes the cases of redundantly actuated structures. This use of distributed actuators for end effector trajectory control is contrasted with the use of only the joint actuators in feedforward. The method proposed here is shown to substantially reduce the induced vibrations in the structure. The results are experimentally verified using a flexible two link articulated truss structure with distributed electro-strictive actuators and joint motors. We also present a novel strain based control scheme for electro-strictive actuators which is very effective in reducing hysterisis and other non-linear effects pre-dominant in such actuators.

The remainder of the paper is organized in the following format. Modeling of flexible multibodies with joint and distributed actuators, formulation of the problem and the solution methodology are presented in Section 2. Section 3 deals with an application of the proposed method to a two-link flexible truss and presents experimental results. Our conclusions are made in Section 4.

2. Formulation

The inverse dynamics of a flexible multi-body is a non-linear problem. We solve this non-linear problem recursively, one element of the multi-body at a time. This algorithm, proposed by Bayo in [3], for general multi-body inverse dynamics involves, 1) studying

an individual component (link) in the chain; 2) coupling the equations of the individual links; and 3) recursively converging to the desired actuator inputs and corresponding displacements. Following this general procedure, we propose a new scheme which incorporates distributed actuators in the solution of the inverse dynamics problem. This approach is presented in the following section.

2.1 Equation of motion of an individual link

We start by studying the dynamics of a single link. To simplify the equations, we consider a link with a revolute joint, however the formulation is similar for a general element of a given multibody with other types of joints like the translational type. The flexible link depicted in Figure 1 forms part of a multi-link (multi-body) system, and has a total length L, mass per unit length $\bar{m}$, area moment of inertia I, cross-sectional area A, Youngs modulus E, shear modulus G, and shear coefficient k. A tip mass of magnitude M_t is attached at one end, and a hub with rotary inertia I_h at the other end. A point P at a distance x from the center of the hub has undergone elastic deflections of magnitudes u_x and u_y, and rotation of θ, defined with respect to a nominal position characterized by the moving frame $(\bar{e}_1, \bar{e}_2)$ that rotates at a specified angular velocity and acceleration ω_h and α_h respectively, and a linear acceleration of a_h. This definition of motion with respect to the nominal frame permits the linearization of the single link's dynamic equations. Incorporating the kinematic model followed by Naganathan and Soni [10], the linear and angular accelerations (a_p and α_p respectively) can be written in vectorial notation as

$$a_p = \omega_h \times (\omega_h \times r) + \alpha_h \times r + 2\,\omega_h \times v_{rel} + a_h + a_{rel} \tag{1a}$$

$$\alpha_p = \alpha_h + \ddot{\theta} \tag{1b}$$

where $r \triangleq (x + u_x)\bar{e}_1(t) + u_y \bar{e}_2(t)$, v_{rel} is the relative velocity of point P, whose relative acceleration is a_{rel}. The components of acceleration vectors satisfy the following equations

$$a_x = -\omega_h{}^2 u_x - \alpha_h u_y - 2\,\omega_h \dot{u}_y + \ddot{u}_x - \omega_h{}^2 x + a_{hx} \tag{2a}$$

$$a_y = -\alpha_h u_x - \omega_h{}^2 u_y + 2\,\omega_h \dot{u}_x + \ddot{u}_y - \alpha_h x + a_{hy} \tag{2b}$$

$$\alpha_p = \alpha_h + \ddot{\theta} \tag{2c}$$

where the subscripts x and y denote components along the $\bar{e}_1$ and $\bar{e}_2$ directions. Now using the Timoshenko beam theory, which includes the effects of shear deformation and rotary inertia, the principle of virtual displacements can be used directly to generate the following equations of motion

$$\int_0^L [\bar{m}\, a_x\, \delta u_x + \bar{m}\, a_y\, \delta u_y + \bar{m}\, \eta^2 \alpha_p\, \delta\theta\,]\, dx + I_h(\alpha_h + \ddot{\theta}_h)\delta\theta_h + M_t\, a_t\, \delta u_t +$$

$$\int_0^L [EI\, \theta'\delta\theta' + GAk(\theta - u'_y)\,\delta(\theta - u'_y) + EAu'_x\, \delta u'_x\,]dx =$$

$$T\, \delta\theta_h + R_{ty}\, \delta u_{ty} + R_{tx}\, \delta u_{tx} + T_t\, \delta\theta_t \tag{3}$$

where η is the radius of gyration of the section. The subscripts h and t indicate the hub and tip respectively, and the symbol $'$ denotes the spatial derivative. δu_x, δu_y and $\delta\theta$ represent a set of virtual elastic displacements. T is the unknown torque to be applied at the hub so that the prescribed tip motion is obtained. Note that the hub acceleration is decomposed into the nominal acceleration α_h and the acceleration due to elastic deflections. Also observe that the reactions at the hub do not have any effect in the total virtual work. As shown later, this constraint is met by imposing the constraint that the hub moves along the nominal path without any elastic deformations. The displacement field of equation (3) can be discretized using the finite element method (FEM) as follows

$$u_x(x,t) = \sum_1^N H_i(x) u_x{}^i(t)\ ;\ u_y(x,t) = \sum_1^N H_i(x) u_y{}^i(t)\ ;\ \theta(x,t) = \sum_1^N H_i(x)\theta^i(t) \tag{4}$$

where H_i are interpolation functions whose order depends on the number of nodes, N, in the elements ; $u_x{}^i$, $u_y{}^i$ and θ^i indicate the nodal deflections. It should be noted here that other alternative approaches, like the modal superposition method may be followed to generate the system equations. The approach chosen is dependent on the ease and accuracy of the particular method. Substituting equations (2) and (4) in the virtual work expression (equation 3), and following standard procedures for the formulation and assemblage of element matrices [11], the equation of motion can be written as [3]

$$M\ddot{z} + \left[C + C_c(\omega_h)\right]\dot{z} + \left[K + K_c(\alpha_h,\omega_h)\right] z = B_T T + B_p V_p + F. \qquad (5)$$

Where z is an R^n vector of the finite element degrees of freedom. M and K belong to $R^{n\times n}$ and are the conventional finite element mass and stiffness matrices respectively; C_c and $K_c \in R^{n\times n}$ and are the time varying Coriolis and centrifugal stiffness matrices, respectively. The $R^{n\times n}$ matrix C represents the internal viscous damping of the material. T is the unknown joint actuation. $F \in R^n$ contains the reactions at the end of the link, and the known forces produced by the rotating frame effect. The distributed actuator inputs $V_p \in R^{np}$ are the equivalent nodal forces at the FEM degrees of freedom, where np is the number of distributed actuator inputs. B_T and B_p are constant matrices input influence matrices of dimensions R^n and $R^{n\times np}$, respectively. The set of finite element equations (5) is partitioned as follows

$$M\begin{bmatrix}\ddot{\theta}_h\\ \ddot{z}_i\\ \ddot{z}_t\end{bmatrix} + \left[C + C_c(\omega_h)\right]\begin{bmatrix}\dot{\theta}_h\\ \dot{z}_i\\ \dot{z}_t\end{bmatrix} + \left[K + K_c(\alpha_h,\omega_h)\right]\begin{bmatrix}\theta_h\\ z_i\\ z_t\end{bmatrix} = \begin{bmatrix}1\\0\\0\end{bmatrix} T + \begin{bmatrix}B_{p_h}\\ B_{p_i}\\ B_{p_t}\end{bmatrix} V_p + \begin{bmatrix}F_h\\ F_i\\ F_t\end{bmatrix} \qquad (6)$$

where θ_h is the elastic rotation of the hub, z_t is the elastic deflection at the tip in the y direction, and the other $n-2$ finite element degrees of freedom are included in the vector z_i. The force vector, F, and the B_p and B_T matrices are also partitioned similarly.

2.2 Minimization Objective

The requirement is to accurately track the end effector of the link along the given nominal trajectory without overshoot and residual vibrations. If the distributed actuators were not available, then the exact tip trajectory tracking requirement defines the joint input torque T. Our objective is is to use the additional actuation available through the distributed actuators to reduce the ensuing structural vibrations at locations away from the control point during this motion by minimizing $J(T,V_p)$, a measure of elastic deflections

in the structure defined as follows

$$J(T,V_p) \triangleq \int_{-\infty}^{\infty} z(t)^T z(t) dt. \tag{7}$$

Mathematically the objective can be stated as

$$\min_{(T,V_p) \in \bar{T}} J(T,V_p). \tag{8}$$

Where $\bar{T}$ is the set of all pairs of stable actuator inputs that when used to actuate the system defined by equation (6) yields $z_t(t) = 0$ for all t.

2.3 Solution Methodology

An iterative scheme is described below for each link. Equation (6) can be rewritten as

$$M\ddot{z} + C\dot{z} + Kz = B_T T + B_p V_p + F - C_c(\omega_h)\,\dot{z} - K_c(\alpha_h,\omega_h)\,z \tag{9}$$

where the time dependent Coriolis and centrifugal terms are kept on the RHS of the equation. A study of the influence of the Coriolis and centrifugal effects on the inverse dynamics has been presented by Gofron and Shabana [12]. The iteration procedure starts with the absence of the last two terms involving C_c and K_c in the right hand side. Then, the system of equations can be transformed into independent sets of simultaneous complex equations by means of the Fourier transform. For each of the evaluation frequency ω, equation (9) becomes

$$\left[M + \frac{1}{i\omega}C - \frac{1}{\omega^2}K\right] \begin{bmatrix} \hat{\ddot{z}}_h \\ \hat{\ddot{z}}_i \\ \hat{\ddot{z}}_t \end{bmatrix} = \begin{bmatrix} \hat{T} \\ 0 \\ 0 \end{bmatrix} + \begin{bmatrix} \hat{F}_h \\ \hat{F}_i \\ \hat{F}_t \end{bmatrix} + \begin{bmatrix} B_{p_h} \\ B_{p_i} \\ B_{p_t} \end{bmatrix} \hat{V}_p \tag{10}$$

where the symbol $\hat{}$ stands for Fourier transform, and $\hat{F}$ represents the known forcing terms. After the first iteration it will also include the updated contributions from the Coriolis and centrifugal terms appearing in the RHS of equation (9). For any $\omega \neq 0$, the matrix

$$H \triangleq \left[M + \frac{1}{i\omega}C - \frac{1}{\omega^2}K\right] \tag{11}$$

is a complex, symmetric and invertible matrix. For $\omega = 0$ the system undergoes a rigid body motion and $H \triangleq M$, the positive definite invertible mass matrix. Let $G \triangleq H^{-1}$. Then the above equation can be re-written as

$$\begin{bmatrix} \ddot{\hat{z}}_h \\ \ddot{\hat{z}}_i \\ \ddot{\hat{z}}_t \end{bmatrix} = \begin{bmatrix} G_{hh} & G_{hi} & G_{ht} \\ G_{ih} & G_{ii} & G_{it} \\ G_{th} & G_{ti} & G_{tt} \end{bmatrix} \left\{ \begin{bmatrix} \hat{T}(\omega) \\ 0 \\ 0 \end{bmatrix} + \begin{bmatrix} \hat{F}_h \\ \hat{F}_i \\ \hat{F}_t \end{bmatrix} + \begin{bmatrix} B_{p_h} \\ B_{p_i} \\ B_{p_t} \end{bmatrix} \hat{V}_p \right\}. \tag{12}$$

The condition that the tip should follow the nominal motion, is equivalent to $\ddot{\hat{z}}_t = 0$ for all ω. This induces a relationship between the joint actuation and the distributed actuator inputs and is obtained from the last row of the previous equation.

$$\hat{T} = -G_{th}^{-1} \begin{bmatrix} G_{th} & G_{ti} & G_{tt} \end{bmatrix} (\hat{F} + B_p \hat{V}_p). \tag{13}$$

Substituting this expression for the input hub torque in equation (8) and using the property that $\ddot{\hat{z}} = -\omega^2 \hat{z}$ yields

$$\hat{z} = -\frac{1}{\omega^2} (A\hat{V}_p + B). \tag{14}$$

Where

$$A \triangleq [-G_{th}^{-1} G B_T (G_{th} \; G_{ti} \; G_{tt}) + G] B_p \tag{15}$$

and

$$B \triangleq [-G_{th}^{-1} G B_T (G_{th} \; G_{ti} \; G_{tt}) + G] \hat{F}. \tag{16}$$

Next we determine $\hat{V}_p$. Using Parseval's theorem, minimizing $J(T, V_p)$ in equation (8) is equivalent to minimizing $\|\hat{z}\|_2^2$ at each ω. This is a standard least squares approximation problem [13] and has one of the solutions for the distributed actuator inputs as,

$$\hat{V}_p = -U \begin{bmatrix} \Sigma^{-1} & 0 \\ 0 & 0 \end{bmatrix} V^* B \tag{17}$$

where Σ, U and V define the standard singular value decomposition of A as follows

$$V^* A U = \begin{bmatrix} \Sigma & 0 \\ 0 & 0 \end{bmatrix}, \tag{18}$$

and the conjugate transpose matrix operator is denoted by $*$. This solution is unique in the sense that it also minimizes $\| \hat{V}_p \|_2$ over all possible $\| \hat{z} \|_2^2$ minimizing solutions. In addition if A has rank np, which is the number of distributed actuator inputs, then the least squares approximation yields

$$\hat{V}_p = -(A^* A)^{-1} A^* B \ . \tag{19}$$

A sufficient and necessary condition for A to have rank np is given next.

Lemma

$$\text{rank } [A] = np \ \text{ iff } \ \text{rank } [B_T \,|\, B_p] = np+1 \tag{20}$$

Proof

$$\text{Rank } [B_T] = 1 \implies \text{rank } [GB_T(G_{th}\ G_{ti}\ G_{tt})] = 1$$

$$\implies \text{rank} \left[\bar{A} \triangleq [-G_{th}^{-1} GB_T(G_{th}\ G_{ti}\ G_{tt}) + G] \right] \geq n-1$$

because G is invertible with rank n. Since $B_T = [1\ 0\ 0]^*$, it follows that $[1\ 0\ 0]^*$ lies in the null space of $\bar{A}$. Hence rank $\bar{A}$ is $n-1$. Noting that $A = \bar{A}\ B_p$, the lemma follows easily. □

The above lemma states that if all the columns of the input matrices B_T and B_p are independent, then the solution for $\hat{V}_p$ is given by equation (19), thus the computationally expensive singular value decomposition given by equation (18) can be avoided. The independency of the input influence matrix columns imply that the different modes of the structure are acted upon in different ratios by the different inputs. If the actuations of two inputs were similar on all the modes, then they can be lumped together to be considered as a single input in the computations. This distribution of actuation effort depends on the mode-shapes of the structure and the actuator placement, and can be modeled easily using FEM [14]. In the problem at hand, the best placement for a given trajectory depends not only on the structure but also the component frequencies of the desired motion. Thus the optimal placement of the actuator would in general be trajectory

dependent. In most structures, such a freedom of changing the actuator placement with the prescribed trajectory is not available. The design of such structures with fixed actuator placements, is based on minimizing the induced structural vibrations over sets of disturbances with a specified energy [14]. In systems where the required motions are largely repetitive, the actuator placement can be optimized over a specified set of trajectories; this warrants a separate treatment to be considered in a future work.

The iteration procedure continues as follows. The corresponding joint torque component, $\hat{T}$ is evaluated from equation (13). An inverse Fourier transform evaluation yields the feedforward inputs and completes the first iteration. The results of this first iteration are the joint torques, T^1 and the distributed inputs V_p^1. Next a forward dynamics analysis is carried out to compute K_c and C_c. F in the RHS of equation (9) is updated and the process is repeated to find the new input torques and voltages. The process is stopped at the n^{th} iteration if $\| T^n - T^{n-1} \|_2 + \| V_p^n - V_p^{n-1} \|_2 < \varepsilon$, where ε is some small positive constant. It may be noted that for slow motions the terms involving K_c and C_c are small relative to the other terms in equation (5) and the iterations converge in a few steps [3].

2.4 Algorithm for the Multi-Link Case

In the previous sub-section the procedure to evaluate the joint actuations of a single link was presented. This is recursively extended for multi-link flexible manipulators. An algorithm is presented below:

1. Define the nominal motion (Inverse Kinematics of rigid manipulator).
2. For each link j, starting from the last one in the chain:
   a) Compute torque (or force) T^j and distributed actuator inputs $P_v{}^j$
      imposing $z_t{}^j = 0$ (Section 2)
   b) Compute the link reaction forces R^j from equilibrium.
3. Use equation (5) to compute the elastic displacement and joint angles.

4. Compute the inputs for the next link, $j-1$.

This concludes the methodology. In the next section we present an application to a two-link flexible manipulator.

3. Experimental Verification

An experimental truss structure developed at UCSB is shown in Figure 2. The structure has 16 spans and two articulations forming a planar manipulator. The trusses are made of aluminum and have lumped masses (net 2 *Kgs* for each link) distributed along their lengths in order to lower the links modal frequencies and hence the control sample rate. In addition, the first (base) and the second links have tip loads of 3.5 and 1 *Kgs* respectively. These loads further increase the flexibility of the structure and the natural frequencies of the first and second links with clamped free boundary conditions are 0.6 Hz and 1.2 Hz respectively. Actuation consists of low-inertia dc-motors at the two joints and an active bay (Figure 3) with four electro-strictive actuators. Sensing consists of resolvers at the joints and collocated strain sensors on the four electro-strictive actuators. In addition, an optical sensor measures the position of an infra-red LED mounted about the midpoint of the the first link, thus providing information of the induced structural vibrations during the tracking operation. The entire structure is supported on air bearings and controlled with an Intel 386-based PC, servo amplifiers for the motors and 150V servo amplifiers for the electro-strictive actuators.

A major concern in the use of electro-strictive actuators is their non-linear applied voltage to effective strain behavior. Temperature dependent variations of this relationship, and the presence of hysterisis prevents their effective use as precision actuators. Several techniques have been discussed in [15] to alleviate this problem. These include biasing the electro-strictor, linearizing the model for small inputs, and non-linear models. We propose a closed loop cascade controller (see Figure 4) with a feedback control based on the effective strain induced by these actuators. A strain gauge collocated with the

electro-strictive actuator is used as sensor for feedback. In our experiments a simple proportional controller yielded excellent results as seen by plot of effective strain versus the command strain (Figure 5) where hysterisis and other non-linear behavior of the electrostrictors are eliminated when a feedback is used. Such a cascade control scheme is particularly effective here because the actuator dynamics are much faster than the dominant modes of the multibody.

To evaluate the proposed use of distributed actuators developed in Section 2, we apply it to track the end-effector of the two link flexible manipulator. The desired trajectory of the end-effector is a series of rest to rest motions, while the first link is stationary. The nominal motion of the second link is shown in Figure 6. Our objective is to track the desired trajectory and minimize the vibrations in the first link which is equipped with electro-strictive actuators. To evaluate the vibration reduction achieved, we conduct the following tracking experiments: (1) feedforward of torques computed without inverse dynamics, i.e. assuming the links to be rigid; (2) using the torques computed by inverse dynamics for only the joint actuators; and (3) incorporating the distributed electrostrictive actuators on the first truss along with joint actuators in the inverse dynamics computation and using these as feedforward. In each case a joint based PD controller was used for controlling errors due to unmodeled dynamics, friction and other modeling errors. The stability of such joint based controllers are discussed in [9]. The results of our experiments are presented below.

Plots of the inputs to the electro-strictor and joint motors are presented in Figures 7, 8 and 9. Note that the actuations start before the tip trajectory begins. This non-causality due to the propagation delays is reduced when additional actuation is available through the piezos as seen in Figure 9. To illustrate the viability of the proposed method we plot the transverse structural deflections at the midpoint of the first link (Figure 10) during the motion obtained by an infra-red led mounted on the structure and an over-head optical sensor. These elastic deflections in the structure are considerably reduced when electro-

strictive actuators are also used in addition to the joint motors. On the contrary if inverse dynamics is not used and the rigid body torques are used then the resulting motion has much larger vibrations.

Thus the incorporation of electro-strictive actuators results in a significant reduction in the structural vibrations and demonstrates the viability of the proposed method. The consequent reduction (50%) in the induced vibrations of the structure allows the use of lighter elements and therefore smaller joint actuators, especially in space structures where the loads are mainly inertial.

4. Conclusion

Typically distributed actuators like the electro-strictive ones cannot garner enough actuation to cause large motions in the multibody system. However they could be very effective in reducing structural deformation. To reduce such vibrations by the use of distributed actuators in feedforward aiding joint actuators for trajectory tracking is a novel idea developed in this paper. The method proposed is extremely efficient as it optimaly reduces structural vibrations and the theory developed was verified by experiments. The use of the redundant distributed actuators seems promising in the slewing control of flexible manipulators and other space structures, and motivates further work on distributed actuators for the control of flexible multibodies. In particular, for systems with largely repetitive trajectory tracking requirements, future work will address the actuator design problems like placement and sizing, from a vibration minimization perspective.

Acknowledgement

Support from Air Force Office of Scientific Research through grant F49620-91-C-0095 and the Astro Aerospace Corporation are gratefully acknowledged. The authors also thank Mr. Dave Bothman and Mr. John M. Hutchinson for their generous help in the experiments.

References

1. Bayo, E. 'A finite-element approach to control the end-point motion of a single-link flexible robot,' *Journal of Robotic Systems* **4**, 1987, pp. 63-75.

2. Book, W. J., ' An inverse dynamic method yielding flexible manipulator state trajectories,' *Proceedings of American Control Conference*, San Diego, CA, 1990, pp. 186-193.

3. Bayo, E., Serna, M. A., Papadopoulos, P., and Stubbe, J., 'Inverse dynamics and kinematics of multi-link elastic robots. An iterative frequency domain approach,' *The International Journal of Robotics Research* **8**, 1989, pp. 49-62.

4. Ledesma, R., Bayo, E., 'A non-recursive lagrangian solution to the non-causal inverse dynamics of flexible multibody systems: The planar case,' *International Journal of Numerical Methods in Engineering*, accepted for publication, 1993.

5. Moulin, H., and Bayo, E., 'On the end point trajectory tracking for flexible manipulators through non-causal inverse dynamics,' *Journal of Dynamic Systems, Measurement and Control* **113**, 1991, pp. 320-324.

6. Mierovitch, L., and Baruh, H., 'Control of self-adjoint distributed-parameter systems,' *AIAA Journal* **5**, 1980, pp. 60-66.

7. Balas, M. J., 'Active control of flexible systems,' *Journal of Optimization theory and Applications* **25**, 1987, pp. 415-436.

8. Fanson, J. L., and Garba, J. A., 'Experimental studies of active members in control of large space structures,' *Proceedings of the 29th AIAA SDM Conference*, Williamsburg, VA, 1988, pp. 9-17.

9. Paden, B., Chen, D., Ledesma, R., and Bayo, E., ' Exponentially stable tracking control for multi-joint flexible-link manipulators,' *ASME Journal of Dynamic Systems, Measurement and Control* **115**, 1993, pp. 53-59.

10. Naganathan, G., and Soni, A. H., 'Coupling effects of kinematics and flexibility in manipulators,' *International Journal of Robotics Research* **6**, 1987, pp. 75-85.

11. Bathe, K. J., 'Finite element procedures in engineering analysis,' *Prentice Hall, Englewood Cliffs, New Jersey*, 1982.

12. Gofron, M., and Shabana, A., 'Effects of the deformation in the inertia forces on the inverse dynamics of flexible mechanical systems,' *Journal of Nonlinear Dynamics*, 1993, to appear.

13. Stewart, G. W., 'Introduction to matrix computations,' *Academic Press Inc.*, 1973, pp. 319-325.

14. Devasia, S., Meressi, T., Paden, B., and Bayo, E., 'Piezo-electric actuator design for vibration suppression: Placement and sizing,' *Journal of Guidance, Dynamics and Control*, 1992, to appear.

15. Crawley, E. F., and Anderson, E. H., 'Detailed models of piezoceramic actuation of beams,' *Journal of Intelligent Material Systems and Structures* **1**, 1990, pp. 4-25.

List of Figures

Figure 1. A single flexible link.

Figure 2. Experimental smart flexible structure.

Figure 3. The active bay in link 1.

Figure 4. The closeloop control scheme.

Figure 5. Effect of feedback on the effective strain.

Figure 6a. Desired nominal rotations of the second link.

Figure 6b. Desired nominal accelerations of the second link.

Figure 7. Command strain input to the electro-strictor.

Figure 8. Applied joint torques to link 1.

Figure 9. Applied joint torques to link 2.

Figure 10. Elastic vibrations on the first link.

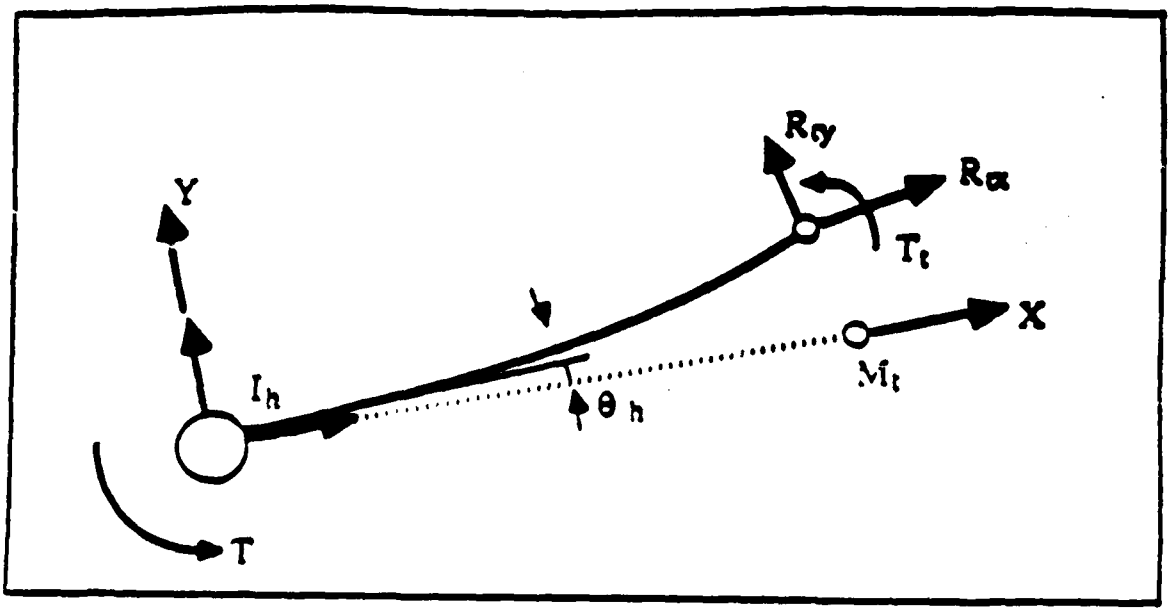
Rcy
Rα
Y
Tt
X
Ih
Mt
θ h
T

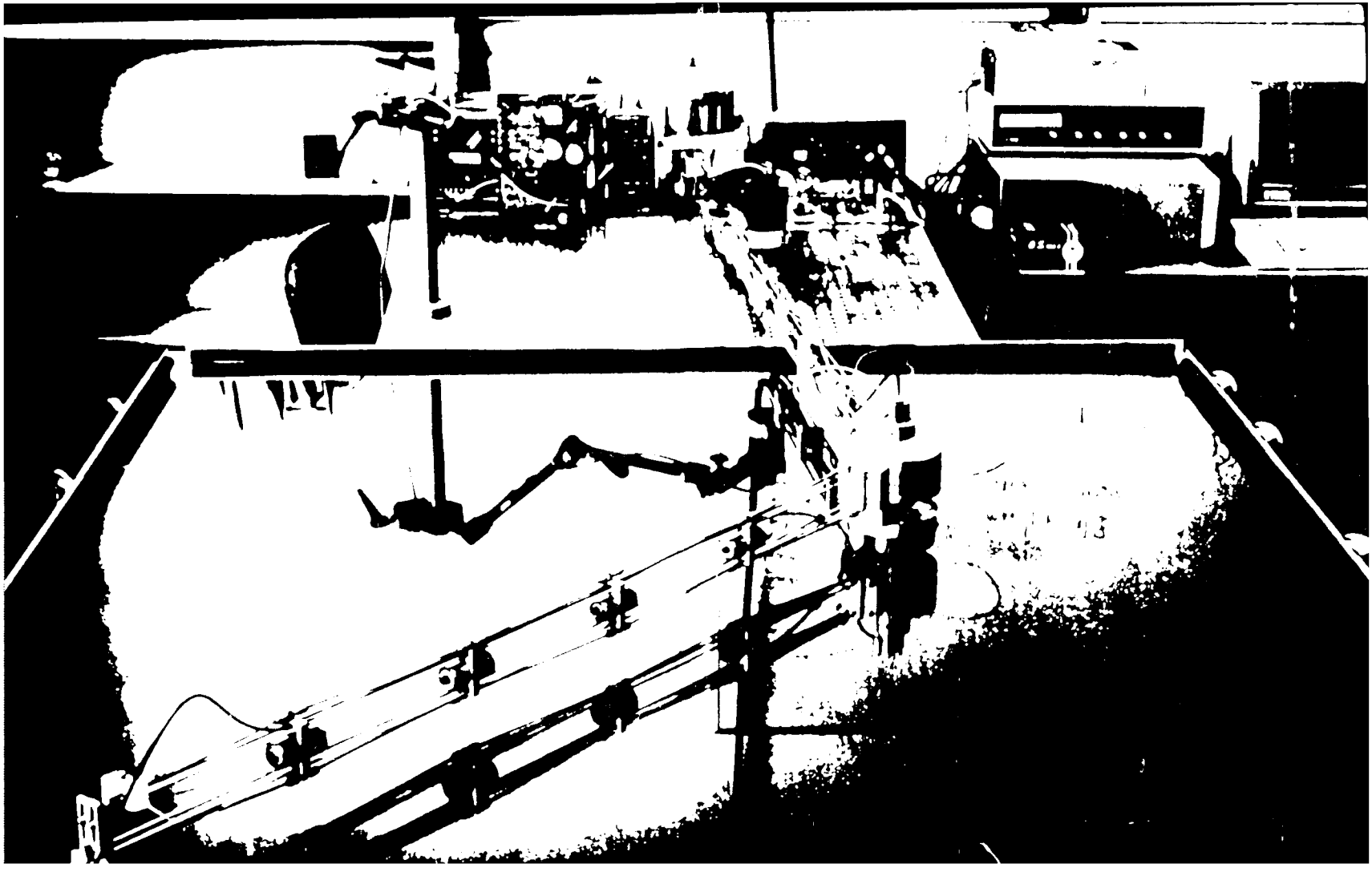

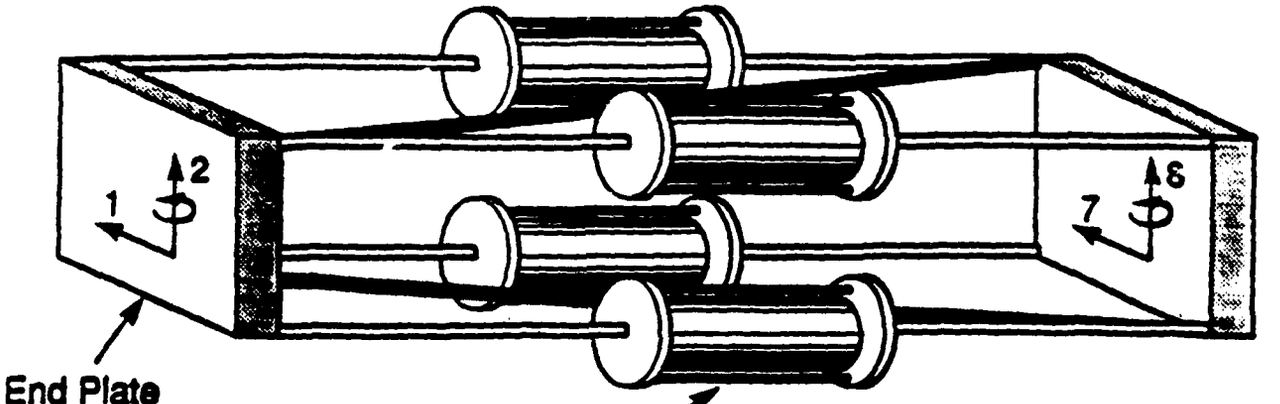

1,2,7,8: FEM Degrees of freedom

Fig 3

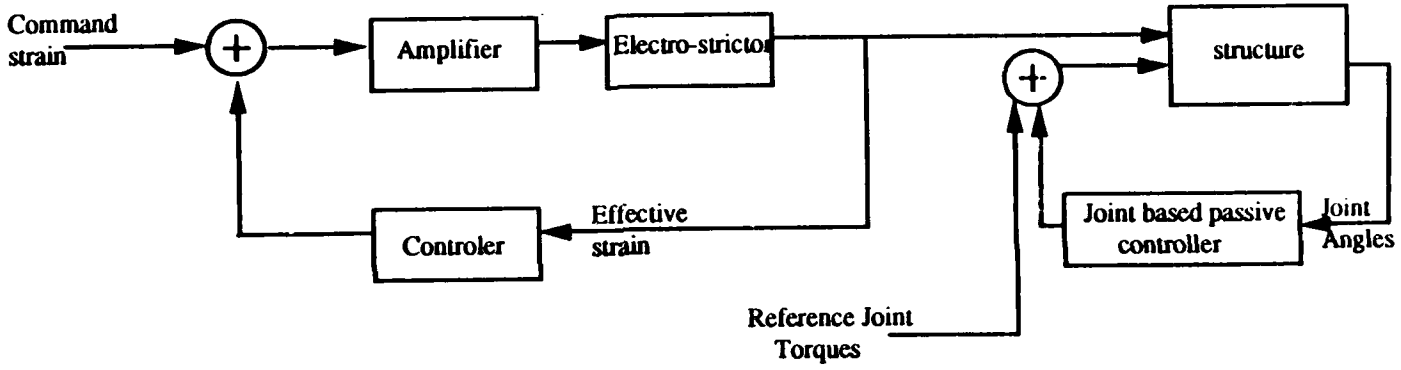
Command
strain
Amplifier
Electro-strictor
structure
Controler
Effective
strain
Joint based passive
controller
Joint
Angles
Reference Joint
Torques

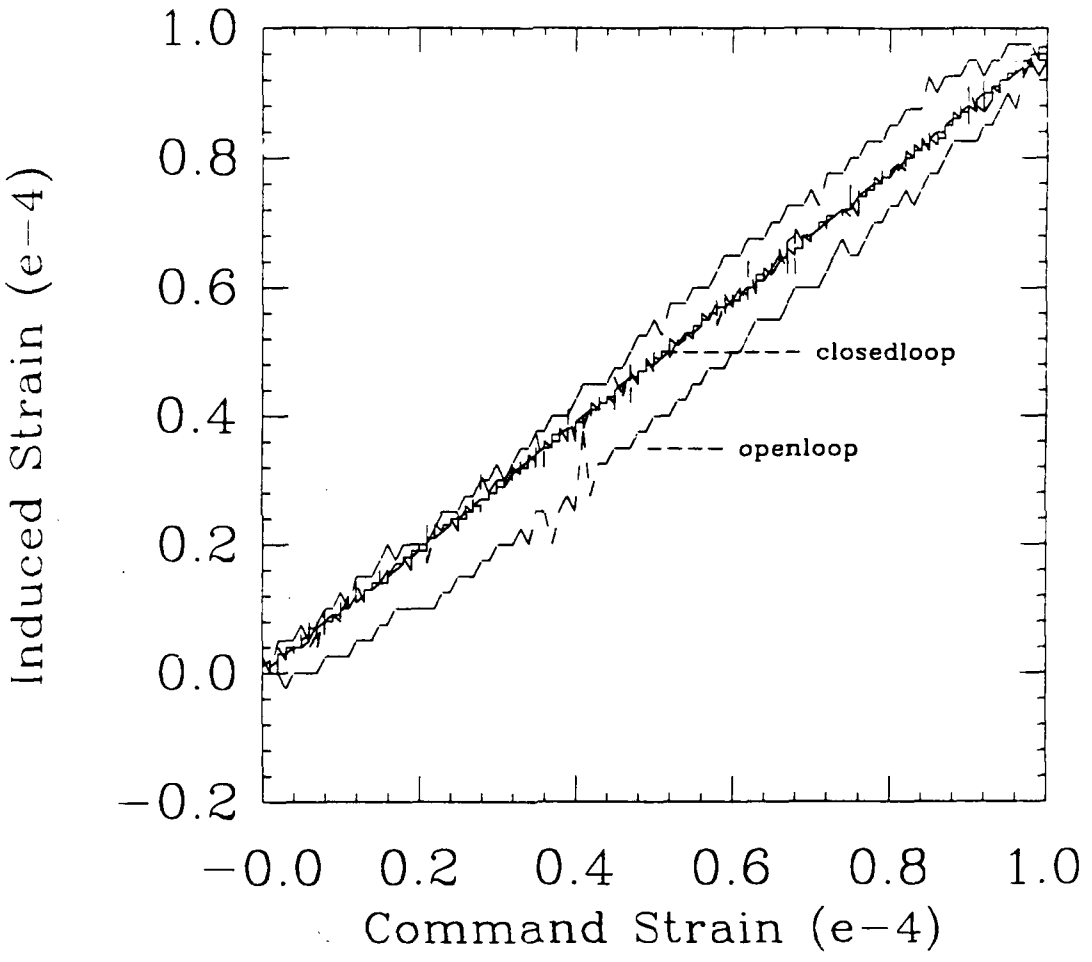
1.0
0.8
0.6
0.4
0.2
0.0
−0.2
Induced Strain (e−4)
closedloop
openloop
−0.0
0.2
0.4
0.6
0.8
1.0
Command Strain (e−4)

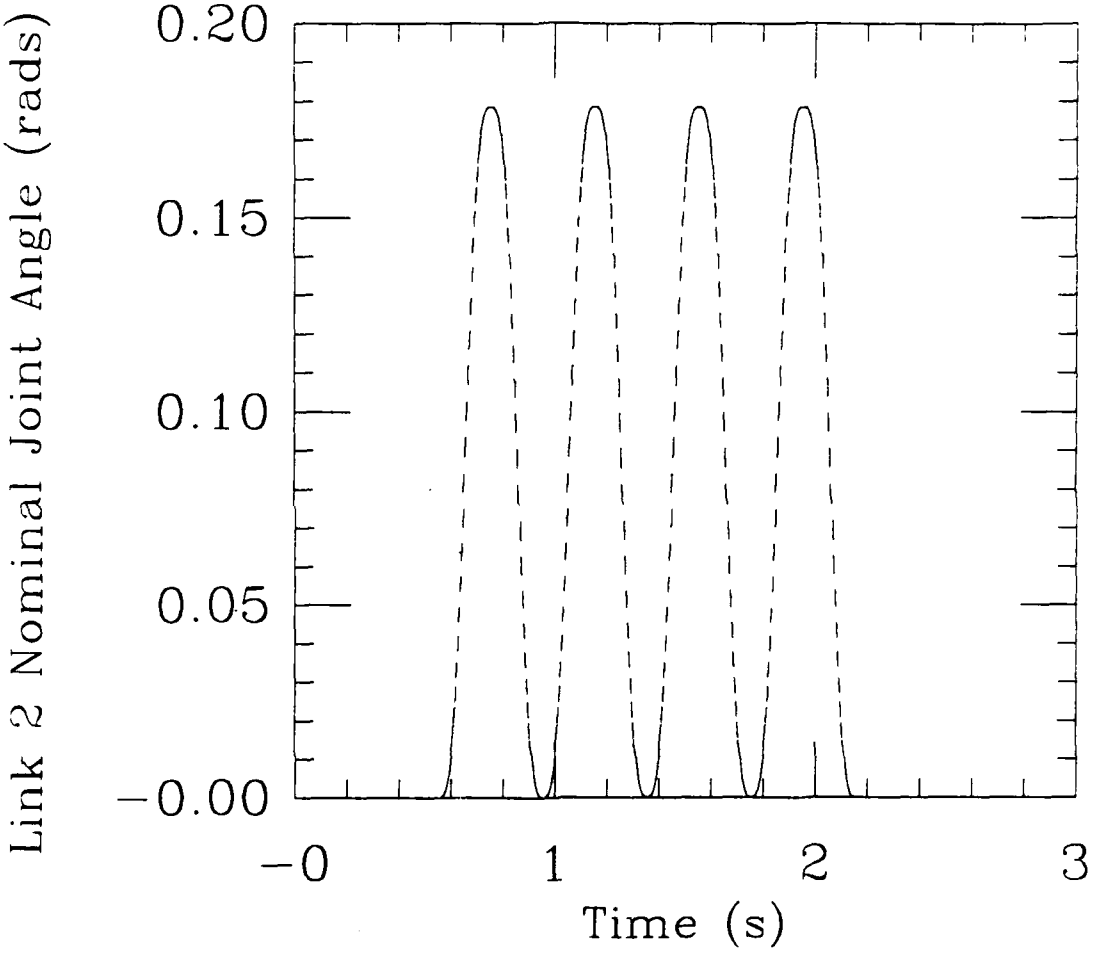
Link 2 Nominal Joint Angle (rads)
0.20
0.15
0.10
0.05
−0.00
−0
1
2
3
Time (s)

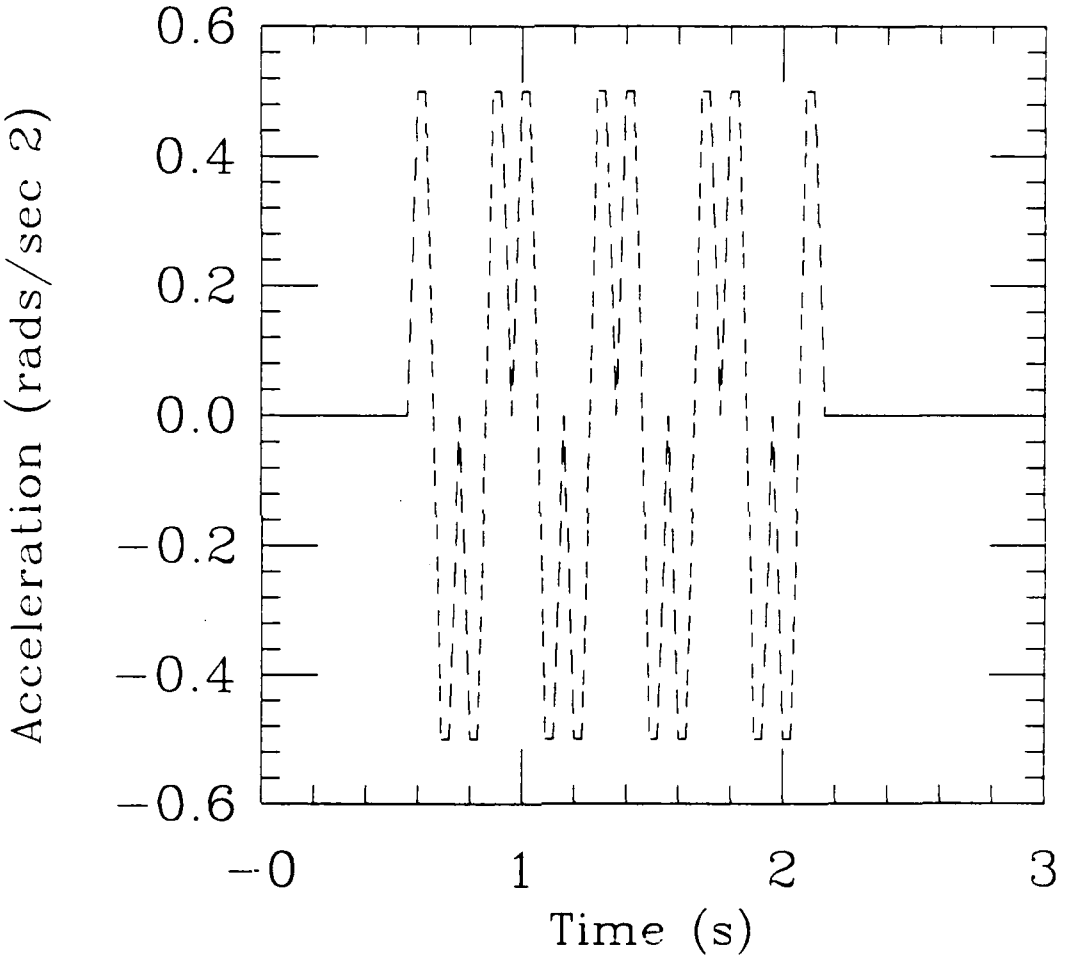
0.6
0.4
0.2
0.0
−0.2
−0.4
−0.6
Acceleration (rads/sec 2)
−0
1
2
3
Time (s)

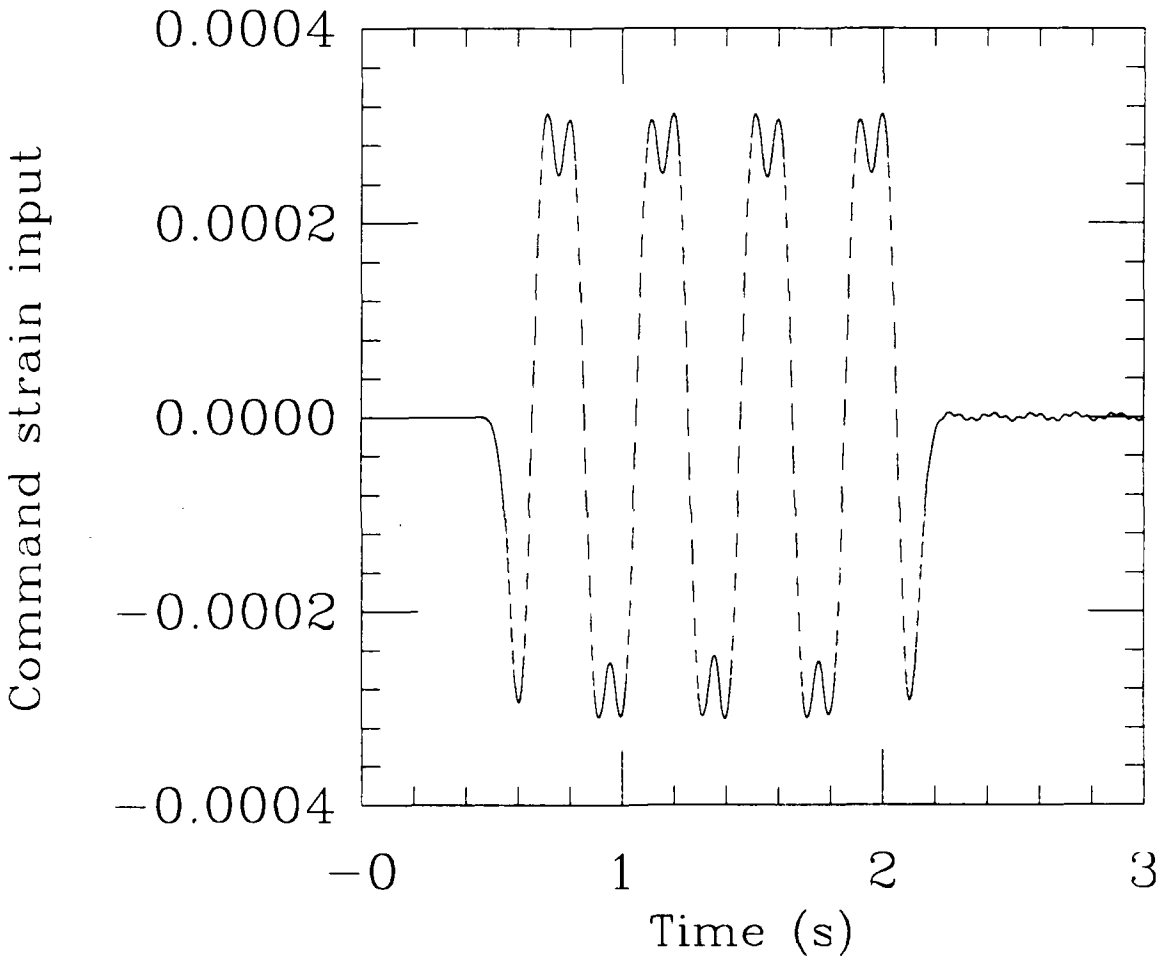
0.0004
0.0002
0.0000
−0.0002
−0.0004
Command strain input
−0
1
2
3
Time (s)

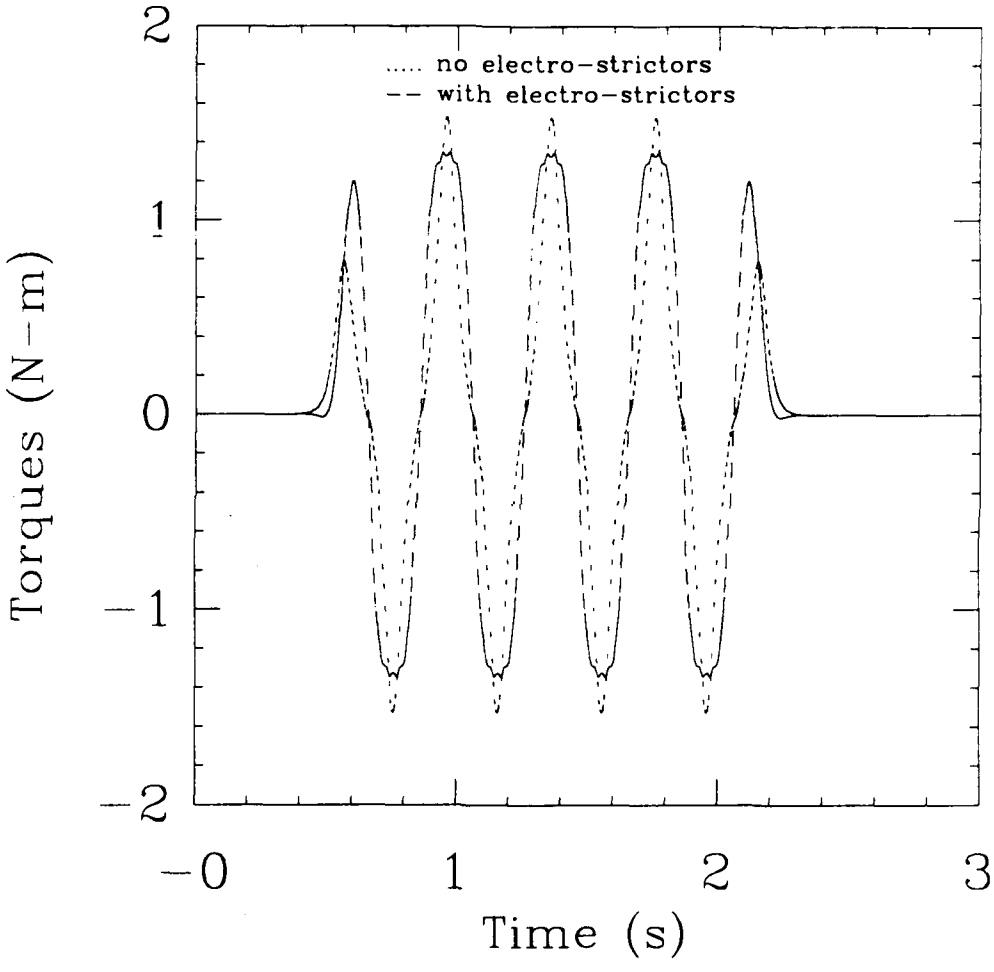
..... no electro-strictors
-- with electro-strictors
Torques (N-m)
2
1
0
-1
-2
-0
1
2
3
Time (s)

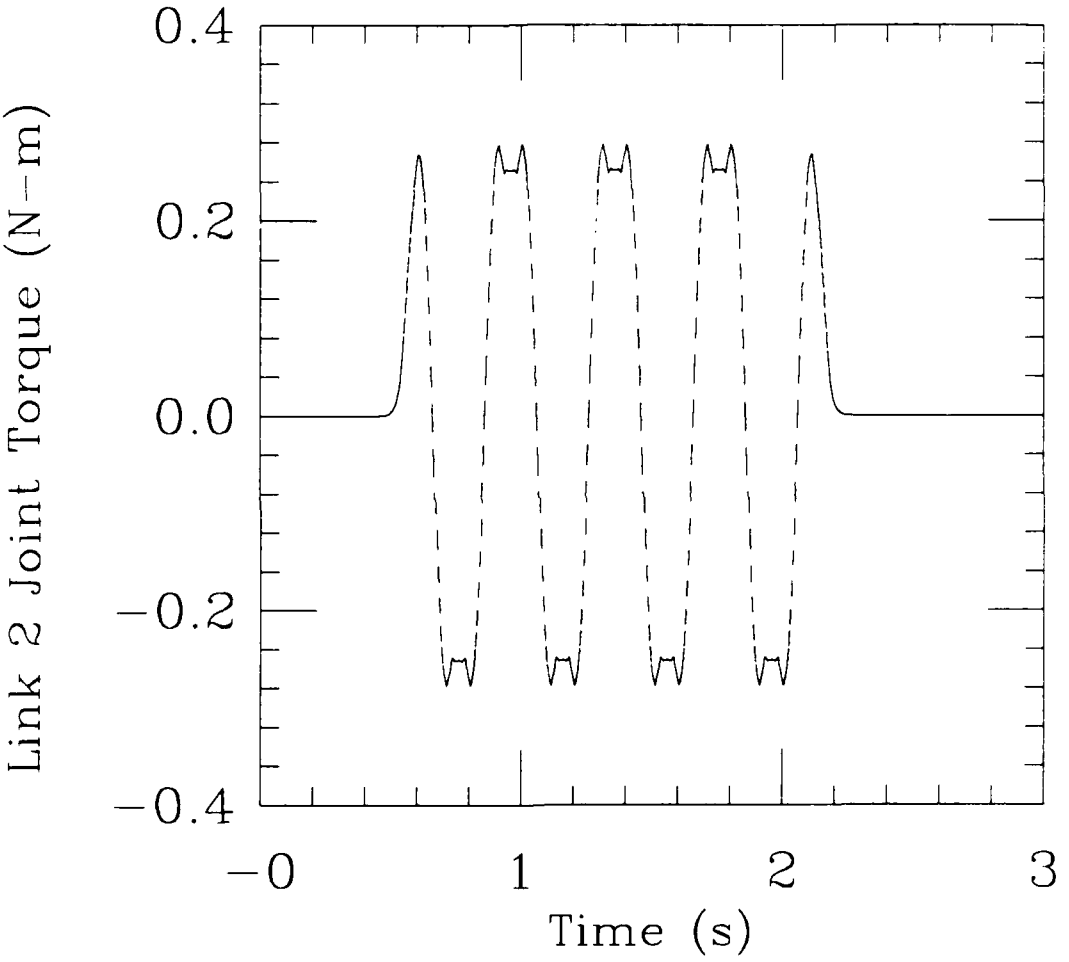
0.4
0.2
0.0
−0.2
−0.4
Link 2 Joint Torque (N−m)
−0
1
2
3
Time (s)

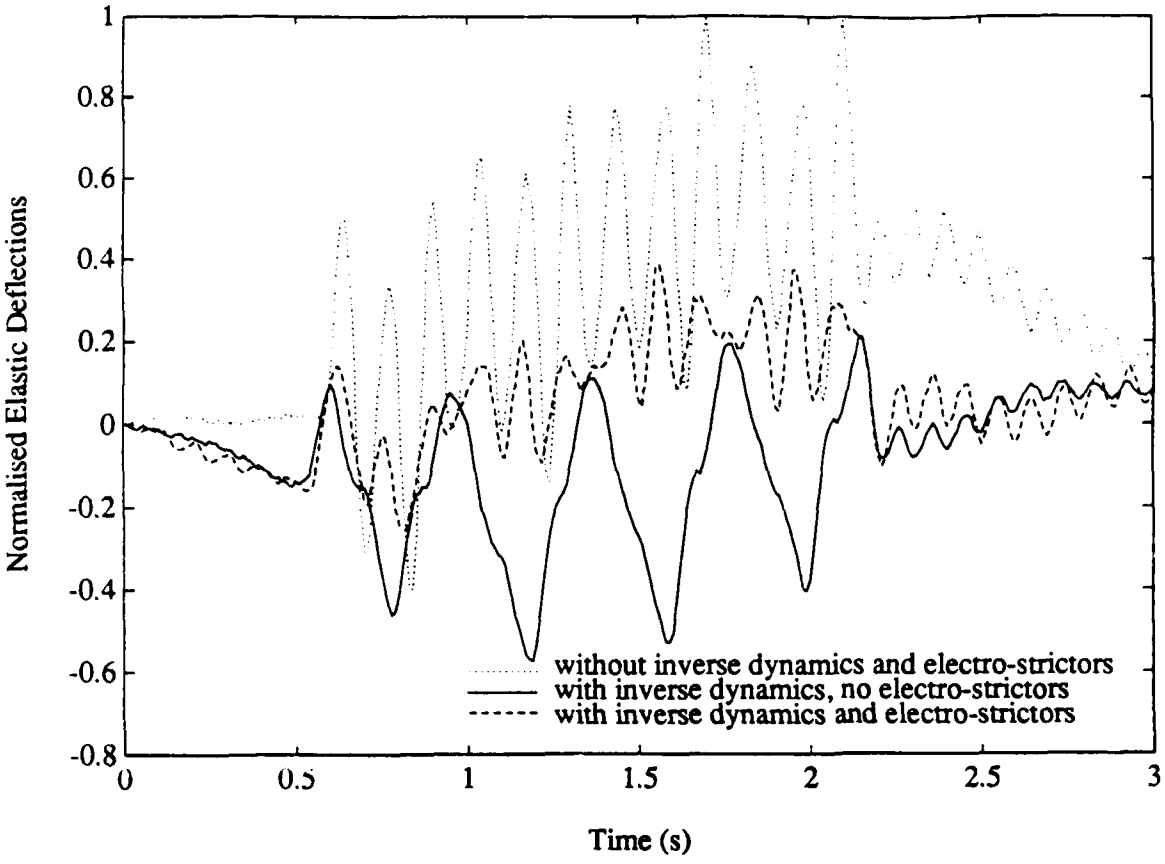
Normalised Elastic Deflections
Time (s)
without inverse dynamics and electro-strictors
with inverse dynamics, no electro-strictors
with inverse dynamics and electro-strictors
1
0.8
0.6
0.4
0.2
0
-0.2
-0.4
-0.6
-0.8
0
0.5
1
1.5
2
2.5
3

American Control Conference
San Francisco, California • June 1993

VIBRATION CONTROL OF AN EXPERIMENTAL TWO-LINK MANIPULATOR

*Santosh Devasia** Brad Paden** Eduardo Bayo**

Dept. of Mechanical & Environmental Engineering
University of California, Santa Barbara, CA 93106

Abstract

In this paper we address the problem of actuator placement for articulated flexible structures. Specifically, the placement of a single active bay on an articulated truss is formulated and solved for the UCSB/Astro-Aerospace truss. We observe that controllability grammian methods are not reliable in general and that better placements are achieved using *closed-loop* performance measures. Some preliminary vibration damping experiments are also described.

1. Introduction

The control of large flexible structures has been considered for some time [1]. However, the recent application of piezoelectric materials by Crawley [2] for actuation of flexible structures has added a new dimension to this problem because these actuators can be distributed along structural members for vibration and shape control. This paper deals with the problem of actuator placement to achieve optimal damping of vibrations in articulated flexible structures (AFS) through the example of an experimental two-link two-joint truss structure. The key issue in such optimizations is the use of a suitable design evaluation measure. Once a numerically tractable measure is available, a combined structure-controller design optimization can be carried out. We approach the problem in two steps, first, different measures to perform design evaluation in linear structures are studied, and second, we extend two of these measures to articulated flexible structures (AFS) with non-linear dynamics.

For structures with linear dynamics, our goal is to find the placement to maximize modal damping when feedback control is applied. Similar problems has been studied previously literature. In Crawley's early work the actuator was simply placed with one bending mode in mind at the location of maximum strain for that mode [2]. However the placement problem for the case with two or more controlled modes was not addressed. Kondoh *et al* [3] used the linear quadratic-optimal control framework to perform sensor and actuator placement, but formulated the problem such that the solution is initial condition dependent -- this dependence is removed here. Controllability was used as a performance measure for placement of a point actuator in [4]. Our main result for the linear case states that methods based on the controllability grammian can yield less effective placement results for vibration damping than those based on closed-loop performance measures.

Next, we consider the non-linear problem of placing piezo-electric vibration dampers in articulated flexible structures (AFS). The placement problem for these jointed structures is complicated by their nonlinear dynamics. Even with small linear vibrations about a given rigid body configuration, a good placement for one configuration should not necessarily work well after the structure's joints are rotated. With a finite-element model, we have indeed observed a large variation in modal frequencies (for the linearized dynamics) as the joint angles are varied. However, we have discovered that for some structures (and ours in particular) nodal rotations associated with the mode *shapes* are relatively invariant to configurations and uniformly good placements are possible! Two methods of placement are explored. The first is based on the simple rate based damping controller where placements are chosen to maximize the decay rate of vibrations. The second method optimizes placement based on closed-loop performance of Linear-Quadratic Regulator. The two methods are contrasted using a finite-element model of our structure.

The remainder of the paper is organized in the following format. In section 2 we describe the experimental setup and modeling. Section 3 formulates measures to be used for actuator placement in linear structures and discusses the performance measures. Section 4 deals with the extension of the measures to articulated flexible structures along with an example and presents simulation and preliminary experimental results. Our conclusions are made in section 5.

Experimental Set-up

The effectiveness of distributed actuators has been demonstrated for vibration reduction [1]. Such structures exhibit residual vibrations due to imperfections in the controller and disturbances like impacts, thermal heating and microgravity. For example, in space station mobile transporter manipulators, gear trains exhibit substantial friction, stiction and backlash. Under such conditions, joint actuators are ineffective in controlling low amplitude structural vibrations. The proper placement of distributed actuators is critical to the control of such vibrations.

The example we consider is an experimental two-link truss structure (figure 1 and shown in the video) developed at UCSB. The structure has 16 spans and two articulations forming a planar manipulator. The trusses are made of aluminum and have lumped masses (net 2 Kgs for each link) distributed along their lengths in order to lower the modal frequencies and hence the control sample rate. In addition, the first and the second links have tip loads of 3.5 and 1 Kgs respectively, and their lengths are 1.8 and 1.1 m respectively. Actuation consists of low-inertia dc-motors at the two joints and one active bay (Figure 2) with four piezo-electric actuators. Sensing consists of resolvers at the joints and co-located strain sensors on the four piezo-electric actuators. The entire structure is supported on air bearings and controlled with an Intel 386-based PC, servo amplifiers for the motors and 150V servo amplifiers for the Piezos.

Our interest is to study piezo actuator placement for optimally controlling structural vibrations. A related issue is the implementation of controllers for the distributed actuators. The problems of implementation include de-poling, nonlinearity, hysteresis, and creep effects in the piezo actuator [5]. De-poling may be avoided by maintaining the applied field below the coercive field. Within the de-poling limits, the nonlinearity between applied electric field and the resulting actuation strain may require the use of more complex models [6]. An alternative is the linearization of this relationship about the operating point [7]. Creep and strain rate dependence of the actuator become important at large strains and low frequencies. Hysteresis also plays an important role at low frequencies. Significant performance improvement over such behavior is possible by commanding the induced charge rather than the voltage applied to the actuator [8]. Other issues related to actuator dynamics are considered in [9] and [10]. We note that the Piezos have fast dynamics relative to electromagnetic actuators and are attractive in this regard.

* Supported by the Astro Aerospace Corp. under P.O. 104236.

** Supported by the U.S. Airforce under grant F49620-91-C-0095.

System Model

The modeling of actuator/structure interaction using finite dimensional models has been studied in detail in [5]. Following a similar approach, low amplitude motions relative to a given rigid body equilibrium configuration x_o of an articulated flexible structure is approximated using the Finite Element Method (FEM) [11], and can be written as

$$M_{p,\theta}\ddot{x} + D_{p,\theta}\dot{x} + K_{p,\theta}x = \bar{B}_{p,\theta}u_p \qquad (2.1a)$$

where $x \in R^n$ denotes the flexible degrees of freedom. $M_{p,\theta}$, $D_{p,\theta}$ and, $K_{p,\theta}$, are the mass, damping and stiffness matrices respectively. $p \in R^1$ denotes the placement, $\theta \in R^2$ is the joint angle vector of the structure, and $u_p \in R^1$ is the input voltage to the actuator. Note that joint motor torques do not appear in the equations as the joints are assumed to be locked due to static friction. The effect of the piezo actuators is modeled as two point moments M (figure 3) acting at the ends of the piezo ([5] and[12]) and is included in the $\bar{B}_{p,\theta}$ matrix. The output $y \in R^1$ is obtained from a strain gauge co-located with the actuator and is linear in the state [13]

$$y = \bar{C}_{p,\theta}x\ . \qquad (2.1b)$$

From equation (2.1) it is seen that for each placement p, the system can be considered as a family of linear systems parametrized by θ. Noting that at each equilibrium point is defined by $x = \dot{x} = 0_{n\times 1}$, the state equation (2.1) can be rewritten as

$$\dot{z}(t) = A_{p,\theta}z(t) + B_{p,\theta}u(t) \qquad (2.2a)$$

$$y(t) = C_{p,\theta}z(t)\ . \qquad (2.2b)$$

where

$$z = \begin{bmatrix} x^T & \dot{x}^T \end{bmatrix}^T \in R^{2n}\ , \qquad (2.2c)$$

$$A_{p,\theta} = \begin{bmatrix} O_{n\times n} & I_{n\times n} \\ -M_{p,\theta}^{-1}K_{p,\theta} & -M_{p,\theta}^{-1}D_{p,\theta} \end{bmatrix} \in R^{2n\times 2n}\ , \qquad (2.2d)$$

$$B_{p,\theta} = \begin{bmatrix} O_{n\times 1} \\ -M_{p,\theta}^{-1}\bar{B}_{p,\theta} \end{bmatrix} \in R^{2n\times 1}\ , \qquad (2.2e)$$

and

$$C_{p,\theta} = \begin{bmatrix} \bar{C}_{p,\theta} & O_{1\times n} \end{bmatrix} \in R^{1\times 2n}\ . \qquad (2.2f)$$

3. Actuator Placement for Linear Systems

In this section we formulate three optimization problems for determining a good placement of the piezo actuator for the linearized system. Our objective being an actuator placement to achieve optimal vibration damping in the elastic modes. In words they are the following. (1) Subject to the constraint that co-located damping control is used, find the placement that maximizes damping uniformly in the modes. (2) Assuming the system is detectable and stabilizable, find the placement that minimizes a standard linear quadratic cost functional uniformly in initial conditions. (3) Find the placement that maximizes the minimum eigenvalue of the controllability grammian (as is done for the actuator placement problem by Arbel [4]).

Passive Damping Case

For the first optimization problem, we assume a pure co-located damping control given by

$$v(t) = -k_d\bar{C}_{p,\theta}\dot{x} \qquad (3.1)$$

where k_d is the scalar controller gain. With this control the state-space description (2.2) becomes

$$\dot{z}(t) = A\ z(t) \qquad (3.2)$$

where

$$A \triangleq A_{p,\theta} + -k_d\,\bar{B}_{p,\theta}\begin{bmatrix} O_{1\times n} & \bar{C}_{p,\theta} \end{bmatrix} \qquad (3.4)$$

The advantage of such a co-located passive control is that controllers designed for a finite-dimensional model remains stable with the infinite dimensional plant provided that actuator dynamics can be neglected [14]. Since the bandwidth of a piezo is only limited by its capacitance, actuator dynamics can be justifiably ignored for large space structures. The implementation issues of such controllers have been addressed in [5] and [10].

We measure the system performance for a particular choice of controller, placement and piezo length by the rate of decay of system states and therefore seek to place the poles of the system far into the left half of the complex plane. More formally, we perform the following optimization

$$\min_p \max_i \mathrm{Re}\,\lambda_i(A) \qquad (3.5)$$

where $\lambda_i(A)$ is the i^{th} eigenvalue of A, and p is one of the span midpoints.

Linear Quadratic Regulator Case

The Linear Quadratic Regulator (LQR) is attractive because the controller stabilizes the closed loop system and also allows for user defined weights on the inputs and states. LQR optimization has been used to reduce the structural vibrations in the control of large flexible structures in [15] and [16] but the formulations were initial condition dependent -- this dependency is removed here. For the system described by equation (2.2), consider the infinite-horizon time-optimal control problem of minimizing a quadratic cost functional given by

$$J_v \triangleq \int_0^\infty [\,Rv(t)^2 + z^T(t)Qz(t)\,]dt \qquad (3.6)$$

where R is a positive scalar and Q is positive semi-definite matrix such that the pair $(A_{p,\theta}, Q^{1/2})$ is observable. Provided system (2.2) satisfies the standard conditions of stabilizability and detectability, the minimum cost $\min_v J_v$ is given by $z^T(t_0)Pz(t_0)$ where P is the unique nonnegative-definite solution to the algebraic Ricatti equation[17]

$$PA_{p,\theta} + A_{p,\theta}{}^TP - PB_{p,\theta}R^{-1}B_{p,\theta}{}^TP + Q = 0. \qquad (3.7)$$

The corresponding control is

$$v(t) = -R^{-1}B_{p,\theta}{}^TPz(t). \qquad (3.8)$$

We propose minimizing J_v for the worst case initial condition and therefore pose the following optimization for computing the placement.

$$\min_p \max_{\|z_0\|=1} z_0^TPz_0\,, \qquad z_0 = z(t_0). \qquad (3.9)$$

This method optimizes performance uniformly in initial conditions in contrast to the approach by Kondoh *et al* [3] where a solution sensitive to initial conditions is proposed.

Controllability Grammian Method

Finally, we describe a placement procedure based on the controllability grammian proposed by [4]. This method is useful, but has certain disadvantages discussed in the following section. Assuming that the matrix $A_{p,\theta}$ in the state space description (2.2) is stable, as the final time T tends to infinity, it can be shown that the finite time controllability grammian $W(0,T)$ approaches W, the solution of the Lyapunov equation

$$WA_{p,\theta}{}^T + A_{p,\theta}W + B_{p,\theta}B_{p,\theta}{}^T = 0. \qquad (3.10)$$

Based on Arbel's method we perform the optimization

$$\max_p \min_i \lambda_i(W) \qquad (3.11)$$

to maximize the controllability of all the modes. This approach is discussed in the following sub-section.

Discussion of the Controllability Grammian based Measure

We discuss in this sub-section the drawbacks of the controllability grammian method applied by Arbel [4]. The cost for the minimum energy control given initial condition $z(t_0)$ and final condition $z(T)$ is

$$J \triangleq \left[z(T) - e^{A_{p,\theta}(T-t_0)} z(t_0) \right]' W^{-1}(0,T) \left[z(T) - e^{A_{p,\theta}(T-t_0)} z(t_0) \right] \tag{3.12}$$

where $e^{A_{p,\theta}(T-t_0)}$ is the state transition matrix. J is the energy required to deviate from the natural motion of the system, which would have reached the state $e^{A_{p,\theta}(T-t_0)} z(t_0)$ at time T without the application of any control. Arbel's method is based on optimizing J *over all possible initial and final conditions* and results in minimizing the maximum eigenvalue of the inverse of the controllability grammian, $W^{-1}(0,T)$, over different actuator positions. In contrast we are interested in a particular final condition namely zero. The control cost J_r for this finite time regulator problem ($z(T) = 0$) is given by

$$J_r \triangleq \left[e^{A_{p,\theta}(T-t_0)} z(t_0) \right]' W^{-1}(0,T) \left[e^{A_{p,\theta}(T-t_0)} z(t_0) \right] \tag{3.13}$$

which differs from J significantly. Next we show that the maximum eigenvalue of $W^{-1}(0,T)$ increases as the system poles move far into the left half of the complex plane. Thus J increases as the system becomes more damped! Let γ be an eigenvalue of W and let v be the corresponding eigenvector such that $\| v \|_2 = 1$. Pre- and post-multiplying the Lyapunov equation (3.10) by v^T and v respectively, we obtain

$$v^T W A_{p,\theta}{}^T v + v^T A_{p,\theta} W v + v^T B_{p,\theta} B_{p,\theta}{}^T v = 0 \tag{3.14}$$

Then

$$\gamma = -\frac{v^T B_{p,\theta} B_{p,\theta}{}^T v}{2 v^T A_{p,\theta} v} \leq \frac{|\max_i \lambda_i(B_{p,\theta} B_{p,\theta}{}^T)|}{\min_j |\lambda_j(A_{p,\theta})|} \tag{3.15}$$

The above result implies that for a given $B_{p,\theta}$ the eigenvalues of W^{-1} increase if the eigenvalues of $A_{p,\theta}$ move into the left half plane. Hence Arbel's approach deems the system as less controllable and therefore not desirable even though the above shifting of the poles is advantageous for vibration reduction.

This decrease in controllability can be easily illustrated through a scalar example described by

$$\dot{x}(t) = -ax(t) + bu(t). \tag{3.16}$$

Using Arbel's method, for a large final time T, the eigenvalue of $W(0,T)$ tends to $\frac{b^2}{2a}$ which decreases as a increases, and subsequently the controllability measure deems the system as less controllable even though from a vibration reduction perspective it is more desirable. A similar effect is seen in flexible structures with large decay rates in the higher modes [13]. Arbel's placement method would therefore push the placement towards locations where the higher modes have maximum strain. However, due to lower decay rates, control of the lower modes is more critical from a vibration suppression perspective. Thus for vibration reduction, care must be exercised when using the controllability grammian based measures.

4. Actuator Placement For AFS

In this section we formulate the problem for the placement of distributed actuators in a general articulated flexible structure (AFS). The set of equilibria in AFS consists of rigid body configurations with zero elastic deformations. Our control objective is to obtain uniformly good regulation of elastic deformations at any equilibrium state (rigid body configuration) of the articulated structure. This implies that the set of desired trajectories X_d, are constant trajectories. Our approach is based on linearization (Section 2) of the system equations at each equilibrium point in the set X_e followed by a local cost measure (Section 3) evaluation at these equilibrium points. In the following sub-section we describe this procedure.

Problem Statement

A local cost functional $c(x_e, p)$ is defined for every placement p and rigid body configuration x_e of the articulated flexible structure as follows. For the passive damping controller (3.5) the local cost function is defined as

$$c(x_e, p) \triangleq \max_i \operatorname{Re} \lambda_i(A) \tag{4.1a}$$

and

$$c(x_e, p) \triangleq \max_{\|z\|=1} z^T P z_0, \qquad z_0 = z(t_0). \tag{4.1b}$$

for the LQR controller (3.9). Based on cost measures evaluated through local linearization (section 3) we can state the placement problem as

$$\min_{p \in X_p} C(p) \tag{4.2}$$

where the functional $C(p)$ assigns a global cost for each placement by evaluating a suitable norm on the function $c(\cdot, p): X_e \to R^1$. If for example, the set of equilibrium points, X_e, is contained in R^n, then two possible choices of the the function $C(p)$ are the average and worst case:

$$\frac{\int_{X_e} c(x_e, p) dx}{\int_{X_e} dx} \quad \text{and} \tag{4.3}$$

$$\max_{x_e \in X_e} c(x_e, p). \tag{4.4}$$

These measures are used to numerically solve the problem of placing distributed Piezo-electric actuators in a two-link flexible manipulator-strictive in the next section.

Example

For the two-link flexible manipulator (figure 1), we study the distributed actuator placement to optimally control small structural vibrations when the joint motors are effectively locked because of static friction. This corresponds to clamped boundary conditions at the joints. Our objective being an actuator placement in the truss structure to achieve optimal vibration damping in the elastic modes over a set of rigid body equilibrium configurations. We study the actuator placement at a single shoulder joint configuration because the system dynamics are independent of the shoulder joint angle. Also, the elbow joint θ is constrained by $|\theta| \leq 90^\circ$ in the experiment. Then by symmetry it is sufficient to study the problem for elbow joint angles between 0° and 90°. Hence the set of equilibrium states X_e, containing rigid body configurations with zero elastic deflections, is parametrized by the elbow joint angle θ and is independent of the placement p.

The two measures defined in the above sub-section are used to generate solutions to the placement problem of the piezo-actuators. The passive co-located damping controller considered is parametrized by a scalar feedback gain K_d and the feedback law can be written as [13]

$$u = -K_d \left[O_{1 \times n} \;\; \bar{C}_{p,\theta} \right] z. \tag{4.5}$$

While computing the cost, an optimization is also performed over the scalar controller gain K_d. This implies that the local measure $c(p, x_e)$, with the passive damping controller is given by

$$c(p, x_e) \triangleq \min_{K_d \in R^1} \max_i \operatorname{Re} \lambda_i(A). \tag{4.6}$$

For the LQR controller based measure, weighting matrix Q is chosen to be uniform in the elastic displacements as

$$Q = \begin{bmatrix} I_{n \times n} & O_{n \times n} \\ O_{n \times n} & O_{n \times n} \end{bmatrix}. \tag{4.7}$$

The choice of the weight R on the control input depends on the de-poling limit of the actuator and the initial conditions. For a given R, and optimal placement p_{op} and the maximum input voltage $u_{max}(R)$ over all the configurations is found.

This variation of $u_{max}(R)$ as a function of R and α (the bound on the initial conditions i.e. $|x_0| \leq \alpha$) is shown in figure 4. Based on de-poling limits for the actuator, the maximum applied voltage is limited to $300V$ which corresponds to an applied field of $2\ MV/m$. For $\alpha = 1e-3$, corresponding to a maximum transverse elastic deflections of approximately $3cm$, $R = 1e-6$ falls in the suitable region, with maximum input voltages below the actuator de-poling limit.

For the averaging global measure defined by equation (4.3), the passive damping based measure yielded a placement at the root of the first link, while the second case of LQR based measures resulted in a placement at the root of the second link (figures 8,9). It is seen in these figures that the placements obtained are relatively "good" over all joint configurations.

Discussion

As the joint angle θ varies from 0 to 90^o, there is a substantial variation in the system eigenvalues. This is represented in figure 5, where the variation of the lowest modal frequency with elbow joint angle is shown. This significant (40% increase) change in the modal frequencies might deem uniformly good placements impossible. The uniformity of placement location is a desirable result because it implies that a single placement is effective in reducing vibrations at the different configurations. The placement based on passive damping controller is seen to be invariant with joint configuration. For the LQR case the resultant global optimal placement is not the best for certain configurations, however the increase in cost is negligible (1%) as seen in figure 9a. This near optimality over all configurations is attributed to the relative invariance of the eigenvector components associated with the nodal rotations at different joint angles.

The placement invariance is due to the fact that in our example the *eigenvectors* are relatively invariant with the joint configuration. This is illustrated in figure 6, where the projection of the eigenvectors, associated with the least two eigenvalues, onto the rotary elastic displacements at the FEM nodes of the manipulator model is shown. These correspond to the spatial derivative of the projection of the eigenvectors onto the transverse elastic displacements of the manipulator. Note that these *rotary* mode shapes shown in figure 6, vary little with joint angle. As the placement varies over the length of the manipulator, the relative control over each mode and its variation are determined by these mode shapes [10]. Consequently, the invariance of these mode shapes with the joint angle implies the relative invariance of the distribution of effective control over different modes. It is this control distribution of the different modes that determines the cost for the possible placement and therefore its invariance results in a uniformly good placement.

The performance measure based on passive damping is determined by the distance of system eigenvalues from the imaginary axis. This distance is an estimate of the slowest decay rate of elastic perturbations in the structure. In our example, the decay rate tends to increase with the elbow joint-angle as shown in figure 7. This is mainly due to the increase in the system natural frequencies, but with constant structural damping. For such a system, the elastic vibration modes associated with higher modal frequencies tend to have higher decay rates. Thus in the case of the passive controller based performance measure, it is the variation of the mode associated with the lowest frequency that determines the cost and therefore the placement. To control a single eigenvector, the optimal placement is at the location of maximum strain [18] where the effective control over that mode is maximized. Hence the passive damping based measure yields the placement at the first span of the structure. As discussed above, this placement is uniformly good for all joint configurations because nodal rotations associated with the mode shapes are relatively invariant.

The LQR based performance measure resulted in a placement where the quadratic cost functional given by equation (2.7) is minimized. The optimization of this quadratic cost functional results in a compromise placement between high decay rates of perturbations and small control effort. Note that the placement obtained by using this performance measure is relatively good over all configurations. Thus the invariance of the mode shapes aided in placements which were near-optimal

The reader is cautioned that this invariance in the mode-shapes need not be true for all AFS. The variations in the mode shapes and the modal frequencies with configuration can in general affect the placement. Hence it is not always possible to find placements that are uniformly good over different configurations. In such circumstances the placement should be based on either the average performance or worst case performance described in section 2, and then the resulting placement yields the best achievable performance.

Preliminary experimental results for co-located passive damping based controllers are given in figure 10, where we show the frequency response between the elastic vibrations at the end of first link span 8 obtained through an optical sensor and input to the base joint actuator. We obtain a 7db improvement in vibration suppression at the first pin-free resonance.

6. Conclusion

In this paper we formulated the actuator placement for both linear and articulated flexible structures. It was shown that the controllability grammian based placement technique is not suitable for vibration damping problems. For general articulated structures, two closed loop performance criterions were used to derive objective functions for optimum placement of actuators. The procedures, developed independent of initial conditions and formulated as eigenvalue problems, are easy to compute. In the example two-link manipulator, these measures are computationally tractable and effective to solve the distributed actuator placement problem for optimal structural vibration reduction. An important observation is that the mode shapes associated with nodal rotations for the example two-link flexible manipulator are relatively invariant with joint configuration. This invariance resulted in a placement which is effective in reducing vibrations over all the different configurations.

The measures suggested in this paper can also be used for actuator placement in set point controllers of non-linear systems. In this sense the approach is a modest attempt at the larger problem of non-linear actuator placement. The existence and computability of optimal designs for general trajectory tracking in non-linear systems is the subject of further work.

Acknowledgment

Support from the Air Force Office of Scientific Research through grant F9620-91-C-0095 and the Astro Aerospace Corporation is gratefully acknowledged.

References

1. L. Meirovitch and H. Baruh, "Control of Self-Adjoint Distributed-Parameter Systems," *AIAA Journal*, vol. 5, No 1, pp. 60-66, 1980.
2. E. F. Crawley and J. De Luis, "Use of Piezoelectric Actuators as Elements of Intelligent Structures," *AIAA Journal*, vol. 25, No 10, pp. 1373-1385, 1985.
3. S. Kondoh, C. Yatomi, and Koichi Inoue, "The Positioning of Sensors and Actuators in the Vibration Control of Flexible Systems," *JSME International Journal*, vol. 33, No.2, pp. 145-152, 1990.
4. A. Arbel, "Controllability Measures and Actuator Placement in Oscillatory Systems," *Int. J. Control*, vol. 33, No.3, pp. 565-574, 1981.
5. E. F. Crawley and E. H. Anderson, "Detailed Models of Piezoceramic Actuation of Beams," *J. of Intell. Mater. Syst. and Struct.*, vol. 1, pp. 4-25, Jan, 1990.
6. J. L. Fanson, G. H. Blackwood, and C-C. Chu, Crawley E. F., and Lazarus K.B., "Induced Strain Actuation of Isotropic and Anisotropic Plates," *AIAA Paper 89-1326, 30th AIAA Structural, Structural Dynamics and Materials Conference*, Mobile, AL, 1989.
7. J. De Luis, "Design and Implementation of Optimal Controllers for Intelligent Structures Using Infinite Order Structural Models," *PhD Thesis*, MIT, Cambridge, MA, 1989.
8. R.H. Comstock, "Charge Control of Piezoelectric Actuators as Elements of Intelligent Structures," AIAA

Journal, vol. 25, No 10, pp. AIAA paper 86-0878, Oct 1987.

9. J.L. Fanson and J.A. Garba, "Experimental Studies of Active members in Control of Large Space Structures," *Proc. AIAA 29th SDM Conf.*, pp. 9-17, 1988.
10. J.L. Fanson and T.K. Caughey, "Positive Position Feedback Control for Large Space Structures," *AIAA Journal*, vol. 28, No.4, pp. 717-724, April 1990.
11. E. Bayo, M.A. Serna, P. Papadopoulos, and J. Stubbe, "Inverse Dynamics and Kinematics of Multi-Link Elastic Robots. An Iterative Frequency Domain Approach," *The International J. of Robotics Research*, vol. 8, No 6, Dec 1989.
12. C. J. Goh and T. K. Caughey, "On the Stability Problem Caused by Finite Actuator Dynamics in the Collocated Control of Large Space structures," *Int. J. Control*, vol. 41, No. 3, pp. 787-802, 1985.
13. S. Devasia, T. Meressi, B. Paden, and E. Bayo, "Piezo-Electric Actuator Design for Vibration Suppression: Placement and Sizing," *Proc. of CDC*, Dec,1992.
14. A. Bhaya and C. A. Desoer, "On the Design of Large Flexible Space Structures(LFSS)," *IEEE trans. on Automatic Control*, vol. AC-30, No.11, pp. 1118-1120, Nov,1985.
15. T. Bailey and J. E. Hubbard Jr., "Distributed Piezoelectric-Polymer Active Vibration Control of a Cantilever Beam," *J. Guidance, Control and Dynamics*, vol. 8 , pp. 605-611, Sept-Oct, 1985.
16. S. Fisher, "Application of Actuators to Control Beam Flexure in a Large Space Structure," *J. Guidance*, vol. 12, No.6, pp. 874-879, Dec 1989.
17. H. Kwakernaak and R. Sivan, *Linear Optimal Control Systems*, Wiley-Interscience, 1972.
18. E. F. Crawley and J. De Luis, "Use of Piezo-ceramics as distributed actuators in large space structures," *AIAA Journal*, pp. 126-133, 1985.

Figure 1. Experimental smart flexible structure

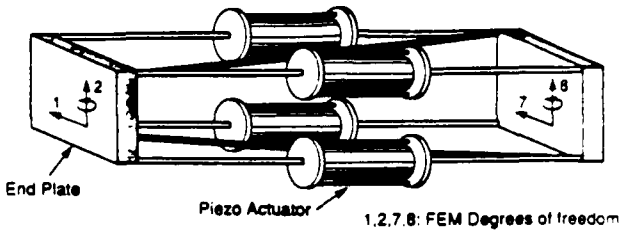

Figure 2. The active bay

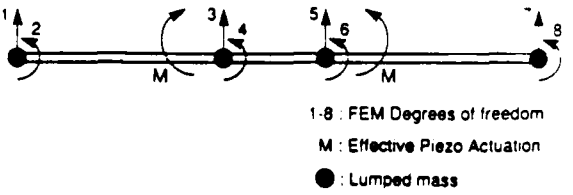

Figure 3. Equivalent FEM representation

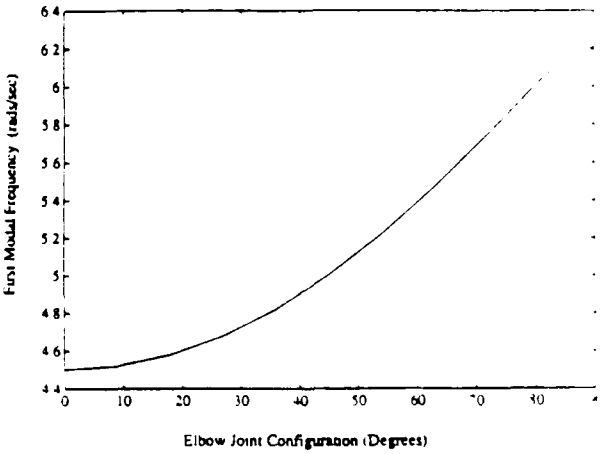

Figure 4. Variation of first modal frequency of the structure

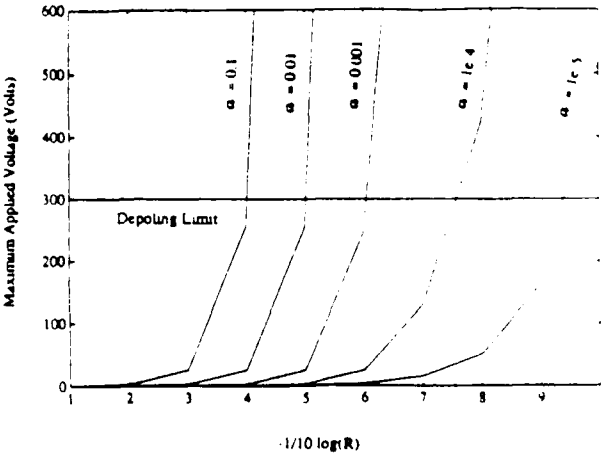

Figure 5. Variation of maximum applied voltage

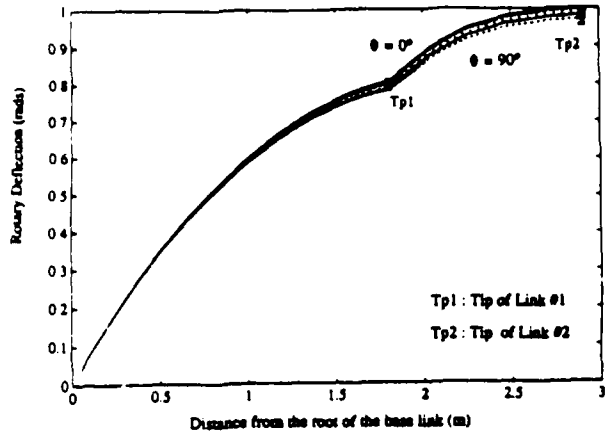

Figure 6a. Variation of 1st eigenvector nodal rotation components

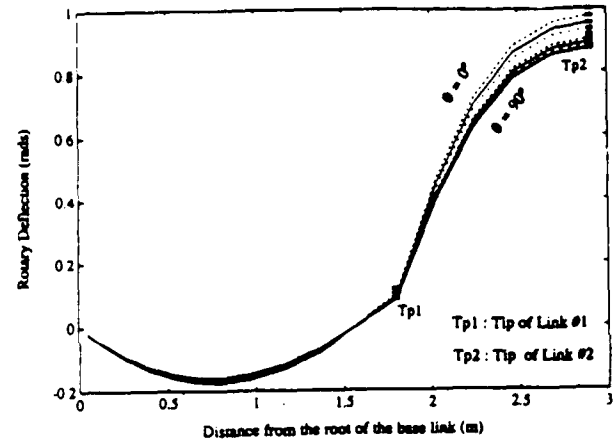

Figure 6b Variation of 2nd eigenvector nodal rotation components

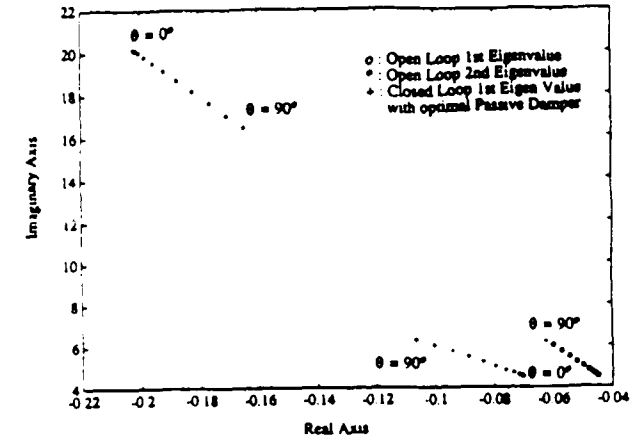

Figure 7. Variation of eigenvalues with joint configuration

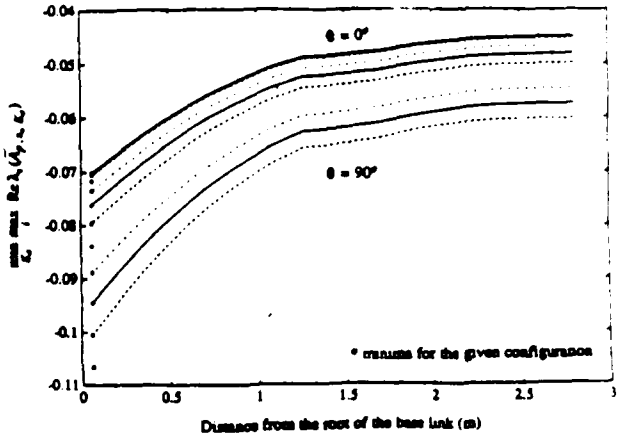

Figure 8. Variation of passive damping based cost over joint configuration

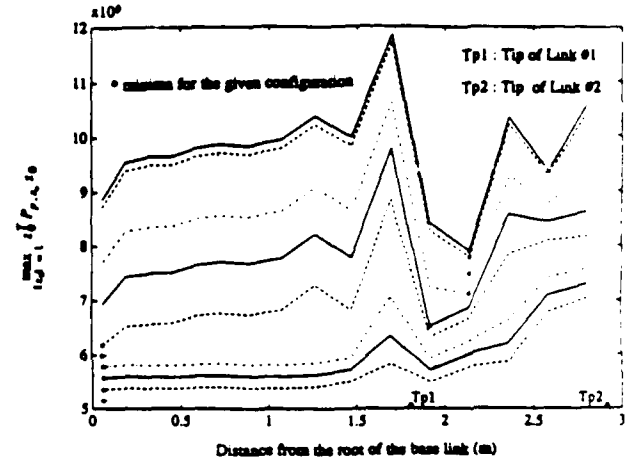

Figure 9. Variation of LQR based cost over different configurations

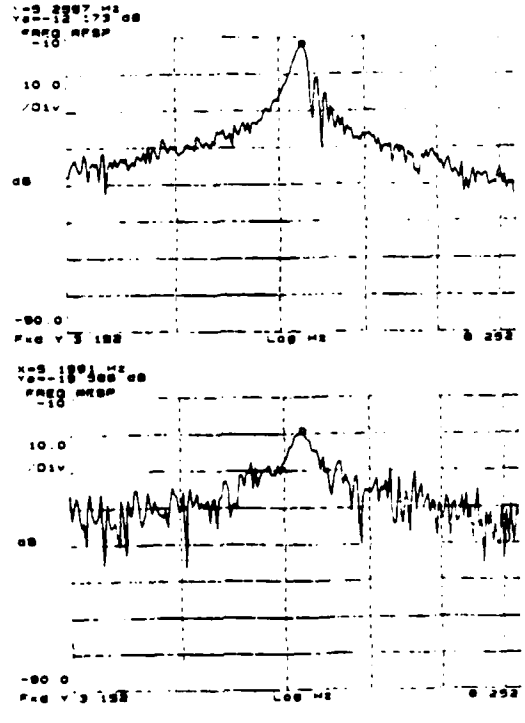

Figure 10. Frequency response from joint actuator to vibrations at the end of span 8 in the first link

INTERNATIONAL JOURNAL FOR NUMERICAL METHODS IN ENGINEERING, VOL. 36, 2725–2741 (1993)

A NON-RECURSIVE LAGRANGIAN SOLUTION OF THE NON-CAUSAL INVERSE DYNAMICS OF FLEXIBLE MULTIBODY SYSTEMS: THE PLANAR CASE

RAGNAR LEDESMA AND EDUARDO BAYO

Department of Mechanical Engineering, University of California, Santa Barbara, CA 93106, U.S.A.

SUMMARY

A technique is presented for solving the inverse dynamics of flexible planar multibody systems. This technique yields the non-causal joint efforts (inverse dynamics) as well as the internal states (inverse kinematics) that produce a prescribed nominal trajectory of the end effector. A non-recursive Lagrangian approach is used in formulating the equations of motion as well as in solving the inverse dynamics equations. Contrary to the recursive method previously presented, the proposed method solves the inverse problem in a systematic and direct manner for both open-chain as well as closed-chain configurations. Numerical simulation shows that the proposed procedure provides an excellent tracking of the desired end effector trajectory.

1. INTRODUCTION

Accurate positioning and vibration minimization of flexible multibody systems have generated considerable interest from the computational dynamics and controls communities. The advent of the new generation of very fast, lightweight robots and flexible articulated space structures has made the control of structural vibrations an important practical problem in the manufacturing and space industries, respectively.

There is a large body of literature dealing with the forward dynamic analysis of flexible multibody systems, *i.e.* the determination of the resulting motion when the joint forces and external forces are given. Several authors[1–10] have proposed the use of floating reference frames, while others[11–13] have put forward the use of inertial reference frames. Winfrey[1] proposed the superposition of linear deflection of flexible bodies to the non-linear rigid body motion. Bahgat and Willmert[2] presented a finite element approach for vibration analysis of planar mechanisms using the assumption that rigid body motion is determined by rigid body kinematic analysis and the elastic response is driven by the inertial forces generated by the rigid body motion. Likins[3] considered the coupling effects of rigid body motion and elastic deformation in the analysis of tree-structured flexible systems. De Veubeke[4] proposed the use of quasi-co-ordinates and a mean axis co-ordinate system to simplify the equations of motion. Song and Haug[5] proposed the use of centre-of-mass co-ordinates and elastic deflections as generalized co-ordinates for the analysis of planar mechanisms composed of beam elements. Shabana and Wehage[6] used the generalized co-ordinate partitioning method in the analysis of inertia-variant flexible mechanical systems. Sunada and Dubowsky[7] used four-by-four matrix methods and component mode synthesis to analyse three-dimensional flexible robots. Agrawal and Shabana[8] investigated the dynamic characteristics of general inertia-variant flexible multibody systems using Euler parameters for rigid body co-ordinates and different finite element mass formulations. Kim and Haug[9] extended

0029–5981/93/162725–17$13.50

Received 6 May 1992
Revised 21 December 1992

the recursive formulations for the dynamics of rigid multibodies to open-chain and closed-chain flexible multibody systems. Vukasovic *et al.*[10] presented the use of fully Cartesian co-ordinates in the analysis of flexible multibody systems. The efficiency of this approach lies in the fact that only the coupling terms between rigid and elastic co-ordinates become time-variant.

Different approaches which use the inertial frame of reference to describe the large overall motion of flexible beams have been proposed by Simo and Vu-Quoc,[11] Cardona and Geradin[12] and Avello *et al.*,[13] among others. The use of an inertial frame of reference leads to linear, uncoupled inertia terms in the expression for kinetic energy, while the expression for the potential energy functional becomes non-linear. Essential to this type of formulation is the use of finite strain and finite rotation theories that are capable of treating large deformations and large rotations. This approach has the advantage that it captures the non-linear stiffening effects that become important at large speeds of operation. However, it has the disadvantage of having a more involved implementation than the formulation based on the use of floating reference frames.

On the other hand, numerous control approaches have also been proposed for the position control of flexible multibody systems. An early work was that of Cannon and Schmitz,[14] who presented an optimal linear quadratic technique to control the tip trajectory of a single-link flexible robot arm. Singh and Schy[15] proposed a joint space close-loop control for elastic robots by applying a causal non-linear inversion and modal damping. Siciliano and Book[16] presented a singular perturbation approach to identify reduced-order systems used to obtain a collocated control scheme. Pfeiffer[17] suggested a multistage control strategy consisting of a feedforward based on rigid body inverse dynamics, and a stabilizing feedback on the linearized system around the rigid trajectory. De Luca *et al.*[18] proposed a closed-loop control scheme consisting of a model-based feedforward term and a linear feedback on joint angles. Oakley and Cannon[19] implemented a multilink arm controller based on the LQG design of the linearized arm.

Looking at the vibration minimization problem from another perspective, Bayo[20] presented the solution of the inverse dynamics of a single-link flexible arm in the frequency domain. The inverse dynamics yields a non-causal or time-delayed joint torque (applied in negative time and future time) that is capable of positioning the end effector according to a desired trajectory. Bayo and Moulin[21] extended the inverse dynamics to the time domain by making use of a bilateral convolution integral. Essential to the inverse dynamics of elastic multibodies is the realization that the joint efforts start actuating before the end effector or control point does. Consequently, for a small amount of time the joint forces do not cause any tip motion. This effect is called non-causality and the inverse dynamics has to account for it. This also constitutes a difference of significant importance between the rigid and flexible multibodies because in the rigid case the inverse dynamics is causal (instant response), whereas it is non-causal (time-anticipatory response) in the flexible case. As shown by Bayo and Moulin,[21] the causal integration of the inverse dynamics of the flexible case leads to unstable results. Kwon and Book[22] also proposed a solution for the inverse problem for a single-link flexible arm by dividing the inverse system into a causal part and an anticausal part to calculate the joint torque and state variables in the time domain for a given end effector trajectory. Bayo *et al.*[23] solved the multilink case using a recursive procedure suitable for open-chain configurations. The importance of using the inverse dynamics approach to vibration control has been demonstrated recently by Paden *et al.*[24] who have used passive feedback and feedforward of the inverse dynamics torque to achieve an exponentially stable tracking control law that yields excellent end-point tracking of flexible multibody systems.

Recursive methods are limited to open-chain configurations, since for closed-chain systems they require *ad hoc* procedures[23] that strongly depend on the given configurations. This limitation motivated the research described in this paper in which we present a non-recursive

Lagrangian approach for the solution of the non-causal (time-anticipatory) inverse dynamics of flexible multibody systems. This method provides a systematic way of generating and solving the inverse problem for open-chain as well as closed-chain systems in either the frequency or the time domain. In the next sections, the equations of motion are formulated and a solution procedure for the inverse dynamics of general planar flexible multibody systems is proposed. Simulation results for open-chain and closed-chain configurations are presented to illustrate the accuracy of the method.

2. MATHEMATICAL FORMULATION

In this paper, the floating frame of reference is used to represent the kinematics of the deformable bodies comprising the planar multibody system. Hence, the configuration of a typical component of a planar multibody shown in Figure 1 can be described by two sets of co-ordinates: the first set corresponds to the rigid body co-ordinates representing the location and orientation of the body axes with respect to the inertial frame; the second set corresponds to the so-called deformation co-ordinates or nodal deformations representing the deformation of the body with respect to the body axes. Using the aforementioned choice of co-ordinates, the location of an arbitrary point P in a planar deformable body i is given by[25]

$$\mathbf{r}^i = \mathbf{R}^i + \mathbf{A}^i\mathbf{u}^i \tag{1}$$

where $\mathbf{R}^i$ is the location of the origin of the body axes with respect to the inertial frame, $\mathbf{u}^i$ is the location of point P with respect to the body axes, and $\mathbf{A}^i$ is the rotation transformation matrix from the body axes to the inertial frame. In the planar case, the transformation matrix is given by

$$\mathbf{A}^i = \begin{bmatrix} \cos\theta^i & -\sin\theta^i \\ \sin\theta^i & \cos\theta^i \end{bmatrix} \tag{2}$$

where θ^i is the angle of rotation of the body axes with respect to the inertial frame. The vector $\mathbf{u}^i$ can be decomposed into

$$\mathbf{u}^i = \mathbf{u}_r^i + \mathbf{u}_f^i \tag{3}$$

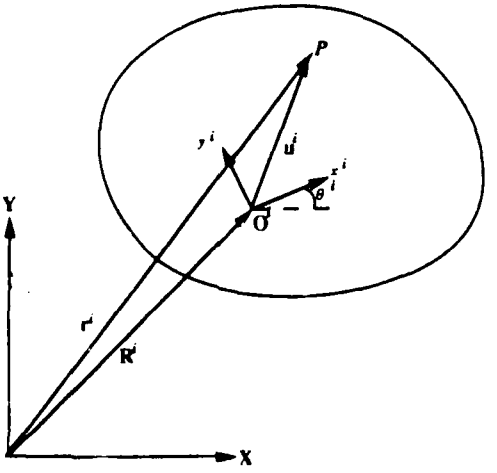

Figure 1. Reference co-ordinates for a planar body

where $\mathbf{u}_r^i$ is the position vector of point P in the undeformed state with respect to the body axes, and $\mathbf{u}_f^i$ is the deformation vector of point P with respect to the body axes. The deformation vector $\mathbf{u}_f^i$ can be expressed in terms of the nodal deformations by using a finite element discretization scheme

$$\mathbf{u}_f^i = \mathbf{N}^i \mathbf{q}_f^i \tag{4}$$

where $\mathbf{N}^i$ is the shape function matrix and $\mathbf{q}_f^i$ is the nodal deformation vector.

When reference co-ordinates such as those described above are employed in multibody systems, the system is then represented in terms of the co-ordinates $\mathbf{q}^T = [\mathbf{R}, \theta, \mathbf{q}_f]$. These co-ordinates are not independent because the motion of specific points in different bodies are related according to the type of mechanical joint that interconnects them. Moreover, in flexible mechanical systems the deformation of a component affects the configuration of adjacent components. As a consequence, the interdependence of the generalized co-ordinates is expressed by a vector of kinematic constraint equations, such as

$$\Phi(\mathbf{q}, t) = 0 \tag{5}$$

where $\mathbf{q}$ is the total vector of system generalized co-ordinates, t is time, and Φ is the vector of linearly independent holonomic constraint equations. These constraint equations can be further classified into: (1) rigid body constraints where only rigid body variables are involved in the constraint equation; (2) joint constraints where both rigid body and deformation co-ordinates are included in the constraint equation; (3) time-dependent constraints wherein the constraint equations can be explicit functions of time as well as generalized co-ordinates, as in the case of imposing the co-ordinates of the end-effector to follow a desired trajectory. To illustrate the construction of constraint equations, take the case of a revolute joint which connects two flexible planar bodies i and j at points P and Q shown in Figure 2. The two constraint equations corresponding to the constraint condition that requires points P and Q to be coincident can be written as

$$(\mathbf{R}^i + \mathbf{A}^i \mathbf{u}_P^i) - (\mathbf{R}^j + \mathbf{A}^j \mathbf{u}_Q^j) = 0 \tag{6}$$

We note that the constraint equation exemplified by equation (6) forms a set of coupled non-linear algebraic equations in the rigid body co-ordinates and deformation co-ordinates.

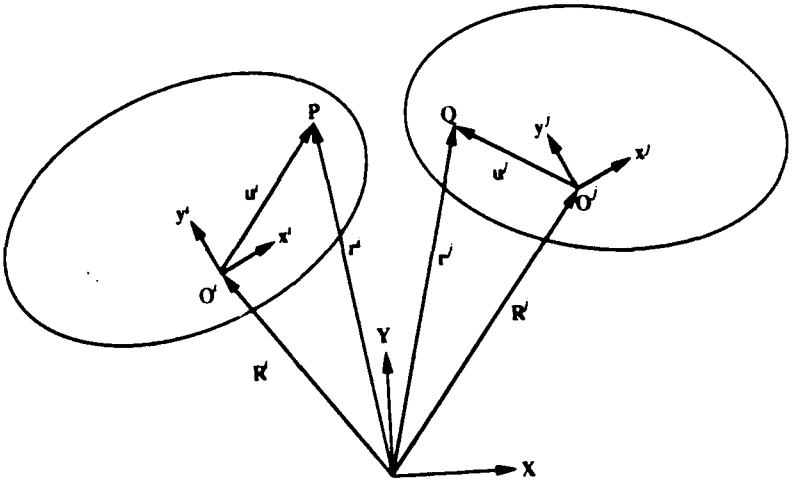

Figure 2. A pair of flexible planar bodies

Considering the rigid body and deformation co-ordinates described above as generalized co-ordinates, and following standard procedures in multibody dynamics, the constrained equations of motion become[25]

$$\mathbf{M}(\mathbf{q})\ddot{\mathbf{q}} + \mathbf{C}\dot{\mathbf{q}} + \mathbf{K}\mathbf{q} + \boldsymbol{\Phi}_{\mathbf{q}}^{\mathrm{T}}\boldsymbol{\lambda} = \mathbf{Q}_{\mathrm{e}} + \mathbf{Q}_{\mathrm{v}}(\mathbf{q}, \dot{\mathbf{q}}) \tag{7}$$

where $\mathbf{M}$, $\mathbf{C}$ and $\mathbf{K}$ are the system mass, damping and stiffness matrices, respectively, $\boldsymbol{\lambda}$ is the vector of Lagrange multipliers associated with the constraints, $\boldsymbol{\Phi}_{\mathbf{q}}$ is the constraint Jacobian matrix, $\mathbf{Q}_{\mathrm{e}}$ is the vector of applied external forces, and $\mathbf{Q}_{\mathrm{v}}$ is the quadratic velocity vector. The quadratic velocity vector contains the centrifugal forces and Coriolis forces that result from the differentiation of the kinetic energy expression with respect to the generalized co-ordinates.

2.1. *Forward dynamics*

In a forward dynamic analysis, *i.e.* finding the resulting motion given the applied joint forces and external forces, equations (5) and (7) form a mixed system of differential-algebraic equations that have to be solved simultaneously. As explained in the next section, the solution to the inverse dynamics problem requires a forward dynamic analysis within an iteration process. We solve the forward dynamics problem by using the augmented Lagrangian penalty formulation.[26] Applying the augmented Lagrangian penalty formulation to equations (5) and (7) results in the following equation:

$$\mathbf{M}(\mathbf{q})\ddot{\mathbf{q}} + \mathbf{C}\mathbf{q} + \mathbf{K}\mathbf{q} + \boldsymbol{\Phi}_{\mathbf{q}}^{\mathrm{T}}\boldsymbol{\alpha}[\ddot{\boldsymbol{\Phi}} + 2\boldsymbol{\mu}\boldsymbol{\omega}\dot{\boldsymbol{\Phi}} + \boldsymbol{\omega}^2\boldsymbol{\Phi}] = \mathbf{Q}_{\mathrm{e}} + \mathbf{Q}_{\mathrm{v}}(\dot{\mathbf{q}}, \mathbf{q}) - \boldsymbol{\Phi}_{\mathbf{q}}^{\mathrm{T}}\boldsymbol{\lambda}^{*} \tag{8}$$

where $\boldsymbol{\alpha}$ is a diagonal matrix of penalty factors whose elements are large real numbers that will assure the satisfaction of constraints, and $\boldsymbol{\omega}$ and $\boldsymbol{\mu}$ are diagonal matrices representing the natural frequencies and damping characteristics of the dynamic penalty system associated with the constraints. Values of α in the range $10^3 < \alpha < 10^6$ provide excellent results when working in double precision. The augmented Lagrangian method requires an iteration for the correct value of the Lagrange multipliers. The iterative equation for the Lagrange multipliers is given by

$$\boldsymbol{\lambda}_{i+1}^{*} + \boldsymbol{\lambda}_{i}^{*} + \boldsymbol{\alpha}[\ddot{\boldsymbol{\Phi}} + 2\boldsymbol{\mu}\boldsymbol{\omega}\dot{\boldsymbol{\Phi}} + \boldsymbol{\omega}^2\boldsymbol{\Phi}] \tag{9}$$

The iterative process described by equation (9) involves only a few additional operations during each iteration but it significantly improves the convergence of the forward dynamics solution as compared to the standard penalty method.[26]

The augmented Lagrangian penalty formulation has several advantages over the standard algorithms used in solving differential-algebraic equations. First, the method obviates the need to solve a mixed set of differential-algebraic equations and does not increase the number of equations to account for the constraints. Second, this method allows the use of standard unconditionally stable algorithms without the need of further stabilization techniques to control the violation of constraints during the integration process. Third, the method can handle redundant constraints and allows the multibody system to undergo singular positions. Fourth, the constraint forces (Lagrange multipliers) can be obtained as a by-product of the integration without having to integrate additional equations. Finally, the method assures convergence independent of the penalty values used.

2.2. *Inverse kinematics and inverse dynamics*

In the context of end-point motion and vibration control, inverse dynamics refers to the problem of finding the actuating forces or torques that will cause the end point of a flexible

multibody system to follow a desired trajectory. Moulin and Bayo[27] showed that because of the non-minimum-phase character of the inverse problem, the *unique stable solution* is found to be *non-causal*, i.e. actuation in required before the end-point has started to move as well as after the end-point has stopped. These findings have led to new theoretical discoveries in the inversion of non-linear non-minimum-phase systems such as flexible multibodies.[28,29] In addition, the fact that the stable solution starts at negative time and extends into future time precludes the standard time-domain integration schemes currently available in multibody computer codes from obtaining the proper inverse solution. These codes will yield causal, and hence unstable, results and therefore are valid only for the forward dynamics. The integration process is therefore essential to obtain non-causal solutions, and the time-anticipatory effect can be obtained by integrating in the frequency domain or in the time domain using the bilateral Laplace transform.

It is important to note that when the dynamic effects of the elastic modes are small (quasi-rigid cases), causal inverse solutions may be obtained by regularizing the problem with the addition of artificial damping either through the damping matrix or the numerical integration scheme. However, this *ad hoc* process changes the nature of the problem and does not yield the desired time delay effect.

Previous solutions[21,23] to the inverse problem relied on a pinned–free finite element model of a flexible beam, and the equation for the inverse dynamics torque was formulated by imposing the condition that the transverse deformation of the free end of each link be zero throughout the motion. This type of model led to a recursive scheme to solve the inverse dynamics of multilink flexible manipulators. This recursive procedure is suitable for open-chain but not for closed-chain configurations.

In this section, we describe a non-recursive Lagrangian approach to solve the general planar inverse dynamics problem. Compared to the recursive procedure, this non-recursive Lagrangian approach is more systematic and becomes the only choice when closed-chain systems are encountered. We model the elastic links under pinned–pinned boundary conditions. This allows us to express the end effector trajectory in terms of the rigid body co-ordinates only and, in addition, leads to a simplified form of the inverse kinematics equations for the internal states. Once the correct internal states are known, the equations of motion give an explicit expression for the inverse dynamics torque.

In partitioned form, equation (7) can be written as

$$\begin{bmatrix} \mathbf{m}_{RR} & \mathbf{m}_{R\theta} & \mathbf{m}_{Rf} \\ \mathbf{m}_{\theta R} & \mathbf{m}_{\theta\theta} & \mathbf{m}_{\theta f} \\ \mathbf{m}_{fR} & \mathbf{m}_{f\theta} & \mathbf{m}_{ff} \end{bmatrix} \begin{bmatrix} \ddot{\mathbf{R}} \\ \ddot{\theta} \\ \ddot{\mathbf{q}}_f \end{bmatrix} + \begin{bmatrix} 0 & 0 & 0 \\ 0 & 0 & 0 \\ 0 & 0 & \mathbf{c}_{ff} \end{bmatrix} \begin{bmatrix} \dot{\mathbf{R}} \\ \dot{\theta} \\ \dot{\mathbf{q}}_f \end{bmatrix} + \begin{bmatrix} 0 & 0 & 0 \\ 0 & 0 & 0 \\ 0 & 0 & \mathbf{k}_{ff} \end{bmatrix} \begin{bmatrix} \mathbf{R} \\ \theta \\ \mathbf{q}_f \end{bmatrix}$$

$$+ \begin{bmatrix} \boldsymbol{\Phi}_R^T \\ \boldsymbol{\Phi}_\theta^T \\ \boldsymbol{\Phi}_{q_f}^T \end{bmatrix} \lambda = \begin{bmatrix} \mathbf{Q}_{eR} \\ \mathbf{Q}_{e\theta} \\ \mathbf{Q}_{ef} \end{bmatrix} + \begin{bmatrix} \mathbf{Q}_{vR} \\ \mathbf{Q}_{v\theta} \\ \mathbf{Q}_{vf} \end{bmatrix} \tag{10}$$

The second set of equations in equation (10) can be rearranged to express the externally applied joint forces as

$$\mathbf{Q}_{e\theta} = \mathbf{m}_{\theta R}\ddot{\mathbf{R}} + \mathbf{m}_{\theta\theta}\ddot{\theta} + \mathbf{m}_{\theta f}\ddot{\mathbf{q}}_f + \boldsymbol{\Phi}_\theta^T\boldsymbol{\lambda} - \mathbf{Q}_{v\theta} \tag{11}$$

Equation (11) constitutes the inverse dynamics equation that yields the joint forces (torques) necessary for the end-point to follow a prescribed trajectory. In order to obtain $\mathbf{Q}_{e\theta}$, the nodal acceleration vector $\ddot{\mathbf{q}}_f$ is needed. This vector can be obtained from the third set of equations in

equation (10), which can be written as

$$\mathbf{m}_{ff}\ddot{\mathbf{q}}_f + \mathbf{c}_{ff}\dot{\mathbf{q}}_f + \mathbf{k}_{ff}\mathbf{q}_f = \mathbf{Q}_{ef} + \mathbf{Q}_{vf} - \boldsymbol{\Phi}_{q_f}^{\mathrm{T}}\boldsymbol{\lambda} - \mathbf{m}_{fR}\ddot{\mathbf{R}} - \mathbf{m}_{f\theta}\ddot{\theta} \tag{12}$$

The vector of applied nodal forces $\mathbf{Q}_{ef}$ can be expressed in terms of the externally applied torques through the following mapping:

$$\mathbf{Q}_{ef} = \mathbf{G}_f\mathbf{Q}_{e\theta} \tag{13}$$

where in the planar case, the matrix $\mathbf{G}_f$ is a constant Boolean matrix which maps the externally applied torques to the vector of externally applied nodal forces. For example, in the open-chain planar multibody system shown in Figure 3, the Boolean matrix $\mathbf{G}_f$ is constructed such that the external moment on the node located at the base of the first link is equal to the base motor torque, the moment on the node located at the tip of the first link is the negative of the elbow motor torque, the external moment on the node located at the base of the second link is equal to the elbow motor torque, and all other external forces are zero. The same technique can be applied for the closed-chain multibody system shown in Figure 9, where the Boolean matrix $\mathbf{G}_f$ is constructed such that the externally applied nodal forces are equal to the motor torques at the rotational degree of freedom of the nodes where the motors are located and zero elsewhere. Substituting equations (11) and (13) into equation (12) results in

$$\mathbf{m}_{ff}\ddot{\mathbf{q}}_f + \mathbf{c}_{ff}\dot{\mathbf{q}}_f + \mathbf{k}_{ff}\mathbf{q}_f = \mathbf{G}_f\mathbf{m}_{\theta f}\ddot{\mathbf{q}}_f + \mathbf{F}_1(\lambda, \mathbf{q}_r, \dot{\mathbf{q}}_r, \ddot{\mathbf{q}}_r, \mathbf{q}_f, \dot{\mathbf{q}}_f) \tag{14}$$

where $\mathbf{F}_1$ is a force vector that includes the inertial terms, reaction terms between contiguous bodies and quadratic velocity terms.

The problem statement for the inverse kinematics is that of finding the non-causal internal states $\mathbf{q}_f$ so that the end-point co-ordinates characterized by a subset of the rigid body co-ordinates $\mathbf{q}_r$ follow a prescribed trajectory. The inverse kinematic equations of equation (14) are non-linear in the variable $\mathbf{q}_f$. The non-linear non-causal inversion cannot be carried out by standard numerical integration of ODEs. It requires a linearization process in either the frequency domain or the time domain, or splitting the linearized system into its causal and anticausal components.

The key to the linearization process for the non-recursive approach relies on decomposing the inertial coupling submatrix $\mathbf{m}_{\theta f}$ into the sum of a time-invariant matrix and a time-varying matrix

$$\mathbf{m}_{\theta f} = \mathbf{m}_{\theta f}^{c} + \mathbf{m}_{\theta f}^{t} \tag{15}$$

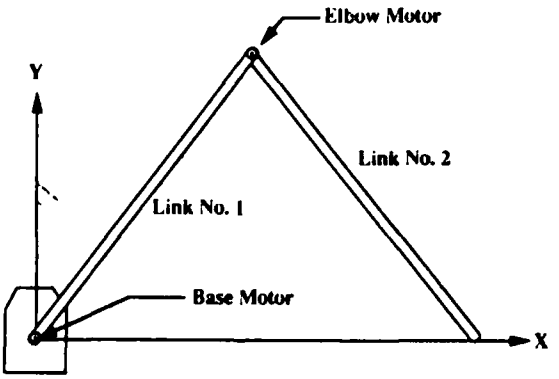

Figure 3. Open-chain flexible multibody system

where $\mathbf{m}_{\theta f}^{c}$ and $\mathbf{m}_{\theta f}^{l}$ are the time-invariant part and time-varyng part of $\mathbf{m}_{\theta f}$, respectively. This decomposition is essential for the iteration process needed to obtain the non-causal solution to the non-linear inversion problem. Substituting equation (15) into Equation (14), we obtain the inverse kinematics equation of motion for the nodal displacements $\mathbf{q}_f$:

$$\mathbf{m}_{ff}^{*}\ddot{\mathbf{q}}_f + \mathbf{c}_{ff}\dot{\mathbf{q}}_f + \mathbf{k}_{ff}\mathbf{q}_f = \mathbf{F}(\lambda, \mathbf{q}_r, \dot{\mathbf{q}}_r, \ddot{\mathbf{q}}_r, \mathbf{q}_f, \dot{\mathbf{q}}_f, \ddot{\mathbf{q}}_f) \tag{16}$$

where

$$\mathbf{m}_{ff}^{*} = \mathbf{m}_{ff} - \mathbf{G}_f \mathbf{m}_{\theta f}^{c} \tag{17}$$

The mass matrix $\mathbf{m}_{ff}^{*}$ is non-symmetric and it is precisely the non-symmetry of the mass matrix that produces internal states which are non-causal with respect to the end-point motion when non-causal techniques are employed to obtain the proper inversion of the non-linear, non-minimum problem characterized by equation (16). The non-linear inversion can now be carried out efficiently in the frequency domain, since the leading matrices have been constructed such that they remain constant throughout the motion. We thus solve equation (16) iteratively in the frequency domain to yield the nodal deformation vector $\mathbf{q}_f$ that is non-causal with respect to the end-point motion.

In the frequency domain, equation (16) can be written as a set of complex equations for a particular frequency $\bar{\omega}$

$$\left[\mathbf{m}_{ff}^{*} + \frac{1}{i\bar{\omega}}\mathbf{c}_{ff} - \frac{1}{\bar{\omega}^2}\mathbf{k}_{ff}\right]\hat{\ddot{\mathbf{q}}}_f(\bar{\omega}) = \hat{\mathbf{F}}(\bar{\omega}) \tag{18}$$

where $\hat{\ddot{\mathbf{q}}}_f(\bar{\omega})$ is the Fourier transform of $\ddot{\mathbf{q}}_f(t)$ and $\hat{\mathbf{F}}(\bar{\omega})$ is the Fourier transform of $\mathbf{F}(t)$. Equation (18) is based on the assumption that $\ddot{\mathbf{q}}_f(t)$ and $\mathbf{F}(t)$ are Fourier-transformable. This assumption is valid for slewing motions which are from rest to rest. The nodal acceleration vector $\hat{\ddot{\mathbf{q}}}_f(\bar{\omega})$ can be obtained directly from equation (18) for each frequency $\bar{\omega}$. The leading matrix of equation (18) is a complex regular matrix that is invertible for all frequencies except $\bar{\omega} = 0$. However, for $\bar{\omega} = 0$, the system undergoes a rigid body motion determined only by the invertible mass matrix $\mathbf{m}_{ff}^{*}$. However, we note that the forcing vector on the right-hand side of equation (18) depends on the nodal deformations, velocities and accelerations. We use a successive substitution scheme to iterate for the nodal deformations, velocities and accelerations. Finally, the nodal accelerations in the time domain may be obtained through the application of the inverse Fourier transform, i.e.

$$\ddot{\mathbf{q}}_f(t) = \frac{1}{2\pi}\int_{-\infty}^{\infty} \hat{\ddot{\mathbf{q}}}_f(\bar{\omega})\, e^{i\bar{\omega}t}\, d\bar{\omega} \tag{19}$$

Once the non-causal nodal accelerations are known, equation (11) can be used to compute explicitly the non-causal inverse dynamics joint efforts that will move the end effector according to a desired trajectory. We note, however, that the inverse dynamics torque and internal states given by equations (11) and (16), respectively, depend on the Lagrange multipliers and rigid body co-ordinates, which in turn depend on the internal states and the applied torque. Moreover, the rigid body co-ordinates and Lagrange multipliers are different from their nominal values when the components of the multibody system are flexible. Therefore, a forward dynamic analysis is required to obtain an improved estimate of the generalized co-ordinates and Lagrange multipliers. In order to ensure that the iteration process converges to obtain the joint efforts that will cause the end-effector to follow the desired trajectory, the forward dynamics analysis is carried out with the additional constraint that the co-ordinates of the end-point follow the desired trajectory. These additional constraints have corresponding Lagrange multipliers which act as correcting terms to the joint efforts that have previously been calculated.

It is important to note that the computation of the nodal acceleration vector in each iteration can also be carried out in the time domain through the use of the bilateral Laplace transform

$$\ddot{\mathbf{q}}_f(t) = \int_{-\infty}^{\infty} \sum_{i=1}^{i=n} \mathbf{h}_i(t-\tau) f_i(\tau)\, d\tau \tag{20}$$

where $\mathbf{h}_i(t)$ is the acceleration response vector to an impulse applied to the ith degree of freedom and $f_i(t)$ is the ith component of the forcing term on the right-hand side of equation (16). We note that the integration from $-\infty$ to ∞ is necessary to capture the non-causal effects.

To summarize, the procedure for obtaining the inverse dynamics solution for flexible multibody systems involves the following steps:

Algorithm

1. Perform a rigid body inverse dynamic analysis to obtain the nominal values of the rigid body co-ordinates $\mathbf{q}_r$ and Lagrange multipliers λ.
2. Solve the inverse kinematics equation in the frequency domain through equation (16) or in the time domain through equation (20) to obtain the time-delayed nodal accelerations $\ddot{\mathbf{q}}_f$.
3. Compute the inverse dynamics joint efforts $\mathbf{Q}_{c\theta}$ using equation (11).
4. Perform a forward dynamic analysis using equation (8) to obtain new values for the generalized co-ordinates and Lagrange multipliers.
5. Repeat steps 2–4 until convergence in the inverse dynamics torques is achieved.

It is worthwhile to compare the recursive procedure[23] and the non-recursive Lagrangian procedure for the inverse dynamics of multibody systems. In the former method, each body in the multibody system is analysed sequentially starting from the last element in the chain. For each element, the joint torques are determined first under the assumption that the rigid body co-ordinates are moving according to the nominal trajectory. With the joint actuation known for this component, a forward dynamic analysis is carried out to determine the nodal deformations, and the reaction forces from the next element in the chain are subsequently determined from equilibrium considerations. This recursive method works very well for open-chain systems, but it is not suitable for closed-chain systems because it requires the analyst to cut the loop of the closed chain and account for the reaction forces at the cuts through *ad hoc* procedures. The non-recursive Lagrangian method avoids this problem since the reaction between system components are automatically accounted for by the Lagrange multipliers and no distinction is made between open-chain and closed-chain configurations. The non-recursive procedure is thus more systematic and general.

3. SIMULATION RESULTS

In this section we present the results of numerical simulations that verify the procedure discussed above. First, we apply the proposed non-recursive Lagrangian approach to an open-chain flexible multibody system and compare the results with those obtained by the recursive method[23] to test the validity of the proposed procedure. Next, we present the results of the application of the non-recursive Lagrangian approach to a closed-chain flexible multibody system to determine the inverse dynamics torque that will produce the desired motion at the end effector.

3.1. Open-chain multibody system

Figure 3 shows a two-link flexible multibody system in the horizontal plane. The end-point of the second link is specified to move along the x-axis according to the acceleration profile

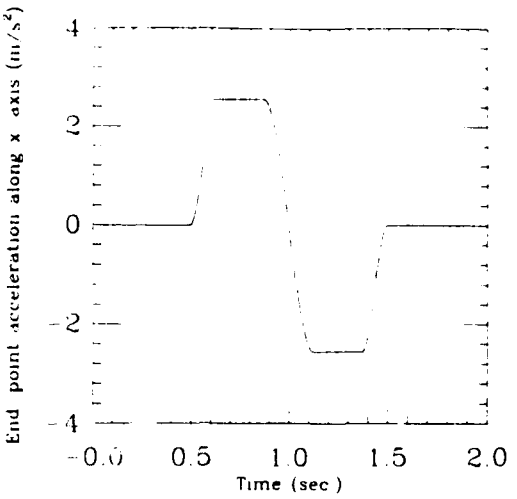

Figure 4. End-point acceleration along the x-axis

described by Figure 4, which corresponds to an end-point displacement of 0·483 meters along the x-axis. The geometric and material properties of the links are as follows:

First link:

Length 0·66 m
Cross-sectional area $1{\cdot}2 \times 10^{-4}$ m^2
Cross-sectional second moment of area $2{\cdot}3 \times 10^{-10}$ m^4

Second link:

Length: 0·66 m
Cross-sectional area $4{\cdot}0 \times 10^{-5}$ m^2
Cross-sectional second moment of area $8{\cdot}5 \times 10^{-12}$ m^4

The two links share the following properties:

Young's modulus 14 GPa
Mass density 2715 kg/m^3

In Figure 5, the inverse dynamics torque profile for the base motor using the non-recursive method is superimposed on the inverse dynamics torque profile determined by the recursive method. The inverse dynamics torque profiles for the elbow motor computed by the two aforementioned methods are superimposed in Figure 6. Both the recursive and non-recursive formulations yield the same result and can be superimposed on each other (solid curve), thus validating the proposed method. The corresponding rigid body torques are also shown as dashed curves in Figures 5 and 6 to illustrate the pre-actuation and post-actuation present in the inverse dynamics flexible torque profiles.

Figure 7 shows comparison of the elastic angular rotation at the base of the second link obtained by a feedforward of the inverse dynamics torque (solid curve) to that obtained by a feedforward of the rigid body torque (dashed curve). We observe that while the inverse dynamics torque does not induce residual vibration, the rigid body torque induces substantial residual oscillation.

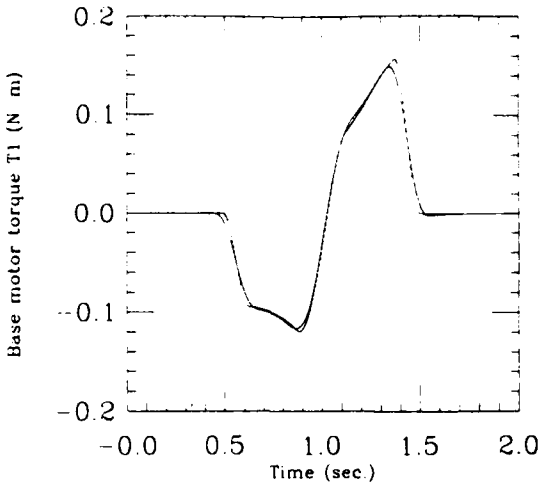

Figure 5. Base motor inverse dynamics (——) and rigid (. . . . .) torques

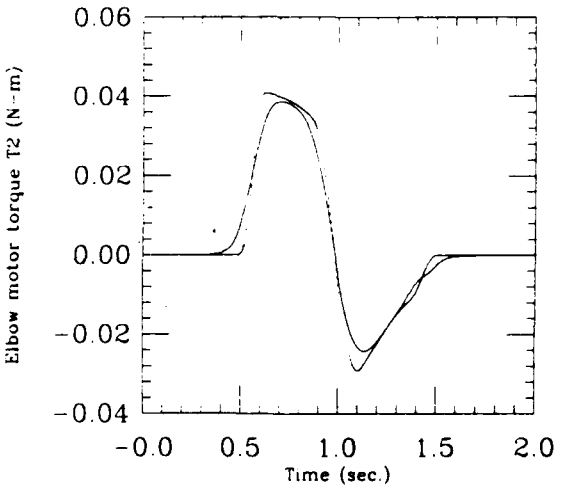

Figure 6. Elbow motor inverse dynamics (——) and rigid (. . . . .) torques

Figure 8 shows a comparison of the vertical tip error obtained by a feedforward of the inverse dynamics torque obtained using the non-recursive approach (solid curve) and the vertical tip error obtained by a feedforward of the rigid body torque (dashed curve). We observe that while the inverse dynamics torque provides an excellent tracking of the tip trajectory, the rigid body torque induces a large oscillation in the tip motion.

3.2. Closed-chain multibody system

Figure 9 shows a closed-chain flexible multibody system made up of four flexible links with two joints which are fixed against translation relative to the ground. As in the open-chain case, the multibody system is assumed to lie on a horizontal plane so that gravity effects are neglected. The

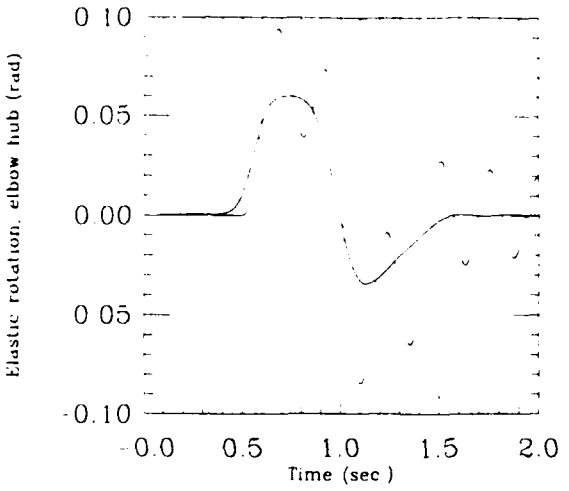

Figure 7. Elastic hub rotation: inverse dynamics (——) vs. rigid (. . . . . .) torques

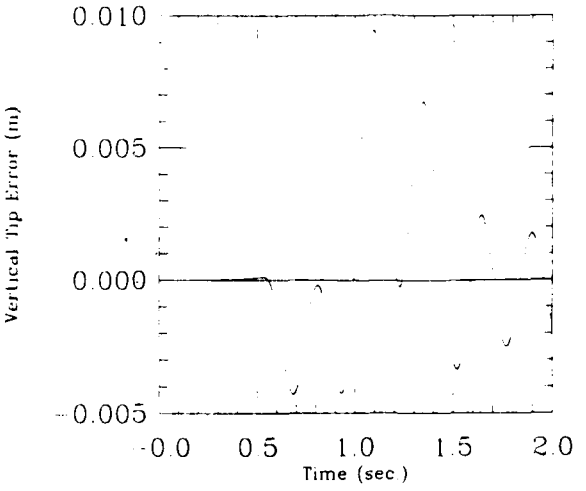

Figure 8. Vertical tip error: inverse dynamics (——) vs. rigid (. . . . . .) torques

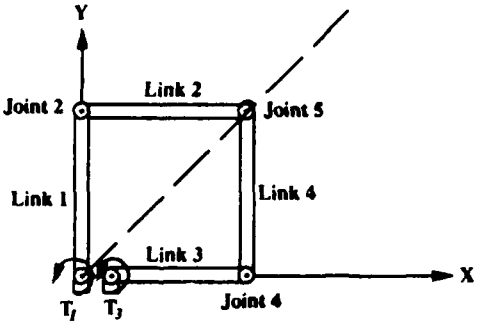

Figure 9. Closed-chain flexible multibody system

desired trajectory of joint 5 is a straight line at 45° with respect to the x- and y-axis. The x- and y-components of the acceleration of joint 5 are specified to follow the acceleration profile shown in Figure 10. The four links share the following geometric and material properties:

Length 0·60 m
Cross-sectional area $4{\cdot}0 \times 10^{-5}$ m^2
Cross-sectional second moment of area $8{\cdot}5 \times 10^{-12}$ m^4
Young's modulus 14 GPa
Mass density 2715 kg/m^3

Figure 11 shows the inverse dynamics torque profile at joint 1 obtained by the non-recursive method (solid curve). The rigid body inverse dynamics torque profile is superimposed for

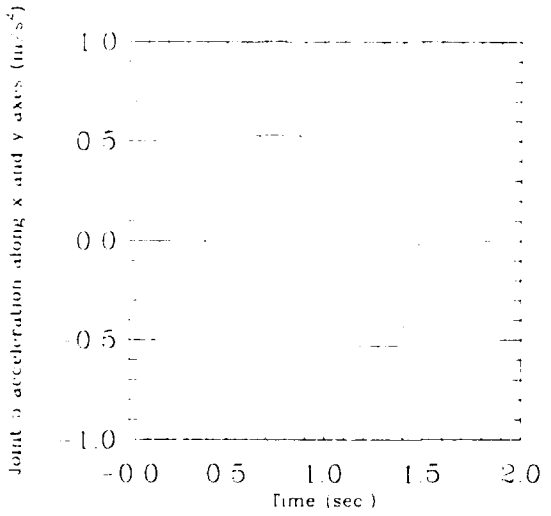

Figure 10. End-point acceleration along the x- and y-axis

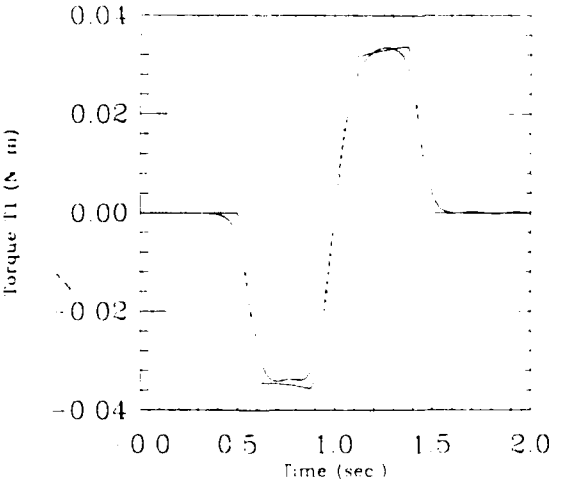

Figure 11. Joint 1 inverse dynamics (——) and rigid (. . . . . .) torques

comparison (dashed curve). The figure shows the non-causal (time-anticipatory) character of the solution for the inverse problem. Figure 12 shows the inverse dynamic torque profile (solid curve) at joint 3 superimposed with the corresponding rigid body torque profile (dashed curve). Again, the time delay due to the non-causality of the solution is seen in this figure.

Figure 13 shows the elastic angular rotation at the base of the first link obtained by a feedforward of the inverse dynamics torque (solid curve). Superimpossed in the same figure is the corresponding elastic angular rotation obtained by a feedforward of the rigid body torque (dashed curve). Whereas the rigid body torque produces residual angular rotations, the inverse dynamic torque does not show residual angular rotations. As a matter of fact, it was observed in the simulations that the rigid body torques produced residual vibration in all the nodal

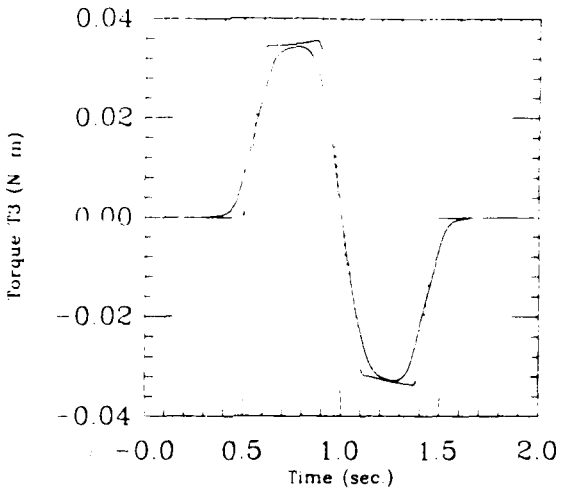

Figure 12. Joint 3 inverse dynamics (——) and rigid (. . . . .) torques

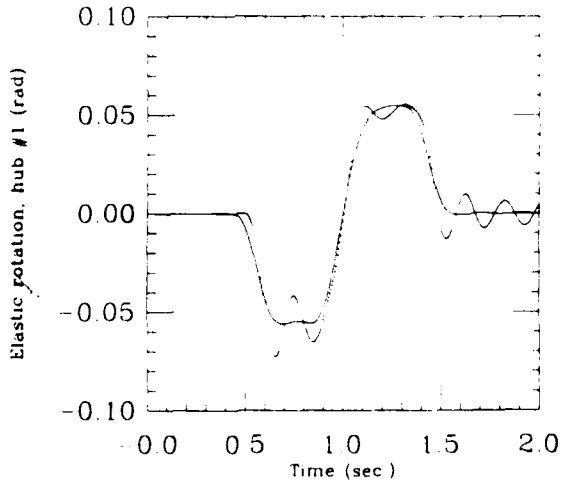

Figure 13. Elastic hub rotation: inverse dynamics (——) vs. rigid (. . . . .) torques

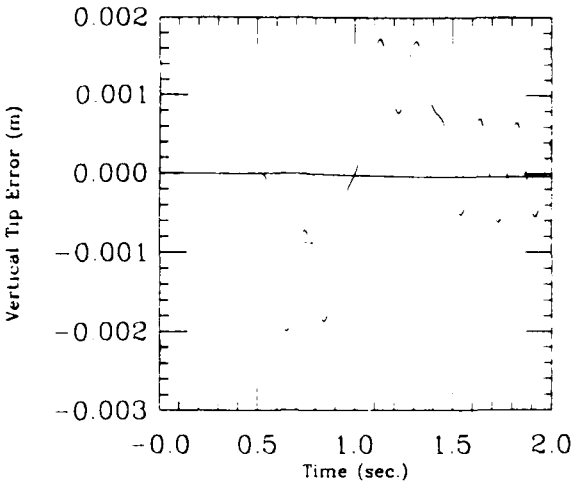

Figure 14. Vertical tip error: inverse dynamics (——) vs. rigid (. . . . .) torques

deformations while the inverse dynamics torques eliminated the residual oscillation. Furthermore, the inverse dynamics torques produced nodal deformations which exhibited non-causal characteristics with respect to the end-point motion. Figure 14 shows a comparison of the vertical tip error at joint 5 obtained by a feedforward of the inverse dynamics torque (solid curve) with the tip error resulting from a feedforward of the rigid body torque (dashed curve). This figure shows that the inverse dynamics torque provides an excellent tracking of the desired end effector trajectory whereas the rigid body torque again induces substantial vibration on the end-point motion.

The numerical simulations reported in this paper were carried out using a single-processor Sun Sparcstation 1. For the open-chain multibody system, the CPU time was 14 s for the recursive method and 37 s for the non-recursive method. As expected, the recursive method is more efficient than the non-recursive method for open-chain problems since the former solves the system equations one link at a time, hence significantly reducing the dimension of the problem. However the non-recursive method can easily be amended to take advantage of parallel processors, hence enabling the method to become more attractive when multiprocessors are used.

For the closed-chain multibody system presented above, the non-recursive method was used to solve the inverse dynamics problem with a CPU time of 96 s. The use of the recursive procedure for the closed-chain system would require an *ad hoc* procedure where the analyst must decide where to cut the chain and impose proper boundary conditions on the resulting tree-structured open-chain system. Hence, the recursive method becomes too cumbersome for the inverse dynamics of closed-chain systems, and for this reason it was not used to simulate the closed-chain system.

4. CONCLUSION

A non-recursive Lagrangian approach for the inverse dynamics of flexible multibody systems has been presented. The procedure is capable of solving for the non-causal inverse dynamics torque profiles of both open-chain and closed-chain flexible multibody systems in a unified and systematic manner. The method is found to produce an excellent tracking of the desired trajectory

of the end effector. In a future paper, we will address the inverse dynamics problem for flexible multibody systems undergoing motion in three dimensions. New problems arise in the three-dimensional case, since the actuating torque vectors have directions which are time-varying and non-linear functions of the rigid body co-ordinates, in contrast to the planar case where the applied torque vectors have directions fixed perpendicular to the plane of the multibody system. In addition, controllability and accessability issues need to be addressed.

ACKNOWLEDGEMENTS

The support of this work by the Air Force Office of Scientific Research under contract F49620-91-C-0095 and by TRW are gratefully acknowledged.

REFERENCES

1. R. C. Winfrey, 'Elastic link mechanism dynamics,' *ASME J. Eng. Ind.*, **B93**, 268–272 (1971).
2. B. M. Bahgat and K. D. Willmert, 'Finite element vibrational analysis of planar mechanisms,' *Mech. Machine Theory*, **8**, 497–516 (1973).
3. P. W. Likins, 'Dynamic analysis of a system of hinge connected rigid bodies with nonrigid appendages,' *NASA Technical Report 32-1576*, Feb. 1974
4. B. F. De Veubeke, 'The dynamics of flexible bodies,' *Int. J. Eng. Sci.*, **14**, 895–913 (1976).
5. J. O. Song and E. J. Haug, 'Dynamic analysis of planar flexible mechanisms,' *Comput. Methods Appl. Mech. Eng.*, **24**, 359–381 (1980).
6. A. A. Shabana and R. A. Wehage, 'A co-ordinate reduction technique for transient analysis of spatial substructures with large angular rotations,' *J. Struct. Mech.*, **11**, 401–431 (1983).
7. W. Sunada and S. Dubowsky, 'On the dynamic analysis and behavior of industrial robotic manipulators with elastic members,' *ASME J. Mechanisms, Transmissions Automation Des.*, **105**, 42–51 (1983).
8. O. P. Agrawal and A. A. Shabana, 'Application of deformable body mean axis to flexible multibody system dynamics,' *Comput Methods Appl. Mech. Eng.*, **56**, 217–245 (1986).
9. S. S. Kim and E. J. Haug, 'A recursive formulation for flexible multibody dynamics. Part 1. Open-loop systems,' *Comput. Methods Appl. Mech. Eng.*, **71**, 293–314 (1988).
10. N. Vukasovic, J. Celigueta, J. Garcia de Jalon and E. Bayo, 'Flexible multibody dynamics based on a fully Cartesian system of support coordinates,' *ASME J. Mech. Des.*, **114**, (1992).
11. J. C. Simo and L. Vu-Quoc, 'On the dynamics of flexible beams under large overall motions—the planar case. Parts 1 & 2,' *J. Appl. Mech.*, **53**, 849–863 (1986).
12. A. Cardona and M. Geradin, 'A beam finite element non-linear theory with finite rotations,' *Int. j. numer. methods eng.*, **26**, 2403–2438 (1988).
13. A. Avello, J. Garcia de Jalon and E. Bayo, 'Dynamics of flexible multibody systems with Cartesian coordinates and large deformation theory,' *Int. j. numer. methods eng.*, **32**, 1543–1563 (1991).
14. R. H. Cannon and E. Schmitz, 'Initial experiments on end-point control of a flexible one-link robot,' *Int. J. Robotics Res.*, **3**(3), 62–75 (1984).
15. S. N. Singh and A. A. Schy, 'Control of elastic robotic systems by nonlinear inversion and modal damping,' *ASME J. Dyn. Syst. Measurement Control*, **108**, 180–189 (1986).
16. B. Siciliano and W. J. Book, 'A singular perturbation approach to control light-weight flexible manipulators,' *Int. J Robotics Res.*, **7**(4), 79–90, (1988).
17. F. G. Pfeiffer, 'A feedforward decoupling concept for the control of elastic robots,' *J. Robotic Syst.*, **6**, 407–416 (1989).
18. A. De Luca, L. Lanari, P. Lucibello, S. Panzieri and G. Ulivi, 'Control experiments on a two-link robot with a flexible forearm,' *Proc. 29th IEEE Conf on Decision and Control*, Vol. 2, Honolulu, Hawaii, December 1990, pp. 520–527.
19. C. M. Oakley and R. H. Cannon, 'Anatomy of an experimental two-link flexible manipulator under end-point control,' *Proc. 29th IEEE Conf. on Decision and Control*, Vol. 2, Honolulu, Hawaii, December 1990, pp. 507–513.
20. E. Bayo, 'A finite-element approach to control the end-point motion of a single-link flexible robot,' *J. Robotic Syst.*, **4**, 63–75 (1987).
21. E. Bayo and H. Moulin, 'An efficient computation of the inverse dynamics of flexible manipulators in the time domain,' *Proc. IEEE Conf. on Robotics and Automation*, Scottsdale, Arizona, 1989, pp. 710–715.
22. D. S. Kwon and W. J. Book, 'An inverse dynamic method yielding flexible manipulator state trajectories,' *Proc American Control Conference*, Vol. 1, San Diego, California, 1990, pp. 186–193.
23. E. Bayo, P. Papadopoulos, J. Stubbe and M. Serna, 'Inverse kinematics and dynamics of a multi-link elastic robot: an iterative frequency domain', *Int. J. Robotics Res.*, **8**(6), 49–62 (1989).
24. B. Paden, D. Chen, R. Ledesma and E. Bayo, 'Exponentially stable tracking control for multi-joint flexible-link manipulators,' *ASME J. Dyn. Syst. Measurement Control* (accepted).

25. A. A. Shabana, *Dynamics of Multibody Systems*, Wiley, New York, 1989.
26. E. Bayo, J. Garcia de Jalon, A. Avello and J. Cuadrado, 'An efficient computational method for real time multibody dynamic simulation in fully Cartesian coordinates,' *Comput. Methods Appl. Mech. Eng.*, **92**, 377–395 (1991).
27. H. Moulin and E. Bayo, 'On the end-point trajectory tracking for flexible manipulators through non-causal inverse dynamics,' *ASME J. Dyn. Syst. Measurement Control*, **113**, 320–324 (1991).
28. B. Paden and D. Chen, 'Zero dynamics and inversion of nonlinear systems,' *Proc. U.S.-Japan Conference on Flexible Automation*, San Francisco, California, 1992.
29. B. Paden and D. Chen, 'A state-space condition for the invertibility of nonlinear nonminimum phase systems,' *Proc. ASME Winter Annual Meeting*, Anaheim, California, 1992.

A Lagrangian Approach to the Non-causal Inverse Dynamics of Flexible Multibody Systems: The Three-Dimensional Case

Ragnar Ledesma

Eduardo Bayo

Department of Mechanical Engineering
University of California
Santa Barbara, CA 93106

ABSTRACT

This paper addresses the problem of end-point trajectory tracking in flexible multibody systems through the use of inverse dynamics. A global Lagrangian approach is employed in formulating the system equations of motion, and an iterative procedure is proposed to achieve end-point trajectory tracking in three-dimensional, flexible multibody systems. Each iteration involves firstly, a recursive inverse kinematics procedure wherein elastic displacements are determined in terms of the rigid body coordinates and Lagrange multipliers, secondly, an explicit computation of the inverse dynamic joint actuation, and thirdly, a non-recursive forward dynamic analysis wherein generalized coordinates and Lagrange multipliers are determined in terms of the joint actuation and desired end-point coordinates. In contrast with the recursive methods previously proposed, this new method is the most general since it is suitable for both open-chain and closed-chain configurations of three-dimensional multibody systems. The algorithm yields stable, *non-causal* actuating joint torques and associated Lagrange multipliers that account for the constraint forces between flexible multibody components.

1. Introduction

The effect of elastic deformation on the dynamics of multibody systems has been vigorously studied during the past thirty years. In particular, the modeling of multibody components as elastic beams has received considerable attention as made evident in the survey papers of Lowen and Jandrastis,[1] Erdman and Sandor,[2] Modi,[3] and more recently by Lowen and Chassapis.[4] A specific area of interest with regards to flexible multibody systems, especially in the aerospace and robotics industries, is in controlling the motion of a specified point in the multibody system. In most cases, the control objective is to have the end-point of the multibody system follow a desired trajectory. Various feedback control strategies for the problem of end-point trajectory tracking have been proposed, and the survey papers of Balas[5] and Book[6] present some of the approaches advanced by the controls community towards this problem.

The problem of end-point trajectory tracking in flexible multibody systems has led to the development of computational methods commonly referred to as inverse dynamics. Inverse dynamics deals with the problem of determining the joint actuation that will cause a specified control point in the flexible multibody system to follow a desired trajectory. The pioneering work of Reference 7 on the trajectory control of a single flexible link through inverse dynamics showed that the inverse dynamic torque is *non-causal* with respect to the end-point motion, *i.e.*, actuation is required before the end-point has started to move as well as after the end-point has stopped. Moulin[8] demonstrated that because of the non-minimum phase character of the inverse dynamics for the trajectory tracking problem, the only bounded solution for the inverse dynamic torque has to be non-causal. Bayo, *et. al.*,[9] extended the inverse dynamics to planar, multiple-link systems using an iterative frequency domain approach. The recursive method proposed in that study is suitable for planar open-chain systems, but required an *ad hoc* procedure for planar closed-chain systems. A time domain inverse dynamics technique based on the non-causal impulse response function was presented by Bayo and Moulin[10] for the single link system, with provisions for extension to multiple link systems. An equivalent time domain approach for a single link arm was proposed by Kwon and Book[11] where the

non-causality of the computed torque was captured by dividing the inverse system into causal and anticausal parts. Recently, a more systematic and more general non-recursive, frequency domain method for the inverse dynamics of *planar* multibody systems was proposed in Reference 12. This method includes the constraint forces between the multibody components in the equations of motion, and the method is found suitable for both open-chain and closed-chain configurations of planar multibody systems. The effect of Coriolis forces and centrifugal forces on the inverse dynamics of constrained mechanical systems was presented by Gofron and Shabana.[13]

The inverse dynamics approach to end-point trajectory tracking of open-chain flexible multibody systems was recently applied to the three-dimensional problem by Ledesma, *et. al.*,[14] where a recursive procedure was proposed to simultaneously track a desired end-point trajectory and minimize motion-induced vibrations through the combined use of lumped inverse dynamic torques and distributed piezoelectric actuators. The recursive procedure required a controlled motor at each intermediate revolute joint and three motors at the ground. This procedure is effective for open-chain systems, but it is not valid for closed-chain systems because in such systems, the number of required control inputs is less than the number of joints.

In this paper, we present a general computational approach for the solution of the *non-causal* inverse dynamics of three-dimensional, flexible multibody systems, that is suitable for both open-chain and closed-chain configurations. With this work, we present a methodology that is suitable for all multibody systems, ranging from the single link case to three-dimensional systems with general topologies. The equations of motion are formulated in Section 2 and an iterative algorithm is subsequently developed. Simulation results for open-chain and closed-chain configurations are presented in Section 3 to demonstrate the validity and accuracy of the method.

2. Problem Formulation

In this section, we derive the governing equations of motion for a flexible multibody system by using a global Lagrangian approach, and develop a solution for the inverse dynamics problem that is suitable for both open-chain and closed-chain configurations. Crucial to the success of the proposed procedure is the use of the correct, *non-causal* Lagrange multipliers that account for the constraint forces between flexible multibody components. These Lagrange multipliers are determined in a forward dynamic analysis, which in turn, require the unknown inverse dynamic actuations. Therefore, the proposed solution is an iterative procedure which converges to the stable, non-causal inverse dynamic actuations and the associated Lagrange multipliers.

Consider an n-body flexible multibody system such as that shown in Fig. 1. A typical multibody component, say body i, is shown in Fig. 1 along with the floating reference frame associated with that body. The generalized coordinates consist of rigid body coordinates $\mathbf{q}_r^i$ which describe the position and orientation of the floating reference frame associated with each multibody component, and deformation coordinates $\mathbf{q}_f^i$ which describe the deformation of the flexible body with respect to its floating reference frame. The rigid body coordinates $\mathbf{q}_r^i$ consist of the Cartesian coordinates $\mathbf{R}^i$ which describe the position of the origin of the floating reference frame associated with body i, and a set of Euler parameters θ^i which describe the orientation of the floating frame. The use of Euler parameters among several choices of orientation coordinates will be explained later in the section describing the inverse dynamics solution procedure. The deformation from the nominal configuration is assumed to be small, so that the different bending and torsional modes are decoupled. For the sake of completeness, we summarize in the following equations the basic kinematic expressions that lead to the general equations of motion for flexible multibody systems. A more detailed formulation is found in Reference 15. With the above choice of coordinates, the position of an arbitrary point P in body i is given by

$$\mathbf{r}^i = \mathbf{R}^i + \mathbf{A}^i \mathbf{u}^i \tag{1}$$

where $\mathbf{R}^i$ is the location of the origin of the body axes with respect to the inertial frame, $\mathbf{u}^i$ is the location of point P with respect to the body axes, and $\mathbf{A}^i$ is the rotation transformation matrix from the body axes to the inertial frame. In the three-dimensional case, the rotation transformation matrix is given by

$$\mathbf{A}^i = \begin{bmatrix} 2(\theta_0^2 + \theta_1^2) - 1 & 2(\theta_1\theta_2 - \theta_0\theta_3) & 2(\theta_1\theta_3 + \theta_0\theta_2) \\ 2(\theta_1\theta_2 + \theta_0\theta_3) & 2(\theta_0^2 + \theta_2^2) - 1 & 2(\theta_2\theta_3 - \theta_0\theta_1) \\ 2(\theta_1\theta_3 - \theta_0\theta_2) & 2(\theta_2\theta_3 + \theta_0\theta_1) & 2(\theta_0^2 + \theta_3^2) - 1 \end{bmatrix}^i \tag{2}$$

where the orientation coordinates are represented by four Euler parameters θ_0^i, θ_1^i, θ_2^i, and θ_3^i which satisfy the following identity:

$$\sum_{k=0}^{3} (\theta_k^i)^2 = 1. \tag{3}$$

The position vector with respect to the body axes, $\mathbf{u}^i$, can be decomposed into

$$\mathbf{u}^i = \mathbf{u}_r^i + \mathbf{u}_f^i \tag{4}$$

where $\mathbf{u}_r^i$ is the position vector of point P *in the undeformed* state with respect to the body axes, and $\mathbf{u}_f^i$ is the deformation vector of point P with respect to the body axes. The deformation vector $\mathbf{u}_f^i$ can be expressed in terms of the nodal deformations by using a finite element discretization scheme, hence

$$\mathbf{u}_f^i = \mathbf{N}^i \, \mathbf{q}_f^i \tag{5}$$

where $\mathbf{N}^i$ is the shape function matrix and $\mathbf{q}_f^i$ is the nodal deformation vector. Differentiating Eq. (1) with respect to time, we obtain the following expression for the velocity vector in terms of the rigid body coordinates and nodal deformation coordinates: [15]

$$\dot{\mathbf{r}}^i = \dot{\mathbf{R}}^i - 2\,\mathbf{A}^i\,\tilde{\mathbf{u}}^i\,\mathbf{E}^i\,\dot{\theta}^i + \mathbf{A}^i\,\mathbf{N}^i\,\dot{\mathbf{q}}_f^i \tag{6}$$

where $\dot{(\,)}$ represents differentiation with respect to time, $\mathbf{E}^i$ is a matrix that depends linearly on the Euler parameters and is given by

$$\mathbf{E}^i = \begin{bmatrix} -\theta_1 & \theta_0 & \theta_3 & -\theta_2 \\ -\theta_2 & -\theta_3 & \theta_0 & \theta_1 \\ -\theta_3 & \theta_2 & -\theta_1 & \theta_0 \end{bmatrix}^i \tag{7}$$

and $\tilde{\mathbf{u}}^i$ is a 3 x 3 skew-symmetric matrix given by

$$\tilde{\mathbf{u}}^i = \begin{bmatrix} 0 & -u_z & u_y \\ u_z & 0 & -u_x \\ -u_y & u_x & 0 \end{bmatrix}^i \tag{8}$$

in which u_x, u_y, and u_z are the coordinates of the generic point P with respect to the body axes, in the deformed configuration.

Considering the reference coordinates $\mathbf{q}^T = [\,\mathbf{R}^T, \theta^T, \mathbf{q}_f^T\,]$ as generalized coordinates for the flexible multibody system, these coordinates are not independent because the motion of specific points in different bodies are related according to the type of mechanical joints that interconnect them. Moreover, in flexible mechanical systems, the deformation of a component affects the configuration of adjacent components. As a consequence, the interdependence of the generalized coordinates is expressed by a vector of kinematic constraint equations, such as

$$\Phi(\mathbf{q},t) = 0 \tag{9}$$

where $\mathbf{q}$ is the total vector of system generalized coordinates, t is time, and Φ is the vector of linearly independent holonomic constraint equations. These constraint equations can be further classified into:

1. rigid body constraints where only rigid body variables are involved in the constraint equation;
2. joint constraints where both rigid body and deformation coordinates are included in the constraint equation; and
3. rheonomic constraints wherein the constraint equations can be explicit functions of time as well as generalized coordinates.

The third type of constraint becomes active, for example, in the case of imposing the coordinates of the end-effector to follow a desired trajectory. To illustrate the construction of constraint equations, take the case of a spherical joint which connects two flexible bodies i and j at points P and Q shown in Fig. 2. The three constraint equations corresponding to the constraint condition that requires points P and Q to be coincident

can be written as

$$\left[\mathbf{R}^i + \mathbf{A}^i\,\mathbf{u}^i_P\right] - \left[\mathbf{R}^j + \mathbf{A}^j\,\mathbf{u}^j_Q\right] = 0. \tag{10}$$

We note that the constraint equation exemplified by Eq. (10) forms a set of coupled nonlinear algebraic equations in the rigid body coordinates and deformation coordinates.

Considering the rigid body and deformation coordinates described above as generalized coordinates, and following standard procedures in multibody dynamics, the constrained equations of motion become [15]

$$\mathbf{M}(\mathbf{q})\,\ddot{\mathbf{q}} + \mathbf{C}\,\dot{\mathbf{q}} + \mathbf{K}\,\mathbf{q} + \Phi_{\mathbf{q}}^{\mathrm{T}}\,\lambda = \mathbf{Q}_e + \mathbf{Q}_v(\mathbf{q},\dot{\mathbf{q}}) \tag{11}$$

where $\mathbf{M}$, $\mathbf{C}$ and $\mathbf{K}$ are the system mass, damping and stiffness matrices, respectively, λ is the vector of Lagrange multipliers associated with the constraints, $\Phi_{\mathbf{q}}$ is the constraint Jacobian matrix, $\mathbf{Q}_e$ is the vector of applied external forces, and $\mathbf{Q}_v$ is the quadratic velocity vector. The quadratic velocity vector contains the centrifugal forces and Coriolis forces that result from the differentiation of the kinetic energy expression with respect to the generalized coordinates. Geometric stiffening due to high rotation rates can also be added to the vector $\mathbf{Q}_v$.

2.1. Forward Dynamics

In a forward dynamic analysis, *i.e.*, finding the resulting motion given the applied joint forces and external forces, Eqs. (9) and (11) constitute a mixed system of differential-algebraic equations that have to be integrated simultaneously. As explained in the next section, the solution to the inverse dynamics problem requires a forward dynamic analysis within an iteration process. We solve the forward dynamics problem by using the augmented Lagrangian penalty formulation.[16] Applying the augmented Lagrangian penalty formulation to Eqs. (9) and (11) results in the following equation:

$$\mathbf{M}(\mathbf{q})\,\ddot{\mathbf{q}} + \mathbf{C}\,\dot{\mathbf{q}} + \mathbf{K}\,\mathbf{q} + \Phi_{\mathbf{q}}^{\mathrm{T}}\,\alpha\left[\ddot{\Phi} + 2\,\mu\,\omega\,\dot{\Phi} + \omega^2\,\Phi\right] = \mathbf{Q}_e + \mathbf{Q}_v(\dot{\mathbf{q}},\mathbf{q}) - \Phi_{\mathbf{q}}^{\mathrm{T}}\,\lambda^* \tag{12}$$

where α is a diagonal matrix of penalty factors whose elements are large real numbers that will assure the satisfaction of constraints, ω and μ are diagonal matrices representing the natural frequencies and damping characteristics of the *dynamic penalty system* associated with the constraints. Values of α in the range $10^3 < \alpha < 10^6$ provide excellent results when working in double precision. The augmented Lagrangian method requires an iteration for the correct value of the Lagrange multipliers. The iterative equation for the Lagrange multipliers is given by

$$\lambda_{i+1}^{*} = \lambda_i^{*} + \alpha \left[\ddot{\Phi} + 2\,\mu\,\omega\,\dot{\Phi} + \omega^2\,\Phi \right]. \tag{13}$$

The iterative process described by Eq. (13) involves only a few additional operations during each iteration but it significantly improves the convergence of the forward dynamics solution as compared to the standard penalty method.[16]

The augmented Lagrangian penalty formulation has several advantages over the standard algorithms used in solving differential-algebraic equations. First, the method obviates the need to solve a mixed set of differential-algebraic equations and does not increase the number of equations to account for the constraints. Second, this method allows the use of standard unconditionally stable algorithms without the need of further stabilization techniques to control the violation of constraints during the integration process. Third, the method can handle redundant constraints and allows the multibody system to undergo singular positions. Fourth, the constraint forces (Lagrange multipliers) can be obtained as a by-product of the integration without having to integrate additional equations for them. Finally, the method assures convergence independent of the penalty values used.

2.2. Inverse Kinematics and Inverse Dynamics

Gofron and Shabana[17] have proposed a solution to the inverse dynamics problem by integrating Eq. (12) directly and solving for the joint actuation from the Lagrange multipliers thus obtained. This method leads to a causal solution which relies on the presence of damping forces in order to obtain a stable solution. In contrast, the method presented

in this paper does not rely on damping to produce a stable solution. Moulin and Bayo [18] recognized that because of the non-minimum phase character of the inverse problem, the *unique stable solution* should be *non-causal*, *i.e.*, actuation is required before the end-point has started to move as well as after the end-point has stopped. These findings have been corroborated by Paden and Chen[19] in their theoretical work on the inversion of non-linear non-minimum phase systems such as flexible multibodies. The proper integration is of crucial importance in obtaining non-causal solutions, and as previously demonstrated in the planar inverse dynamics problem, the time-anticipatory effect can be automatically obtained by integrating in the frequency domain[9] or in the time domain by using the non-causal impulse response function and the bilateral Laplace transform.[10]

A previously proposed solution to the three-dimensional inverse dynamics problem[14] relied on a pinned-free finite element model of a flexible beam, and the equation for the inverse dynamics torque was formulated by imposing the condition that the torsional deformation and the two transverse deformations of the free end of each link be zero throughout the motion. This limited type of model led to a recursive scheme to solve the inverse dynamics of flexible multibody systems, and is found suitable for open-chain configurations but not for closed-chain configurations.

In this section, we describe an iterative Lagrangian procedure to solve the three-dimensional inverse dynamics problem for either open-chain or closed-chain topologies. Our overall strategy is to first solve the inverse kinematics problem, *i.e.*, finding the unknown rigid body coordinates $\mathbf{q}_r$ and flexible body displacements $\mathbf{q}_f$, given the desired end-point coordinates as explicit functions of time. Having determined the correct generalized coordinates and their time derivatives, the inverse dynamics joint torques can be obtained explicitly from the equations of motion. Compared to the recursive procedure cited above, this new approach is more systematic and becomes the only choice when closed-chain systems are encountered. We model the elastic links under pinned-pinned boundary conditions. Furthermore, since torsional deformations cause deviations from the nominal configuration further down the chain, we model the elastic link as fixed with respect to torsion at the distal end of the link.

Our goal then is to formulate an inverse kinematics equation that is linearized about the nominal motion, so that the elastic displacements, which are non-causal with respect to the end-point motion, can be determined through a frequency domain analysis. This is possible only if the leading matrix of the linearized equation is time-invariant and if the forcing term is Fourier transformable. This objective has been achieved in the planar case with the use of reference coordinates for the rigid body variables to describe the position and orientation of the floating reference frame.[12]

The three-dimensional inverse kinematics problem presents additional difficulties not found in the planar case. First, unlike the planar case, the three-dimensional torque vectors change directions in time, so that the external force vector $\mathbf{Q}_e$ in Eq. (11) becomes a nonlinear function of the rigid body orientation coordinates. To overcome this difficulty, a proper parametrization of the rigid body coordinates and proper bases for the joint torques are necessary to attain the stated objectives in forming the linearized inverse kinematics equations. As described later in this section, the desired form of the linearized inverse kinematics equation is possible if Euler parameters are used to describe the rigid body orientation and if the base torque vector of each multibody component is expressed in terms of components along the associated floating reference frame.

A second difficulty that appears in the three-dimensional inverse dynamics problem is that the end-point vibration in the plane defined by the revolute joint axis and the member axis can not be controlled by the torque applied at the revolute joint. This suggests that additional actuation is necessary to control the end-point motion when the multibody system reaches an "inaccessible" configuration.[20] This problem has been addressed in Reference 14 wherein one motor at each intermediate joint and three motors at the ground were proposed to control the end-point motion for all possible configurations of a certain class of open-chain, flexible multibody systems. The problem of "inaccessibility" in open-chain systems, however, can be completely avoided simply through a judicious design of the orientation of the joint motors so that end-point vibration is controllable for all possible configurations. For closed-chain systems, "inaccessible" configurations do not occur, hence the controllability of the end-point motion is

assured without the need for extra actuation.

Consider again the system equations of motion expressed by Eq. (11). For a typical multibody component, say body i, the equations of motion can be written in the following partitioned form:

$$\begin{bmatrix} m_{RR} & m_{R\theta} & m_{Rf} \\ m_{\theta R} & m_{\theta\theta} & m_{\theta f} \\ m_{fR} & m_{f\theta} & m_{ff} \end{bmatrix} \begin{bmatrix} \ddot{\mathbf{R}} \\ \ddot{\theta} \\ \ddot{q}_f \end{bmatrix} + \begin{bmatrix} 0 & 0 & 0 \\ 0 & 0 & 0 \\ 0 & 0 & c_{ff} \end{bmatrix} \begin{bmatrix} \dot{\mathbf{R}} \\ \dot{\theta} \\ \dot{q}_f \end{bmatrix} + \begin{bmatrix} 0 & 0 & 0 \\ 0 & 0 & 0 \\ 0 & 0 & k_{ff} \end{bmatrix} \begin{bmatrix} \mathbf{R} \\ \theta \\ q_f \end{bmatrix} + \begin{bmatrix} \Phi_R^T \\ \Phi_\theta^T \\ \Phi_f^T \end{bmatrix} \lambda = \begin{bmatrix} Q_{eR} \\ Q_{e\theta} \\ Q_{ef} \end{bmatrix} + \begin{bmatrix} Q_{vR} \\ Q_{v\theta} \\ Q_{vf} \end{bmatrix} . \tag{14}$$

The elements of the mass matrix and quadratic velocity force vector corresponding to an isoparametric, three-dimensional curved beam finite element are given in the Appendix.

Let us define τ^i as the torque vector at the base of body i, whose three components τ_r^i, τ_s^i, and τ_t^i are parallel to the associated floating reference axes r^i, s^i, and t^i, respectively. If we use Euler parameters as the rigid body orientation coordinates, the externally applied joint forces $\mathbf{Q}_{e\theta}^i$ associated with the rigid body rotation of body i can be expressed as

$$\mathbf{Q}_{e\theta}^i = [\mathbf{G}^i]^T \{\tau^i - [\mathbf{A}^i]^T \mathbf{A}^{i+1} \tau^{i+1}\} \tag{15}$$

where τ^i is the base torque acting on body i and whose components are parallel to the floating reference axes associated with body i; τ^{i+1} is the vector of joint torques and reaction moments transmitted from body i to body $i+1$, and whose components are parallel to the floating reference axes associated with body $i+1$; $\mathbf{A}^i$ and $\mathbf{A}^{i+1}$ are body axes to inertial axes rotation transformation matrices for bodies i and $i+1$, respectively; and $\mathbf{G}^i$ is a matrix that maps the derivatives of the Euler parameters describing the orientation of the reference frame of body i to the angular velocity of this reference frame, and is given by $\mathbf{G}^i = 2\,\mathbf{E}^i$. Combining Eq. (15) with the second set of equations in Eq. (14) yields

$$[\mathbf{G}^i]^T \{\tau^i - [\mathbf{A}^i]^T \mathbf{A}^{i+1} \tau^{i+1}\} = m_{\theta R}^i \ddot{\mathbf{R}}^i + m_{\theta\theta}^i \ddot{\theta}^i + m_{\theta f}^i \ddot{q}_f^i + \Phi_\theta^T \lambda - Q_{v\theta}^i. \tag{16}$$

If we pre-multiply both sides of Eq. (16) by $\frac{1}{4}\mathbf{G}^i$ and use the identity

$$\frac{1}{4}\mathbf{G}\,\mathbf{G}^T = \mathbf{I}_3 \tag{17}$$

where $\mathbf{I}_3$ is the 3×3 identity matrix, we can get the following result after expanding the inertia matrices and quadratic velocity vectors found in Eq. (16), (the reader is referred to the Appendix for the expressions for the inertia matrices and quadratic velocity vectors in terms of the invariants of the motion):

$$\tau^i = [\mathbf{A}^i]^T\,\mathbf{A}^{i+1}\,\tau^{i+1} + \frac{1}{4}\mathbf{G}^i\,\mathbf{m}_{\theta R}\,\ddot{\mathbf{R}}^i + \mathbf{J}^i\,\mathbf{G}^i\,\ddot{\theta}^i + \mathbf{J}_f^i\,\ddot{\mathbf{q}}_f^i + \frac{1}{4}\mathbf{G}^i\,\Phi_\theta^T\,\lambda$$

$$+ \frac{1}{2}\mathbf{G}^i\,[\dot{\mathbf{G}}^i]^T\,\{\mathbf{J}^i\,\mathbf{G}^i\,\dot{\theta}^i + \mathbf{J}_f^i\,\dot{\mathbf{q}}_f^i\} \tag{18}$$

where $\mathbf{J}^i$ is the 3×3 inertia tensor of body i with respect to the origin of the floating reference frame and measured relative to this frame, and $\mathbf{J}_f^i$ is the inertia matrix coupling the rigid body rotation and the elastic deformation. The key to obtaining a time-invariant leading matrix, that is necessary in transforming the linearized equations of motion into the frequency domain, is the fact that the inertial coupling matrix $\mathbf{J}_f^i$ can be decomposed into the sum of a time-invariant matrix and a time-varying matrix, *i.e.*,

$$\mathbf{J}_f^i = \mathbf{J}_{fc}^i + \mathbf{J}_{ft}^i \tag{19}$$

where $\mathbf{J}_{fc}^i$ and $\mathbf{J}_{ft}^i$ are the time-invariant part and time-varying part of $\mathbf{J}_f^i$, respectively. This decomposition is essential to the formulation of the inverse kinematics equations that lead to non-causal solutions to the nonlinear inversion problem. This is also the reason for selecting Euler parameters as rigid body orientation coordinates over other types of singularity-free coordinates such as natural coordinates,[21] where the decomposition of the inertial coupling matrix into time-invariant and time-varying parts is multiplicative rather than additive as in Eq. (19). Introducing this decomposition into Eq. (18) results in the following expression for the base torque on body i:

$$\tau^i = [\mathbf{A}^i]^T\,\mathbf{A}^{i+1}\,\tau^{i+1} + \mathbf{T}_b^i + \mathbf{J}_{fc}^i\,\ddot{\mathbf{q}}_f^i \tag{20}$$

where $\mathbf{T}_b^i$ is a torque vector given by

$$\mathbf{T}_b^i = \frac{1}{4}\mathbf{G}^i\ \mathbf{m}_{\theta R}^i\ \ddot{\mathbf{R}}^i + \mathbf{J}^i\ \mathbf{G}^i\ \ddot{\theta}^i + \mathbf{J}_{ft}^i\ \ddot{\mathbf{q}}_f^i + \frac{1}{4}\mathbf{G}^i\ \Phi_{\theta}^{iT}\ \lambda$$

$$+ \frac{1}{2}\mathbf{G}^i\ [\dot{\mathbf{G}}^i]^T\ \{\mathbf{J}^i\ \mathbf{G}^i\ \dot{\theta}^i + \mathbf{J}_f^i\ \dot{\mathbf{q}}_f^i\}. \tag{21}$$

Considering the equations of motion associated with the elastic degrees of freedom, the externally applied force vector due to the joint torques acting on body i can be expressed as

$$\mathbf{Q}_{ef}^i = \mathbf{N}_b^T\ \tau^i - \mathbf{N}_t^T\ [\mathbf{A}^i]^T\ \mathbf{A}^{i+1}\ \tau^{i+1} \tag{22}$$

where $\mathbf{N}_b$ and $\mathbf{N}_t$ are the shape function matrices associated with a torque vector acting on node b (base) and at node t (tip) of the finite element mesh, respectively. Combining Eq. (22) with the third set of equations in Eq. (14) yields the following inverse kinematics equations for body i:

$$\tilde{\mathbf{m}}_{ff}^i\ \ddot{\mathbf{q}}_f^i + \mathbf{c}_{ff}^i\ \dot{\mathbf{q}}_f^i + \mathbf{k}_{ff}^i\ \mathbf{q}_f^i = \mathbf{F}^i(\lambda, \mathbf{q}_r^i, \dot{\mathbf{q}}_r^i, \ddot{\mathbf{q}}_r^i, \mathbf{q}_f^i, \dot{\mathbf{q}}_f^i, \ddot{\mathbf{q}}_f^i) \tag{23}$$

where the modified mass matrix is given by

$$\tilde{\mathbf{m}}_{ff}^i = \mathbf{m}_{ff}^i - \mathbf{N}_b^T\ \mathbf{J}_c^i \tag{24}$$

and the motion-induced force vector acting on the elastic degrees of freedom is given by

$$\mathbf{F}^i = \mathbf{N}_b^T\ \{[\mathbf{A}^i]^T\ \mathbf{A}^{i+1}\ \tau^{i+1} + \mathbf{T}_b^i\} - \mathbf{N}_t^T\ [\mathbf{A}^i]^T\ \mathbf{A}^{i+1}\ \tau^{i+1}$$

$$+ \mathbf{Q}_{vf}^i - \Phi_{qf}^{iT}\ \lambda - \mathbf{m}_{fR}^i\ \ddot{\mathbf{R}}^i - \mathbf{m}_{f\theta}^i\ \ddot{\theta}^i. \tag{25}$$

The modified mass matrix $\tilde{\mathbf{m}}_{ff}^i$ is nonsymmetric and it is precisely this nonsymmetry that produces elastic displacements which are non-causal with respect to the end-point motion when non-causal techniques are employed to obtain the proper inversion of the nonlinear, non-minimum phase systems. Furthermore, inspection of Eqs.(23)-(25) shows that the inverse kinematics equation for body i assumes that the base torque vector τ^{i+1} is known beforehand. This suggests some form of recursive algorithm for the inverse kinematics, *i.e.*, finding the elastic displacements starting from the end-point, and

proceeding to the base of the multibody system (inboard direction). This procedure is straightforward for open-chain configurations. However, for closed-chain configurations, we need to take the additional step of cutting the chain at the joint that is defined as the end-point, and then proceed as in the open-chain case, since the constraint forces at the cut are automatically accounted for by the vector of Lagrange multipliers.

The nonlinear inversion can now be carried out efficiently in the frequency domain since the leading matrices have been constructed such that they remain constant throughout the motion. Our strategy is to solve Eq. (23) in the frequency domain to obtain the nodal deformation vector $\mathbf{q}_f$ that is non-causal with respect to the end-point motion. In the frequency domain, Eq. (23) can be written as a set of complex equations for a particular frequency ω

$$\left[\bar{\mathbf{m}}^i_{ff} + \frac{1}{i\omega} \mathbf{c}^i_{ff} - \frac{1}{\omega^2} \mathbf{k}^i_{ff} \right] \hat{\ddot{\mathbf{q}}}^i_f(\omega) = \hat{\mathbf{F}}^i(\omega) \tag{26}$$

where $\hat{\ddot{\mathbf{q}}}^i_f(\omega)$ is the Fourier transform of $\ddot{\mathbf{q}}^i_f(t)$ and $\hat{\mathbf{F}}^i(\omega)$ is the Fourier transform of $\mathbf{F}^i(t)$. Eq. (26) is based on the assumption that $\ddot{\mathbf{q}}^i_f(t)$ and $\mathbf{F}^i(t)$ are Fourier transformable. This assumption is valid for slewing motions which are from rest to rest. The nodal acceleration vector $\hat{\ddot{\mathbf{q}}}^i_f(\omega)$ can be obtained directly from Eq. (26) for each frequency ω. The leading matrix of Eq. (26) is a complex regular matrix that is invertible for all frequencies except for $\omega = 0$. However, for $\omega = 0$, the system undergoes a rigid body motion, and the leading matrix will be determined only by $\mathbf{m}_{ff}$ which is positive definite and therefore invertible. We note, however, that the forcing vector on the right hand side of Eq. (26) depends on the elastic deformations, velocities and accelerations. Therefore, an iterative process is needed to obtain the solution to the differential equations which are nonlinear in $\mathbf{q}^i_f$. We start the iteration process by assuming zero elastic deformations, velocities and accelerations for the initial calculation of the forcing vector $\mathbf{F}^i(t)$, and use a successive substitution scheme to converge to the correct solution. Finally, the elastic displacements and their derivatives in the time domain may be obtained through the application of the inverse Fourier transform, *e.g.*,

$$\ddot{\mathbf{q}}_f^j(t) = \frac{1}{2\pi} \int_{-\infty}^{\infty} \hat{\ddot{\mathbf{q}}}_f^j(\omega)\, e^{i\omega t}\, d\omega. \tag{27}$$

Alternately, the computation of the elastic displacements and their derivatives in each iteration can also be carried out in the time domain through the use of the non-causal impulse response function and the bilateral Laplace transform, *e.g.*,

$$\ddot{\mathbf{q}}_f(t) = \int_{-\infty}^{\infty} \sum_{j=1}^{j=n} \mathbf{h}_j(t-\tau)\, f_j(\tau)\, d\tau \tag{28}$$

where $\mathbf{h}_j(t)$ is the non-causal acceleration response vector to an impulse applied to the j^{th} degree of freedom and $f_j(t)$ is the j^{th} component of the forcing term on the right hand side of Eq. (23). We note that the integration from $-\infty$ to ∞ is necessary to capture the non-causal effects.

Once the non-causal elastic displacements and their derivatives are known, Eq. (18) can be used to explicitly compute the non-causal inverse dynamics joint efforts that will move the end effector according to a desired trajectory. We note, however, that the joint torques and elastic displacements given by Eqs. (18) and (23), respectively, depend on the Lagrange multipliers and rigid body coordinates, which in turn depend on the elastic displacements and the applied torque. Moreover, the rigid body coordinates and Lagrange multipliers are different from their nominal values when the components of the multibody system are flexible. Therefore, a forward dynamic analysis is required to obtain an improved estimate of the generalized coordinates and Lagrange multipliers. In order to ensure that the iteration process converges to obtain the joint efforts that will cause the end-effector to follow the desired trajectory, the forward dynamics analysis is carried out with the additional constraint that the coordinates of the end-point follow the desired trajectory. These additional constraints have corresponding Lagrange multipliers which act as correcting terms to the joint efforts that have been previously calculated. We also note that this iteration process takes into account the effect of the nonlinear coupling between the rigid body coordinates and the deformation coordinates in the computation of the joint efforts. The iterative procedure is found to be convergent for multibody

systems with moderately flexible members and with moderate rotation rates.

To summarize, the procedure for obtaining the inverse dynamics solution for three-dimensional, flexible multibody systems involve the following steps:

Algorithm:

1. Perform a rigid body inverse dynamic analysis to obtain the nominal values of the rigid body coordinates $\mathbf{q}_r$ and Lagrange multipliers λ.
2. Solve the inverse kinematics equation in the frequency domain through Eq. (23) or in the time domain through Eq. (28) to obtain the time-delayed elastic displacements and their time derivatives.
3. Compute the inverse dynamics joint efforts τ using Eq. (18).
4. Perform a forward dynamic analysis using Eqs. (12) and (13) to obtain new values for the generalized coordinates and Lagrange multipliers.
5. Repeat steps 2 through 4 until convergence in the inverse dynamics torques is achieved.

It is worthwhile to compare the recursive procedure proposed in Reference 14 and the algorithm proposed in this paper. The most important difference between the two methods is that the former method assumes that the dependence of rigid body coordinates on the elastic displacements are made negligible through the action of control forces so that the rigid body coordinates take on values corresponding to the nominal motion. This assumption is not made in the present method and consequently, the solution of the inverse kinematics equation of Eq. (23) would require an iteration for the rigid body coordinates $\mathbf{q}_r$ as well as the Lagrange multipliers λ that are needed as inputs to the inverse kinematics equation. A consequence of the above assumption in the previously proposed recursive procedure is that control inputs were required at all intermediate joints in the multibody system. This requirement is acceptable in open-chain configurations, but not practical in closed-chain configurations because the number of system degrees of freedom is less than the number of joints in a closed-chain multibody system. The present procedure takes advantage of this fact and allows the analyst to

choose *a priori* which joints in the multibody system are the control joints. Therefore, the present algorithm is more general and more systematic than the previously proposed procedure, although it requires more computational effort.

3. Simulation Results and Discussion

We present in this section some results of the numerical implementation of the procedure discussed above. First, we apply the procedure proposed in this paper to the inverse dynamics of a two-link, open-chain flexible multibody system undergoing motion in three-dimensional space, and compare the results with those obtained by the previously proposed recursive procedure.[14] Next, we present some simulation results of the application of the present procedure to the inverse dynamics of a closed-chain, flexible multibody system undergoing three-dimensional motion.

3.1. Open-Chain Multibody System

The iterative procedure discussed in the preceding section is applied to the three-dimensional open-chain flexible manipulator shown in Fig. 3. The multibody system is controlled by three motors at the base and one motor at the intermediate revolute joint. The desired motion is to have the end-point remain in the x_2–x_3 plane with the x_2 coordinate and x_3 coordinate of the end-point following the trajectories shown in Fig. 4. Gravitational forces are neglected. The two links share the following geometric and material properties:

Length: 1.0 *m*

Cross section dimensions: 1.0 *cm* x 1.0 *cm*

Young's modulus: 70 *GPa*

Shear modulus: 27 *GPa*

Mass density: 2715 kg/m^3

Tip mass: 0.1 *kg*

We perform two sets of computations for the example considered: 1) using the recursive procedure proposed in Reference 14; and 2) using the iterative procedure proposed in this paper. In the open-chain case, each intermediate joint needs to be controlled, and we therefore expect very similar results from both methods. Plots of inverse dynamic joint torques needed to track the desired end-point trajectory are shown in Figs. 5a and 5b. The results obtained from the two methods superimpose, thus validating the method proposed in this paper. Plots of the corresponding rigid body torques are also shown in the figures to illustrate the non-causal nature of the inverse dynamic torques. In Figs. 5a-b, the dashed curves refer to the inverse dynamic torques, while the solid curves refer to the rigid body torques. Transverse deflections induced by the motion at third points in the two links are shown in Figs. 6-7. In these figures, the dashed curves are transverse deflections caused by the inverse dynamic torques, while the solid curves are deflections caused by the rigid body torques. In Fig. 6, one vibration mode with a frequency of approximately $30\,Hz$ dominates the response, while in Fig. 7, two vibration modes at frequencies of approximately $3.4\,Hz$ and $30\,Hz$ dominate the response. The higher frequency corresponds to the first bending mode of a single link and characterizes the so-called "fast subsystem" while the lower frequency corresponds to the "slow subsystem" formed by the assembly of the multibody components. Rayleigh damping was used in the numerical simulation, with damping coefficients of 0.4% and 3.8% corresponding to frequencies of $3.4\,Hz$ and $30\,Hz$, respectively. We observe that the inverse dynamic torques minimize the residual structural vibrations that would otherwise be present if rigid body torques were used to actuate the flexible multibody system.

3.2. Closed-Chain Multibody System

Fig. 8 shows a closed-chain, three-dimensional flexible multibody system, where the selected control torques are shown in the figure. Joints 1-4 are revolute joints while joint 5 is a spherical joint. The desired end-point (joint 5) trajectory is a motion in the x_2–x_3 plane with the x_2 coordinate and x_3 coordinate of the end-point following the trajectories shown in Fig. 9. As in the open-chain case, gravitational forces are not

considered in order to focus on the inertial effects on the dynamics of the system. The four links share the following geometric and material properties:

Length: 1.0 m

Cross section dimensions: 1.0 cm x 1.0 cm

Young's modulus: 40 GPa

Shear modulus: 15 GPa

Mass density: 2715 kg/m^3

Tip mass: 0.1 kg

The present procedure is applied to the closed-chain system by introducing a cut at the end-point (joint 5), thus creating two open-chain systems. The internal constraint forces exposed by the cut are automatically taken into account by the Lagrange multipliers in the equations of motion. Figs. 10a and 10b show joint torques T_2 and T_3, respectively, that are needed to achieve the desired end-point trajectory. In these figures, the dashed curves refer to the inverse dynamic torques obtained by the present procedure, while the solid curves refer to the corresponding rigid body torques. Figs. 11 and 12 show the transverse deflections at a third point in link #2, obtained from a feedforward of the inverse dynamic torques (dashed curve) and the corresponding deflection obtained from a feedforward of the rigid body torque (solid curve). Again, we observe that the inverse dynamic torques minimize the residual structural vibrations that are otherwise present when rigid body torques are used to actuate the system. It is also interesting to look at the Lagrange multipliers that represent the reaction forces between multibody components. Fig. 13 shows a typical Lagrange multiplier associated with the inverse dynamic torques (dashed curve) and the corresponding nominal Lagrange multiplier associated with the rigid multibody system (solid curve). We observe that pre-actuation and post-actuation are also exhibited by the Lagrange multipliers in an inverse dynamics calculation.

4. Conclusion

We have presented a new iterative procedure for determining the inverse dynamic torques that are needed for end-point trajectory tracking in three-dimensional flexible multibody systems. An iterative procedure is necessary because of the interdependence between the elastic coordinates, the rigid body coordinates and the associated Lagrange multipliers in the system equations of motion. This procedure is valid for both open-chain and closed-chain configurations, and differs from the previously proposed recursive procedures in the sense that the rigid body coordinates are not assumed to follow the nominal motion. The conditions for trajectory tracking are now met in a more general way through the satisfaction of rheonomic constraint conditions. The new method is shown to yield the same results as those obtained with the recursive procedures for open-chain systems with normal link flexibilities and normal rotation rates. For closed-chain systems, however, this new method is the only valid procedure for determining the inverse dynamic torques since in this case, the number of control torques is smaller than the number of joints and therefore, the recursive methods can not be applied.

Further research is needed to address the inverse dynamics problem wherein the contribution of the quadratic force vector $\mathbf{Q}_{vf}$ to the generalized elastic forces is considerable enough to yield errors in the feedforward control law. This case arises when the rotation rates are high or when the structural components are extremely compliant. It has been reported that this problem can be mitigated by introducing damping into the structure.[17] An issue that still needs to be resolved is how to introduce distributed actuation that may necessary beyond that provided by structural damping that is inherent in the material. In a separate paper,[14] we have addressed this issue through the use of electrostrictive actuators that are distributed along the span of the structure.

Acknowledgement

The support of this work by the Air Force Office of Scientific Research under contract no. F49620-91-C-0095 is gratefully acknowledged.

Appendix

The elements of the mass matrix and quadratic velocity force vector in Eq. (14) can be expressed in terms of the so-called invariants of the motion which need to be computed only once at the start of the simulation. For each component of the flexible multibody system, the invariants of the motion can be expressed by the following integrals:

$$\mathbf{Z}_1 = \int_V \mathbf{u}_r \, \rho \, dV \tag{A.1}$$

$$\mathbf{Z}_2 = \int_V \mathbf{N} \, \rho \, dV \tag{A.2}$$

$$\mathbf{Z}_3 = \int_V \begin{bmatrix} (u_{r_2}^2 + u_{r_3}^2) & -u_{r_1}u_{r_2} & -u_{r_1}u_{r_3} \\ -u_{r_2}u_{r_1} & (u_{r_3}^2 + u_{r_1}^2) & -u_{r_2}u_{r_3} \\ -u_{r_3}u_{r_1} & -u_{r_3}u_{r_2} & (u_{r_1}^2 + u_{r_2}^2) \end{bmatrix} \rho \, dV \tag{A.3}$$

$$\mathbf{Z}_4^{ij} = \int_V u_{r_i} \, \mathbf{N}_j \, \rho \, dV, \quad i, j = 1,2,3 \tag{A.4}$$

$$\mathbf{Z}_5^{ij} = \int_V \mathbf{N}_i^T \mathbf{N}_j \, \rho \, dV, \quad i, j = 1,2,3 \tag{A.5}$$

where ρ is the mass density, V is the volume of the component, $\mathbf{N}$ is the shape function matrix, and $\mathbf{N}_j$ is the j^{th} row of the shape function matrix. We observe that the motion invariant $\mathbf{Z}_1$ is a measure of the first moment of the undeformed component about the body axes, and the motion invariant $\mathbf{Z}_3$ is the inertia tensor of the undeformed component with respect to the body axes.

Closed-form expressions for the motion invariants corresponding to the three-dimensional, Bernoulli-Euler straight beam element are given in Reference 15. In this paper, however, we use the variable-node, isoparametric, three-dimensional curved beam element developed by Bathe and Bolourchi[22] to model the flexible links. As a result, the motion invariants can be expressed in terms of integrals which are evaluated numerically through Gaussian quadrature.

The components of the mass matrix, expressed in terms of the invariants of the motion are given by the following:

$$\mathbf{m}_{RR} = m\ \mathbf{I}_3 \tag{A.6}$$

$$\mathbf{m}_{R\theta} = -\mathbf{A}\,\tilde{\mathbf{S}}\,\mathbf{G} \tag{A.7}$$

$$\mathbf{m}_{Rf} = \mathbf{A}\,\mathbf{Z}_2 \tag{A.8}$$

$$\mathbf{m}_{\theta\theta} = \mathbf{G}^T\,\mathbf{J}\,\mathbf{G}\,;\quad \mathbf{J} = [\mathbf{Z}_3 + \mathbf{J}_1 + \mathbf{J}_2] \tag{A.9}$$

$$\mathbf{m}_{\theta f} = \mathbf{G}^T\,\mathbf{J}_f\,;\quad \mathbf{J}_f = [\mathbf{J}_{fc} + \mathbf{J}_{ft}] \tag{A.10}$$

$$\mathbf{m}_{ff} = \mathbf{Z}_5^{11} + \mathbf{Z}_5^{22} + \mathbf{Z}_5^{33} \tag{A.11}$$

where, in Eq. (A.6), m is the total mass of the component, and the tilde symbol above the vector in Eq. (A.7) refers to the skew-symmetric matrix operator. The matrices $\mathbf{S}$, $\mathbf{J}_{fc}$, $\mathbf{J}_{ft}$, $\mathbf{J}_1$, and $\mathbf{J}_2$ are given by

$$\mathbf{S} = \mathbf{Z}_1 + \mathbf{Z}_2\,\mathbf{q}_f \tag{A.12}$$

$$\mathbf{J}_{fc} = \begin{bmatrix} \mathbf{Z}_4^{23} - \mathbf{Z}_4^{32} \\ \mathbf{Z}_4^{31} - \mathbf{Z}_4^{13} \\ \mathbf{Z}_4^{12} - \mathbf{Z}_4^{21} \end{bmatrix} \tag{A.13}$$

$$\mathbf{J}_{ft} = \begin{bmatrix} \mathbf{q}_f^T (\mathbf{Z}_5^{23} - \mathbf{Z}_5^{32}) \\ \mathbf{q}_f^T (\mathbf{Z}_5^{31} - \mathbf{Z}_5^{13}) \\ \mathbf{q}_f^T (\mathbf{Z}_5^{12} - \mathbf{Z}_5^{21}) \end{bmatrix} \tag{A.14}$$

$$\mathbf{J}_1 = \begin{bmatrix} (p_{22} + p_{33}) & -p_{12} & -p_{13} \\ -p_{21} & (p_{11} + p_{33}) & -p_{23} \\ -p_{31} & -p_{32} & (p_{11} + p_{22}) \end{bmatrix} \tag{A.15}$$

$$\mathbf{J}_2 = \begin{bmatrix} (q_{22} + q_{33}) & -q_{12} & -q_{13} \\ -q_{21} & (q_{11} + q_{33}) & -q_{23} \\ -q_{31} & -q_{32} & (q_{11} + q_{22}) \end{bmatrix} \tag{A.16}$$

in which

$$p_{ij} = [\mathbf{Z}_4^{ij} + \mathbf{Z}_4^{ji}]\,\mathbf{q}_f\,,\quad i, j = 1,2,3 \tag{A.17}$$

and

$$q_{ij} = \mathbf{q}_f^T\,\mathbf{Z}_5^{ij}\,\mathbf{q}_f\,,\quad i, j = 1,2,3. \tag{A.18}$$

The quadratic velocity force vectors are given by

$$\mathbf{Q}_{vR} = -\mathbf{A}\{\tilde{\omega}^2\,\mathbf{S} + 2\,\tilde{\omega}\,\mathbf{Z}_2\,\dot{\mathbf{q}}_f\} \tag{A.19}$$

$$\mathbf{Q}_{v\theta} = -2\,\dot{\mathbf{G}}^T\{\mathbf{J}\,\omega + \mathbf{J}_f\,\dot{\mathbf{q}}_f\} \tag{A.20}$$

$$\mathbf{Q}_{vf} = -[\tilde{\omega}^2]^*\,[\mathbf{Z}_4^{11} + \mathbf{Z}_4^{22} + \mathbf{Z}_4^{22}]^T - [\tilde{\omega}^2]^*\,\mathbf{m}_{ff}\,\mathbf{q}_f - [2\,\tilde{\omega}]^*\,\mathbf{m}_{ff}\,\dot{\mathbf{q}}_f \tag{A.21}$$

where ω is the absolute angular velocity of the body axes, whose components are expressed with respect to the body axes and given by

$$\omega = \mathbf{G}\,\dot{\theta} \tag{A.22}$$

and the matrices $[\tilde{\omega}^2]^*$ and $[2\,\tilde{\omega}]^*$ are block diagonal matrices whose diagonal elements are $\tilde{\omega}^2$ and $2\,\tilde{\omega}$, respectively.

References

1. G. G. Lowen and W. G. Jandrastis, "Survey of investigations into the dynamic behavior of mechanisms containing links with distributed mass and elasticity," *Mechanism and Machine Theory*, vol. 7, pp. 3-17, 1972.

2. A. G. Erdman and G. N. Sandor, "Kineto-elastodynamics - a review of the state of the art and trends," *Mechanism and Machine Theory*, vol. 7, pp. 19-33, 1972.

3. V. J. Modi, "Attitude dynamics of satellites with flexible appendages - a brief review," *Journal of Spacecraft and Rockets*, vol. 11, pp. 743-751, 1974.

4. G. G. Lowen and C. Chassapis, "The elastic behavior of linkage: an update." *Mechanism and Machine Theory*, vol. 21, pp. 33-42, 1986.

5. M. J. Balas, "Trends in large space structure control theory: fondest hopes, wildest dreams," *IEEE Transactions on Automatic Control*, vol. AC-27, no. 3, pp. 522-535, 1982.

6. W. J. Book, "Modeling, design, and control of flexible manipulator arms: status and trends," *Proceedings, NASA Conference on Space Telerobotics*, vol. 3, pp. 11-24, January, 1989.

7. E. Bayo, "A finite-element approach to control the end-point motion of a single-link flexible robot," *Journal of Robotic Systems*, vol. 4, no. 1, pp. 63-75, 1987.

8. H. Moulin, "Problems in the inverse dynamics solution for flexible manipulators," *PhD. Thesis*, University of California, Santa Barbara, 1989.

9. E. Bayo, P. Papadopoulos, J. Stubbe and M. Serna, "Inverse kinematics and dynamics of a multi-link elastic robot: an iterative frequency domain," *International Journal of Robotics Research*, vol. 8, no. 6, pp. 49-62, 1989.

10. E. Bayo and H. Moulin, "An efficient computation of the inverse dynamics of flexible manipulators in the time domain," *Proceedings, IEEE Conference on Robotics and Automation*, pp. 710-715, Scottsdale, Arizona, 1989.

11. D. S. Kwon and W. J. Book, "An inverse dynamic method yielding flexible manipulator state trajectories," *Proceedings, American Control Conference* , vol. 1, pp. 186-193, San Diego, California, 1990.

12. R. Ledesma and E. Bayo, "A non-recursive Lagrangian approach to the inverse dynamics of flexible multibody systems: the planar case," *International Journal for Numerical Methods in Engineering*, vol. 36, no. 16, pp. 2725-2741, 1993.

13. M. Gofron and A Shabana, "Effect of the deformation in the inertia forces on the inverse dynamics of flexible mechanical systems," *Nonlinear Dynamics*. To appear.

14. R. Ledesma, S. Devasia and E. Bayo, "Inverse dynamics of spatial open-chain flexible manipulators with lumped and distributed actuators," *Journal of Robotic Systems*, 1994. To appear.

15. A. A. Shabana, *Dynamics of Multibody Systems*, John Wiley & Sons, Inc., 1989.

16. E. Bayo, J. Garcia de Jalon and M. Serna, "A modified lagrangian formulation for the dynamic analysis of constrained mechanical systems," *Computer Methods in Applied Mechanics and Engineering*, vol. 71, pp. 183-195, Nov. 1988.

17. M. Gofron and A. Shabana, "Control structure interaction in the nonlinear analysis of flexible mechanical systems," *Nonlinear Dynamics*, vol. 4, pp. 183-206, 1993.

18. H. Moulin and E. Bayo, "On the end-point trajectory tracking for flexible manipulators through non-causal inverse dynamics," *ASME Journal of Dynamic Systems, Measurement and Control*, vol. 113, no. 2, pp. 320-324, June 1991.

19. B. Paden and D. Chen, "Zero dynamics and inversion of nonlinear systems," *Proceedings, U.S.-Japan Conference on Flexible Automation*, San Francisco, California, 1992.

20. S. Tosunoglu, S. Lin and D. Tesar, "Accessibility and controllability of flexible robotic manipulators," *ASME Journal of Dynamic Systems, Measurement, and Control*, vol. 114, pp. 50-58, March 1992.

21. J. Garcia de Jalon, J. Unda and A. Avello, "Natural coordinates for the computer analysis of multibody systems," *Computer Methods in Applied Mechanics and Engineering*, vol. 56, pp. 309-327, 1986.

22. K. J. Bathe and S. Bolourchi, "Large deformation analysis of three-dimensional beam structures," *International Journal for Numerical Methods in Engineering*, vol. 14, no. 7, pp. 961-986, 1979.

List of Figures

Fig. 1: A three-dimensional flexible multibody system

Fig. 2: A pair of flexible bodies connected by a spherical joint

Fig. 3: A two-link, three-dimensional, flexible open-chain system

Fig. 4: Nominal end-point coordinates for the open-chain system

Fig. 5: Rigid (solid) vs. flexible (dashed) torques: (a) base torque T_0; (b) joint torque T_3

Fig. 6: Link #1 transverse deflection along s-axis: rigid (solid) vs. flexible (dashed)

Fig. 7: Link #2 transverse deflection along t-axis: rigid (solid) vs. flexible (dashed)

Fig. 8: A three-dimensional, flexible closed-chain system

Fig. 9: Nominal end-point coordinates for the closed-chain system

Fig. 10: Rigid (solid) vs. flexible (dashed) torques: (a) joint torque T_2; (b) joint torque T_3

Fig. 11: Link #2 transverse deflection along s-axis: rigid (solid) vs. flexible (dashed)

Fig. 12: Link #2 transverse deflection along t-axis: rigid (solid) vs. flexible (dashed)

Fig. 13: Comparison of Lagrange multipliers: nominal (solid) vs. flexible (dashed)

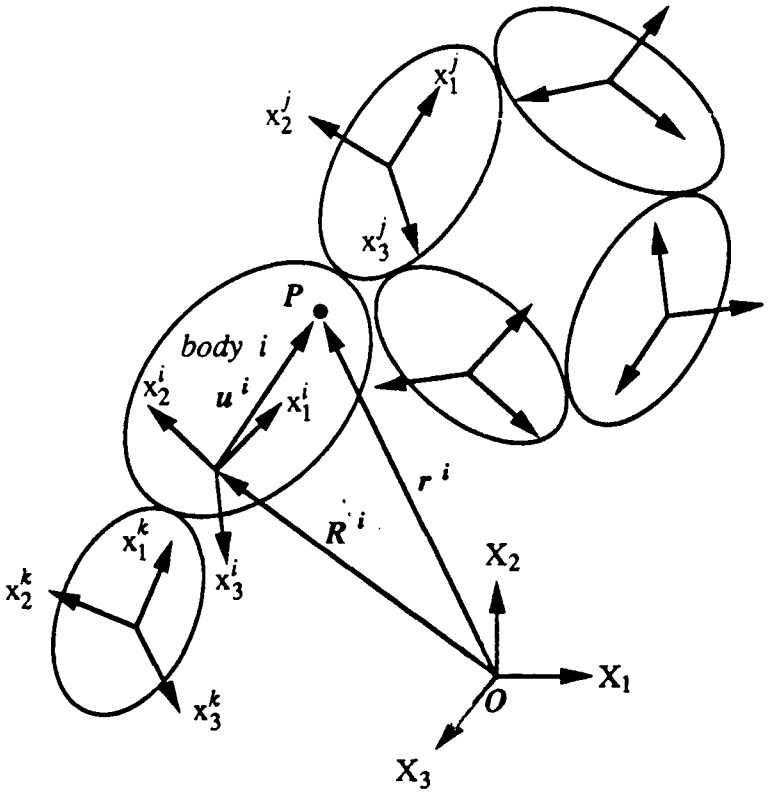
x_1^j
x_2^j
x_3^j
P
body i
x_2^i
u^i
x_1^i
r^i
R^i
x_1^k
x_2^k
x_3^i
x_3^k
X_2
X_1
O
X_3

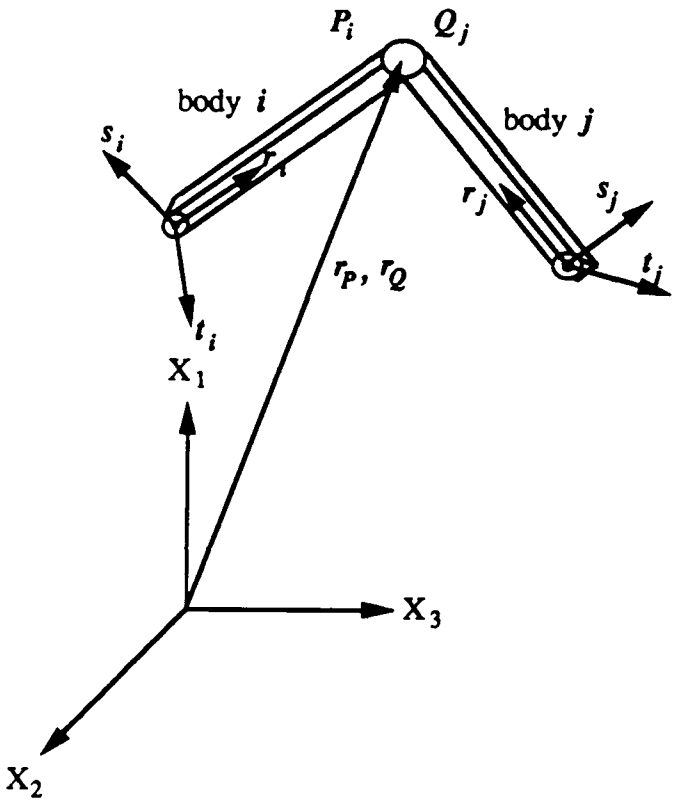
P_i
Q_j
body i
body j
s_i
r_i
r_j
s_j
t_j
r_P, r_Q
t_i
X_1
X_3
X_2

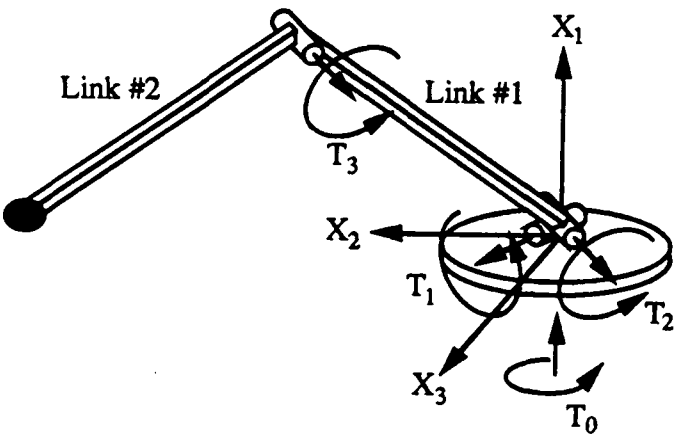
Link #2
Link #1
X_1
T_3
X_2
T_1
T_2
X_3
T_0

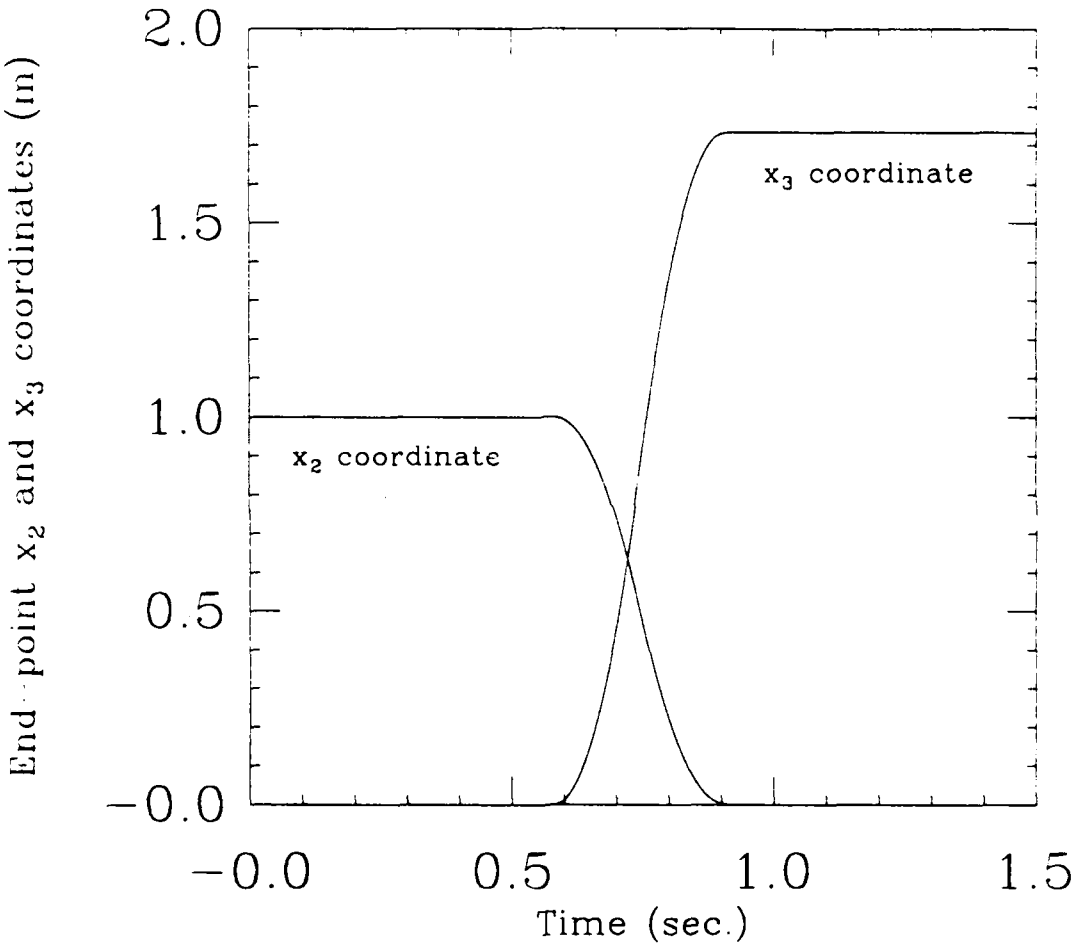
2.0
1.5
1.0
0.5
−0.0
−0.0
0.5
1.0
1.5
End-point x_2 and x_3 coordinates (m)
Time (sec.)
x_3 coordinate
x_2 coordinate

Fig. 4

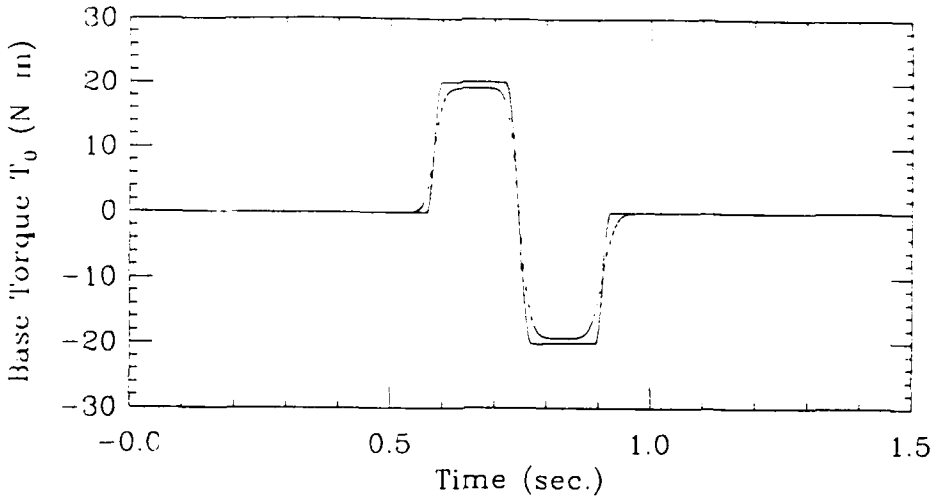
Base Torque T_0 (N m)
30
20
10
0
-10
-20
-30
-0.0
0.5
1.0
1.5
Time (sec.)

Fig 5a

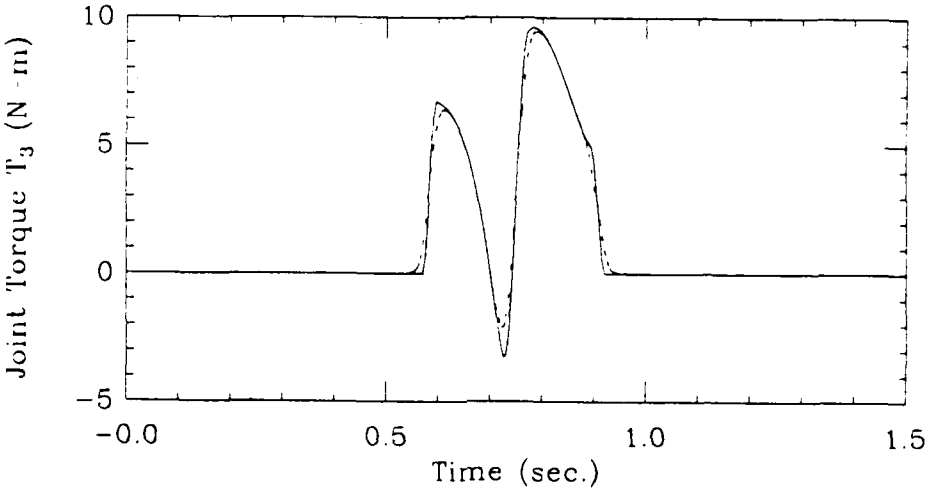
Joint Torque T_3 (N m)
10
5
0
-5
-0.0
0.5
1.0
1.5
Time (sec.)

Fig 5

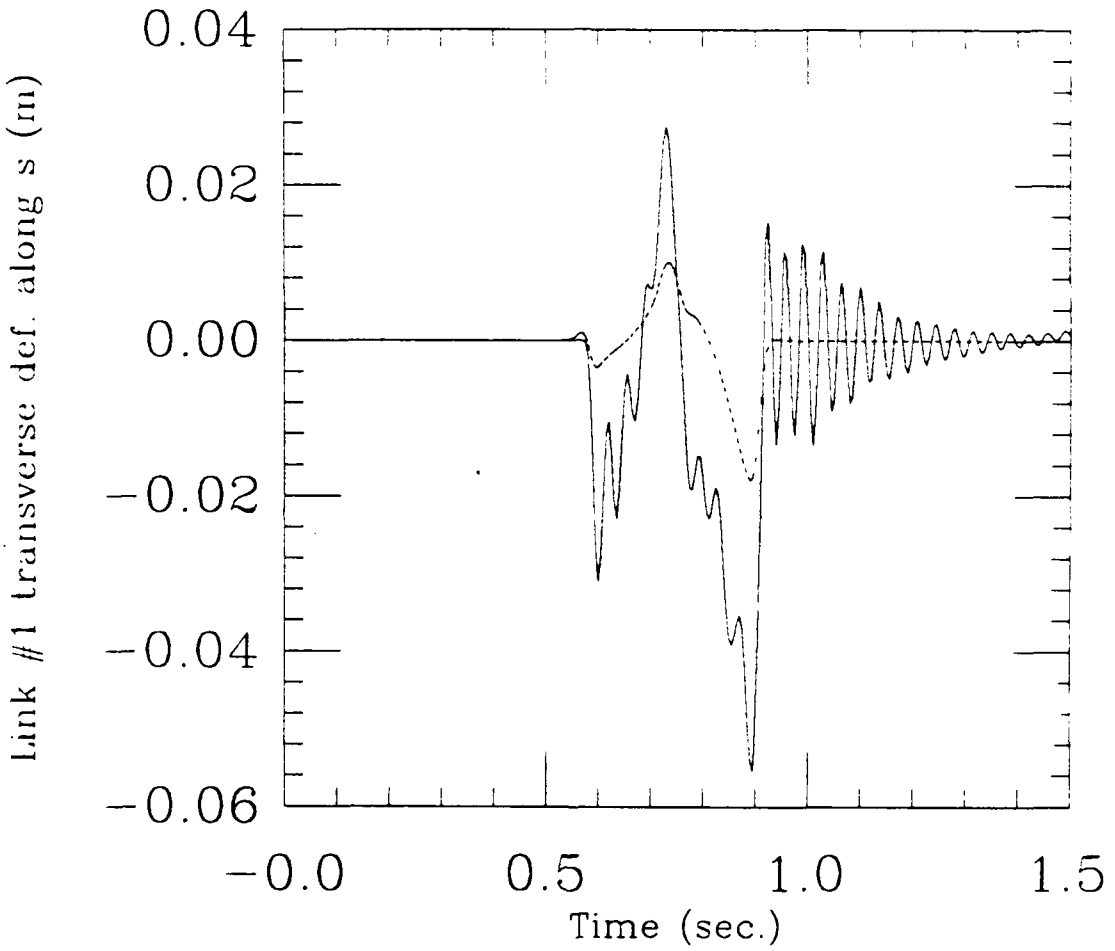
0.04
0.02
0.00
−0.02
−0.04
−0.06
−0.0
0.5
1.0
1.5
Time (sec.)
Link #1 transverse def. along s (m)

Fig 6

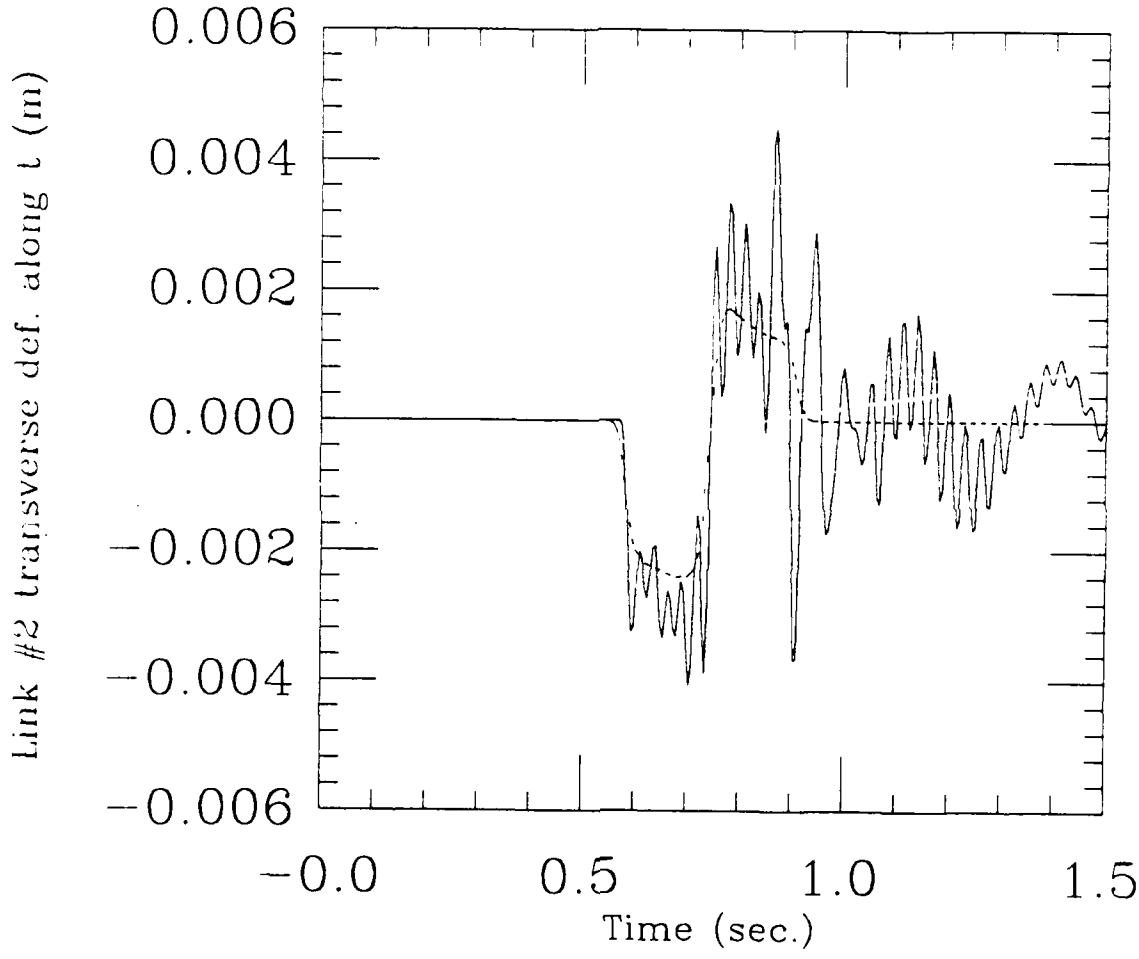
0.006
0.004
0.002
0.000
−0.002
−0.004
−0.006
Link #2 transverse def. along L (m)
−0.0
0.5
1.0
1.5
Time (sec.)

fig. 7

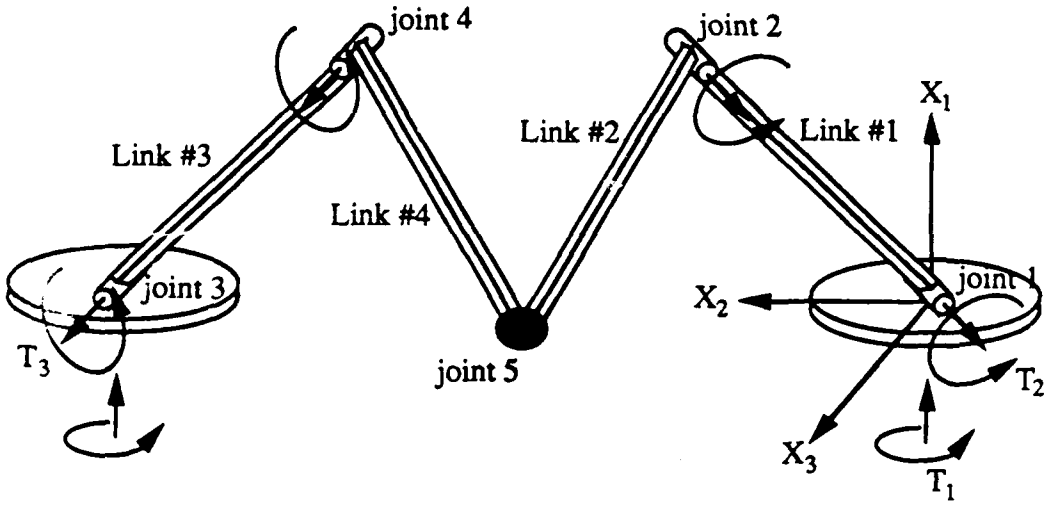
joint 4
joint 2
Link #3
Link #2
Link #1
Link #4
joint 3
joint 1
joint 5
X_1
X_2
X_3
T_1
T_2
T_3

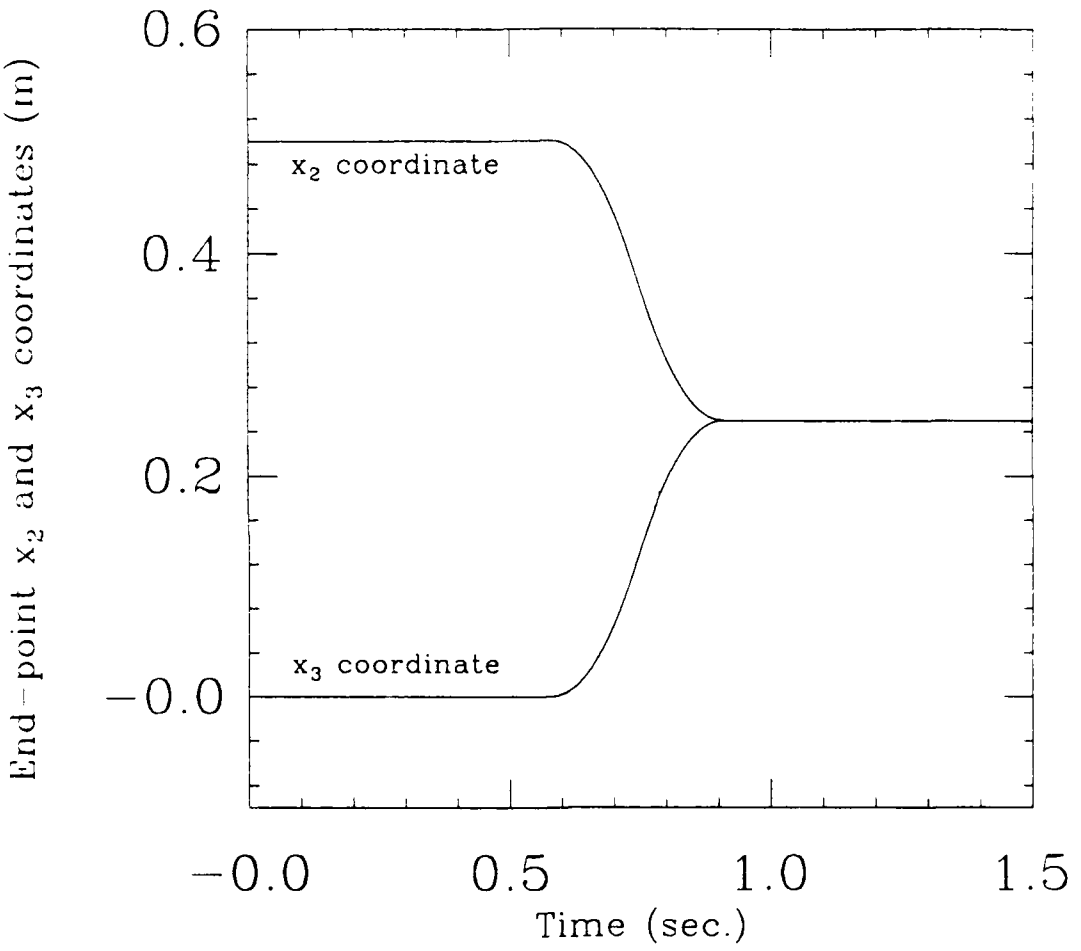
0.6
0.4
0.2
−0.0
End−point x_2 and x_3 coordinates (m)
x_2 coordinate
x_3 coordinate
−0.0
0.5
1.0
1.5
Time (sec.)

Fig. 7

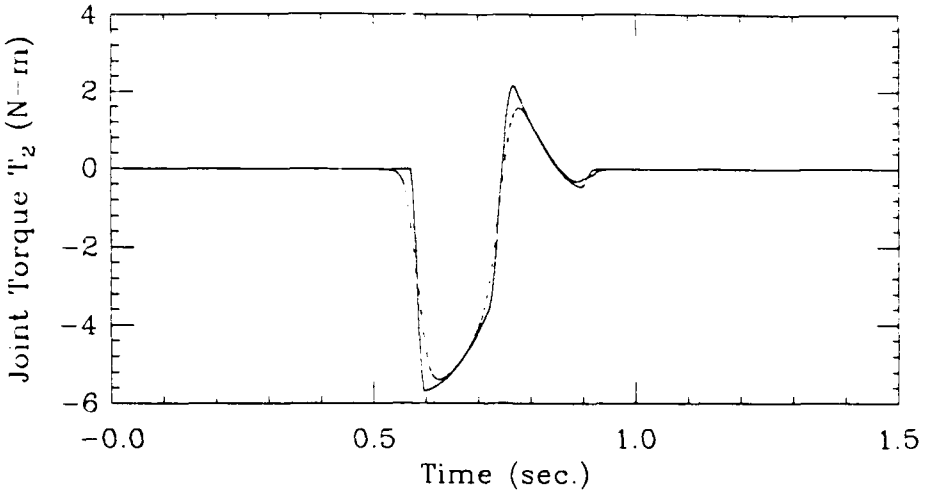

fig. 10a

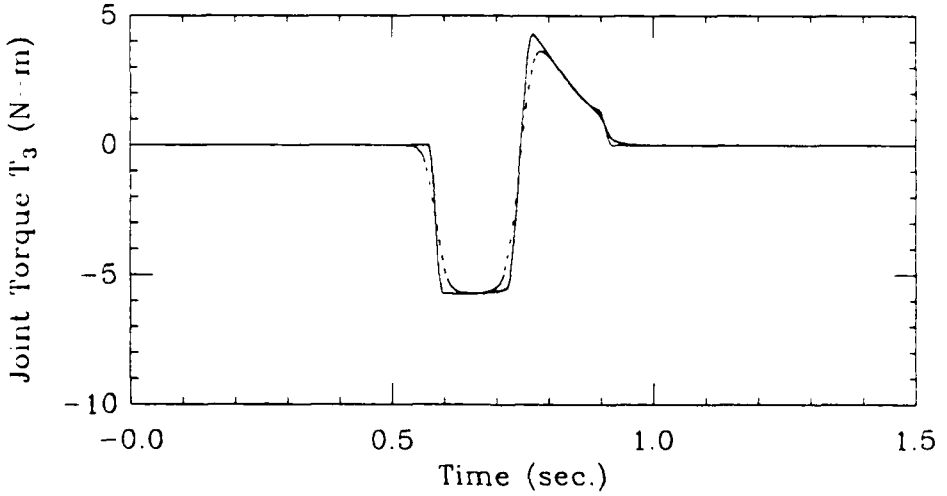

fig. 10b

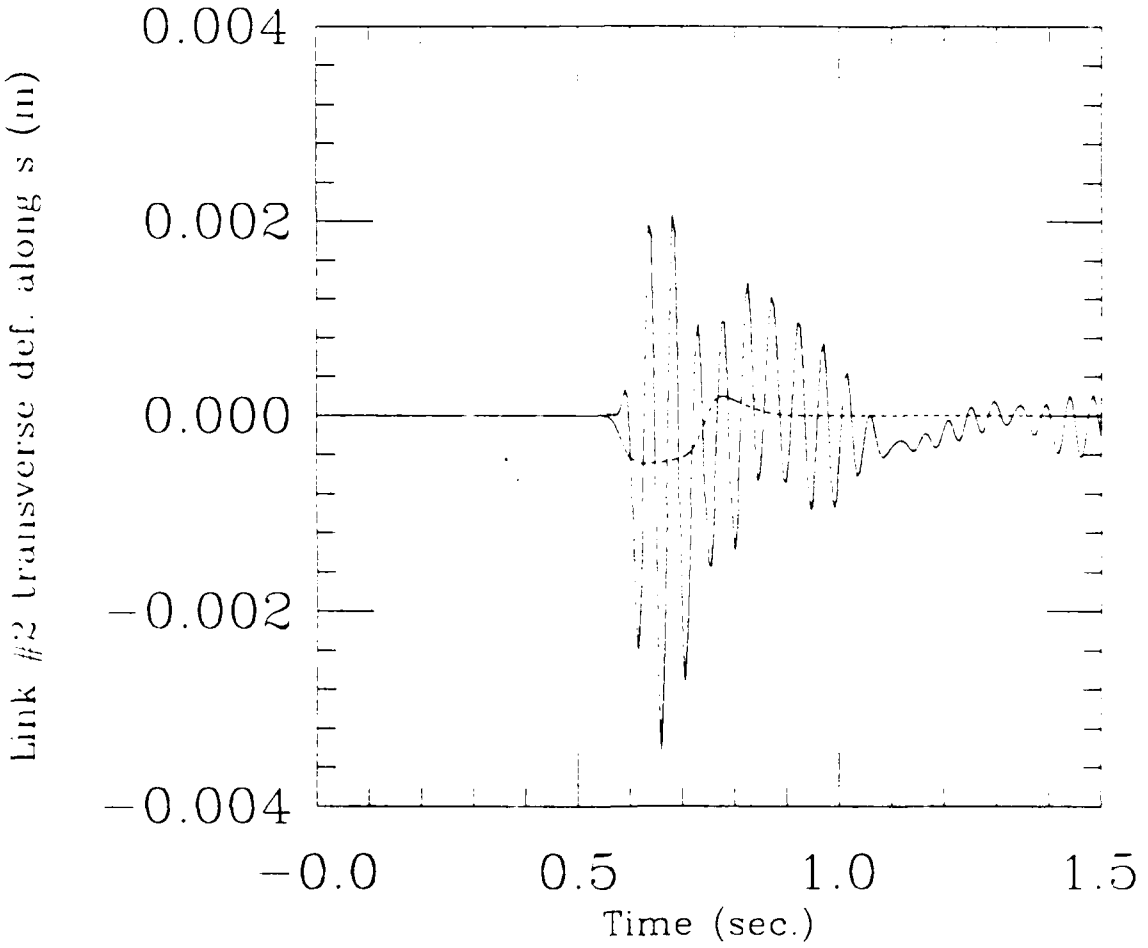
0.004
0.002
0.000
−0.002
−0.004
−0.0
0.5
1.0
1.5
Time (sec.)
Link #2 transverse def. along s (m)

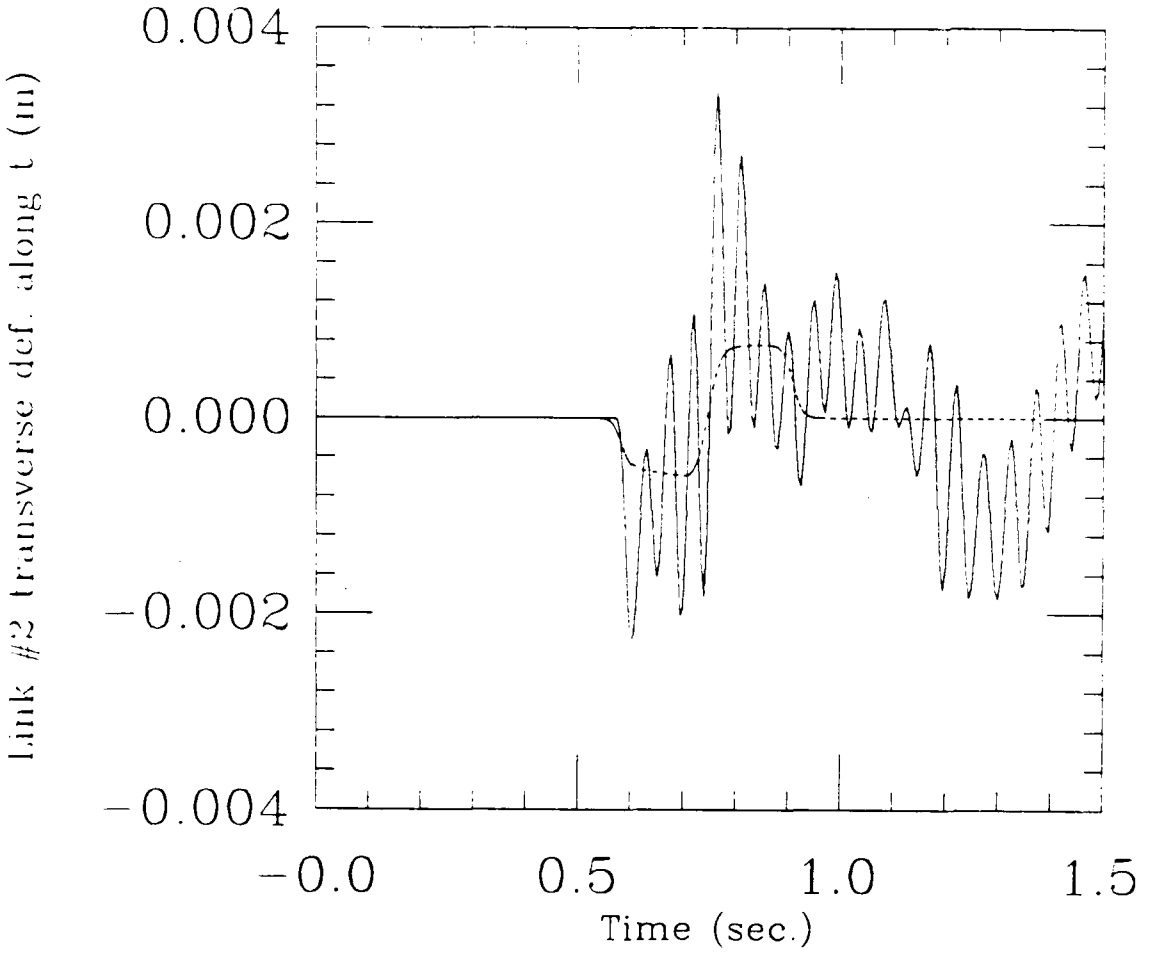
0.004
0.002
0.000
−0.002
−0.004
−0.0
0.5
1.0
1.5
Time (sec.)
Link #2 transverse def. along t (m)

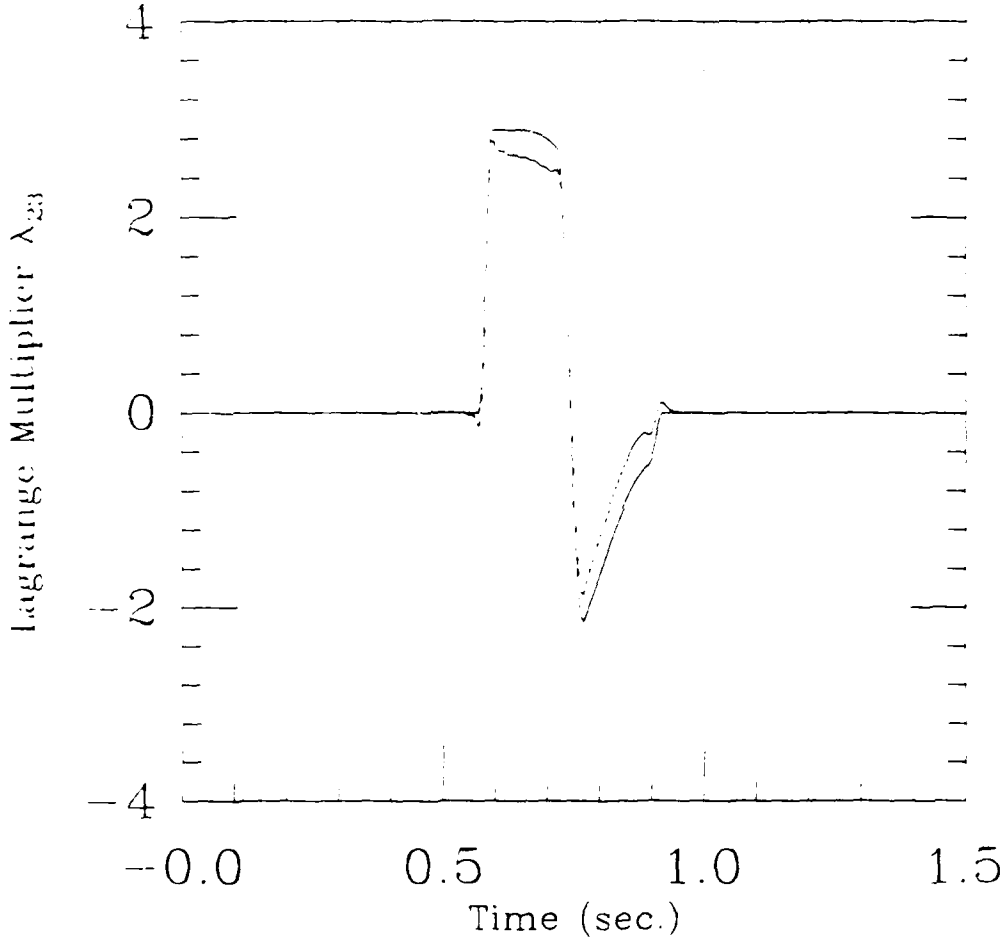

Fig. 13

To appear in the Journal of Robotic Systems
Vol 11, 1994

Inverse Dynamics of Spatial Open-Chain Flexible Manipulators with Lumped and Distributed Actuators

Ragnar Ledesma

Santosh Devasia

Eduardo Bayo

Department of Mechanical Engineering
University of California
Santa Barbara, CA 93106

ABSTRACT

This paper addresses the problem of inverse dynamics for three-dimensional flexible manipulators with both lumped and distributed actuators. A recursive procedure is presented for computing the lumped inverse dynamic torques and the distributed piezoelectric actuator inputs for simultaneously tracking a prescribed end-point trajectory and reducing induced vibrations in the manipulator. The procedure sequentially solves for the non-causal inverse dynamic torques and piezoelectric voltages applied to each link in the manipulator, starting from the last element in the chain and proceeding to the base element. The method allows trajectory tracking wherein controllability of the structural vibrations is assured in all possible configurations through the use of only one motor at each intermediate joint and three motors at the ground. Numerical simulation shows that the elastic vibrations can be reduced significantly through the use of distributed actuators while at the same time satisfying the trajectory tracking requirement through the use of inverse dynamics.

1. Introduction

The control of flexible manipulators is becoming a more important area of research as more stringent demands are placed on these multibody systems. For example, current developments in orbiting space manipulators and cranes require their different components to be positioned accurately in order to fulfill mission requirements. In most cases, the control objectives for these structures are end-point tracking in a slewing maneuver and minimizing the structural vibrations that result from the slewing motion. Several approaches towards these objectives have been suggested from different segments of the scientific community. Some researchers have suggested the improvement of the dynamic properties of the structure through the use of composite materials tailored for higher damping capabilities along with shape optimization to maximize the stiffness to mass ratio.[1] A second approach is to implement feedback control on the joint actuators through the use of a variety of control strategies (the reader is referred to Reference 2 for a survey of the state of the art in the control of flexible manipulators). Recent studies in this area which include valuable experimental results have been reported in References 345 and 6. Thirdly, the use of distributed active control members such as piezoceramics to damp out the elastic vibrations has been proposed.[7] Finally, a fourth method is to compute the inverse dynamic joint torques that will cause the control point to follow the desired trajectory.[8910] The computed torque technique has been validated with experimental results in the study done by Paden, *et. al.*,[11] wherein passive feedback and feedforward of the inverse dynamic torques were used to achieve an exponentially stable tracking control law in flexible, multi-link systems. However, it is desirable to not only track a desired trajectory but also minimize the subsequent elastic deformations in the structure. To achieve this goal, we combine the third and fourth approaches and present in this paper a new scheme for simultaneous trajectory tracking and vibration minimization for open-chain flexible articulated structures. The major contributions of this paper are the extension of the inverse dynamics formulation to three-dimensional open-chain manipulators and the combined application of inverse dynamics and distributed piezoelectric actuation to track trajectories and reduce vibrations simultaneously.

Trajectory tracking in planar flexible articulated structures has been addressed by Bayo,[8] Bayo and Moulin,[9] and also by Kwon and Book.[10] The researchers cited above

have considered the non-minimum phase character of the system when solving for the inverse dynamic torques that are required for end-point trajectory tracking in slewing motions that are confined in a plane. The results of the above studies lead to the conclusion that the unique stable solution for the inverse dynamic torques are non-causal with respect to the end-point motion. This non-causality can be captured either through integration in the frequency domain,[8] or by computing for the inverse transfer function in the frequency domain and subsequently integrating in the time domain through the use of bilateral convolution integrals,[9] or by dividing the solution into causal and anticausal parts and integrating in the time domain.[10] In our opinion, the frequency domain approach involves a simpler formulation than the time domain approach, when the equations of motion can be linearized about the nominal motion so that the Fourier transforms of the deformation coordinates and base torques can be explicitly expressed. Bayo, *et. al.*,[12] extended the computed torque technique to multiple flexible links in a planar, open-chain configuration by using a recursive method that computes for the inverse dynamic torques starting from the last component in the chain and continuing to the first link at the base of the chain. The recursive method entails an inverse dynamic analysis for the non-causal joint torques and a forward dynamic analysis for the reaction forces between contiguous links in the chain. The inverse dynamic torques so determined achieve end-point tracking but do not minimize the elastic vibrations. In this paper, we extend the application of inverse dynamics to simultaneous trajectory tracking and vibration reduction by combining inverse dynamic joint torques with distributed piezoelectric actuators in three-dimensional, open-chain flexible manipulators. In the present work, the inverse dynamic torques and the piezoelectric voltages are simultaneously computed so that the non-causal joint torques assure end-point tracking while the distributed piezoelectric actuators reduce the elastic vibrations that are induced by the slewing motion.

We develop in the present study a recursive computational algorithm that allows end-point trajectory tracking of three-dimensional open-chain manipulators through the use of only one motor at each intermediate joint and three motors at the ground, as opposed to the method proposed in Reference 13 where three motors were proposed at each joint. Our method achieves the trajectory tracking requirement with the use of

reduced number of actuators and in addition, the elastic vibrations are reduced through the use of distributed piezoelectric actuators. The extension of the frequency domain recursive inverse dynamics procedure[12] to three-dimensional flexible manipulators is not trivial and presents two main difficulties. First, unlike the two-dimensional case, the three-dimensional joint torque vectors change direction in time and become functions of the rigid body orientation coordinates. Consequently, if the torque vectors are expressed in terms of components along the inertial frame axes, the force vectors due to these torques become nonlinear functions of rigid body orientation coordinates and torque components, for which the Fourier transforms may not exist. Second, in the three-dimensional case, the end-point vibration in the plane defined by the revolute joint axis at the base of the link and the member axis can not be controlled by the torque applied at the revolute joint.

The two previously mentioned problems are solved by taking the following steps in the formulation of the solution. First, the nonlinearity in the forcing term due to the joint torques is avoided by expressing the base torque in terms of components along the floating reference frame associated with each multibody component. The base torques are then expressed independent of the rigid body configuration, and as a consequence these torques are Fourier transformable. Secondly, having expressed the base torques in this manner, the bi-axial bending and torsional deformations are decoupled when deformations from the nominal motion are small. Hence, one of the base torque components described above, which refers to the joint torque applied to the revolute joint, controls the end-point deformation in one direction, while the remaining two torque components can be treated as a reaction torsional moment which controls the end-point torsional deformation and a reaction bending moment which controls the lateral deformation in the other direction, respectively. These reaction moments are treated as unknowns which are to be determined along with the inverse dynamic joint torques. Here, it is important to note that in the three-dimensional case, the torsional deformation at the end-point needs to be controlled, since the torsional deformation will result in a displacement from the nominal configuration further down the chain.

The recursive procedure can then be formulated as follows. The last multibody component at the end of the chain is analyzed first to determine the actuating torque and

reaction moments at the base of that multibody component. Each of the other components are subsequently analyzed for the base torques at the proximal end given the desired reaction forces and reaction moments at the distal end. The actuating torques at the base of the chain can then be determined by a simple projection of moments, where the projection matrix depends on the nominal rigid body orientation coordinates. Through the use of the proposed recursive procedure, the end-point trajectory tracking problem of three-dimensional, open-chain flexible manipulators can be accomplished by using only one motor at each intermediate joint and three motors at the ground. In contrast with other proposed approaches that rely on three motors at each intermediate joint,[13] the use of only one motor at each intermediate joint for control purposes minimizes the inertial forces acting on the system, thereby increasing the speed under which the system can effectively operate.

2. Mathematical Formulation

In this section, we formulate the problem and present a solution of simultaneous trajectory tracking and vibration reduction for three-dimensional open-chain flexible manipulators. The problem formulation starts with the equations of motion for each component of an n-link manipulator that is undergoing motion in three dimensional space. The combined objectives of trajectory tracking and vibration reduction are then expressed in the form of a minimization problem that is suitable for numerical computation. The solution procedure presented in this section is a recursive procedure which solves for the required actuating torques and piezoelectric voltages starting from the last multibody component at the end of the chain and proceeding to the first component at the base of the chain.

2.1. Problem Formulation

Consider an n-link, open-chain flexible manipulator shown in Fig. 1. The recursive procedure developed in this paper consists in analyzing each multibody component for the piezoelectric voltages applied across the distributed actuators and the base torques at the proximal end, given the inertial forces due to the nominal motion and the reactions coming from the next component at the other end. A typical multibody component, say

body i, is shown in Fig. 1 along with the floating reference frame associated with that body. The generalized coordinates consists of rigid body coordinates $\mathbf{q}_r$ which describe the position and orientation of the floating reference frame associated with each multibody component, and deformation coordinates $\mathbf{q}_f$ which describe the deformation of the flexible body with respect to its floating reference frame. The deformation from the nominal configuration is assumed to be small, so that the different bending and torsional modes are decoupled. Using the aforementioned coordinates, the equations of motion for a flexible multibody component can be written as[14]

$$\begin{bmatrix} \mathbf{m}_{rr} & \mathbf{m}_{rf} \\ \mathbf{m}_{fr} & \mathbf{m}_{ff} \end{bmatrix} \begin{bmatrix} \ddot{\mathbf{q}}_r \\ \ddot{\mathbf{q}}_f \end{bmatrix} + \begin{bmatrix} 0 & 0 \\ 0 & \mathbf{c}_{ff} \end{bmatrix} \begin{bmatrix} \dot{\mathbf{q}}_r \\ \dot{\mathbf{q}}_f \end{bmatrix} + \begin{bmatrix} 0 & 0 \\ 0 & \mathbf{k}_{ff} \end{bmatrix} \begin{bmatrix} \mathbf{q}_r \\ \mathbf{q}_f \end{bmatrix} = \begin{bmatrix} \mathbf{Q}_{er} \\ \mathbf{Q}_{ef} \end{bmatrix} + \begin{bmatrix} \mathbf{Q}_{vr} \\ \mathbf{Q}_{vf} \end{bmatrix} \tag{1}$$

where $\mathbf{m}_{rr}$ is a configuration-dependent matrix representing the mass and inertia tensor of the deformed body, associated with the rigid body coordinates; $\mathbf{m}_{fr}$ and $\mathbf{m}_{rf}$ are configuration-dependent matrices representing the inertial coupling between the rigid body coordinates and deformation coordinates; and $\mathbf{m}_{ff}$, $\mathbf{c}_{ff}$, and $\mathbf{k}_{ff}$ are the consistent finite element mass, damping, and stiffness matrices, respectively. The force vector $\mathbf{Q}_e$ represents the applied external forces, control forces, and reaction forces coming from adjacent multibody components, while the force vector $\mathbf{Q}_v$ represents the quadratic velocity force vector which includes centrifugal forces and Coriolis forces. Geometric stiffening due to high rotation rates can also be added to the vector $\mathbf{Q}_{vf}$.

The dependence of the rigid body coordinates on the deformation coordinates can be mitigated by assuming that we can find control forces so that the rigid body coordinates follow the nominal motion and therefore, the resulting equations of motion become

$$\mathbf{m}_{ff}\,\ddot{\mathbf{q}}_f + \mathbf{c}_{ff}\,\dot{\mathbf{q}}_f + \mathbf{k}_{ff}\,\mathbf{q}_f = \mathbf{Q}_{ef} + \mathbf{Q}_{vf} - \mathbf{m}_{fr}\,\ddot{\mathbf{q}}_r \tag{2}$$

where $\ddot{\mathbf{q}}_r$ takes values along the nominal motion. Furthermore, the external force vector $\mathbf{Q}_{ef}$ can be decomposed into applied torques, equivalent moments coming from the distributed piezoelectric actuators and reaction forces coming from adjacent multibody components, *i.e.*,

$$\mathbf{Q}_{ef} = \mathbf{B}_\tau\,\tau + \mathbf{B}_p\,\mathbf{V}_p + \mathbf{R} \tag{3}$$

where $\mathbf{B}_\tau$ and $\mathbf{B}_p$ are *constant* matrices that describe the placement of the motors and

piezoelectric actuators, respectively; τ is the vector of base torques measured with respect to the floating reference frame; $\mathbf{V}_p$ is the vector of applied piezoelectric voltages; and $\mathbf{R}$ is the vector of reaction forces coming from adjacent multibody components. The reaction force vector $\mathbf{R}$ consists of three force components and three torque components acting at both ends of the multibody component. The force and torque components are taken along the body axes associated with the multibody. As shown in Fig. 2, these force and torque components are transferred from body j to body i through the rotation transformation

$$\sigma^i = \mathbf{A}^{ij}\, \sigma^j \tag{4}$$

and

$$\tau^i = \mathbf{A}^{ij}\, \tau^j \tag{5}$$

where σ^i and τ^i are the reaction forces and reaction moments, respectively, measured along the body axes of body i, and $\mathbf{A}^{ij}$ is the rotation transformation matrix which projects forces and moments from body j to body i. The transformation matrix $\mathbf{A}^{ij}$ depends on the nominal values of rigid body coordinates $\mathbf{q}_r^i$ and $\mathbf{q}_r^j$.

Following the model proposed by Crawley and Anderson,[15] the piezoelectric actuation can be considered as two self-equilibrating concentrated moments acting at the two ends of the actuator. The magnitude of the concentrated moment is proportional to the voltage applied across the piezoelectric actuator, hence

$$M_p = k_p\, V_p \tag{6}$$

where the proportionality constant k_p is a function of the dimensions and material properties of the piezoceramic material and the link components. As an example, for a 3-element model where the middle element has piezoelectric actuators attached on four sides to control bending in two directions, the influence matrix $\mathbf{B}_p$ can be expressed as

$$\mathbf{B}_p = \begin{bmatrix} 0 & 0 \\ k_p & 0 \\ 0 & k_p \\ \vdots & \vdots \\ -k_p & 0 \\ 0 & -k_p \\ \vdots & \vdots \\ 0 & 0 \end{bmatrix} \tag{7}$$

where the rows having the non-zero coefficients correspond to the rotational degree of freedom of the element in which the piezoelectric actuators are attached. Each column of $\mathbf{B}_p$ corresponds with a specific voltage of a pair of actuators. Hence, $\mathbf{B}_p$ will have as many columns as the number of pairs of piezoelectric actuators. In general, the influence matrix $\mathbf{B}_p$ depends on the sizing and placement of the distributed actuators. Issues concerning the design of so-called smart structures are discussed in Reference 16. In the cited work, the researchers conclude that the optimal placement and sizing of piezoeletric actuators depends on the free vibration modes of the flexible manipulator, the frequency content of the desired motion, and the choice of vibration modes that need to be controlled. As a general rule, distributed actuators are most effective in controlling the vibration modes which do not have nodes near the distributed actuator.

There are two important reasons for expressing the base torques in terms of components along the floating reference frame. First, the influence matrix $\mathbf{B}_\tau$ becomes a constant Boolean matrix because each of the base torque components is associated with a specific rotational deformation degree of freedom. Constant influence matrices $\mathbf{B}_\tau$ and $\mathbf{B}_p$ are necessary in order to obtain the non-causal base torques and piezoelectric voltages in the frequency domain as will be seen in the following section. Second, the base torque components which are associated with the torsional moment and the two bending moments are independent of each other if the corresponding modes of deformation are decoupled, as in the case of small deformation from the nominal configuration. Hence, the influence matrix $\mathbf{B}_\tau$ has independent columns, and this property is useful in finding the solution to the minimization problem described in the next section.

Combining Eqs. (2) and (3), the equations of motion for each multibody component become

$$\mathbf{m}_{ff}\,\ddot{\mathbf{q}}_f + \mathbf{c}_{ff}\,\dot{\mathbf{q}}_f + \mathbf{k}_{ff}\,\mathbf{q}_f = \mathbf{B}_\tau\,\tau + \mathbf{B}_p\,\mathbf{V}_p + \mathbf{F} \tag{8}$$

where

$$\mathbf{F} = \mathbf{R} + \mathbf{Q}_{vf} - \mathbf{m}_{fr}\,\ddot{\mathbf{q}}_r\,. \tag{9}$$

Having derived the equations of motion for each multibody component, the problem statement that this paper addresses can be stated as follows. Given the nominal motion of an open-chain flexible manipulator, we wish to find: 1) the inverse dynamic torques that will cause the end-point of each multibody component to follow the nominal motion; and 2) the piezoelectric voltages that will minimize the induced elastic vibrations during the motion. The problem of simultaneous trajectory tracking and vibration reduction can be stated mathematically as the following minimization problem:

$$\min_{(\tau,\mathbf{V}_p)\,\in\,\bar{T}} J(\tau,\mathbf{V}_p) \tag{10}$$

where $\bar{T}$ is the set of all pairs of stable joint torques and distributed actuator voltages that cause the end-point to follow the nominal motion, and $J(\tau,\mathbf{V}_p)$ is a measure of the elastic vibrations and defined as

$$J(\tau,\mathbf{V}_p) = \int_{-\infty}^{\infty} \mathbf{q}_f(t)^T\,\mathbf{q}_f(t)\,dt. \tag{11}$$

2.2. Solution Procedure

The minimization problem described in the previous subsection presents some unique features that are associated with non-minimum phase systems such as flexible manipulators. The requirement that the pair $(\tau,\mathbf{V}_p)$ should cause the end-point to follow the nominal trajectory admits only non-causal solutions as stable solutions to the minimization problem.[17] As demonstrated by Bayo, *et. al.*,[12] the recursive frequency domain approach can be employed to capture the non-causal (time-anticipatory) nature of the actuating torques in the case of multi-link, planar manipulators. In our approach, each multibody component is modeled by a pinned-free beam and the requirement that the

end-point follows the desired trajectory is satisfied by imposing the condition that the elastic displacement at the tip is zero. In the three-dimensional case, however, we have to impose the additional constraint that the elastic torsional deformation at the tip is zero, because torsional deformations would cause displacements from the nominal configuration further down the chain.

In the frequency domain, Eq. (8) can be expressed as a set of complex equations for a particular frequency $\bar{\omega}$

$$\left[\mathbf{m}_{ff} + \frac{1}{i\omega}\mathbf{c}_{ff} - \frac{1}{\omega^2}\mathbf{k}_{ff} \right] \hat{\ddot{\mathbf{q}}}_f(\bar{\omega}) = \mathbf{B}_\tau \hat{\tau}(\bar{\omega}) + \mathbf{B}_p \hat{\mathbf{V}}_p(\bar{\omega}) + \hat{\mathbf{F}}(\bar{\omega}) \tag{12}$$

where $\hat{\ddot{\mathbf{q}}}_f(\bar{\omega})$, $\hat{\tau}(\bar{\omega})$, $\hat{\mathbf{V}}_p(\bar{\omega})$, and $\hat{\mathbf{F}}(\bar{\omega})$ are the Fourier transforms of $\ddot{\mathbf{q}}_f(t)$, $\tau(t)$, $\mathbf{V}_p(t)$, and $\mathbf{F}(t)$, respectively. Eq. (12) is based on the assumption that the aforementioned Fourier transforms exist, an assumption which is valid for rest to rest slewing motions. We also take note of the fact that the Fourier transforms of the base torques and applied piezoelectric voltages can be explicitly expressed because their respective influence matrices are constant. The leading matrix

$$\hat{\mathbf{H}}(\bar{\omega}) = \left[\mathbf{m}_{ff} + \frac{1}{i\omega}\mathbf{c}_{ff} - \frac{1}{\omega^2}\mathbf{k}_{ff} \right] \tag{13}$$

is a complex regular matrix that is invertible for all frequencies except for $\bar{\omega} = 0$. However, for $\bar{\omega} = 0$, the system undergoes a rigid body motion, and the leading matrix will be determined only by $\mathbf{m}_{ff}$ which is positive definite and therefore invertible. Making use of the fact that the leading matrix is invertible for all frequencies, Eq. (12) can be expressed in the following partitioned form:

$$\begin{Bmatrix} \hat{\ddot{\mathbf{q}}}_h(\bar{\omega}) \\ \hat{\ddot{\mathbf{q}}}_i(\bar{\omega}) \\ \hat{\ddot{\mathbf{q}}}_t(\omega) \end{Bmatrix} = \begin{bmatrix} \hat{\mathbf{G}}_{hh} & \hat{\mathbf{G}}_{hi} & \hat{\mathbf{G}}_{ht} \\ \hat{\mathbf{G}}_{ih} & \hat{\mathbf{G}}_{ii} & \hat{\mathbf{G}}_{it} \\ \hat{\mathbf{G}}_{th} & \hat{\mathbf{G}}_{ti} & \hat{\mathbf{G}}_{tt} \end{bmatrix} \left\{ \begin{bmatrix} \mathbf{I}_3 \\ 0 \\ 0 \end{bmatrix} \hat{\tau}(\bar{\omega}) + \begin{bmatrix} \mathbf{B}_{p_h} \\ \mathbf{B}_{p_i} \\ \mathbf{B}_{p_t} \end{bmatrix} \hat{\mathbf{V}}_p(\bar{\omega}) + \begin{bmatrix} \hat{\mathbf{F}}_h(\bar{\omega}) \\ \hat{\mathbf{F}}_i(\bar{\omega}) \\ \hat{\mathbf{F}}_t(\omega) \end{bmatrix} \right\} \tag{14}$$

where $\hat{\mathbf{G}}(\bar{\omega})$ is the inverse of $\hat{\mathbf{H}}(\bar{\omega})$ and $\mathbf{I}_3$ is the (3 x 3) identity matrix. The subscript h refers to the rotational degrees of freedom at the hub, the subscript t refers to the deformation degrees of freedom at the tip which are to be controlled, and the subscript i refers to the remaining elastic degrees of freedom. The expression for the influence matrix $\mathbf{B}_\tau$

on the right hand side of Eq. (14) makes use of the fact that each of the components of the base torque vector τ is associated with a specific rotational deformation degree of freedom and is independent of the other components.

The condition that the tip should follow the nominal motion is equivalent to imposing the constraint $\ddot{\hat{q}}_t(\bar{\omega}) = 0$ for all $\bar{\omega}$. This constraint results in a relationship between the base torques τ and the distributed piezoelectric actuator inputs $\mathbf{V}_p$. This relationship can be obtained from the last set of equations of Eq. (14) when $\ddot{\hat{q}}_t(\bar{\omega})$ is set to zero, hence giving the following result:

$$\hat{\tau}(\bar{\omega}) = -\hat{\mathbf{G}}_{th}^{-1}\left[\hat{\mathbf{G}}_{th}\ \hat{\mathbf{G}}_{ti}\ \hat{\mathbf{G}}_{tt}\right]\left\{\mathbf{B}_p\ \hat{\mathbf{V}}_p(\bar{\omega}) + \hat{\mathbf{F}}(\bar{\omega})\right\} \tag{15}$$

where the existence of the inverse of $\hat{\mathbf{G}}_{th}$ is assured when the torsional deformation and the bi-axial bending modes are decoupled, which is consistent with the assumption of small deformation from the nominal configuration. Substituting the above expression for the base torque $\hat{\tau}(\bar{\omega})$ in Eq. (13) and using the Fourier transform property $\ddot{\hat{\mathbf{q}}} = -\bar{\omega}^2\,\hat{\mathbf{q}}$ yields the following expression for the elastic displacements in compact form:

$$\hat{q}_f(\bar{\omega}) = -\frac{1}{\omega^2}\left(\mathbf{A}\,\hat{\mathbf{V}}_p + \mathbf{B}\right) \tag{16}$$

where

$$\mathbf{A} = \left[-\hat{\mathbf{G}}\,\mathbf{B}_\tau\,\hat{\mathbf{G}}_{th}^{-1}\left(\hat{\mathbf{G}}_{th}\ \hat{\mathbf{G}}_{ti}\ \hat{\mathbf{G}}_{tt}\right) + \hat{\mathbf{G}}\right]\mathbf{B}_p \tag{17}$$

and

$$\mathbf{B} = \left[-\hat{\mathbf{G}}\,\mathbf{B}_\tau\,\hat{\mathbf{G}}_{th}^{-1}\left(\hat{\mathbf{G}}_{th}\ \hat{\mathbf{G}}_{ti}\ \hat{\mathbf{G}}_{tt}\right) + \hat{\mathbf{G}}\right]\hat{\mathbf{F}}. \tag{18}$$

Employing Parseval's theorem, minimizing $J(\tau, \mathbf{V}_p)$ is equivalent to minimizing the 2-norm $\|\hat{q}_f(\bar{\omega})\|_2^2$ for each $\bar{\omega}$. The minimization problem of Eq. (10) then reduces to a standard least squares approximation problem with the solution

$$\hat{\mathbf{V}}_p = -(\mathbf{A}^*\mathbf{A})^{-1}\,\mathbf{A}^*\,\mathbf{B} \tag{19}$$

where $\mathbf{A}^*$ denotes the conjugate transpose of $\mathbf{A}$. A necessary and sufficient condition for the inverse of $\mathbf{A}^*\mathbf{A}$ to exist is that all the columns of the constant matrices $\mathbf{B}_\tau$ and $\mathbf{B}_p$ are independent. This condition is automatically satisfied because the base torques and the

equivalent concentrated moment due to the distributed piezoelectric actuators do not act on the same degree of freedom in the finite element model.

Having determined the piezoelectric voltages $\hat{V}(\bar{\omega})$ for each frequency $\bar{\omega}$ from Eq. (19), the base torques $\hat{\tau}(\bar{\omega})$ and the elastic displacements $\hat{q}_f(\bar{\omega})$ can be determined from Eqs. (15) and (16), respectively, for the same frequency. The base torques, elastic displacements, and piezoelectric voltages do not need to be determined for the frequency $\bar{\omega} = 0$ because the zero frequency content of these variables can be determined from the zero initial conditions. The base torques, elastic displacements, and the piezoelectric voltages in the time domain can then be obtained by using their respective inverse Fourier transforms

$$\tau(t) = \frac{1}{2\pi} \int_{-\infty}^{\infty} \hat{\tau}(\bar{\omega})\, e^{i\bar{\omega}t}\, d\bar{\omega} \tag{20}$$

$$q_f(t) = \frac{1}{2\pi} \int_{-\infty}^{\infty} \hat{q}_f(\bar{\omega})\, e^{i\bar{\omega}t}\, d\bar{\omega} \tag{21}$$

and

$$V_p(t) = \frac{1}{2\pi} \int_{-\infty}^{\infty} \hat{V}_p(\bar{\omega})\, e^{i\bar{\omega}t}\, d\bar{\omega}. \tag{22}$$

We note, however, that the forcing vector $\mathbf{F}(t)$ in Eq. (8) depends on the elastic nodal deformations and nodal velocities. Therefore, an iteration process is needed to obtain the solution to the nonlinear differential equations. We start the iteration process by assuming zero elastic deformations and velocities for the initial calculation of the forcing vector $\mathbf{F}(t)$ and use a successive substitution scheme to converge to the correct solution. For normal robotics applications, convergence is achieved in two or three iterations.

Once the base torques and the elastic deformations have been determined, the reactions coming from the next multibody component in the proximal direction can be determined from dynamic equilibrium considerations. The reaction forces between components will generally consist of three force components and three torque components. As shown in Fig. 2, the three torque components at the base for body j consist of a

revolute joint actuating torque τ_t, a reaction bending moment τ_s that controls the end-point displacement δ_t in the plane defined by the revolute joint axis and the component's body axis, and a reaction torsional moment τ_r which controls the end-point torsional deformation θ_r for this multibody. Having determined the reaction forces and moments between this multibody and the next multibody component in the proximal direction, the latter multibody can be analyzed using the inverse dynamics procedure discussed above. This multibody component has, at its distal end, the previously computed reaction forces and reaction moments coming from the previous multibody component. These forces and moments are transferred from the previous multibody component to the present multibody by a projection of forces and moments, where the projection matrix depends on the rigid body coordinates. The inverse dynamics analysis therefore involves a procedure which analyzes each multibody body component, starting from the end of the chain and proceeding towards the base of the chain. For each multibody component, the base torques are determined such that the end-point follows the desired trajectory and in addition, the reaction forces and moments at the end-point are in dynamic equilibrium with the previously computed base torques and base forces of the adjacent multibody component in the distal direction. Finally, the base torques of the multibody component at the base of the chain are projected onto a reference frame that defines the joint axes of the three motors at the ground. The three torque components that result from this projection are the required base motor torques at the ground.

To summarize, the procedure for obtaining the inverse dynamic torques and distributed piezoelectric voltages that will simultaneously track a desired end-point trajectory and minimize elastic vibrations in open-chain flexible manipulators involve the following steps:

Algorithm:

1. Define the nominal motion (rigid body inverse kinematics).
2. For each link in the chain, starting from the last link:
   a) Determine the piezoelectric voltages for this link.
   b) Determine the base torques for this link.
   c) Determine the elastic displacements, velocities and accelerations.
   d) Repeat steps (a), (b), and (c) until the base torques and voltages converge to within a desired tolerance.
   e) Determine the reaction forces to the next link by considering dynamic equilibrium for this link.
3. Proceed to the next link in the chain.

The recursive approach presented above solves the trajectory tracking problem one link at a time. In general, there may be global solutions to the nonlinear inversion problem associated with end-effector trajectory tracking, which can potentially have many solutions. Our method, however, yields a solution which can be efficiently computed due to the linearization process that takes place when the ends of each link are constrained to move along their respective nominal trajectories.

In the next section, we consider an example of a class of spatial, open-chain, flexible manipulators where all intermediate joints are revolute joints and all intermediate joint axes are parallel in the nominal configuration. For this class of flexible manipulators, at least three motors are required at the ground in order to achieve end-point tracking for all possible configurations. We illustrate the preceding statement through a simple example involving a single-link flexible manipulator supported by a rotating base and controlled by only two motors at the ground, as shown in Fig. 3. When the manipulator is in the vertical position, the end-point displacement δ_f can not be controlled by two ground motors alone. This is so because as the manipulator gets closer to the vertical position, the torque that is required to control this displacement component becomes so large that it saturates the capacity of the ground motor. Likewise, when the manipulator is in the horizontal position, the end-point rotational displacement θ_f can not be controlled by the two motors alone. Hence, a minimum of three motors at the ground is

necessary to assure that the end-point elastic displacements are controllable for all possible configurations. The requirement of having three motors at the ground is not restrictive because it does not increase the mass that is distributed on the links, and therefore this requirement does not increase the inertial forces acting on the system. The simple algorithm presented herein, and the minimal number of motors required to implement the trajectory tracking procedure should make the proposed approach very attractive in the design and experimentation of spatial, open-chain, flexible manipulators.

3. Simulation Results and Discussion

The recursive procedure discussed in the preceding section is applied to the three-dimensional open-chain flexible manipulator shown in Fig. 4 to demonstrate the validity of the proposed procedure for solving the simultaneous end-point trajectory tracking and vibration reduction problem. The desired motion is to have the end-point remain in the x_2–x_3 plane with the x_2 coordinate and x_3 coordinate of the end-point following the trajectories shown in Fig. 5. The two links share the following geometric and material properties:

Length: 1.0 m
Cross section dimensions: 1.0 cm x 1.0 cm
Young's modulus: 70 GPa
Shear modulus: 27 GPa
Mass density: 2715 kg/m^3
Tip mass: 0.5 kg

The piezoelectric actuators are distributed uniformly on the middle third span of each link. This placement of the distributed actuators assures that the first mode of vibration is minimized. For the example considered herein, the equivalent concentrated moment that results from the applied voltage to the piezoelectric actuator is

$$M_p = 0.2\, V_p . \tag{23}$$

We perform two sets of computations for the example considered: 1) inverse dynamic torques acting alone; and 2) inverse dynamic torques applied together with

distributed piezoelectric actuators. We can compare the results of the two separate numerical experiments to illustrate the effectiveness of the distributed actuators in minimizing elastic vibrations while simultaneously tracking a desired end-point trajectory.

Plots of the inverse dynamic motor torques needed to track the desired end-point trajectory are shown in Figures 6-9. In these plots, the solid curve refers to the inverse dynamic torques that are needed when they are acting alone, and the dashed curves refer to the required inverse dynamic joint torques that are acting together with piezoelectric actuators. We take note of the observation that the inverse dynamic torque profiles exhibit pre-actuation and post-actuation with respect to the end-point motion for both sets of curves. We also note that the inverse dynamic torques are only slightly perturbed by the presence of the distributed piezoelectric actuators.

Figures 10 and 11 show the elastic deformations along the two transverse directions at the proximal third point in each of the two links. The solid curve refers to the elastic deflection caused by the joint actuators acting alone, and the dashed curves refer to the elastic deflection that results when joint torques are acting together with the distributed piezoelectric actuators. The figures show that the distributed actuators can significantly reduce the elastic vibrations that are induced by the slewing motion. Plots of the piezoelectric voltages that are required to obtain the above reductions in the elastic vibrations are shown in Figure 12.

4. Conclusion

We have presented a new recursive computational procedure for determining the inverse dynamic torques and distributed piezoelectric actuator voltages that are needed to simultaneously achieve end-point trajectory tracking and vibration minimization in three-dimensional, open-chain flexible manipulators. The trajectory tracking requirement is achieved for the three-dimensional case with the use of a single actuator at each intermediate joint, as opposed to previous approaches where three actuators have been proposed at each joint. The non-causal inverse dynamic torques and piezoelectric voltages are obtained through integration in the frequency domain. The transformation of the equations of motion into the frequency domain is greatly simplified by expressing the

base torques in terms of components along the associated floating reference frame for each multibody component. End-point displacements in the plane defined by the associated revolute joint axis and the body axis can be controlled by treating the base torque controlling this displacement as an unknown internal reaction moment which is to be determined. Through a recursive procedure, the actuating torques at the proximal revolute joints are determined so that the desired internal reaction moments described above are attained. Finally, the minimal number of motors required at the intermediate joints to implement the tracking control procedure substantially reduces the control effort and weight of the manipulator, and this is an important contribution in the design and experimentation of spatial, open-chain, flexible manipulators.

Further research is needed to address the problem of simultaneous trajectory tracking and vibration minimization of general (open-chain or closed-chain) three-dimensional flexible manipulators. The sensitivity of the method to modeling errors needs to be addressed as well.

Acknowledgement

The support of this work by the Air Force Office of Scientific Research under contract no. F49620-91-C-0095 is gratefully acknowledged.

References

1. D. X. Liao, C. K. Sung and B. S. Thompson, "The design of flexible robotic manipulators with optimal arm geometries fabricated from composite laminates with optimal material properties," *International Journal of of Robotics Research*, vol. 6, no. 3, pp. 116-130, 1987.

2. W. J. Book, "Modeling, design, and control of flexible manipulator arms: status and trends," *Proceedings, NASA Conference on Space Telerobotics*, vol. 3, pp. 11-24, January, 1989.

3. F. Matsuno and Y. Sakawa, "A simple model of flexible manipulators with six axes and vibration control by using accelerometers," *Journal of Robotic Systems*, vol. 7, no. 4, pp. 575-597, 1990.

4. M. Uchiyama, A. Konno, T. Uchiyama and S. Kanda, "Development of a flexible dual-arm manipulator testbed for space robotics," *Proceedings, IEEE International Workshop on Intelligent Robots and Systems*, pp. 375-381, Tsuchiura, Japan, 1990.

5. M. Uchiyama and Z. H. Jiang, "Compensability of end-effector position errors for flexible robot manipulators," *Proceedings, 1991 American Control Conference*, pp. 1873-1878, Boston, 1991.

6. D. M. Gorinevsky, A. V. Lensky and E. Sabitov, "Feedback control of a one-link flexible manipulator with a gear train," *Journal of Robotic Systems*, vol. 8, no. 5, pp. 659-676, 1991.

7. E. F. Crawley and J. de Luis, "Use of piezoceramics as distributed actuators in large space structures," *AIAA Journal*, vol. 25, no. 10, pp. 1373-1385, 1987.

8. E. Bayo, "A finite-element approach to control the end-point motion of a single-link flexible robot," *Journal of Robotic Systems*, vol. 4, no. 1, pp. 63-75, 1987.

9. E. Bayo and H. Moulin, "An efficient computation of the inverse dynamics of flexible manipulators in the time domain," *Proceedings, IEEE Conference on Robotics and Automation*, pp. 710-715, Scottsdale, Arizona, 1989.

10. D. S. Kwon and W. J. Book, "An inverse dynamic method yielding flexible manipulator state trajectories," *Proceedings, American Control Conference* , vol. 1, pp. 186-193, San Diego, California, 1990.

11. B. Paden, D. Chen, R. Ledesma and E. Bayo, "Exponentially stable tracking control for multi-joint flexible-link manipulators," *ASME Journal of Dynamic Systems, Measurement and Control*, March 1993.

12. E. Bayo, P. Papadopoulos, J. Stubbe and M. Serna, "Inverse kinematics and dynamics of a multi-link elastic robot: an iterative frequency domain," *International Journal of Robotics Research*, vol. 8, no. 6, pp. 49-62, 1989.

13. I. Shimoyama and I. J. Oppenheim, "Manipulator with flexible links: a simple model and experiments," *Proceedings, NASA Conference on Space Telerobotics*, vol. 3, pp. 59-68, January, 1989.

14. A. A. Shabana, *Dynamics of Multibody Systems*, John Wiley & Sons, Inc., 1989.

15. E. F. Crawley and E. H. Anderson, "Detailed models of piezoceramic actuation of beams," *Journal of Intelligent Material Systems and Structures*, vol. 1, pp. 4-24, 1990.

16. S. Devasia, T. Meressi, B. Paden and E. Bayo, "Piezoelectric actuator design for vibration suppression: placement and sizing," *AIAA Journal of Guidance, Dynamics and Control*, 1993. To appear.

17. H. Moulin and E. Bayo, "On the end-point trajectory tracking for flexible manipulators through non-causal inverse dynamics," *ASME Journal of Dynamic Systems, Measurement and Control*, vol. 113, no. 2, pp. 320-324, June 1991.

List of Figures

Fig. 1: A three-dimensional open-chain flexible multibody system

Fig. 2: Joint torques, reaction moments, and tip displacements

Fig. 3: A single-link manipulator with only two ground motors

Fig. 4: A two-link, three-dimensional, flexible open-chain system

Fig. 5: Nominal end-point coordinates

Fig. 6: Base motor torque T0: without piezo (solid) vs. with piezo (dotted)

Fig. 7: Joint torque T1: without piezo (solid) vs. with piezo (dotted)

Fig. 8: Joint torque T2: without piezo (solid) vs. with piezo (dotted)

Fig. 9: Joint torque T3: without piezo (solid) vs. with piezo (dotted)

Fig. 10: Deflection along s-axis, without piezo (solid) vs. with piezo (dotted): (a) link #1; (b) link #2

Fig. 11: Deflection along t-axis, without piezo (solid) vs. with piezo (dotted): (a) link #1; (b) link #2

Fig. 12: Piezo voltages: (a) on surface normal to t-axis; (b) on surface normal to s-axis

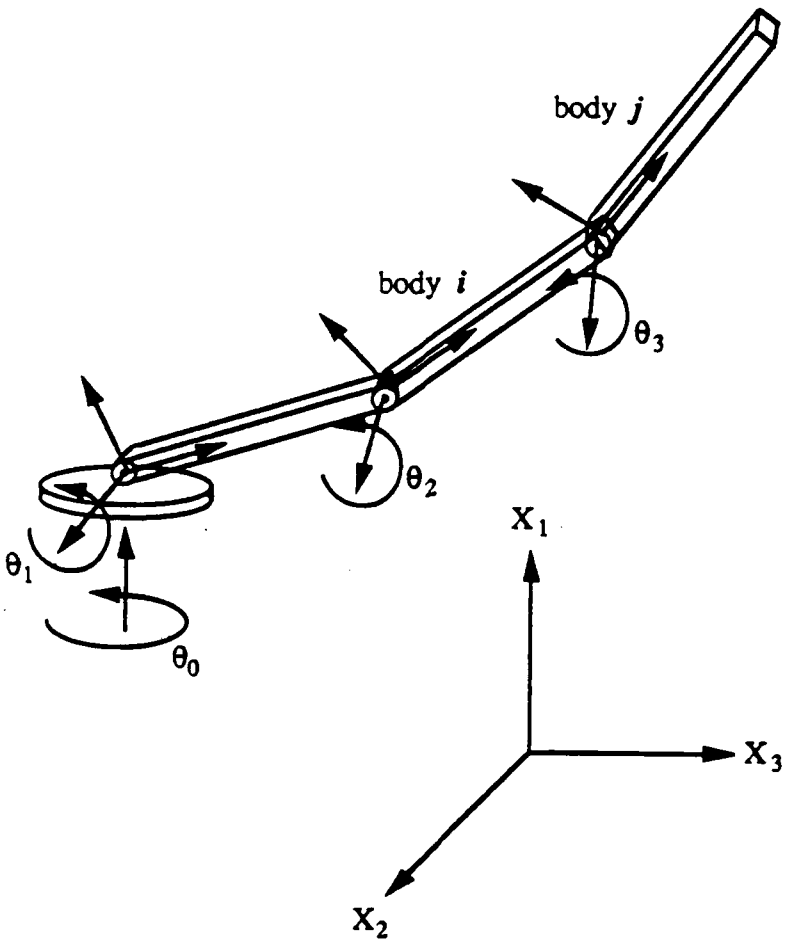
body j
body i
θ3
θ2
θ1
θ0
X1
X3
X2

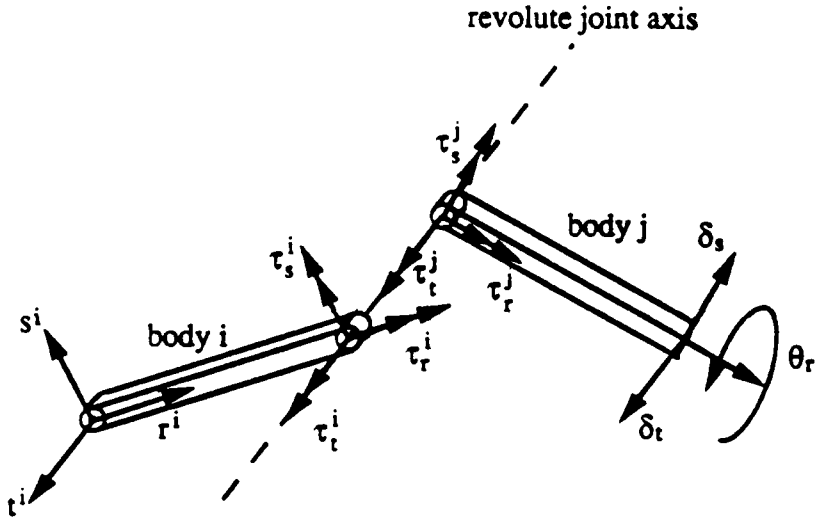
revolute joint axis
τ_s^j
body j
δ_s
τ_s^i
τ_t^j
τ_r^j
s^i
body i
τ_r^i
θ_r
r^i
τ_t^i
δ_t
t^i

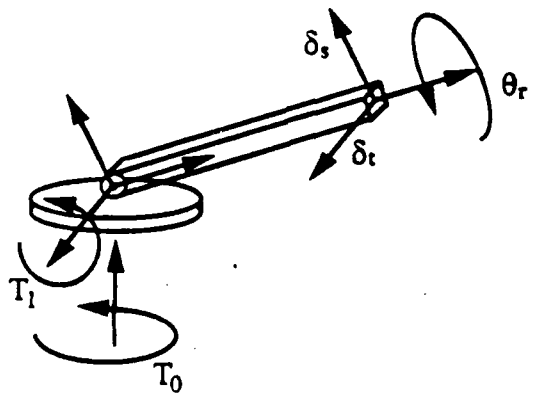
δ_s
θ_r
δ_t
T_1
T_0

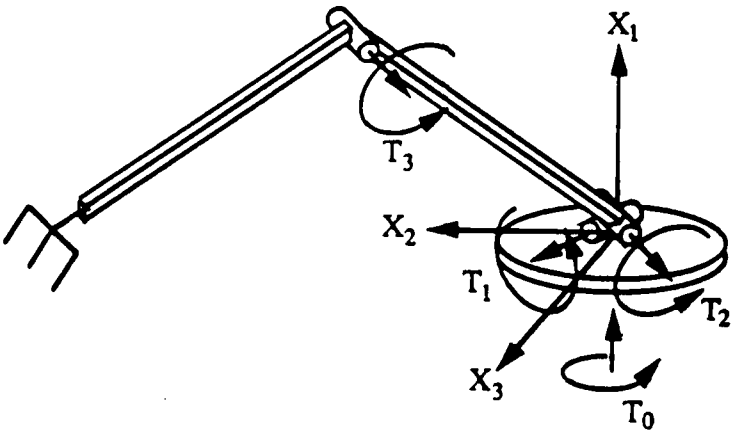
X1
T3
X2
T1
T2
X3
T0

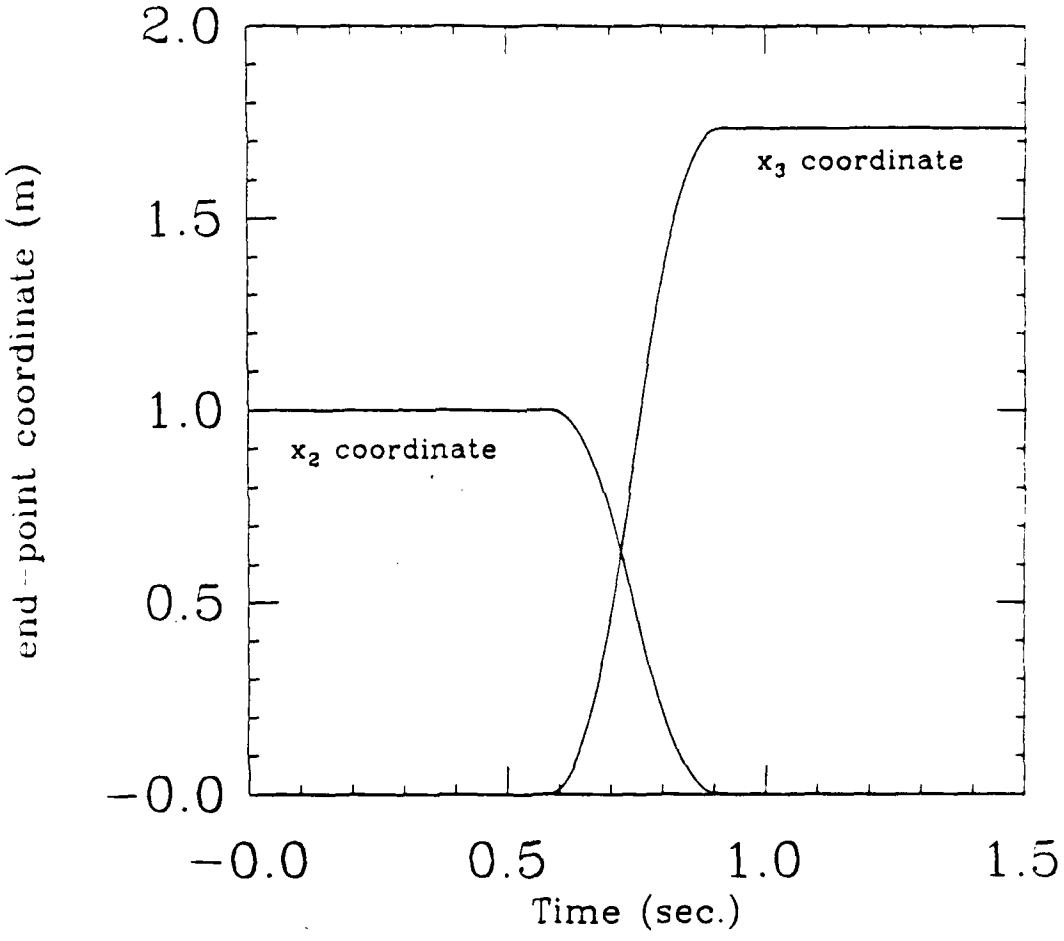
2.0
1.5
1.0
0.5
-0.0
-0.0
0.5
1.0
1.5
end-point coordinate (m)
Time (sec.)
x3 coordinate
x2 coordinate

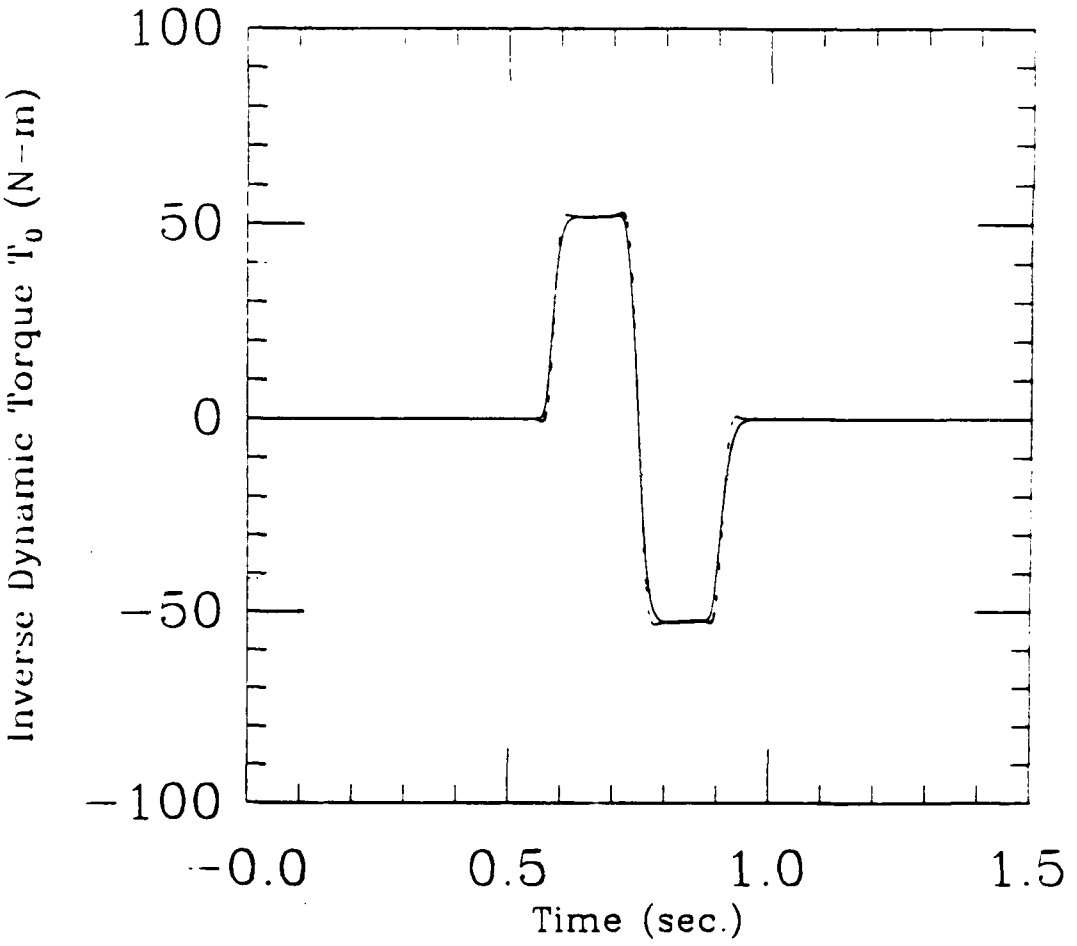
100
50
0
−50
−100
-0.0
0.5
1.0
1.5
Time (sec.)
Inverse Dynamic Torque T_0 (N-m)

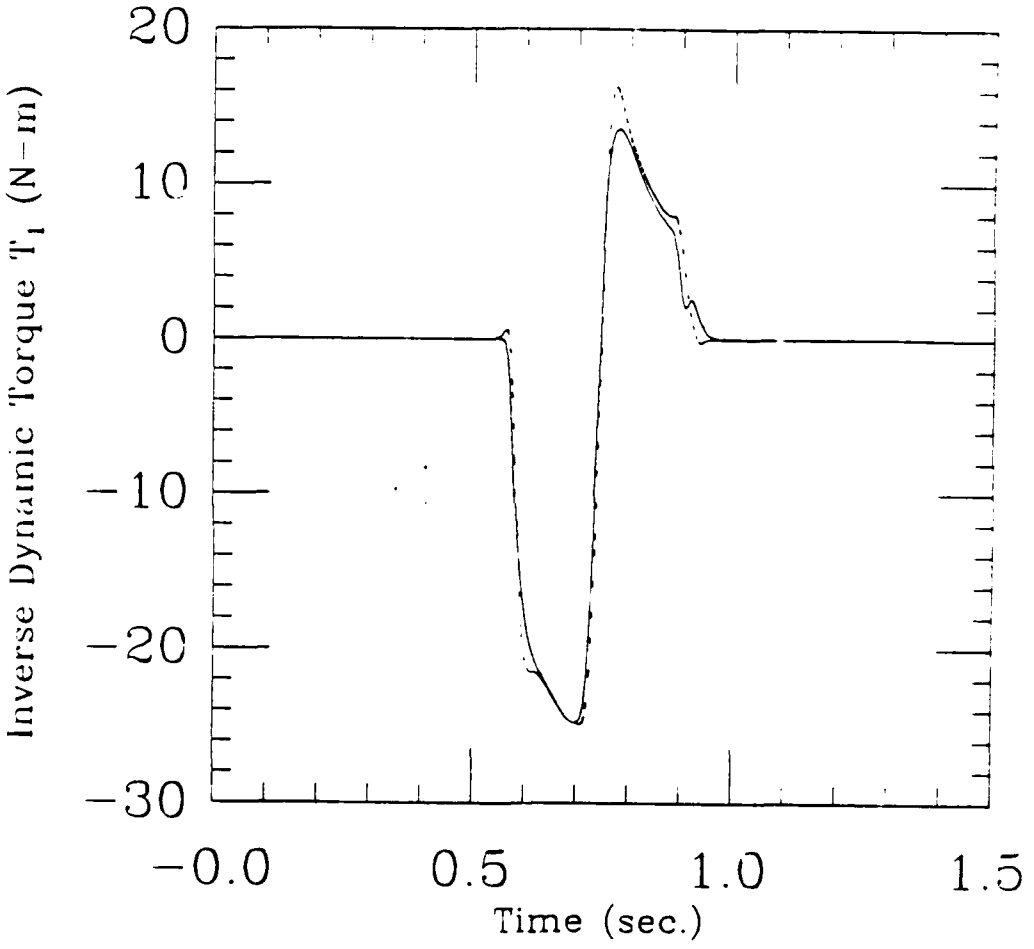
20
10
0
−10
−20
−30
−0.0
0.5
1.0
1.5
Time (sec.)
Inverse Dynamic Torque T_1 (N−m)

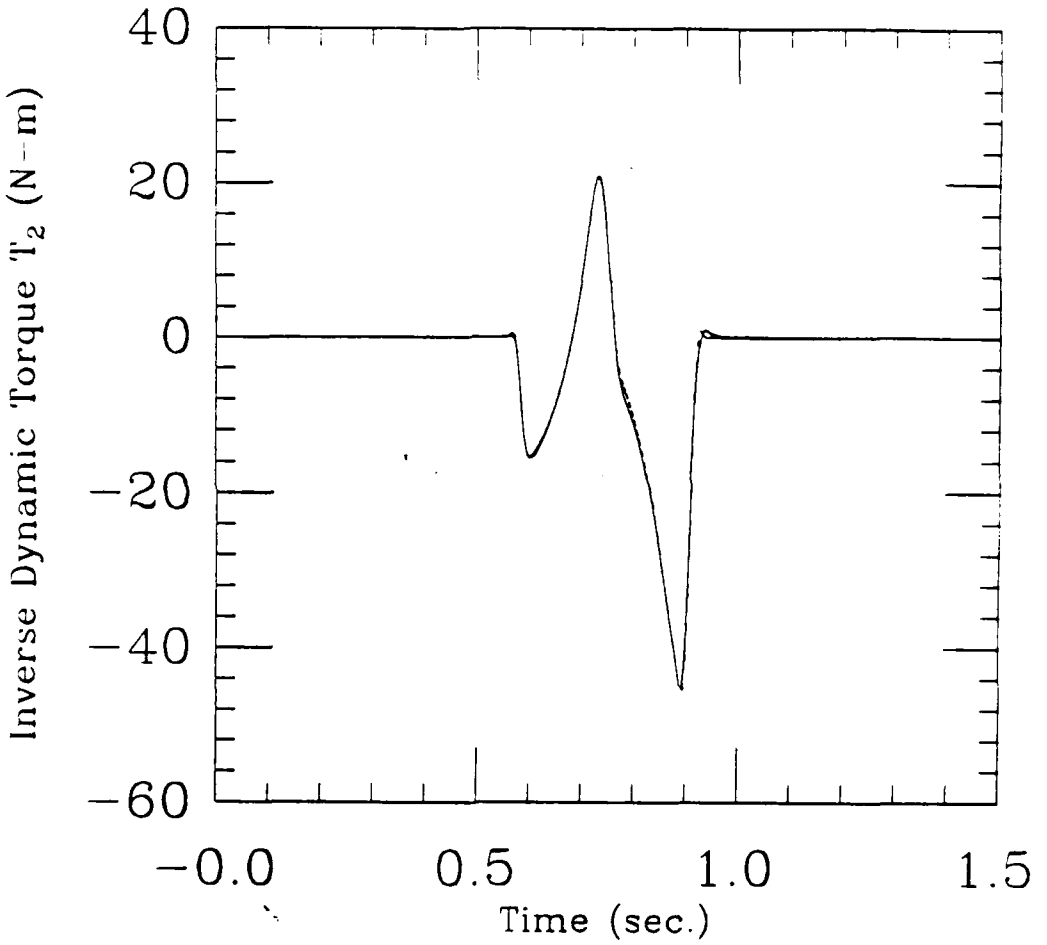
40
20
0
−20
−40
−60
−0.0
0.5
1.0
1.5
Time (sec.)
Inverse Dynamic Torque T_2 (N−m)

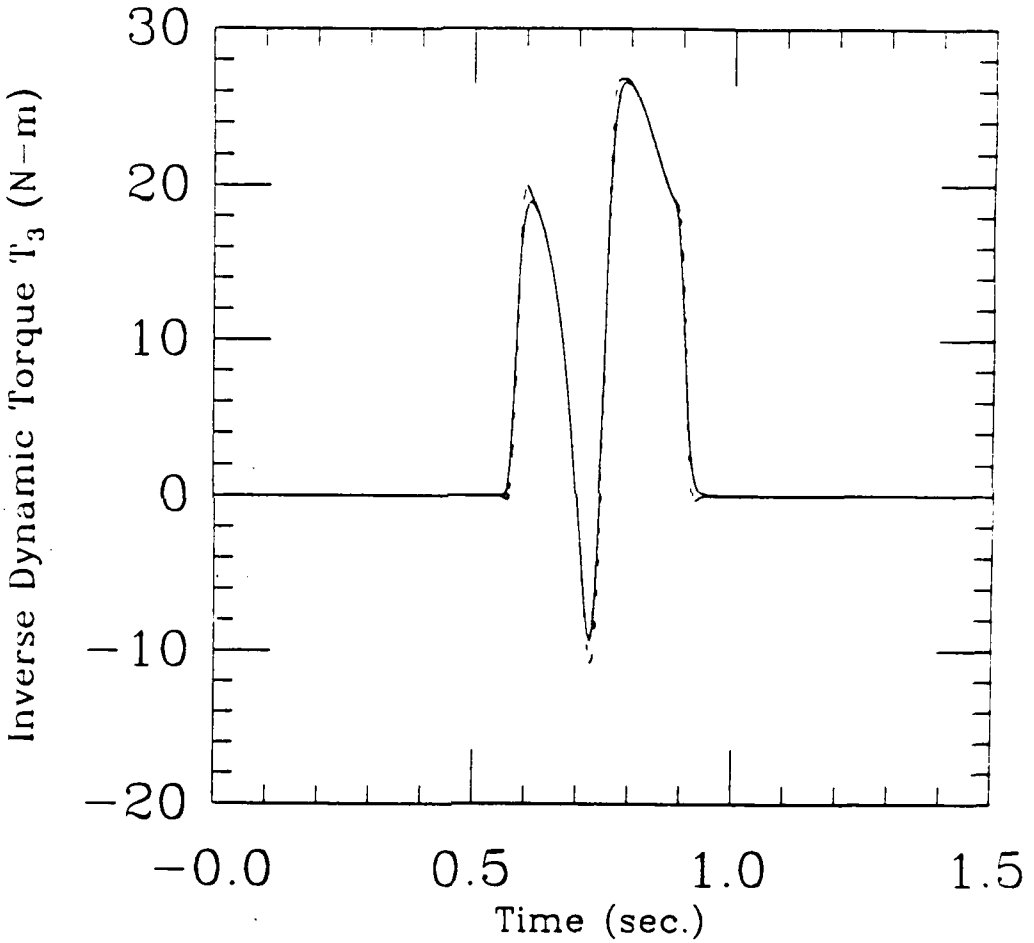
30
20
10
0
−10
−20
−0.0
0.5
1.0
1.5
Time (sec.)
Inverse Dynamic Torque T_3 (N−m)

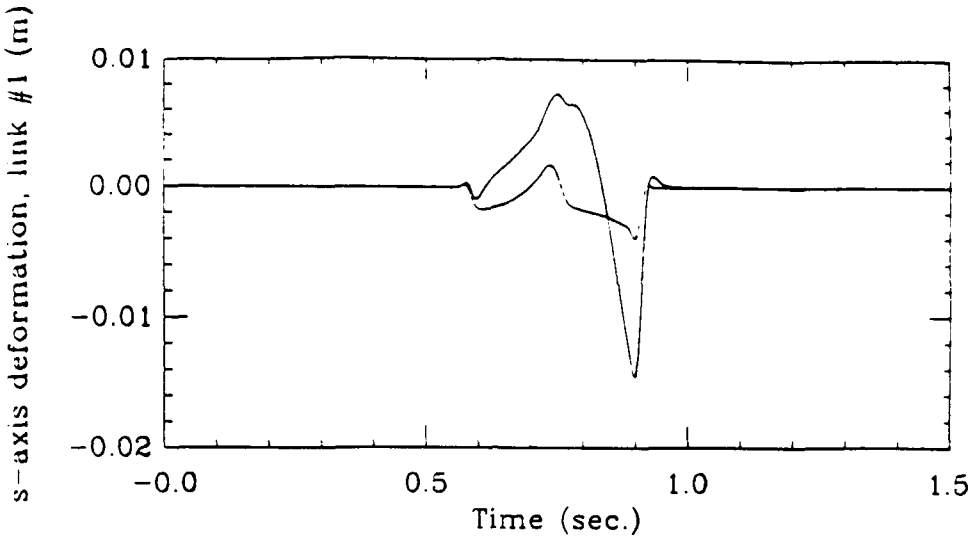
s-axis deformation, link #1 (m)
0.01
0.00
-0.01
-0.02
-0.0
0.5
1.0
1.5
Time (sec.)

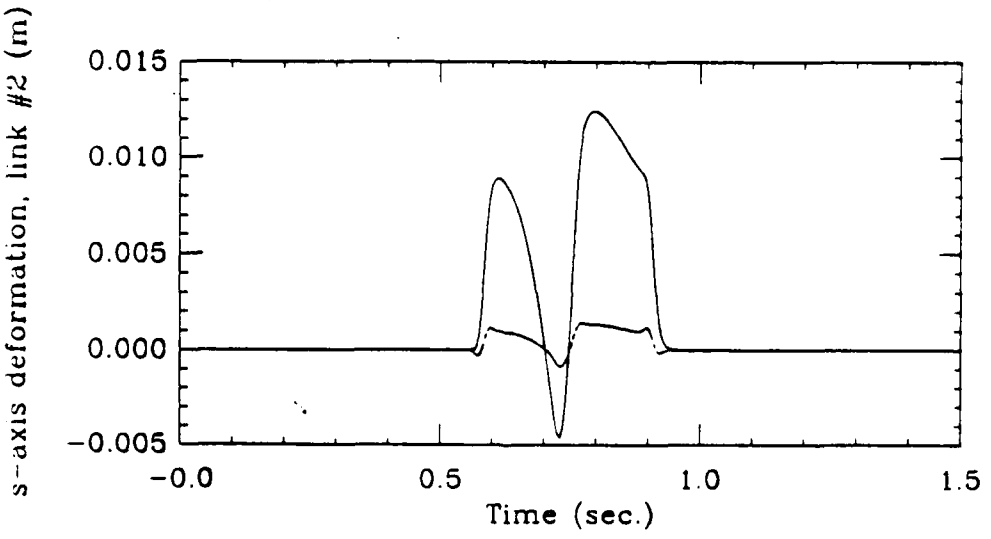
s-axis deformation, link #2 (m)
0.015
0.010
0.005
0.000
-0.005
-0.0
0.5
1.0
1.5
Time (sec.)

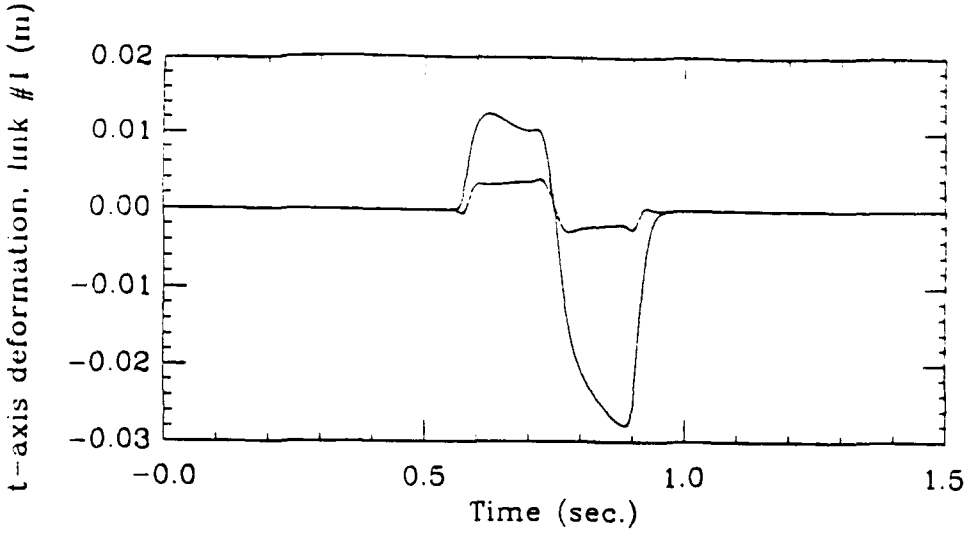
t-axis deformation, link #1 (m)
0.02
0.01
0.00
-0.01
-0.02
-0.03
-0.0
0.5
1.0
1.5
Time (sec.)

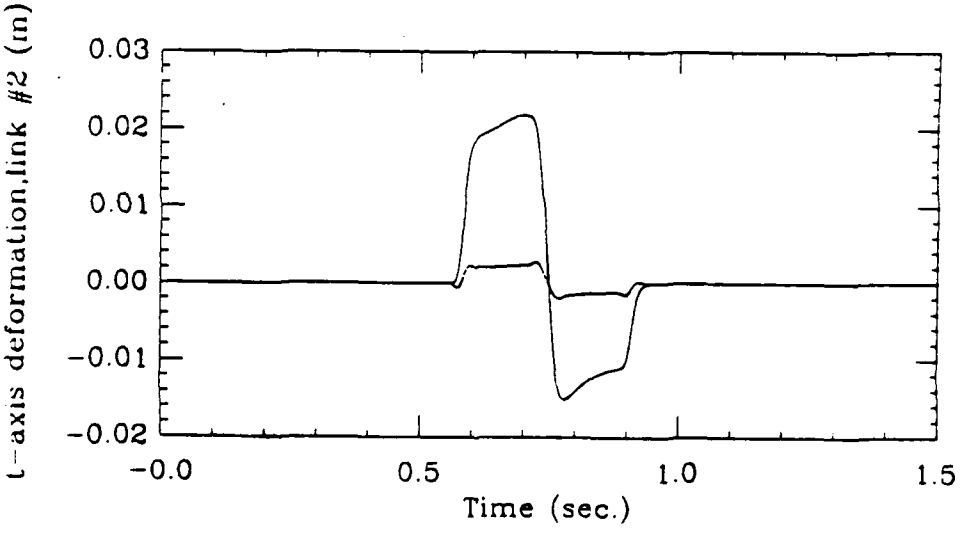
t-axis deformation,link #2 (m)
0.03
0.02
0.01
0.00
-0.01
-0.02
-0.0
0.5
1.0
1.5
Time (sec.)

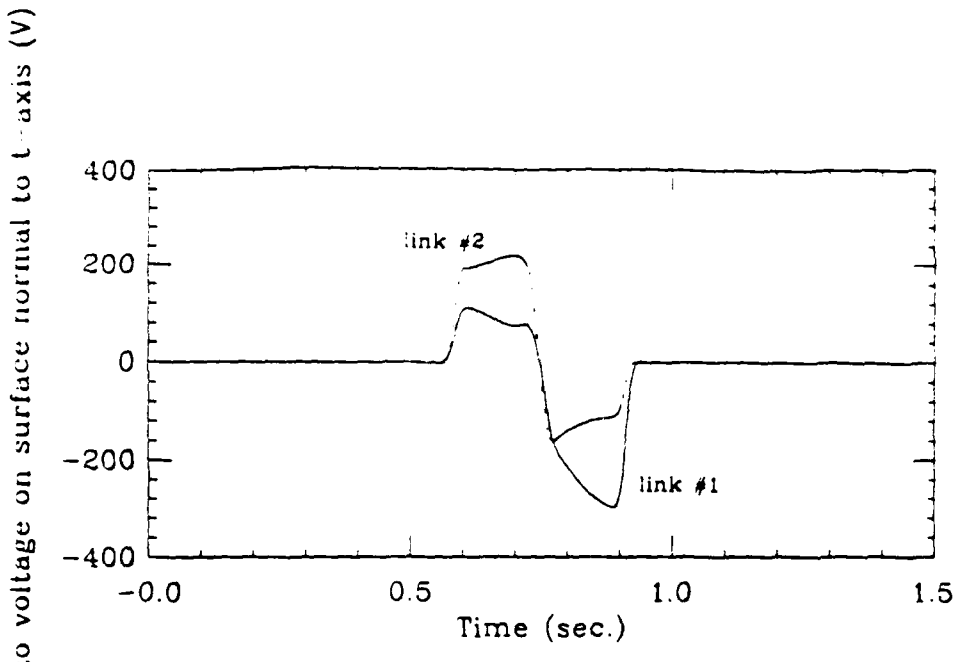
Piezo voltage on surface normal to t-axis (V)
400
200
0
-200
-400
link #2
link #1
-0.0
0.5
1.0
1.5
Time (sec.)

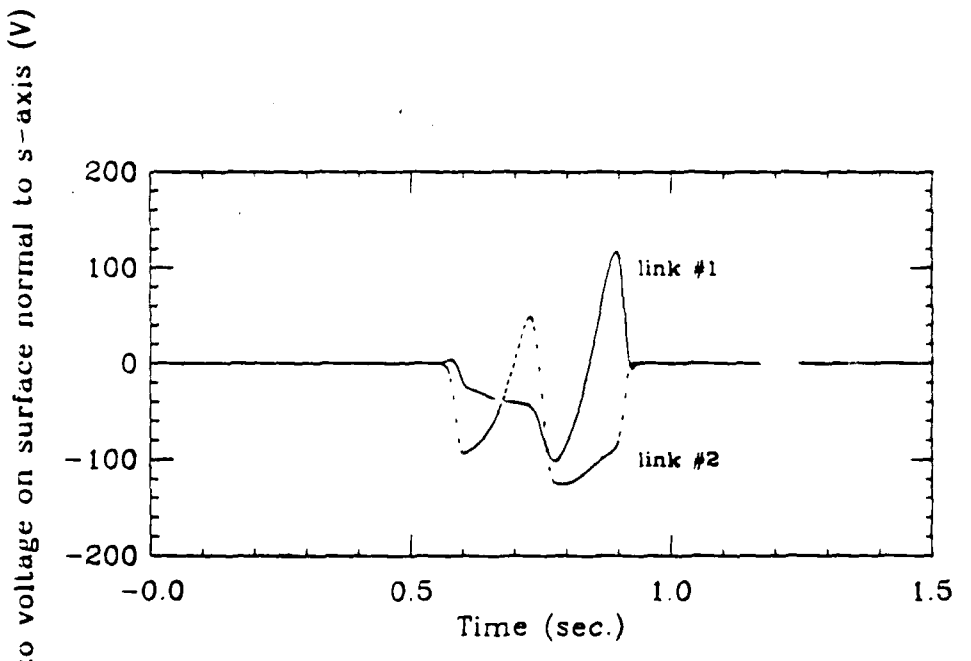
Piezo voltage on surface normal to s-axis (V)
200
100
0
-100
-200
link #1
link #2
-0.0
0.5
1.0
1.5
Time (sec.)

Buckling Control of a Flexible Beam Using Piezoelectric Actuators

T. Meressi and B. Paden

Reprinted from

Journal of Guidance, Control, and Dynamics

Volume 16, Number 5, September-October 1993, Pages 977-980

AIAA

A publication of the
American Institute of Aeronautics and Astronautics, Inc.
The Aerospace Center, 370 L'Enfant Promenade, SW
Washington, DC 20024-2518

Buckling Control of a Flexible Beam Using Piezoelectric Actuators

Tesfay Meressi* and Brad Paden†
University of California, Santa Barbara, Santa Barbara, California 93106

Introduction

ACTIVE damping and control of flexible structures has been an area of research focus for some time.[1] However, the recent application of distributed piezoelectric actuators to structure control by Crawley and De Luis[2] and Bailey and Hubbard[3] has posed new and challenging problems. Following the initial experiments of these researchers, where a single vibrational mode is controlled, Fisher[4] addressed the actuator placement problem to control several modes.

In this Note we address the new problem of buckling control using smart materials. In contrast to the dynamic stability issues of vibration control, buckling is a static instability of axially loaded members of a structure. It is well known that as the axial compressive load P in an initially straight beam increases, the beam remains straight and undeformed until the load reaches a certain critical value $P_{cr,1}$, where the stable equilibrium of the first bending mode bifurcates into one unstable and two stable equilibria (pitchfork bifurcation). The two stable equilibria correspond to buckled configurations.

Here we use piezoelectric actuators and strain gauge sensors to show that buckling of a simply supported beam can be postponed beyond the first critical load. The load deflection characteristic for large deflections of a beam in a buckled configuration is highly nonlinear and involves numerical solution of elliptic integrals. Figure 1a shows a typical load deflection curve where $P_{cr,n}$ is the buckling load of the nth mode. If $P < P_{cr,1}$, the undeflected beam is stable. For $P_{cr,n} < P < P_{cr,n+1}$ all modes are stable except for the first n bending modes. The idea reflected in this Note is the use of feedback control in conjunction with piezoactuators to stabilize the first bending mode beyond $P_{cr,1}$ and achieve a bifurcation diagram of the form shown in Fig. 1b, where the buckling force $P_{cr,1}$ is greater than that for the uncontrolled beam.

We begin by deriving the linearized equation of motion and the associated modal equations of a simply supported flexible beam with piezoelectric actuators subjected to slowly varying axial load. This is followed by the state-space model of the reduced order system and the design of a controller to increase the stiffness or impedance of the first bending mode. We discuss the effect of the unmodeled higher order residual modes and methods of reducing this effect. Our conclusions are made in the last section.

Received Feb. 25, 1992; revision received Oct. 10, 1992; accepted for publication Oct. 19, 1992.

*Research Assistant, Department of Mechanical Engineering.
†Associate Professor, Department of Mechanical Engineering.

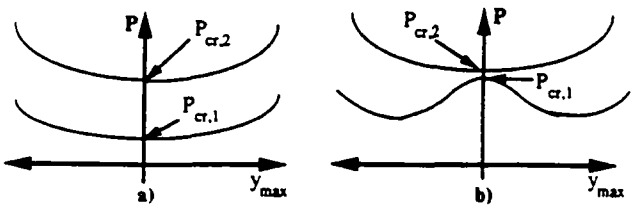

Fig. 1 Load deflection curve of a) uncontrolled beam and b) controlled beam.

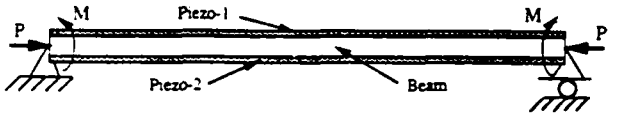

Fig. 2 Simply supported column with piezoelectric actuators.

System Model of a Beam with Piezoactuators

In this section we use a truncated modal expansion of the deflection of a beam to derive a linear finite-dimensional model. We emphasize that the beam is assumed to be uniform with no manufacturing imperfections. Since the aim is to stabilize the beam in its straight configuration, it is natural to assume small deflections and linearize the equations of motion about this configuration. Note that the strain induced by piezoelectric actuators is usually small and, therefore, the small deflection assumption is consistent with the capacity of the actuators.

Figure 2 shows a simply supported uniform beam with piezoelectric actuators of equal thickness bonded to both sides by a suitable adhesive. The beam of width b and thickness t_b is subjected to an axial compressive load, and control moments are applied by the piezoactuators. The actuator being modeled is a piezoelectric polymer, poly vinylidene fluoride. For an axially polarized piezo, a voltage applied across its thickness results in strain along its length. For simplicity the width of each piezolayer is assumed to be the same as that of the beam.

The strain Λ_i developed in an unconstrained piezo is given by $\Lambda_i = v_i(t)d_{31}/t_p$ where $v_i(t)$; $i = 1, 2$ is the voltage applied to the ith piezostrip, d_{31} the piezoelectric strain constant, and t_p the thickness of the piezolayer. If v_1 and v_2 are the voltages applied on the top and bottom piezolayers, respectively, and E_p is the Young's modulus of the piezo, the resulting moment on the piezobeam segment is given by

$$M = bE_p t_p(\Lambda_2 - \Lambda_1)\left(\frac{t_b}{2} + t_a + \frac{t_p}{2}\right)$$

$$= bE_p d_{31}\left(\frac{t_b}{2} + t_a + \frac{t_p}{2}\right)(v_2 - v_1) \triangleq k^*(v_2 - v_1) \tag{1}$$

The equation of motion of the beam can be derived using Hamilton's variational principle.[5] Under small deflection assumption Hamilton's principle yields

$$\rho A\ddot{y} + (EIy'')'' + (Py')' = M\left[\delta'(x - x_2) - \delta'(x - x_1)\right] \tag{2}$$

where ρ is the density of the beam; y is the transverse deflection; $\dot{y}$ and y' are the time and spatial derivatives of y, respectively; EI is the stiffness of the beam; A is the cross-sectional area of the beam; δ' is the spatial derivative of the delta function; and x_1 and x_2 are the locations of the two ends of the piezolayer. The solution to Eq. (2) is obtained as follows.

Unforced Dynamics

The unforced system dynamics are defined by the condition $M = 0$ in Eq. (2). Using separation of variables, we have $y_n(x,t) = \phi_n(x)\eta_n(t)$. Substituting this in Eq. (2) and assuming a simply supported uniform beam (EI constant) of length L, we obtain

$$\eta_n(t) = \sin(\omega_n t + \psi) \quad \text{and} \quad \phi_n(x) = D_n \sin(n\pi x/L)$$

$$n = 1, 2, 3 \ldots \tag{3}$$

If ϕ_n is normalized so that $\int_0^L \phi_n^2\, dx = 1$, the unforced dynamics in modal form becomes

$$y_n(x,t) = \sqrt{2/L}\, \sin(n\pi x/L)\sin(\omega_n t + \psi) \tag{4}$$

To see how the load affects the natural frequencies of the beam, substitute Eq. (4) in Eq. (2) and simplify to get

$$\omega_n^2 = \frac{1}{\rho A}\frac{n^2\pi^2}{L^2}\left[EI\frac{n^2\pi^2}{L^2} - P\right] \tag{5}$$

From Eq. (5) we see that the nth pole pair $\pm j\omega_n$ moves along the imaginary axis toward the origin as P increases from 0 to $P_{cr,n} \triangleq EIn^2\pi^2/L^2$ and becomes real for $P \geq P_{cr,n}$. Hence, when $P = P_{cr,n}$ the beam loses all of its stiffness and buckles in the nth buckling mode.

Forced Response

The deflection of the beam can be written in terms of the modal deflections as

$$y(x,t) = \sum_{n=1}^{n=\infty} y_n(x,t)$$

Substituting this in Eq. (2) we obtain

$$\sum_{n=1}^{n=\infty} \rho A\phi_n\ddot{\eta}_n + \sum_{n=1}^{n=\infty} EI\phi_n''''\eta_n + \sum_{n=1}^{n=\infty} P\eta_n\phi_n''$$

$$= M\left[\delta'(x - x_2) - \delta'(x - x_1)\right] \tag{6}$$

(If the piezoelectric actuators are bonded along the total length of the beam, $x_1 = 0$ and $x_2 = L$.) Multiplying both sides of Eq. (6) by ϕ_n, integrating with respect to x over the beam length, and using the orthogonality of the mode shapes yields

$$\ddot{\eta}_n + \omega_n^2\eta_n = \frac{-2n\pi M}{\rho AL}\sqrt{\frac{2}{L}}\begin{cases} 1 & \text{if } n \text{ is odd} \\ 0 & \text{if } n \text{ is even} \end{cases} \tag{7}$$

If $v_2 = -v_1 \triangleq v$, we have $M = 2k^*v$ and Eq. (7) becomes $\ddot{\eta}_n + \omega_n^2\eta_n = B_n v$, where

$$B_n \triangleq \frac{-4n\pi k^*}{\rho AL}\sqrt{\frac{2}{L}}\begin{cases} 1 & \text{if } n \text{ is odd} \\ 0 & \text{if } n \text{ is even} \end{cases} \tag{8}$$

Since the n even modes are uncontrollable, we expect the beam to buckle in the second mode when $P \geq P_{cr,2}$.

Many control problems aimed at vibration suppression use piezoelectric materials as sensors in the feedback loop. However, due to charge leakage, piezoelectrics are not useful as sensors near 0 Hz as required in this application. Therefore, resistive strain gauge sensors are used as modeled in the next section.

Sensor Modeling

Modal states are estimated from strain gauge measurements at discrete locations. It is easy to see that observability of the modes of the system depends on the location of the sensors; a mode with its node at the location of a strain gauge is unobservable with that sensor. To reduce the number of sensors, modal control of flexible structures is usually based on the first

few modes of vibration. This is justified by the fact that higher vibrational modes are in general difficult to excite and have higher structural damping. However, the unmodeled dynamics can cause instability through what are known as control and observation spillover. It has been shown[1] that both control and observation spillover of unmodeled modes are necessary to cause instability in a closed-loop system.

The sensors are placed so that the second and third modes and their multiples are unobservable. Thus the first and fifth modes are the first two modes in a minimal realization of the system. We ignore higher order modes and discuss the associated spillover problems later. If a small amount of structural damping is present, all of the unobservable modes remain stable even in the presence of spillover. Similarly the dynamics of the even modes are not affected by the control, and hence they remain stable.

We model the sensors as follows. The bending moment at the location of a strain gauge, a distance x from the left end of the beam, is given by[5]

$$M_b = -E_b I_{eq} y''(x,t) = \sqrt{\frac{2}{L}} E_b I_{eq} \frac{\pi^2}{L^2} \sum_{n=1}^{n=\infty} n^2 \eta_n \sin\left(\frac{n\pi x}{L}\right) \quad (9)$$

where E_b is the Young's modulus of the beam material and I_{eq} is the equivalent moment of inertia of the composite piezo-beam segment based on beam material. The resulting strain in a strain gauge attached to one side of the beam is

$$\epsilon = \pm \frac{M_b\left[(t_b/2) + t_a + t_p\right]}{E_b I_{eq}} - \frac{P}{A_{eq} E_b} \quad (10)$$

where A_{eq} is the equivalent area based on beam material. The sign of the first term in Eq. (10) depends on which side of the beam the strain gauge is bonded to. Therefore, the output of a *differential* strain gauge is *independent of the load P* and is given by

$$v_s = 2\epsilon k_g = 2\sqrt{\frac{2}{L}} k_g \frac{\left[(t_b/2) + t_a + t_p\right]\pi^2}{L^2} \sum_{n=1}^{n=\infty}$$

$$\times n^2 \eta_n \sin\left(\frac{n\pi x}{L}\right) \triangleq k_s \sum_{n=1}^{n=\infty} n^2 \eta_n \sin\left(\frac{n\pi x}{L}\right) \quad (11)$$

where k_g is the strain gauge constant. If differential strain gauges are placed at $x = L/3$ and $x = 2L/3$, and the sum of their measurements is taken as the system output, we have

$$v_o \triangleq v_s\left(x = \frac{L}{3}\right) + v_s\left(x = \frac{2L}{3}\right)$$

$$= k_s \sum_{n=1}^{n=\infty} n^2 \eta_n \left(\sin\frac{n\pi}{3} + \sin\frac{2n\pi}{3}\right) \quad (12)$$

Controller Design

If n modal amplitudes and their rates are taken as the states of the system, the state-space representation of the $2n$ dimensional reduced order model with a state vector $\eta_r^T = [\eta_1 \quad \dot{\eta}_1 \quad \cdots \quad \eta_n \quad \dot{\eta}_n]$ becomes

$$\dot{\eta}_r = A_r \eta_r + B_r \nu \qquad \text{and} \qquad V_o = C_r \eta_r \quad (13)$$

where A_r is a $2n \times 2n$ block diagonal matrix, B_r is a $2n \times 1$ input matrix, and ν is input to the system. We assume that the derivative of the sensor output can be computed and define $V_o^T \triangleq [v_o \quad \dot{v}_o]$; and C_r is a $2 \times 2n$ output matrix. If only the first and the fifth modes are included in the reduced order model and a structural damping coefficient ζ is assumed, then

$$A_r = \begin{bmatrix} 0 & 1 & 0 & 0 \\ -\omega_1^2 & -2\zeta\omega_1 & 0 & 0 \\ 0 & 0 & 0 & 1 \\ 0 & 0 & -\omega_5^2 & -2\zeta\omega_5 \end{bmatrix}$$

$$B_r = \frac{-4\pi k^*}{\rho A L}\sqrt{\frac{2}{L}} \begin{bmatrix} 0 \\ 1 \\ 0 \\ 5 \end{bmatrix}, \qquad C_r^T = k_s \begin{bmatrix} \sqrt{3} & 0 \\ 0 & \sqrt{3} \\ -25\sqrt{3} & 0 \\ 0 & -25\sqrt{3} \end{bmatrix} \quad (14)$$

A controller is designed using standard linear quadratic regulator (LQR) design to minimize a cost functional of the form

$$J = \int_0^\infty (\alpha \eta_r^T Q \eta_r + \nu^T R \nu)\, dt \quad (15)$$

where Q and R are positive semidefinite and positive definite weighting matrices, respectively; and α is a scalar. The solution of the corresponding Riccati equation in this method gives an optimal state feedback solution of the form $\nu(t) = -K_r \eta_r(t)$, where K_r is a constant feedback gain matrix. The following parameters were used for simulation.

Beam properties:

$$b_b = 25.4 \text{ mm} \qquad t_b = 1 \text{ mm} \qquad E_b = 5 \text{ GPa}$$

$$\rho_b = 1000 \text{ kg/m}^3 \qquad L_b = 152.4 \text{ mm}$$

Piezoactuaor properties:

$$b_p = b_b \qquad t_p = 110\ \mu\text{m} \qquad E_p = 2 \text{ GPa} \qquad L_p = L_b$$

$$\rho_p = 1780 \text{ kg/m}^3 \qquad d_{31} = 23 \times 10^{-12} \text{ m/V}$$

A strain gauge constant $k_g = 0.01$ V/μ *strain* and structural damping coefficient $\zeta = 0.01$ are assumed. The thickness of the adhesive layer is neglected.

The optimal feedback gain matrix K_r is computed for $P = 4.1 P_{cr,1}$ using $Q = C_r^T C_r$, $R = 1$, and $\alpha = 0.05$. The first mode is stabilized at a load exceeding $P_{cr,2} = 4 P_{cr,1}$ and at this load the uncontrolled second mode is unstable (i.e., the beam is forced to buckle in the second mode). However, it remains to check that this controller stabilizes the system for loads less than $4.1 P_{cr,1}$. For the reduced order system this problem can be reduced to checking the roots of a fourth-degree interval polynomial with each coefficient varying monotonically when the load varies from $P = 0$ to $P = 4.1 P_{cr,1}$. The stability of the system under any fixed axial load $P \le 4.1 P_{cr,1}$ was verified by checking the stability of the two Kharitonov polynomials[6] associated with the fourth-order characteristic equation of the system. The same robustness result can also be obtained numerically using a root locus plot parameterized by P.

The resulting closed-loop response to nonzero initial conditions and the control input voltage to the actuators for the controlled model with a load of $P = 3.8 P_{cr,1}$ are shown in Fig. 3a. The effect of the unmodeled dynamics and methods of reducing this effect is the subject of the next section.

Numerical Evaluation of Spillover

To see the effect of spillover, the same gain K_r is used with an extended evaluation model containing modes 7 and 11 in addition to modes 1 and 5. To reduce the effect of spillover the

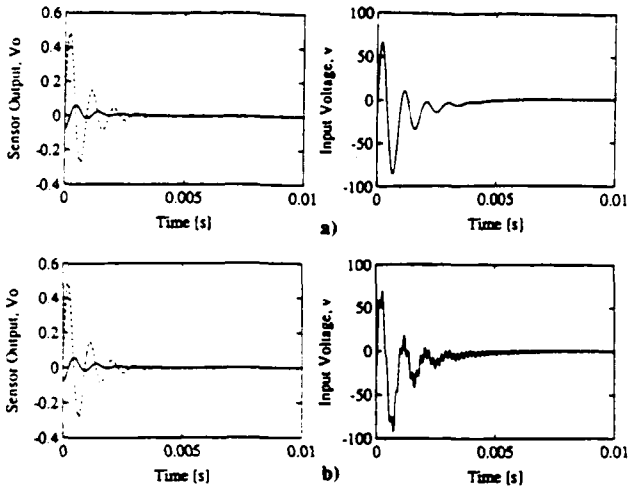

Fig. 3 Closed-loop response to nonzero initial deflection ($P = 3.8P_{cr,1}$): a) reduced order model and b) extended evaluation model.

controlled modes are reconstructed from the output of the extended model using a comb filter selecting modes 1 and 5 (an observer serves this purpose) and these estimates are used for feedback.

The resulting closed-loop response of the augmented system to nonzero initial conditions and the required input voltage to the actuators are shown in Fig. 3b. From Figs. 3a and 3b it can be seen, as expected, that there is no significant effect of the uncontrolled modes on the dynamics of the controlled modes.

Conclusion

In this Note we addressed the problem of buckling control using smart materials, a static instability of axially loaded members of a structure. We showed that the buckling of a flexible beam can be postponed beyond the first critical load by means of feedback using piezoelectric actuators and strain gauge sensors. It is observed that a controller design based on a fixed axial load P_{max} stabilizes the modeled modes for any $P \leq P_{max}$ and, therefore, is robust to slow load variations. Hence buckling in the first mode is inhibited, and the beam can support a load up to the second critical load. Actuator and sensor placement is discussed with regard to problems of spillover. Finally, spillover has not posed serious problems as we are able to design the controller, in the case of a beam, using a low-order model and verify stability for a high-order model.

Acknowledgment

Support from the Air Force Office of Scientific Research through Grant F49620251-C-0095 is gratefully acknowledged.

References

[1]Balas, M. J., "Active Control of Flexible Systems," *Journal of Optimization Theory and Applications*, Vol. 25, No. 3, 1978, pp. 415-436.

[2]Crawley, E. F., and De Luis, J., "Use of Piezoelectric Actuators as Elements of Intelligent Structures," *AIAA Journal*, Vol. 25, No. 10, 1987, pp. 1373-1385.

[3]Bailey, T., and Hubbard, J. E., "Distributed Piezoelectric-Polymer Active Vibration Control of a Cantilever Beam," *Journal of Guidance, Control, and Dynamics*, Vol. 8, No. 5, 1985, pp. 605-611.

[4]Fisher, S., "Application of Actuators to Control Beam Flexure in a Large Space Structure," *Journal of Guidance, Control, and Dynamics*, Vol. 12, No. 6, 1989, pp. 874-879.

[5]Timoshenko, S. P., and Gere, J. M., *Theory of Elastic Stability*, McGraw-Hill, New York, 1961.

[6]Minnichelli, R. J., Anagnost, J. J., and Desoer, C. A., "An Elementary Proof of Kharitonov's Stability Theorem with Extensions," *IEEE Transactions on Automatic Control*, Vol. AC-34, Sept. 1989, pp. 995-998.

JAPAN/USA Symposium on Flexible Automation — Volume 1
ASME 1992

STABLE INVERSION OF NONLINEAR NONMINIMUM PHASE SYSTEMS

Degang Chen
Department of Electrical Engineering
California Institute of Technology
Pasadena, California

Brad Paden
Department of Mechanical Engineering
University of California
Santa Barbara, California

Abstract

This paper addresses the inversion of a nonlinear system of the form $\dot{x}=f(x)+g(x)u$, $y=h(x)$ from the perspective of nonlinear geometric control theory. We use the notion of zero dynamics for obtaining stable, though noncausal, inverses for nonminimum phase systems. This contrasts with the causal inverses proposed by Hirschorn where unstable zero dynamics result in unbounded solutions to the inverse problem. Our results reduce to those of Hirschorn in the case of stable zero dynamics, however. A numerical example is described and the input generated using inversion is compared with that produced using recent results in nonlinear regulation.

Key Words: inversion, output tracking, nonlinear systems, nonminimum phase.

1. Introduction

Output tracking control for nonlinear systems is a challenging problem encountered in the control of articulated flexible space structures, flexible manipulators and elsewhere. There are two basic approaches to this problem. First, asymptotic tracking control using feedback and, second, inversion coupled with stabilization. The second approach offers the potential of exact output tracking without transients, but introduces the problem of inverting nonlinear systems with unstable zero dynamics. Motivated by new results in the control of articulated flexible structures [1, 2, 3], we address the second approach and solve the inversion problem for a class of nonlinear systems with unstable zero dynamics.

For the linear multivariable case, the asymptotic tracking problem was solved by [4, 5] and subsequently crystalized as the internal model principle [6]. The matrix equations defining an asymptotic tracking controller for linear systems were translated to nonlinear partial differential equations in the nonlinear case (see Isidori and Byrnes [7]). Although nonlinear PDE's are only numerically tractable for systems of low order, solutions for tracking periodic trajectories have developed based on Fourier series [8, 9]. Transient response remains a problem, however.

Transient behavior can be precisely controlled using stabilizing feedback together with feed-forward generated by an inverse system. For linear multivariable systems the inversion problem has been resolved to a large degree by Brockett and Mesarovic [10] and Silverman [11]. However, these inverses are all causal. Conditions for the invertibility of nonlinear real-analytic systems have been derived by Hirschorn [12, 13]. Here again, only causal inversion is addressed. Deeply rooted in these inversion results is the notion of relative degree which is important in our work also (although a clear exposition of relative degree for nonlinear systems is fairly recent [14]). Although stable inversion has not been studied in the framework of Brockett and Mesarovic and Hirschorn, approximate noncausal inversion has been used, for example, in linear quadratic optimal tracking [15], etc..

In this chapter we derive bounded inverses to nonlinear systems in an effort to find feed-forward signals for tracking controllers. For systems with unstable zero dynamics these are necessarily noncausal. These results are new for linear as well as nonlinear systems and were motivated by the successful inversion of a flexible manipulator model by Bayo *et al.* [2] using iterative linearization and solution with the Discrete Fourier Transform. Here we seek a geometric interpretation and time-domain solution of the inversion problem for the system

$$\dot{x}=f(x)+g(x)u$$

$$y=h(x).$$

We show that inversion is equivalent to solving a two-point boundary value problem in the general case of unstable zero dynamics. The stable and unstable manifolds of the zero dynamics play a central role in the ideas developed.

The remainder of the chapter is organized as follows. In the next section we define the class of reference trajectories under consideration and state the problem of stable inversion. Section 3 contains the main result and shows that the stable inversion problem reduces to a two-point boundary value problem of reduced-order ordinary differential equations. Section 4 contains an example of a fourth order nonlinear nonminimum-phase system; our stable inversion approach is worked out in detail and compared to the approximate inverse obtained from a nonlinear regulator. Simulation results demonstrate the value of our inverse for dead-beat output tracking.

2. Framework and Problem Statement

We consider a nonlinear system of the form

$$\dot{x} = f(x) + g(x)u \tag{1}$$

$$y = h(x), \tag{2}$$

defined on a neighborhood X of the origin of $\mathbb{R}^n$, with input $u \in \mathbb{R}^m$ and output $y \in \mathbb{R}^p$. The functions $f(x)$, $g_i(x)$ (the ith column of $g(x)$) $i = 1, 2, \cdots, m$ are smooth vector fields and $h_i(x)$ for $i = 1, 2, \cdots, p$ are smooth functions on X, with $f(0) = 0$ and $h(0) = 0$.

In the context of the above system pose the following

Stable Inversion Problem: Given a smooth reference output trajectory $y_d(t)$ with compact support, find a control input $u_d(t)$ and a state trajectory $x_d(t)$ such that

1) u_d and x_d satisfy the differential equation

$$\dot{x}_d(t) = f(x_d(t)) + g(x_d(t))u_d(t), \tag{3}$$

2) exact output tracking is achieved:

$$h(x_d(t)) = y_d(t), \tag{4}$$

3) u_d and x_d are bounded and

$$u_d(t) \to 0, \quad x_d(t) \to 0 \quad \text{as} \quad t \to \pm\infty. \tag{5}$$

Note that here we require $y_d(t)$ to have compact support, that is, there exist t_0 and t_f such that $y_d(t) = 0$ for all $t \le t_0$ and all $t \ge t_f$. However, the development in this chapter can be extended with little effort to cover desired trajectories whose first derivatives have compact support. The extension covers a large class of realistic trajectories.

We call x_d the desired state trajectory and u_d the nominal control input. These can be incorporated into a dead-beat controller by using the nominal control input as a feed-forward signal and $x - x_d$ as an error signal for feedback. The design of the feedback compensator has no general solution yet, but controllers for specific systems have been developed (see e.g. Paden *et al.* [1]).

In solving for the nominal trajectories x_d and u_d the concepts of stable and unstable manifolds of an equilibrium point arise naturally [16]. For the sake of completeness we review the definitions here. Let $z = 0$ be an equilibrium point of an autonomous system defined in a open neighborhood U of the origin of $\mathbb{R}^n$:

$$\dot{z} = f(z), \tag{6}$$

and $\phi_t(z)$ be the flow passing through z at $t = 0$. We define the (local) stable and unstable manifolds W^s, W^u as follows:

$$W^s = \{z \in U \mid \phi_t(z) \in U \ \forall t \ge 0, \phi_t(z) \to 0 \text{ as } t \to \infty\} \tag{7}$$

$$W^u = \{z \in U \mid \phi_t(z) \in U \ \forall t \ge 0, \phi_t(z) \to 0 \text{ as } t \to -\infty\} \tag{8}$$

The equilibrium point $z = 0$ is said to be hyperbolic if the Jacobian matrix Df of f at $z = 0$ has no eigenvalues on the $j\omega$ axis. Let n^s denote the number of eigenvalues of Df in the open left half complex plane, and n^u the number in the open right half plane. Stable and unstable manifolds W^s and W^u exist locally in the neighborhood of hyperbolic fixed point and have dimensions n^s and n^u respectively.

For convenience, we will use the following notation. Let $\mathbb{N} \triangleq \{0, 1, 2, \cdots\}$, $r = (r_1, r_2, \cdots, r_m)' \in \mathbb{N}^m$ and $y = [y_1(t), y_2(t), \cdots, y_m(t)]'$; $t \in \mathbb{R}$. Then we define $|r| \triangleq r_1 + r_2 + \cdots + r_m$ and write

$$y^{(r)} \triangleq \begin{bmatrix} \dfrac{d^{r_1} y_1}{dt^{r_1}} \\ \dfrac{d^{r_2} y_2}{dt^{r_2}} \\ \cdots \\ \dfrac{d^{r_m} y_m}{dt^{r_m}} \end{bmatrix}. \tag{9}$$

We will use the bold number **1** to denote the vector $(1, 1, \cdots, 1)'$ so that

$$y^{(1)} = \dot{y} = \left(\frac{dy_1}{dt}, \frac{dy_2}{dt}, \cdots, \frac{dy_m}{dt}\right)'.$$

If $y: \mathbb{R}^n \to \mathbb{R}^m$ and $f: \mathbb{R}^n \to \mathbb{R}^n$, we define

$$L_f^r y \triangleq \begin{bmatrix} L_f^{r_1} y_1 \\ L_f^{r_2} y_2 \\ \cdots \\ L_f^{r_m} y_m \end{bmatrix}. \tag{10}$$

3. Inversion of Partially Linearizable Systems

Consider a nonlinear system of the form (1) and (2) with the same number m of inputs and outputs which we expand in the following form:

$$\dot{x} = f(x) + \sum_{i=1}^{m} g_i(x) u_i$$

$$y_1 = h_1(x)$$

$$\cdots$$

$$y_m = h_m(x)$$

We assume that the system has well-defined relative degree $r = (r_1, r_2, \cdots, r_m)$ at the equilibrium point 0, that is, (i) for all $1 \le j \le m$, for all $1 \le i \le m$, for all $k < r_i - 1$, and for all x in a neighborhood of the origin,

$$L_{g_j} L_f^k h_i(x) = 0, \tag{11}$$

(ii) the $m \times m$ matrix

$$\beta(x) = \begin{bmatrix} L_{g_1} L_f^{r_1 - 1} h_1(x) & \cdots & L_{g_m} L_f^{r_1 - 1} h_1(x) \\ L_{g_1} L_f^{r_2 - 1} h_2(x) & \cdots & L_{g_m} L_f^{r_2 - 1} h_2(x) \\ \cdots & \cdots & \cdots \\ L_{g_1} L_f^{r_m - 1} h_m(x) & \cdots & L_{g_m} L_f^{r_m - 1} h_m(x) \end{bmatrix} \tag{12}$$

is nonsingular in a neighborhood of the origin.

Under this assumption, the system can be partially linearized. To do this, we differentiate y_i until at least one u_j appears explicitly. This will happen at exactly the r_ith derivative of y_i due to (11). Define $\xi_k^i = y_i^{(k-1)}$ for $i = 1, \cdots, m$ and

$k = 1, \cdots, r_i$, and denote

$$\xi = (\xi_1^1, \xi_2^1, \cdots, \xi_{r_1}^1, \xi_1^2, \cdots, \xi_{r_2}^2, \cdots, \xi_{r_m}^m)'$$

$$= (y_1, \dot{y}_1, \cdots, y_1^{(r_1-1)}, y_2, \cdots, y_2^{(r_2-1)}, \cdots, y_m^{(r_m-1)})'. \quad (13)$$

Choose η, an $n - |r|$ dimensional function on $\mathbb{R}^n$ such that $(\xi', \eta')' = \psi(x)$ forms a change of coordinates with $\psi(0) = 0$ [14]. In this new coordinate system, the system dynamics of equation (1) becomes

$$\begin{cases} \dot{\xi}_1^i = \xi_2^i \\ \cdots \\ \dot{\xi}_{r_i-1}^i = \xi_{r_i}^i & \text{for } i = 1, \cdots, m, \\ \dot{\xi}_{r_i}^i = \alpha_i(\xi, \eta) + \beta_i(\xi, \eta)u \end{cases} \quad (14)$$

$$\dot{\eta} = q_1(\xi, \eta) + q_2(\xi, \eta)u,$$

which, in a more compact form, is equivalent to

$$y^{(r)} = \alpha(\xi, \eta) + \beta(\xi, \eta)u, \quad (15)$$

$$\dot{\eta} = q_1(\xi, \eta) + q_2(\xi, \eta)u, \quad (16)$$

where

$$y = (y_1, y_2, \cdots, y_m)',$$

$$u = (u_1, u_2, \cdots, u_m)',$$

$$\alpha(\xi, \eta) = L_f^r h(\psi^{-1}(\xi, \eta)), \quad (17)$$

$$\beta(\xi, \eta) = L_{g_1} L_f^{r-1} h(\psi^{-1}(\xi, \eta)). \quad (18)$$

Here β is actually the same $\beta(x)$ matrix defined in the equation (12), $\alpha(0, 0) = 0$ since $f(0) = 0$, and

$$h(x) = [h_1(x), h_2(x), \cdots, h_m(x)]',$$

$$g(x) = [g_1(x), g_2(x), \cdots, g_m(x)].$$

Since by the relative degree assumption, $\beta(\xi, \eta)$ is nonsingular, the following feedback control law

$$u \triangleq [\beta(\xi, \eta)]^{-1}[v - \alpha(\xi, \eta)] \quad (19)$$

is well defined and partially linearizes the system such that the input-output relationship is given by a chain of integrators:

$$y^{(r)} = v \quad (20)$$

where $v \in \mathbb{R}^m$ is the new control input. Assume both y and y_d start from rest and choose

$$v = y_d^{(r)}. \quad (21)$$

Then immediately we have

$$\xi = \xi_d$$

$$\triangleq (y_{d1}, \dot{y}_{d1}, \cdots, y_{d1}^{(r_1-1)}, y_{d2}, \cdots, y_{d2}^{(r_2-1)}, \cdots, y_{dm}^{(r_m-1)})' \quad (22)$$

and equation (16) becomes, which we call the *reference dynamics*, or the zero dynamics driven by the reference output trajectory,

$$\dot{\eta} = p(y_d, \dot{\xi}_d, \eta) \quad (23)$$

where

$$p(y_d, \dot{\xi}_d, \eta)$$

$$\triangleq q_1(\xi_d, \eta) + q_2(\xi_d, \eta)[\beta(\xi_d, \eta)]^{-1}[y_d^{(r)} - \alpha(\xi_d, \eta)]. \quad (24)$$

It is clear now that an integration of the reference dynamics gives rise to a trajectory of the original state through the inverse coordinate transformation $x = \Psi^{-1}\begin{pmatrix}\xi\\ \eta\end{pmatrix}$ and an input trajectory by equation (19). Now the question is how to integrate the reference dynamics to generate a bounded input solving the stable inversion problem, since the reference dynamics may be unstable in both positive and negative time directions in general.

For reference trajectories with compact support, the reference dynamics become autonomous zero dynamics for t outside the compact interval $[t_0, t_f]$. Assuming that $\eta = 0$ is a hyperbolic equilibrium point of the autonomous zero dynamics, then there exist stable and unstable manifolds W^s and W^u. Locally W^u can be defined by an equation $B^u(\eta) = 0$ and, similarly, W^s can be defined by $B^s(\eta) = 0$. The following theorem is our main result.

Theorem: The stable inversion problem has a solution if and only if the following two-point boundary value problem has a solution:

$$\dot{\eta} = p(y_d, \dot{\xi}_d, \eta), \quad (23)$$

subject to

$$\begin{aligned} B^u(\eta(t_0)) &= 0, \\ B^s(\eta(t_f)) &= 0. \end{aligned} \quad (25)$$

Proof: (necessity) Suppose $x_d(t)$ and $u_d(t)$ solve the stable inversion problem. Then $x_d(t)$ and $u_d(t)$ satisfy the differential equation (1). Let $(\xi', \eta')' = \psi(x_d)$. Then ξ and η satisfy (1) or equivalently (14) with u substituted by u_d. Besides, since $y = h(x_d) = y_d$ by assumption, $\xi = \xi_d$ and $y^{(r)} = y_d^{(r)}$. Therefore by equation (15)

$$y_d^{(r)} = \alpha(\xi_d, \eta) + \beta(\xi_d, \eta)u_d,$$

which yields

$$u_d = [\beta(\xi_d, \eta)]^{-1}(y_d^{(r)} - \alpha(\xi_d, \eta)).$$

Substituting this into the η dynamics of equation (16) and comparing the resulting right-hand side with the definition of $p(y_d, \dot{\xi}_d, \eta)$ in equation (24), we recognize that η satisfy equation (23).

Now we only need to show that η also satisfies the boundary condition. This is easy. Since by assumption, $x_d(t) \to 0$ as $t \to -\infty$ and $\psi(0) = 0$, thus $\eta(t) \to 0$ as $t \to -\infty$ also. By definition of the unstable manifold, $\eta(t) \in W^u$ for all $t \le t_0$. Therefore, $B^u(\eta(t_0)) = 0$. Similar arguments show that $B^s(\eta(t_f)) = 0$.

(sufficiency) Suppose η_d solves the above two point boundary value problem. Then, η_d is bounded, and $\eta_d(t) \to 0$ as

$t \to \infty$ since $\eta_d(t_f) \in W^s$ and $\eta_d(t) \to 0$ as $t \to -\infty$ since $\eta_d(t_0) \in W^u$. Also, $\xi_d = 0$ for $t \le t_0$ and for $t \ge t_f$.

Let

$$x_d = \psi^{-1}(\xi_d, \eta_d),$$

$$u_d = [\beta(\zeta_d, \eta_d)]^{-1}(y_d^{(r)} - \alpha(\xi_d, \eta_d)).$$

Then, x_d and u_d are bounded, and $x_d(t), u_d(t) \to 0$ as $t \to \infty$ or $t \to -\infty$, since $\psi^{-1}(0, 0) = 0$ and $\alpha(0, 0) = 0$. And by the definition of ξ, $y = y_d$.

This completes the proof.

A geometric interpretation of the $x_d(t)$ evolution is shown in Figure 1. The noncausal part of the nominal control drives the internal states of the system along the unstable manifold of the zero dynamics manifold to a particular initial condition $x_d(t_0)$ while maintaining zero system output. This initial condition guarantees two things: 1) the desired reference output trajectory is easily reproduced with bounded input and states; 2) the internal states land on the stable manifold of the zero dynamics manifold at the end of output tracking. With this nice final condition, the internal states will converge to zero along the stable manifold without affecting the output. This geometrical picture is shown in Figure 1 where for clarity we showed a case of output slewing so that the t_0 and t_f zero dynamics manifolds are separate.

Here we see that the stable inversion problem is transformed into a two-point boundary value problem for which the number of equations is reduced. However, it is still a nontrivial numerical problem. The difficulty arises because of the instability of the reference dynamics in both positive and negative time. Existing approaches, for example the shooting method, do not perform well numerically for unstable systems.

In the case of minimum-phase systems, the reference dynamics is asymptotically stable in the forward time. The size of the stable manifold is the same as that of the zero dynamics manifold and the unstable manifold reduces to the origin only. Therefore, the boundary condition $B^u(\eta(t_0)) = 0$, reduces to $\eta(t_0) = 0$ and $B^s(\eta(t_f)) = 0$ imposes no extra constraints. And the two-point boundary value problem reduces to a simple initial condition problem with an asymptotically stable dynamics, and can be easily integrated in the forward time. This is Hirschorn's approach. Similarly, if the zero dynamics is completely unstable, the two-point boundary value problem reduces to a final-value problem and can be easily integrated in backward time.

Another simple situation is when the stable and unstable part of the reference dynamics can be decoupled by change of coordinates. This happens when the reference dynamics is a linear time-invariant system driven by the reference output and its derivatives. In such cases, we can easily integrate the stable part in forward time and the unstable part in backward time.

4. An Example

In this section, both the inversion and regulator approaches will be applied to a simple nonlinear nonminimum-phase system. The example system is selected such that both the integration of the reference dynamics and the solution to the nonlinear partial differential equations are manageable. The performance of the two approaches is compared.

Now consider a slightly nonlinear single-input single-output system described by the following equations:

$$\begin{bmatrix} \dot{x}_1 \\ \dot{x}_2 \\ \dot{x}_3 \\ \dot{x}_4 \end{bmatrix} = \begin{bmatrix} -x_1 + x_2 \\ -3x_2 + x_1^3 \\ x_1 - 2x_3 \\ -x_4 + x_3^2 \end{bmatrix} + \begin{bmatrix} 0 \\ 2 + \sin^2 x_4 \\ 0 \\ 0 \end{bmatrix} u,$$

$$y = x_1 - 3x_3.$$

The reference output trajectory is given by:

$$y_d = \begin{cases} 2(1 - \cos(t)) & t \in [0, 2\pi], \\ 0 & \text{otherwise}, \end{cases}$$

and is depicted in Figure 2 with a dotted curve.

First, let us consider the regulator approach. The reference signal can be exactly generated by the following linear time-invariant exosystem:

$$\dot{w}_1 = w_2,$$

$$\dot{w}_2 = -w_1,$$

$$\dot{w}_3 = 0,$$

$$y_d = w_3 - w_1.$$

The initial conditions are set and reset as follows:

$$w_1(-\infty) = w_2(-\infty) = w_3(-\infty) = 0;$$

$$w_1(0) = w_3(0) = 2, \quad w_2(0) = 0;$$

$$w_1(2\pi) = w_2(2\pi) = w_3(2\pi) = 0.$$

The zero error manifold, $x = x(w)$ and $u = u(w)$, is obtained by solving a system of nonlinear partial differential equations, which is in general extremely difficult if not impossible. For this example, the partial differential equations are as follows:

$$\frac{\partial x_1(w)}{\partial w_1} w_2 - \frac{\partial x_1(w)}{\partial w_2} w_1 = -x_1(w) + x_2(w),$$

$$\frac{\partial x_2}{\partial w_1} w_2 - \frac{\partial x_2}{\partial w_2} w_1 = -3x_2(w) + x_1^3(w) + (2 + \sin^2 x_4(w))u(w),$$

$$\frac{\partial x_3(w)}{\partial w_1} w_2 - \frac{\partial x_3(w)}{\partial w_2} w_1 = x_1(w) - 2x_3(w),$$

$$\frac{\partial x_4(w)}{\partial w_1} w_2 - \frac{\partial x_4(w)}{\partial w_2} w_1 = -x_4(w) + x_3^2(w),$$

subject to

$$x_1(w) - 3x_3(w) = w_3 - w_1.$$

Fortunately, we are able to get a closed-form solution as follows:

$$x_1(w) = -\frac{5}{2}w_1 - \frac{3}{2}w_2 - 2w_3,$$

$$x_2(w) = -7w_1 - 4w_4 - 2w_3,$$

$$x_3(w) = -\frac{1}{2}(w_1+w_2) - w_3,$$

$$x_4(w) = \frac{7}{20}w_1^2 + \frac{3}{20}w_2^2 + \frac{1}{10}w_1w_2 - w_1w_3 + w_3^2,$$

$$u(w) = (-17w_1 - 7w_2 + 18w_3) / (2 + \sin^2 x_4(w)).$$

Now note that with $u = 0$, the forward system is locally asymptotically stable since the Jacobian matrix of $f(x)$ at $x = 0$ is clearly

$$\begin{bmatrix} -1 & 1 & 0 & 0 \\ 0 & -3 & 0 & 0 \\ 1 & 0 & -2 & 0 \\ 0 & 0 & 0 & -1 \end{bmatrix}$$

and has all its eigenvalues negative. Therefore, for simplicity, we can choose the feedback gain to be zero.

This completes the regulator design. The simulation results are shown in Figure 2 to 4. Figure 2 compares the desired and actual output trajectory, Figure 3 shows the state trajectories solving the partial differential equations, and Figure 4 the actual state trajectories. Note that the output generated by the regulator does asymptotically track the reference trajectory as predicted by theory. This is evidenced by the segments from $t = 4$ to $t = 2\pi$ and $t > 9$. However, there are substantial transient tracking error both when getting onto the zero error manifold and getting off the manifold. This phenomenon is not a special case of this example, but rather generic.

Next, let us consider the stable inversion approach. To partially linearize the system, we differentiate the output y to yield

$$\dot{y} = \dot{x}_1 - 3\dot{x}_3 = -4x_1 + x_2 + 6x_3.$$

Since the control u does not appear explicitly, we differentiate $\dot{y}$ again to yield

$$\ddot{y} = -4(-x_1 + x_2) - 3x_2 + x_1^3 + (2 + \sin^2 x_4)u + 6(x_1 - 2x_3)$$

$$= (10x_1 - 7x_2 - 12x_3 + x_1^3) + (2 + \sin^2 x_4)u \triangleq \alpha(x) + \beta(x)u.$$

Now not only does u appear, its coefficient $\beta(x) \neq 0$ for all x. Hence, we can set

$$u(x) = \frac{1}{\beta(x)}(\ddot{y}_d - \alpha(x)) \tag{26}$$

and introduce a change of coordinates:

$$\begin{bmatrix} y \\ \dot{y} \\ \eta_1 \\ \eta_2 \end{bmatrix} = \begin{bmatrix} y \\ \dot{y} \\ x_3 \\ x_4 \end{bmatrix} = \begin{bmatrix} 1 & 0 & -3 & 0 \\ -4 & 1 & 6 & 0 \\ 0 & 0 & 1 & 0 \\ 0 & 0 & 0 & 1 \end{bmatrix} \begin{bmatrix} x_1 \\ x_2 \\ x_3 \\ x_4 \end{bmatrix}.$$

The inverse transformation is given by:

$$\begin{bmatrix} x_1 \\ x_2 \\ x_3 \\ x_4 \end{bmatrix} = \begin{bmatrix} 1 & 0 & 3 & 0 \\ 4 & 1 & 6 & 0 \\ 0 & 0 & 1 & 0 \\ 0 & 0 & 0 & 1 \end{bmatrix} \begin{bmatrix} y \\ \dot{y} \\ \eta_1 \\ \eta_2 \end{bmatrix}. \tag{27}$$

Using the feedback of equation (26), the system in the new coordinates becomes:

$$\ddot{y} = \ddot{y}_d, \tag{28}$$

$$\dot{\eta}_1 = \eta_1 + y,$$

$$\dot{\eta}_2 = -\eta_2 + \eta_1^2.$$

Since we assume partially (the output part) correct initial conditions, equation (28) leads to

$$y = y_d.$$

Then the above η dynamics with y substituted with y_d characterize our reference dynamics. And for t outside $[t_0, t_f]$, $y_d = 0$, giving the zero dynamics:

$$\dot{\eta}_1 = \eta_1,$$

$$\dot{\eta}_2 = -\eta_2 + \eta_1^2.$$

This is an autonomous system. It is clearly hyperbolic, since its first order approximation has eigenvalues 1 and -1. Therefore there exist stable and unstable manifolds. The stable manifold can be easily seen to be characterized by

$$\eta_1 = 0.$$

And the unstable manifold is characterized by

$$\eta_2 = \frac{\eta_1^2}{3}. \tag{29}$$

Therefore the two-point boundary value problem is given by:

$$\dot{\eta}_1 = \eta_1 + y_d, \qquad \eta_1(t_f) = 0,$$

$$\dot{\eta}_2 = -\eta_2 + \eta_1^2, \qquad \eta_2(t_0) = \frac{\eta_1^2(t_0)}{3}.$$

This particular example is in a triangular form and can be easily solved. For the first equation is antistable with a final value condition, it can be easily integrated backward in time to give η_1. The integration is continued into the time $t < t_0$ and stopped when $|\eta_1|$ is sufficiently small. Once we have η_1, the second equation is a stable system with an initial condition and driven by a known input η_1^2. Integration forward in time is no problem either. For the part of η_2 before t_0, we use the simple algebraic relation of equation (29) since the trajectory remains on the unstable manifold.

Once η_1 and η_2 are calculated, the desired trajectory of the original states can be obtained using the inverse coordinate transformation in equation (27) with $y = y_d$ and $\dot{y} = \dot{y}_d$. Then the nominal control input is calculated according to the linearizing feedback law in equation (26). Note that the η's are

nonzero for $t < t_0$, the u thus obtained is also nonzero for $t < t_0$, corresponding to a noncausal input.

Again, since the forward system is asymptotically stable, we choose zero feedback gain for simplicity. The simulation results are shown in Figures 5 to 7. Figure 5 compares the desired and actual output trajectories, Figure 6 shows the nominal state trajectories by inversion, and Figure 7 the actual state trajectories generated by the truncated nominal input. Note that an almost perfect output tracking is obtained using a mild control effort. A stabilizing feedback loop is expected to improve these small errors.

5. Conclusion

The primary contribution of this chapter is the connection made between zero dynamics and stable inversion of nonlinear systems. These results, in conjunction with Hirschorn's show that there are multiple inverses for nonminimum-phase nonlinear systems – bounded, noncausal solutions produced with our method and unbounded, causal solution produced using Hirschorn's technique. These inversion techniques are fundamental to nonlinear tracking controllers which use feed-forward in conjunction with stabilizing feedback. Future work will include conditions for existence of solutions to the two-point boundary-value problems and global behavior of inverses.

References

1. B. Paden, D. Chen, R. Ledesma, and E. Bayo, "Exponentially Stable Tracking Control for Multi-Link Flexible Manipulators," *to appear in ASME J Dynamics, Measurement and Control.*
2. E. Bayo, M.A. Serna, P. Papadopoulos, and J.R. Stubbe, "Inverse Dynamics and Kinematics of Multi-Link Elastic Robots: An Iterative Frequency-Domain Approach," *Int. J. Robotics Research*, vol. 8(6), pp. 49-62, 1989.
3. D.S. Kwon and W.J. Book, "An Inverse Dynamics Method Yielding Flexible Manipulator State Trajectory," *Proc. 1990 American Control Conference*, pp. 186-193, San Diego, 1990.
4. B.A. Francis, "The Linear Multivariable Regulator Problem," *SIAM J. Control & Optimization*, vol. 15, pp. 486-505, 1977.
5. E.J. Davison, "The Robust Control of a Servomechanism Problem for Linear Time-Invariant Multivariable Systems," *IEEE Trans. on Automatic Control*, vol. AC-21(1), pp. 25-34, 1976.
6. B.A. Francis and W.M. Wonham, "The Internal Model Principle for Linear Multivariable Regulators," *Applied Mathematics & Optimization*, vol. 2(2), pp. 170-194, 1975.
7. A. Isidori and C.I. Byrnes, "Output Regulation of Nonlinear Systems," *IEEE Trans. on Automatic Control*, vol. AC-35(2), pp. 131-140, 1990.
8. P. Lucibello and M.D. Di Benedetto, "Output Tracking for a Nonlinear Flexible Arm," *submitted to J. of ASME.*
9. A. De Luca, L. Lanari, and G. Ulivi, "Output Regulation of a Flexible Robot Arm," *9th Int. Conference on Analysis & Optimization of Systems INRIA*, 1990.
10. R.W. Brockett and M.D. Mesarovic, "The Reproducibility of Multivariable Systems," *J. Mathematical Analysis and Applications*, vol. 11, pp. 548-563, 1965.
11. L.M. Silverman, "Inversion of Multivariable Linear Systems," *IEEE Trans. on Automatic Control*, vol. AC-14(3), pp. 270-276, 1969.
12. R.M. Hirschorn, "Invertibility of Nonlinear Control Systems," *SIAM J. Control & Optimization*, vol. 17(2), pp. 289-297, 1979.
13. R.M. Hirschorn, "Invertibility of Multivariable Nonlinear Control Systems," *IEEE Trans. on Automatic Control*, vol. AC-24(6), pp. 855-865, 1979.
14. A. Isidori, *Nonlinear Control Systems: An Introduction*, Springer-Verlag, New York, 1989.
15. B.D.O. Anderson and J.B. Moor, *Optimal Control - Linear Quadratic Methods*, Prentice-Hall, Englewood Cliffs, New Jersey, 1990.
16. J. Guckenheimer and P. Holmes, *Nonlinear Oscillations, Dynamical Systems, and Bifurcations of Vector Fields*, Springer-Verlag, New York, 1983.

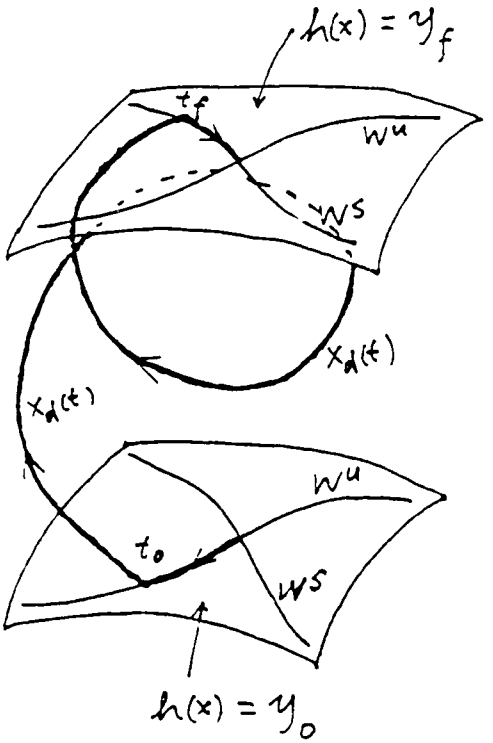

Figure 1.

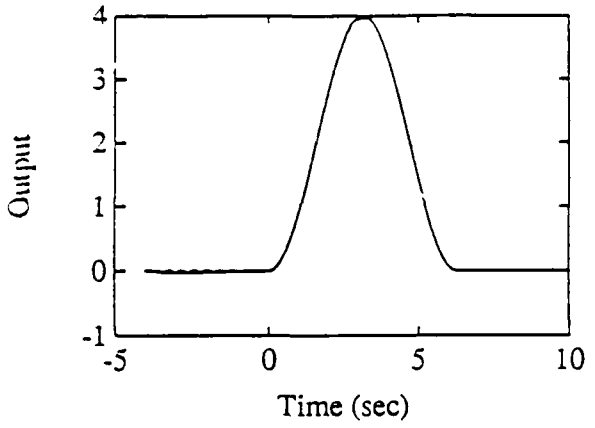

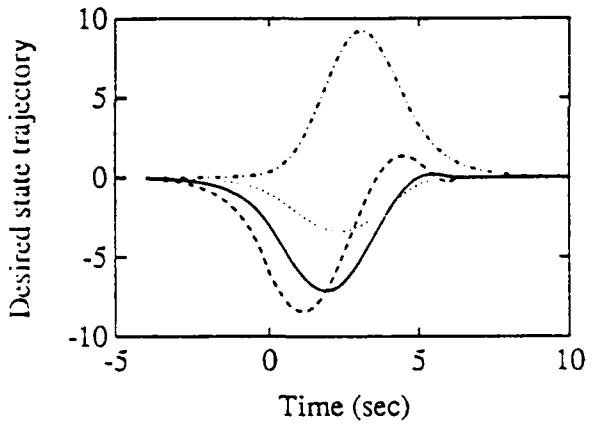

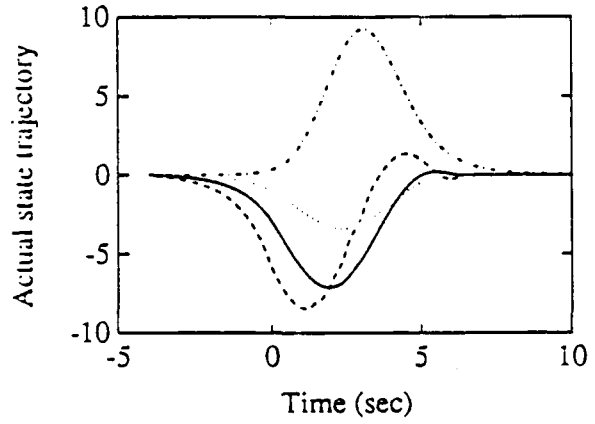

Figure 2. Desired and actual output in inversion approach

Figure 3. Desired state trajectory in inversion approach

Figure 4. Actual state trajectory in inversion approach

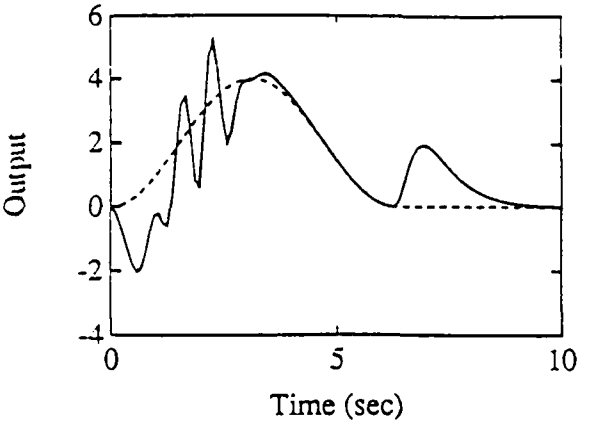

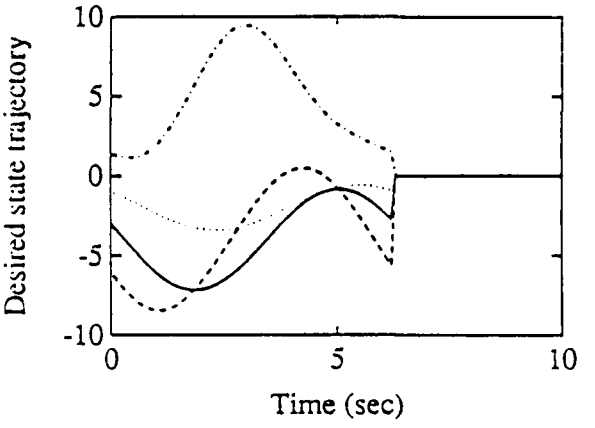

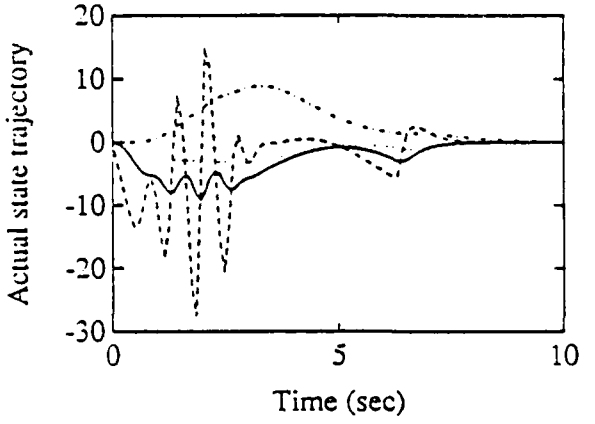

Figure 5. Desired and actual output in regulator approach

Figure 6. Desired state trajectory in regulator approach

Figure 7. Actual state trajectory in regulator approach

DSC-Vol. 43

ADVANCES IN ROBUST AND NONLINEAR CONTROL SYSTEMS

PRESENTED AT
THE WINTER ANNUAL MEETING OF
THE AMERICAN SOCIETY OF MECHANICAL ENGINEERS
ANAHEIM, CALIFORNIA
NOVEMBER 8–13, 1992

SPONSORED BY
THE DYNAMIC SYSTEMS AND CONTROL DIVISION, ASME

EDITED BY
EDUARDO A. MISAWA
OKLAHOMA STATE UNIVERSITY

THE AMERICAN SOCIETY OF MECHANICAL ENGINEERS
345 East 47th Street □□ United Engineering Center □□ New York, N.Y. 10017

DSC-Vol. 43, Advances in Robust and Nonlinear Control Systems
ASME 1992

A STATE-SPACE CONDITION FOR THE INVERTIBILITY OF NONLINEAR NONMINIMUM-PHASE SYSTEMS

Brad Paden and Degang Chen
Department of Mechanical and Environmental Engineering
University of California
Santa Barbara, California

Abstract

This paper addresses the inversion of nonlinear systems of the form $\dot{x} = f(x) + g(x)u$; $y = h(x)$ from the perspective of nonlinear geometric control theory. We use the notion of zero dynamics for obtaining stable, though noncausal, inverses for nonminimum phase systems. This contrasts with the causal inverses proposed by Hirschorn where unstable zero dynamics result in unbounded solutions to the inverse problem. We show that hyperbolicity of the zero dynamics equilibrium guarantees invertibility.

1. Introduction

Inversion of nonlinear nonminimum-phase systems is a challenging problem encountered in the control of articulated flexible space structures, flexible manipulators and elsewhere. A nominal input, derived by inversion, which produces a desired output is an excellent feedforward control which can then be stabilized with feedback. Motivated by [1] results in the control of articulated flexible structures [1] we explore the inversion approach to nonlinear systems with unstable zero dynamics.

An alternative approach is to apply the nonlinear regulator theory and solve the associated partial differential equations. For the linear multivariable case, the asymptotic tracking problem was solved by [2] and subsequently crystalized the internal model principle. The matrix equations defining a asymptotic tracking controller for linear systems are easily solvable but translate to nonlinear partial differential equations in the nonlinear case which pose severe computational problems (see Isidori and Byrnes [3]). This was avoided in flexible robot control by tracking periodic trajectories where Fourier series methods have been applied [4]. The class of periodic trajectories is poorly suited to such systems however.

Transient behavior is an issue in tracking control in contrast to inversion approaches where deadbeat control can be acheived. For linear multivariable systems the inversion problem has been resolved to a large degree by Mesarovic and Brockett [5] and Silverman [6]. However, these inverses are all causal. Conditions for the invertibility of nonlinear real-analytic systems have been derived by Hirshorn [7]. Here again, only causal inversion is addressed. Deeply rooted in these inversion results is the notion of relative degree and is important in our work also (although a clear exposition of relative degree for nonlinear systems is fairly recent[8]).

In this paper we prove a connection between the hyperbolicity of zero dynamics and the invertibility of nonlinear nonminimum phase systems. For systems with unstable zero dynamics these inverses are necessarily noncausal.

The remainder of the paper is organized as follows. In section 2 we review some concepts from nonlinear geometric control theory and formulate our inversion problem. Section 3 contains the main result and shows that invertibilty can be tested by examining the zero-dynamics of the system in question. Our conclusions are made in section 5. The appendix contains a key technical result on the Frechet differentiability of solutions of ordinary differential equations with respect to a control.

2. Framework and Problem Statement

We consider a nonlinear system of the form

$$\dot{x} = f(x) + g(x)u \tag{2.1a}$$

$$y = h(x), \tag{2.1b}$$

defined on a neighborhood X of the origin of R^n, with input $u \in R^m$ and output $y \in R^p$. $f(x)$, $g_i(x)$ (the ith column of $g(x)$) $i=1, 2, \cdots, m$ are smooth vector fields and $h_i(x)$ for $i=1, 2, \cdots, p$ are smooth functions on X, with $f(0)=0$ and $h(0)=0$.

In the context of the above system pose the following

Stable Inversion Problem: Given a smooth "desired" output trajectory $y_d(t)$ with compact support $[0, T]$, find a corresponding control input $u_d(t)$ and a state trajectory $x_d(t)$ such that

1) u_d and x_d satisfy the differential equation

$$\dot{x}_d(t) = f(x_d(t)) + g(x_d(t))u_d(t) \tag{2.2}$$

2) exact output tracking is achieved:

$$h(x_d(t)) = y_d(t), \tag{2.3}$$

3) u_d and x_d are bounded and

$$u_d(t) \to 0, \quad x_d(t) \to 0 \quad \text{as} \quad t \to \pm\infty. \tag{2.4}$$

We call x_d the desired state trajectory and u_d the desired control corresponding to the desired output trajectory. These can be incorporated into a dead-beat controller by using u_d as a feedforward signal and $x - x_d$ as an error signal for feedback. The design of the feedback compensator has no general solution, but controllers for specific systems have been developed (see e.g. Paden et al. [9]).

In solving for the trajectories x_d and u_d the concepts of stable and unstable manifolds of an equilibrium point arise naturally. For the sake of completeness we review the definitions here. Let $z=0$ be an equilibrium point of an autonomous system defined in a open neighborhood U of the origin of R^n:

$$\dot{z} = f(z), \tag{2.5}$$

and $\phi_t(z)$ be the solution passing through z at $t=0$. We define the (local) stable and unstable manifolds W^s, W^u as follows:

$$W^s = \{z \in U \mid \phi_t(z) \to 0 \text{ as } t \to \infty, \text{ and } \phi_t(z) \in U \ \forall\ t \geq 0\}$$

$$W^u = \{z \in U \mid \phi_t(z) \to 0 \text{ as } t \to -\infty, \text{ and } \phi_t(z) \in U \ \forall\ t \leq 0\}.$$

The equilibrium point $z=0$ is said to be hyperbolic if the Jacobian matrix Df of f at $z=0$ has no eigenvalues on the $j\omega$ axis. Let n^s denote the number of eigenvalues of Df in the open left half complex plane, and n^u the number in the open right half plane. In this case, stable and unstable manifolds W^s and W^u exist locally and have dimensions n^s and n^u respectively.

For convenience, we will use the following notation: $N=0, 1, 2, \cdots$, $r=(r_1, r_2, \cdots, r_m)^T \in N^m$ and $y=(y_1(t), y_2(t), \cdots, y_m(t))^T$; $t \in R$. Also define

$$y^{(r)} := \begin{bmatrix} \frac{d^{r_1} y_1}{dt^{r_1}} \\ \frac{d^{r_2} y_2}{dt^{r_2}} \\ \cdots \\ \frac{d^{r_m} y_m}{dt^{r_m}} \end{bmatrix}. \tag{2.6}$$

We will use the bold number $\mathbf{1}$ to denote the vector $(1, 1, \cdots, 1)^T$ so that

$$y^{(1)} = \dot{y} = \left(\frac{dy_1}{dt}, \frac{dy_2}{dt}, \cdots, \frac{dy_m}{dt}\right)^T.$$

If $y: R^n \to R^m$ and $f: R^n \to R^n$, we define $L_f y = \frac{dy}{dx} f(x)$, $L_f^k y = L_f(L_f^{k-1} y)$ and

$$Lfy := \begin{bmatrix} L_f^{r_1} y_1 \\ L_f^{r_2} y_2 \\ \cdots \\ L_f^{r_m} y_m \end{bmatrix}. \tag{2.7}$$

3. Inversion of Partially Linearizable Systems

Consider a nonlinear system of the form (2.1) with the same number m of inputs and outputs which we expand in the following form:

$$\dot{x} = f(x) + \sum_{i=1}^{m} g_i(x) u_i \tag{3.1a}$$

$$y_1 = h_1(x)$$

$$\cdots$$

$$y_m = h_m(x) \tag{3.1b}$$

We assume that the system has well-defined relative degree $r=(r_1, r_2, \cdots, r_m)$ at the equilibrium point 0, that is,

(i) for all $1 \leq j \leq m$, for all $1 \leq i \leq m$, for all $k < r_i - 1$, and for all x in a neighborhood of the origin,

$$L_{g_j} L_f^k h_i(x) = 0, \tag{3.2}$$

(ii) the $m \times m$ matrix

$$\beta(x) = \begin{bmatrix} L_{g_1} L_f^{r_1 - 1} h_1(x) & \cdots & L_{g_m} L_f^{r_1 - 1} h_1(x) \\ L_{g_1} L_f^{r_2 - 1} h_2(x) & \cdots & L_{g_m} L_f^{r_2 - 1} h_2(x) \\ \cdots & \cdots & \cdots \\ L_{g_1} L_f^{r_m - 1} h_m(x) & \cdots & L_{g_m} L_f^{r_m - 1} h_m(x) \end{bmatrix} \tag{3.2}$$

is nonsingular in a neighborhood of the origin.

Under this assumption, the system can be partially linearized. To do this, we differentiate y_i until at least one u_j appear algebraically. This will happen at exactly the r_ith derivative of y_i. Define $\xi_k^i = y_i^{(k-1)}$ for $i=1, \cdots, m$ and $k=1, \cdots, r_i$, and denote

$$\xi = (\xi_1^1, \xi_2^1, \cdots, \xi_{r_1}^1, \xi_1^2, \cdots, \xi_{r_2}^2, \cdots, \xi_{r_m}^m)^T \tag{3.4}$$

$$= (y_1, \dot{y}_1, \cdots, y_1^{(r_1 - 1)}, y_2, \cdots, y_2^{(r_2 - 1)}, \cdots\cdots, y_m^{(r_m - 1)})^T.$$

Choose $\eta(x)$, an $n - |r|$ dimensional function on R^n such that $(\xi^T, \eta^T)^T = \psi(x)$ forms a change of coordinates with 1) $\psi(0) = 0$ and 2) the system dynamics (3.1) become [8]

$$\begin{cases} \dot{\xi}_1^i = \xi_2^i \\ \cdots \\ \dot{\xi}_{r_i - 1}^i = \xi_{r_i}^i \\ \dot{\xi}_{r_i}^i = \alpha_i(\xi, \eta) - \beta_i(\xi, \eta) u \end{cases} \quad \text{for } i = 1, \cdots, m, \tag{3.5a}$$

$$\dot{\eta} = q_1(\xi, \eta) + q_2(\xi, \eta) u, \tag{3.5b}$$

which, in a more compact form, is equivalent to

$$\begin{cases} \dot{\xi}^{(r)} = \alpha(\xi, \eta) + \beta(\xi, \eta) u \\ \dot{\eta} = q_1(\xi, \eta) + q_2(\xi, \eta) u \end{cases}. \tag{3.6}$$

where

$$y = (y_1, y_2, \cdots, y_m)^T,$$

$$u = (u_1, u_2, \cdots, u_m)^T,$$

$$\alpha(\xi, \eta) = L_f^r h(\psi^{-1}(\xi, \eta)),$$

$$\beta(\xi, \eta) = L_g L_f^{r-1} h(\psi^{-1}(\xi, \eta)).$$

This β is actually the same $\beta(x)$ matrix defined in the above, and

$$h(x) = [h_1(x), h_2(x), \cdots, h_m(x)]^T,$$

$$g(x) = [g_1(x), g_2(x), \cdots, g_m(x)].$$

α_i and β_i are the ith row of α and β respectively. By the relative degree assumption, $\beta(\xi, \eta)$ is nonsingular so we can define the feedback control law

$$u := \beta^{-1}(\xi, \eta)[v - \alpha(\xi, \eta)]. \tag{3.7}$$

This control linearizes the input-output behavior to a chain of integrators:

$$y^{(r)} = v \tag{3.8}$$

where $v \in R^m$ is the new control input. Assume both $y(t) \equiv 0$ and $y_d(t) \equiv 0$ for $t < 0$ and choose

$$v = y_d^{(r)}. \tag{3.9}$$

Then immediately we have

$$\xi = \xi_d :=$$

$$(y_{d1}, \dot{y}_{d1}, \cdots, y_{d1}^{(r_1-1)}, y_{d2}, \cdots, y_{d2}^{(r_2-1)}, \cdots\cdots, y_{dm}^{(r_m-1)}) \tag{3.10}$$

and equation (3.6) becomes,

$$\dot{\eta} = p(\xi_d, y_d^{(r)}, \eta) \tag{3.11}$$

where

$$p(y_d, \dot{\xi}_d, \eta) := q_1(\xi_d, \eta) - q_2(\xi_d, \eta)\beta^{-1}(\psi^{-1}(\xi_d, \eta))[y_d^{(r)} - \alpha(\psi^{-1}(\xi_d, \eta))].$$

For brevity we define $\bar{\xi}_d = (\xi_d, y_d^{(r)})$ and write (3.11) as

$$\dot{\eta} = p(\bar{\xi}_d, \eta). \tag{3.11'}$$

We call (3.11') the ξ_d dynamics. Equation (3.11) together with (3.8) determine the linearizing input through (3.7). Our goal is to choose a particular solution of (3.11') such that the resulting input tends to zero at $\pm\infty$ and meets the other requirements of being and inverse to y_d.

For reference trajectories with compact support $[0, T]$, the reference dynamics become autonomous zero dynamics for t outside the interval $[0, T]$. The following theorem is our main result.

Theorem (State-space conditions for existence of inverse): Consider the system

$$\dot{x} = f(x) + g(x)u \tag{3.13a}$$

$$y = h(x) \tag{3.13b}$$

where f, g and h are smooth. Let 0 be an equilibrium point of $\dot{x} = f(x)$ and assume without loss of generality that $h(0) = 0$. If $y_d(t)$ is a smooth desired output with compact support $[0, T]$ and 0 is a hyperbolic equilibrium point of the zero dynamics then there is a solution to the inverse problem provided $\| \bar{\xi}_d \|_\infty := \sup_{t \in [0,T]} \| \bar{\xi}_d(t) \|_2$ is not too large.

Proof: Let

$$y^{(r)} = y_d^{(r)} \tag{3.14a}$$

$$\dot{\eta} = p(\bar{\xi}_d, \eta) \tag{3.14b}$$

be the normal form of the system with initial conditions 0 at $-\infty$ and v chosen to cause tracking of the desired output. We need to find a solution to the η dynamics such that the input u tends to zero at $\pm\infty$. Define $\phi_{t,\tau}^{\bar{\xi}_d}$ be the flow of the η dynamics (3.14b) from time t to time τ. Note that there exists an interval, say, $[0, T]$ outside which y and its derivatives are zero. Hence the η dynamics before 0 and after T are simply the zero dynamics. Since the stable and unstable manifolds of the equilibrium point 0 are indeed smooth manifolds there exists smooth functions $B^s : R^{(n-|r|)} \to R^{(n-|r|-n_u)}$ and $B^u : R^{(n-|r|)} \to R^{(n-|r|-n_s)}$ which define the stable and unstable manifolds.

We claim that $\phi_{0,T}^{\bar{\xi}_d}(W^u) \cap W^s$ is nonempty (an element of this set defines an initial condition for selecting our solution to (3.14b)). That is, the image of the unstable manifold of 0 under the flow $\phi_{0,T}^{\bar{\xi}_d}$ intersects the stable manifold of 0. This is equivalent to the existence of a solution to

$$f(\eta, \xi) := \begin{bmatrix} B^u(\phi_{0,T}^{\bar{\xi}_d}(\eta)) \\ B^s(\eta) \end{bmatrix} = 0 \tag{3.16}$$

For $\xi = 0$ there is a solution since the stable and unstable manifolds intersect at 0. We now employ the implicit function theorem to show existence of solution for $\| \bar{\xi} \|_\infty$ is not too large. Since the intersection of the stable and unstable manifolds intersect transversally at the equilibrium 0 we have that $D_\eta f(0,0)$ is an isomorphism. Also,

$$D_\xi f(0,0) = \begin{bmatrix} DB^u(0) \circ D_\xi \phi_{0,T}^{\bar{\xi}_d} \\ 0 \end{bmatrix}. \tag{3.17}$$

The function B^u is smooth and, by the corollary to the proposition in the Appendix, $D_\xi \phi_{0,T}^{\bar{\xi}_d}$ is continuous. Hence, by the implicit function theorem, there exists a solution η_T to 3.16 when $\| \bar{\xi}_d \|_\infty$ is not too large. By flowing this solution point forward and backward in time we can obtain the inverse.

Define the desired η trajectory by

$$\eta_d(t) = \phi_{T,t}^{\bar{\xi}_d}(\eta_T) \tag{3.18}$$

From this and the desired ξ trajectory we construct the input: $u(t) = \beta(\xi_d, \eta_d)^{-1}(y_d^{(r)} - \alpha(\xi_d, \eta_d))$. Since η_T is on the stable manifold and the $\bar{\xi}_d$ dynamics are the zero dynamics after time T, we have that $\eta \to O$ as $t \to \infty$. Also, $\xi(t) \to 0$ as $t \to \infty$ because y_d has compact support. If follows that both u and x tend to zero as $t \to \infty$. A similar argument applies in backward time. On the interval $[0, T]$ solutions are bounded since they depend continuously on $\bar{\xi}_d$ and $\| \bar{\xi}_d \|_\infty$ is bounded. Hence and inverse exists. □

In the case of minimum phase systems, the reference dynamics is asymptotically stable in forward time. The stable manifold is the dimension as the zero dynamics manifold and the unstable manifold reduces to the origin only. Therefore, the boundary condition $B^u(\eta)=0$, reduces to $\eta=0$ and $B^s(\eta)=0$ imposes no extra constraints. The inverse can be easily integrated in the forward time. This is Hirshorn's approach.

Similarly, if we consider the system as evolving backward in time, and

this reversed system has only the origin as the stable manifold of its zero dynamics then the two point boundary value problem reduces to a final value problem and can be easily integrated in backward time.

Another simple situation is when the stable and unstable part of the reference dynamics can be decoupled by change of coordinates. This happens when the reference dynamics is a linear time-invariant system driven by the reference output and its derivatives. In such cases, we can easily integrate the stable part in forward time and the unstable part in backward time.

4. Conclusion

The primary contribution of this paper is the proof existence of inverses when zero dynamics are hyperbolic. These results, in conjunction with Hirschorn's show that there are multiple inverses for nonminimum phase nonlinear system -- bounded, noncausal solutions produced with our method and unbounded, and causal solutions produced using Hirschorn's method. These inversion techniques are fundamental to nonlinear tracking controllers which use feedforward in conjunction with stabilizing feedback. Future work will include input-output characterizations for existence of solutions to the inverse problem.

Appendix

Proposition: Consider the system

$$\dot{x} = f(x,u); \quad x(0) = x_0 \tag{A.1}$$

on the interval $[0,T]$ where $f: R^n \times R^m \to R^n$ is smooth in x and u and $\|u\|_\infty = \sup_{t \in [0,T]} \|u(t)\|_2 < M$; T is chosen such that solutions exist on $[0,T]$ for all $u \in L_\infty$ satisfying the bound.

Let $\phi_u(t,x_0)$ denote the solution of the differential equation on $[0,T]$. The Frechet derivative, $D_u\phi_u(t,x_0)$: $L_\infty[0,T] \to L_\infty[0,T]$ of the map

$$u(\cdot) \mapsto \phi_u(\cdot,x_0) \tag{A.2}$$

is given by

$$D_u\phi_u(t,x_0)\zeta = \int_0^t \Phi(t,\tau)\frac{\partial f}{\partial u}[\phi_u(\tau,x_0),u(\tau)]\zeta(\tau)d\tau \tag{A.3}$$

where $\Phi(t,\tau)$ is the state transition matrix for

$$\dot{x} = \left[\frac{\partial f}{\partial x}(\phi_u(t,x_0),u(t))\right]x. \tag{A.4}$$

Before proceeding with the proof we establish the following

Lemma: The mapping from $L_\infty[0,T] \to L_\infty[0,T]$ given by

$$u(\cdot) \to \phi_u(\cdot,x_0) \tag{A.5}$$

is Lipshitz in u.

Proof: Define

$$\varepsilon(t) = \|\phi_{u_1}(t,x_0) - \phi_{u_2}(t,x_0)\|_2. \tag{A.6}$$

The one-sided derivative of ε is

$$\dot{\varepsilon}_+(t) = \lim_{h \to 0+} \frac{\varepsilon(t+h) - \varepsilon(t)}{h}$$

$$= m_+\left[\varepsilon(t), f(\phi_{u_1}(t,x_0),u_1(t)) - f(\phi_{u_2}(t,x_0),u_2(t))\right]. \tag{A.7}$$

where $m_+[x,y]$ is the directional derivative of the 2-norm: $m_+[x,y] = \lim_{h \to 0+} \frac{\|x + hy\| - \|x\|}{h}$. The smoothness of f implies its local Lipschitz continuity (in both arguments). Since $m_+[x,y] \le \|y\|$ we have

$$\|f(\phi_{u_1}(t,x_0),u_1(t)) - f(\phi_{u_2}(t,x_0),u_2(t))\|$$

$$\le K[\varepsilon(t) + \|u_1(t) - u_2(t)\|] \tag{A.8}$$

for some real K. This implies

$$\dot{\varepsilon}^+ \le K[\varepsilon + \|u_1 - u_2\|_\infty]. \tag{A.9}$$

By solving this differential inequality we obtain

$$\varepsilon(t) \le (\|u_1 - u_2\|_\infty) K \int_0^t e^{K(t-\tau)}d\tau. \tag{A.10}$$

Therefore we have the desired Lipschitz property with Lipschitz constant $K \int_0^t e^{K(t-\tau)}d\tau$.

Proof of Proposition (see [10] proposition 5.3 for related proof techniques). Let $\varepsilon > 0$. By the Lipschitz continuity of $\phi_u(t,x_0)$ proven in the lemma and the smoothness of f, there exists $r \in (0, (M - \|\zeta\|_\infty)]$ such that

$$\| f(\phi_{u+\zeta}(t,x_0),u+\zeta) - f(\phi_u(t,x_0),u) - \frac{\partial f}{\partial x}(\phi_u(t,x_0),u)[\phi_{u+\zeta}(t,x_0)$$

$$\phi_u(t,x_0)] - \frac{\partial f}{\partial u}(\phi_u(t,x_{0),u})\zeta(t)\|_2 \le \varepsilon\|\zeta\|_\infty \tag{A.11}$$

for all $t \in [0,T]$ and ζ satisfying $\|\zeta\|_\infty < M - \|u\|_\infty$. Define the error between a solution $\phi_u(t,x_0)$ and a perturbed solution $\phi_{u+\zeta}(t,x_0)$ by

$$\delta(t) = \phi_{u+\zeta}(t,x_0) - \phi_u(t,x_0). \tag{A.12}$$

(The idea of the proof is to bound $\dot{\delta}(t) - \dot{\Delta}(t)$ where $\Delta(t)$ is the right-hand side of equation (A.3). We integrate this bound to get a bound on $\delta(t) - \Delta(t)$ and, finally, we show that $\delta(t) = \Delta(t)$ in the limit $\|\zeta\|_\infty \to 0$.)

Differentiating $\delta(t)$ yields

$$\dot{\delta}(t) = f(\phi_{u+\zeta}(t,x_0),u(t) + \zeta(t)) - f(\phi_u(t,x_0),u(t)) \tag{A.13}$$

but this is just the first two terms in (A.11). Hence

$$\|\dot{\delta}(t) - \frac{\partial f}{\partial x}(\phi_u(t,x_0))\delta - \frac{\partial f}{\partial u}\phi_u(t,x_0)\zeta\| \le \varepsilon\|\zeta\|_\infty. \tag{A.14}$$

Define $p(t) = \|\delta(t) - \Delta(t)\|$. The one-sided derivative of $p(t)$ is given by

$$\dot{p}_+(t) = m_+[\delta(t) - \Delta(t), \dot{\delta}(t) - \dot{\Delta}(t)]$$

Expanding $\dot{\Delta}$ in the second argument, using A.14 and the property $m_+[x,y+z] \le m_+[x,y] + \|z\|$ we have

$$\dot{p}_+(t) \le m_+\left[\delta(t) - \Delta(t), \frac{\partial f}{\partial x}(\phi_u(t,x_0),u(t))(\delta(t) - \Delta(t))\right] + \varepsilon\|\zeta\|_\infty \tag{A.15}$$

$$\le Bp(t) + \varepsilon\|\zeta\|_\infty \tag{A.16}$$

where B is a uniform bound on $\frac{\partial f}{\partial x}(\phi_u(t,x_0),u(t))$ for $t \in [0,T]$ and u satisfying $\|u\|_\infty < M$. The existence of the bound follows from basic existence and uniqueness theory for ordinary differential equations, boundedness of u and smoothness of f.

Solving this differential inequality yields

$$p(t) \leq \varepsilon \|\zeta\|_\infty \int_0^t e^{\beta(t-\tau)} d\tau \tag{A.17}$$

We have therefore

$$\lim_{\|\zeta\|_\infty \to 0} \frac{\|\delta - \Delta\|_\infty}{\|\zeta\|_\infty} \leq \varepsilon \int_0^t e^{\beta(t-\tau)} d\tau. \tag{A.18}$$

Since ε can be chosen arbitrarily small, Δ is Frechet derivative evaluated in the direction ζ. □

Corollary $D_u \phi_u(t, x_0)$ is continuous in $u(\cdot)$.

Proof: By inspection of (A.3) we see that the smoothness of f and the continuity of ϕ_u in $u(\cdot)$ implies the statement of the corollary.

References

1. Bayo, E., Serna, M.A., Papadopoulos, P., and Stubbe, J.R., "Inverse dynamics and kinematics of multi-link elastic robots: an iterative frequency-domain approach ," *International Journal of Robotics Research*, vol. 8 no. 6, pp. 49-62, Dec. 1989.
2. B. A. Francis, "The linear multivariable regulator problem," *SIAM J. Control & Optimization*, vol. 15, pp. 486-505, 1977.
3. A. Isidori and C. I. Byrnes, "Output regulation of nonlinear systems," *IEEE Trans. on Automatic Control*, vol. AC-35(2), pp. 131-140, 1990.
4. A. De Luca, L. Lanari, and G. Ulivi, "Output Regulation of a Flexible Robot Arm," *9th Int. Conference on Analysis and Optimization of Systems, INRIA*, 1990.
5. R. W. Brockett and M. D. Mesarovic, "The reproducibility of multivariable systems ," *J. Mathematical Analysis and Applications*, vol. 11, pp. 548-563, 1965.
6. W. M. Silver, "On the equivalence of Lagrangian and Newton-Euler Dynamics for Manipulators," *International Journal of Robotics Research*, vol. 1 No. 2, 1982.
7. R. M. Hirschorn, "Invertibilty of nonlinear control systems," *SIAM J. Control & Optimization*, vol. 17(2), pp. 289-297, 1979.
8. A. Isidori, *Nonlinear Control Systems: An Introduction, 2nd edition* , Springer-Verlag, 1989.
9. B. Paden, D. Chen, R. Ledesma, and E. Bayo, "Exponentially stable tracking control for multi-link flexible manipulators ," *to appear in ASME J. Dynamic Systems Measurement and Control.*
10. R. H. Martin, *Nonlinear Operators and Differential Equations in Banach Spaces*, Wiley, 1976.